

TRIESKOVÉ A BEZTRIESKOVÉ OBRÁBANIE DREVA 2024

CHIP AND CHIPLESS WOODWORKING PROCESSES 2024

Vedecký časopis // Scientific journal



TECHNICKÁ UNIVERZITA VO ZVOLENE // TECHNICAL UNIVERSITY IN ZVOLEN
DREVÁRSKA FAKULTA // FACULTY OF WOOD SCIENCES AND TECHNOLOGY
KATEDRA OBRÁBANIA DREVA // DEPARTMENT OF WOODWORKING

TECHNICKÁ UNIVERZITA VO ZVOLENE // TECHNICAL UNIVERSITY IN ZVOLEN
DREVÁRSKA FAKULTA // FACULTY OF WOOD SCIENCES AND TECHNOLOGY
KATEDRA OBRÁBANIA DREVA // DEPARTMENT OF WOODWORKING



TRIESKOVÉ A BEZTRIESKOVÉ OBRÁBANIE DREVA 2024

CHIP AND CHIPLESS WOODWORKING PROCESSES 2024

Vedecký časopis // Scientific journal



Trieskové a beztrieskové obrábanie dreva (ISSN 2453-904X (print), ISSN 1339-8350

(online)) je vedecký časopis uverejňujúci recenzované pôvodné vedecké práce, z oblasti technického a technologického výskumu trieskového delenie a obrábanie dreva, procesu tvorby triesky, kvality vytváraného povrchu a fyzikálno-mechanických vlastnostiach triesky. Súčasťou zamerania časopisu je i problematika termickej a hydrotermickej úpravy drevnej hmoty teplom a realizácie týchto procesov. Časopis vychádza s dvojročnou periodicitou v elektronickej a printovej forme.

Chip and chipless woodworking processes (ISSN 2453-904X (print), ISSN 1339-8350

(online)) is a scientific journal publishing the reviewed original scientific works focusing on the technical and technological research of chip separation and wood processing, the process of making chips, the quality of created surface as well as the physico-mechanical chips characteristics. The journal focuses also on the issue of thermal and hydrothermal modification of the wood pulp by heat and how these processes are realized. The journal is published in a twoyear periodicity in an electronic and a print form.

Redakčná rada/Editorial Board

Predseda redakčnej rady/Editorial Board Chief

Ladislav DZURENDA

Členovia edičnej rady/Editorial Board Members

Zhivko GOCHEV, Ján SEDLIAČIK, Kazimierz A. ORLOWSKI, Grzegorz KOWALUK, Alena OČKAJOVA, Miroslav KOPECKY, Tomasz ROGOZIŃSKI, Richard KMINIAK

Zodpovední vedeckí redaktori/Responsible scientific editors

Ladislav DZURENDA

Adrián BANSKI

Technický redaktor/Technical Editor

Silvia NEMCOVA

Redakcia/Editorial office

Technická univerzita vo Zvolene/ Technical university in Zvolen

Drevárska fakulta/ Faculty of Wood Sciences and Technology

Katedra obrábania dreva/ Department of Woodworking

T. G. Masaryka 24

960 01 Zvolen

Vydavateľ/Publisher

Technická univerzita vo Zvolene/Technical university in Zvolen,

T. G. Masaryka 24

960 01 Zvolen, IČO 00397440, 2024

Náklad (Circulation) 80 výtlačkov, rozsah (Pages) 220 strán

Tlač (Printed by) Vydavateľstvo Technickej univerzity vo Zvolene.

Vydanie I. – september

Periodikum s periodicitou raz za dva roky. Za vedeckú úroveň tejto publikácie zodpovedajú autori.

Všetky práva vyhradené. Nijaká časť textu ani ilustrácie nemôžu byť použité na ďalšie šírenie akoukoľvek formou bez predchádzajúceho súhlasu autorov alebo vydavateľa.

© Technická univerzita vo Zvolene

ISSN 2453-904X (print), ISSN 1339-8350 (online)

CONTENTS

ADAMČÍK Lukáš – KMINIAK Richard – BANSKI Adrián – DUDIAK Michal – PAVELLA Filip Tibor: Mutual comparison of methodologies of line and area surface roughness measurement of steamed beech wood after CNC milling	7
ADAMČÍK Lukáš – KMINIAK Richard – DARABOŠOVÁ Anna – ČABALOVÁ Iveta: Use of areal surface texture parameters for quantification of porosity of particleboards in the evaluation of their density	17
BORYSIUK Piotr – PIECH Radosław – AURIGA Radosław: Biocomposite based on starch and pine wood particles	25
ČUCHOR Tomáš – KOLEDA Peter – KMINIAK Richard: Analysis of power consumption during milling the wood-based materials	33
DELIISKI Nencho – DZURENDA Ladislav – ANGESKI Dimitar – VITCHEV Pavlin – ATANASOVA Krasimira: Computing the specific heat capacities and energy consumption of logs subjected to defrosting. Part 1. Calculating the specific heat capacities of frozen wood	39
DELIISKI Nencho – DZURENDA Ladislav – ANGESKI Dimitar – VITCHEV Pavlin – ATANASOVA Krasimira: Computing the specific heat capacities and energy consumption of logs subjected to defrosting Part 2. Calculating the energy required to defrost logs	45
DUDIAK Michal – BANSKI Adrián: Acidity of steamed beech sapwood and false heartwood	53
DUDIAK Michal – KMINIAK Richard – BANSKI Adrián: The effect of steaming alder wood on the quality of the milled wood surface	61
DZURENDA Ladislav – DUDIAK Michal: Heat consumption for the elimination of color differences of beech sapwood and false heartwood by the steaming process	73
GEJDOŠ Miloš – TOMČÍK Daniel: Dust monitoring in urban heating plants on forest biomass	79
GOCHEV Zhivko – VITCHEV Pavlin: Effect of lens focal length in CO ₂ laser engraving	85
HANINCOVÁ Lud'ka – NOVÁK VÍT – PROCHÁZKA Jiří – MATROSZ Radek: Tool Coatings and Their Effect on Cutting Force Reduction in CNC MDF Milling	95

JURKOVIČ Peter – NOVÁK Igor – MATYAŠOVSKÝ Ján – KLEINOVÁ Angela – MIČUŠÍK Matej – SEDLIAČIK Ján: Surface and adhesive properties of beech wood treated by low temperature plasma and saturated water steam	103
KLEMENT Ivan – VILKOVSKÁ Tatiana – VILKOVSKÝ Peter – SUČHTA Aleksandra – BARAŇSKI Jacek: Cupping deformation during drying of beech wood (<i>Fagus sylvatica</i> L.)	109
KOLEDA Pavol: Chip color analysis using the program Matlab	117
KOLEDA Peter – HORTOBÁGYI Áron – KMINIAK Richard Experimental analysis of parameters influence of woodbased materials milling on vibrations amplitude	123
KOVATCHEV Georgy: Influence of V-belt type on the vibration of a woodworking milling machine at idle	129
KUČERKA Martin – ADAMČÍK Lukáš – JÚDA Martin – KMINIAK Richard – OČKAJOVÁ Alena: Comparison of particles from the sanding process of spruce and oak on a narrow belt sander	135
KWIDZIŃSKI Zdzisław – PEŁDZIK Marta – WILCZYŃSKI Adam – ROGOZIŃSKI Tomasz – DREW CZYŃSKI Marcin: Efficiency of integrated technological modules in mass production processes of wooden door frames	143
MATYAŠOVSKÝ Ján – SEDLIAČIK Ján – NOVÁK Igor– JURKOVIČ Peter – DUCHOVIČ Peter: Keratin as environmentally friendly formaldehyde scavengers from wood-based panels	149
OČKAJOVÁ Alena – BANSKI Adrián – KUČERKA Martin – VYHNÁLIKOVÁ Zuzana: Examples of safety and health risk factors in woodworking industry in Slovak Republic	159
POTOK Zbigniew – PRAŁAT Barbara – PEŁDZIK Marta – WIADEREK Krzysztof – ROGOZIŃSKI Tomasz: Specific cutting work at drilling particleboards made of an alternative raw material	169
SLABEJOVÁ Gabriela – ŠMIDRIAKOVÁ Mária – ADAMČÍK Lukáš – VIDHOLDOVÁ Zuzana: Surface Roughness of Oil Surface Finishes on Beech Wood if The Recommended Application Procedure is Not Followed	175
SZWAJKA Krzysztof – ZIELIŃSKA-SZWAJKA Joanna: Identification of the workpiece material based on the of signals from the cutting zone	187

ŠTEFANČIN Lukáš – IGAZ Rastislav – KUBOVSKÝ Ivan – KMINIAK Richard: Comparison of kerf widths in CO2 laser cutting of wood-based materials	193
ULIČNÝ Hugo M. – VILKOVSKÝ Peter – KLEMENT Ivan: Monitoring the dimensional stability of hornbeam lumber in the process of air drying	201
ZIELIŇSKA-SZWAJKA Joanna – SZWAJKA Krzysztof: Model of energy consumption in drilling processes of wood-based materials based on cutting force	209
VIDHOLDOVÁ Zuzana – SLABEJOVÁ Gabriela: Decay resistance valuation for false heartwood and mature beech wood	215



MUTUAL COMPARISON OF METHODOLOGIES OF LINE AND AREA SURFACE ROUGHNESS MEASUREMENT OF STEAMED BEECH WOOD AFTER CNC MILLING

Lukáš Adamčík – Richard Kminiak – Adrián Banski – Michal Dudiak
– Filip Tibor Pavella

Abstract

Wood milling is a process in which the correct setting of parameters is important. These are most often optimized with regard to the quality of the created surface. The most commonly used methodologies are measuring the roughness of wood. Currently, there are two types of measurements – line and area surface roughness measurement. Both methods were used to compare the effect of steaming modes on roughness parameters. The experiment showed that line measurement of wood roughness provides a more detailed analysis of individual factors on surface roughness. Area surface roughness measurement, on the other hand, evaluates the complex overall change in surface roughness. For these reasons, the conclusions of the individual methodologies therefore differ. However, both methods have their significant advantages as well as disadvantages.

Key words: beech wood, steaming, roughness, digital microscopy, methodology

INTRODUCTION

Wood milling is a process that also significantly contributes to the creation of the final quality of the created surface (Kminiak and Gaff, 2015). Although the surface roughness changes in the next technological operation – sanding, improperly performed milling (with inappropriately set machining parameters) can lead to extensive damage to the wood surface. This damage often cannot be removed by sanding or filling with filler. Optimization of milling parameters should therefore be carried out with regard to the quality of the created surface (Atanasov et al., 2023; Keturakis and Juodeikienė, 2007; Wei et al., 2021). In the field of wood processing technology as well as research on the properties of wood surfaces or wood materials, there is a large number of research dealing with roughness (Gurau *et al.* 2007; Henke *et al.* 2022; Malkoçoğlu, 2007). Most authors measure roughness with a stylus profilometer (Chuchala *et al.* 2023; İşleyen and Karamanoğlu, 2019; Kilic *et al.* 2006). However, roughness measurements by optical methods are also in the foreground – digital profilometers or digital microscopes combined with the properties of profilometers. With their development, methodologies for measuring area surface parameters of roughness of materials have also developed (Blateyron, 2013; Nagalingam et al., 2021). This surface assessment represents a very fast method of measurement, which contains many points in the evaluated area, from which the areal

surface texture parameters are determined. The basis of evaluation is no longer 1 profile, but an area on which it is possible to capture the irregularities present in both anatomical directions at once. Especially when evaluating the roughness of the wood surface, this difference can significantly help to research the effects of individual factors. While in the case of profile traces it is necessary to consider unevenness in the direction perpendicular to the grain (alternation of earlywood and latewood), dales formed by cellular elements (Kang et al., 2023), in the direction parallel to the grain, the dominant unevenness is created rather by milling (cycloidal movement of the tool). These mixed effects are difficult to discuss when measured separately in two directions. Very often, they lead to different conclusions. Nevertheless, line roughness measurement has its justification, especially when analysing separately acting factors. However, if we look at the overall surface changes (i.e. unevenness created by milling and at the same time unevenness formed by cellular elements), which are common especially in the processing of thermally modified wood (Corleto et al., 2020), it is advisable to use measurement by areal surface texture parameters.

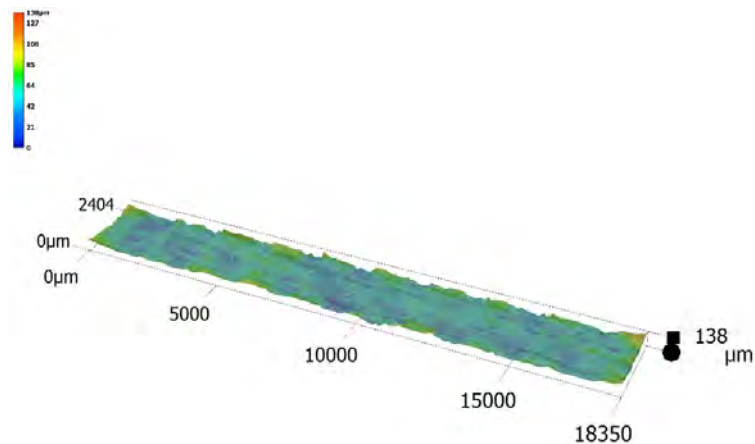


Fig. 1 Unevenness of the surface of beech wood created by milling (cycloidal movement) and cellular elements. Image magnification 100×

Fig. 1 shows an example of a digital image that is scanned from the surface of beech wood. The figure shows that when evaluated by the linear parameters of roughness, in the direction parallel to the grain (at a length of 12.5 mm), the dominant unevenness will be created by the movement of the cutter. These can change due to steaming modes, as the physical and mechanical properties of wood as a processed material also change. On the other hand, in the direction perpendicular to the grain, the unevenness created by the cell elements present will be dominant in the individual profile tracks. Thus, when measuring in the direction perpendicular to the grain, important and not negligible “waves” after the cycloidal movement of the instrument are absent. When measuring parallel to the grain, on the other hand, the unevenness formed by the cellular elements is absent. These are not only negligible for beech, but especially for wood species with deep pores on the surface, such as oak. However, the thermal modification of wood by steaming affects the entire system comprehensively. Demonstrably increases the quality of the milled surface in many cases (Korkut et al., 2012; Shukla, 2019). At the same time, however, it also causes the collapse

of cell walls, which leads to the closure of pores on the surface and, to a certain extent, to an improvement in quality (A. Bakar et al. 2013).

The aim of this paper is to compare two types of methodologies – linear and area surface measurement of wood roughness. The comparison will be carried out on beech wood that has been thermally modified by steaming. The methodologies will compare the effect of steaming modes on roughness parameters. Subsequently, the conclusions from both methodologies will be compared with each other.

MATERIALS AND METHODS

Sample preparation

For the preparation of the samples, boards from European beech (*Fagus sylvatica* L.) with wood moisture from 54.7 % to 58.2 % were used. The plates were then divided into five groups and thermally modified by steaming in the APDZ 240 autoclave (Himmasch AD, Bulgaria) in the company Sundermann s.r.o., Slovakia. Steaming took place according to the conditions specified in Table 1.

Table 1 Temperatures and time of individual steaming modes

Groups	Conditions of steaming modes	
	Temperatures [°C]	Duration [h]
Unmodified (UM)	-	
I.	95	
II.	115	6
III.	125	
IV.	135	

All boards were then dried in the SUZAR KC 1/50 drying kiln (SUZAR s.r.o., Slovakia). After drying, the samples were moved to indoor conditions, where they gradually reached an equilibrium wood moisture content of 8 to 10%. Samples with dimensions of 20 × 70 × 400 mm (thickness × width × length) were manipulated using a circular saw.

CNC Sample Milling

The dimensions of the samples were determined as the most optimal with regard to the design of the SCM Tech Z5 CNC machining center (Scm Group, Rimini, Italy) and the design of the mechanical clamps. A Klein T143 spiral milling cutter (Sistemi Srl, Pesaro, Italy) with a diameter of 20 mm and three cutting edges was used for milling beech samples. CNC milling was carried out in two passes of the tool through the workpiece – the first pass ensured the removal of unevenness created after planing and thicknessing. The second pass created the final quality of the created surface. The thickness of the removed layer during milling was 1 mm, the tool speed was 18,000 rpm and the feed speed was 14 m·min⁻¹.

Measuring the roughness of wood

Wood roughness measurements were performed on a Keyence VHX-7000 digital microscope (Keyence, Japan) with a VH-Z100R objective lens (with 100× zoom selected). On one sample, 10 surfaces were digitally scanned in the direction perpendicular to the grain and in the direction parallel to the grain (the size of the scanned image was 3 × 18 mm). The following conditions were set for the line measurement of wood roughness: λ_c (L-filter) = 2.5 mm, λ_s (S-filter) = 8 μm according to the recommendations of ISO 21920-3 (STN EN ISO 21920-3:, 2022). On each scanned image, 2 profile tracks were digitally translated, i.e. 2 roughness parameters were obtained. For the area surface measurement of wood roughness, 5 evaluated areas were evenly distributed on the scanned image. According to the recommendations of ISO 25178-3 ("EN ISO 25178-3. Geometrical product specifications (GPS) Surface texture: Areal Part 3: Specification operators," 2012) was chosen as the evaluated surface S-L surface, i.e. a square with sizes of 2.5 × 2.5 mm. The filters chosen were S-filter = 25 μm and L-filter = 2.5 mm. Line as well as surface roughness was measured for each steaming mode.

RESULTS AND DISCUSSION

The measurement outliers were first removed from the measured data set. Subsequently, descriptive statistics were performed – arithmetic averages and standard deviations of the parameter Ra in the direction perpendicular to the grain and in the direction parallel to the grain for all steaming modes. Likewise, the arithmetic means of the parameter and the standard deviations of Sa for all steaming modes were also found. The results of descriptive statistics are presented in Table 2.

Table 2 Arithmetic averages of the parameters Ra and Sz for all steaming modes. The values in parentheses represent the standard deviation

Steaming mode	Ra (in the direction perpendicular to the grain) [μm]	Ra (in the direction parallel to the grain) [μm]	Sa (evaluated area) [μm]
UM	6,10 (0,82)	7,70 (2,35)	14,95 (1,91)
I.	6,24 (0,83)	6,41 (1,50)	14,07 (3,01)
II.	6,56 (1,53)	6,66 (1,42)	12,21 (2,57)
III.	6,42 (0,72)	6,69 (1,58)	11,69 (1,51)
IV.	5,89 (1,41)	6,31 (1,73)	11,30 (1,82)

In the second step, a one-factor analysis of variance (ANOVA) was performed as part of inductive statistics. The analysis showed that the steaming mode has a statistically significant effect on the line roughness measurement methodology (A – in the direction perpendicular to the grain $p = 0.000$, B – in the direction parallel to the grain $p = 0.000$) as well as in the area roughness measurement methodology ($p = 0.000$).

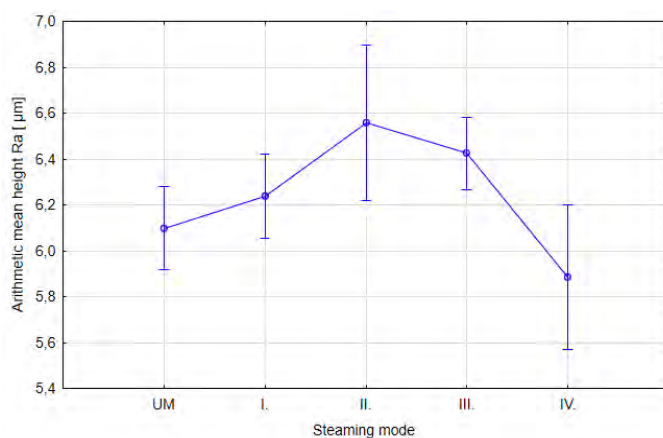


Fig. 2 Line roughness of the surface expressed by the parameter Ra for individual steaming modes (measurement in the direction perpendicular to the grain)

The measurement of roughness in the direction perpendicular to the grain (Fig. 2) shows that with increasing steaming temperature to mode II, there is an increase in roughness. The increase is statistically significant compared to unmodified beech wood (UM). With this measurement, it was found that up to a certain vaporization temperature, there is a deterioration in the quality of the surface formed for this direction. It has been found that differently milled zones of earlywood and latewood are involved in the formation of roughness. However, since the second steaming mode, the opposite trend has been measured – this roughness has decreased with increasing temperature. Under Mode III, this reduction was not yet statistically significant, but it decreased statistically significantly with higher temperatures. Under Mode IV, the roughness of the surface of beech wood decreased so much that it was lower than that of unmodified beech wood. The conclusion from this direction of measurement is that as the steaming temperature increases, the surface roughness increases up to 115 °C. Subsequently, however, with the increase in temperature, it decreases and thus the quality of the surface after milling of such modified wood increases.

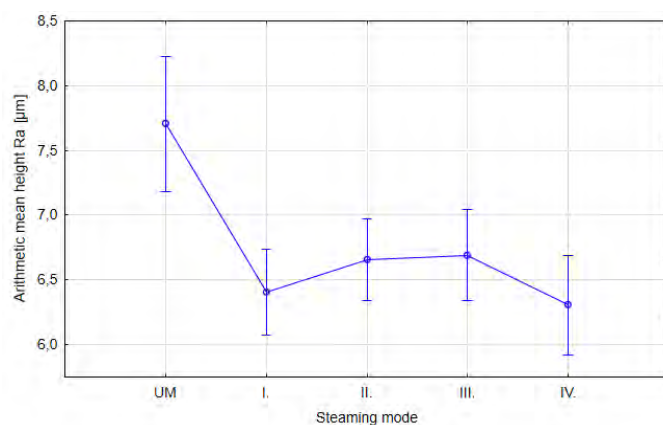


Fig. 3 Line surface roughness expressed by parameter Ra for individual steaming modes (measurement in the direction parallel to the grain)

Line measurement of roughness in the direction parallel to the grain (Fig. 3) shows that wood steaming already at the temperature of mode I causes a sharp, statistically significant decrease in roughness. In this respect, the surface is defined mainly by the formation of characteristic waves. These were most common with unmodified wood. Since steaming caused a change in the properties of beech wood at an increased temperature (already at 95 °C), waves stopped forming on the surface after the cutter movement. Although there was a slight increase in the averages of the Ra parameter with a further increase in temperature, this increase is not statistically significant, even in the last IV steaming mode. The conclusion of this methodology for measuring roughness in the direction parallel to the grain is that steaming causes changes in the level of roughness created by the movement of the tool. Up to 135 °C, there is no further significant increase or decrease in roughness. From a temperature of 95 °C, however, the surface roughness is significantly lower than in the case of unmodified wood.

Line measurements of surface roughness in the previous steps brought results in the independent action of two important factors – cell structure and tool, on the surface roughness of beech wood. A significant disadvantage of this method is that a large number of profile tracks are required to ensure the relevance of the results. This is time-consuming and often does not bring the desired results. Line roughness measurement is also problematic in the repeatability of the measurement. The reason for this is that the placement of digital profile traces (this also applies to stylus profilometers and the placement of their measuring tips on the measured surface) is highly dependent on the device operator.

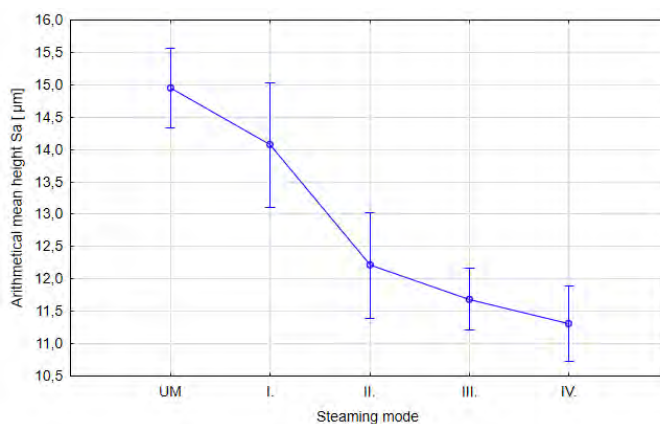


Fig. 3 Surface roughness expressed by the parameter Sa for individual steaming modes (measurement of roughness on the evaluated area)

Area measurement of wood roughness, on the other hand, is a faster method with better repeatability of the measurement. With a clearly defined size of the digital surface image, even several operators of the measuring device will achieve the same results. In Fig. 3, it is possible to see the evolution of the areal surface texture parameter Sa, which is equivalent to the parameter Ra. From the graph it can be observed that a significant decrease in roughness due to increased temperature occurs only in the second steaming mode. Subsequently, the roughness decreases, but there is no statistically significant change between the second and third steaming modes. Another statistically significant decrease

was measured in the IV steaming mode. The conclusion of the applied surface method of measuring roughness is that as the steaming point increases, the roughness decreases (and thus the quality improves) to a temperature of 135 °C. At the same time, this method comprehensively assessed all surface unevenness present on the evaluated surface – i.e. the development of unevenness between earlywood and latewood or cellular elements as pores on the surface, as well as waves on the surface after cycloidal movement of the tool.

CONCLUSION

The experiment conducted shows the following about the individual methodologies used:

- Line roughness as a measurement methodology provides important information about the effect of individual factors on surface roughness. It is used for a more detailed analysis, but it is a more time-consuming method. According to the recommendations of technical standards, line roughness parameters should be measured in the direction with larger, dominant unevenness. However, when researching the roughness of the surface of wood, especially native wood, it is advisable to measure the roughness in both directions. This will make it possible to obtain more detailed information from the measurements.
- If we talk about longitudinal milling, the roughness of the wood surface will be formed as follows in the individual directions of the wood: in the direction perpendicular to the grain, it will be formed by unevenly milled earlywood and latewood, as well as deep cellular elements present; in the direction parallel to the grain will be formed by the cycloidal movement of the cutter.
- Surface roughness parameters were a faster method that evaluated the change in surface roughness comprehensively – i.e. on the entire evaluated surface. The method is particularly suitable for evaluating the surface of treated thermally modified wood, where high temperatures affect the overall structure of the wood and changes occur both in the properties of the wood and in the cellular elements.
- Surface measurement of surface roughness is suitable if the aim of the research is to determine the effect of thermal modification modes on the change in the overall surface roughness, without considering changes in individual directions. Line roughness measurement, on the other hand, provides deeper answers to what happens to the surface of the wood in the direction perpendicular to the grain and in the direction parallel to the grain. Each of the methodologies examined is therefore characterized by special advantages.

Acknowledgement:

This experimental research was prepared within the grant project supported by the Slovak Research and Development Agency under the Contract No. APVV-21-0051 "Research of false heartwood and sapwood of *Fagus sylvatica* L. wood in order to eliminate color differences by the process of thermal treatment with saturated water steam" as the result of the work of the author and the considerable assistance of the APVV agency. The contribution was also prepared within the project agency IPA TUZVO, which contributed significantly to the creation of this contribution through the project: IPA TUZVO ESG grant no. 10/2024 "Progressive methods of optimizing CNC wood milling strategies with focus on machined surface properties".

REFERENCES

1. Atanasov, V., Kovatchev, G., Todorov, T. (2023). Study of the Influence of Basic Process Parameters on the Roughness of Surfaces During Milling of Scots Pine Wood. *Acta Facultatis Xylogiae Zvolen* 65, 89–98.
2. Blateyron, F. (2013). The Areal Field Parameters, in: Leach, R. (Ed.), *Characterisation of Areal Surface Texture*. Earlywooder, Berlin, Heidelberg, pp. 15–43. https://doi.org/10.1007/978-3-642-36458-7_2
3. Chuchala, D., Orłowski, K.A., Hiziroglu, S., Wilmańska, A., Pradlik, A., Mietka, K. (2023). Analysis of surface roughness of chemically impregnated Scots pine processed using frame-sawing machine. *Wood Material Science & Engineering* 18, 1809–1815. <https://doi.org/10.1080/17480272.2023.2221655>
4. Corleto, R., Gaff, M., Niemz, P., Sethy, A.K., Todaro, L., Ditommaso, G., Razaeei, F., Sikora, A., Kaplan, L., Das, S., Kamboj, G., Gašparik, M., Kačík, F., Macků, J. (2020). Effect of thermal modification on properties and milling behaviour of African padauk (*Pterocarpus soyauxii* Taub.) wood. *Journal of Materials Research and Technology* 9, 9315–9327. <https://doi.org/10.1016/j.jmrt.2020.06.018>
5. EN ISO 25178-3. Geometrical product specifications (GPS) Surface texture: Areal Part 3: Specification operators, 2012.
6. Gurau, L., Mansfield-Williams, H., Irle, M. (2007). Separation of processing roughness from anatomical irregularities and fuzziness to evaluate the effect of grit size on sanded European oak. *Forest Products Journal* 57, 110–116.
7. Henke, M., Lis, B., Krystofiak, T. (2022). Evaluation of Surface Roughness Parameters of HDF for Finishing under Industrial Conditions. *Materials* 15, 6359. <https://doi.org/10.3390/ma15186359>
8. İşleyen, Ü.K., Karamanoğlu, M. (2019). The influence of machining parameters on surface roughness of MDF in milling operation. *BioRes* 14, 3266–3277. <https://doi.org/10.15376/biores.14.2.3266-3277>
9. Kang, C.-W., Hashitsume, K., Jang, E., Kolya, H. (2023). Relationship Between Wood Anatomical Features and Surface Roughness Characteristics. *Wood Research* 68, 455–464. <https://doi.org/10.37763/wr.1336-4561/68.3.455464>
10. Keturakis, G., Juodeikienė, I. (2007). Investigation of Milled Wood Surface Roughness. *Materials Science* 13.
11. Kilić, M., Hiziroglu, S., Burdurlu, E. (2006). Effect of machining on surface roughness of wood. *Building and Environment* 41, 1074–1078. <https://doi.org/10.1016/j.buildenv.2005.05.008>
12. Kminiak, R., Gaff, M. (2015). Roughness of Surface Created by Transversal Sawing of Spruce, Beech, and Oak Wood. *BioResources* 10, 2873–2887. <https://doi.org/10.15376/biores.10.2.2873-2887>
13. Korkut, S., Korkut, D.S., Kocaefe, D., Elustondo, D., Bajraktari, A., Çakıcıer, N. (2012). Effect of thermal modification on the properties of narrow-leaved ash and chestnut. *Industrial Crops and Products* 35, 287–294. <https://doi.org/10.1016/j.indcrop.2011.07.016>
14. Malkoçoğlu, A. (2007). Machining properties and surface roughness of various wood species planed in different conditions. *Building and Environment - BLDG ENVIRON* 42, 2562–2567. <https://doi.org/10.1016/j.buildenv.2006.08.028>

15. Nagalingam, A.P., Vohra, M.S., Kapur, P., Yeo, S.H. (2021). Effect of Cut-Off, Evaluation Length, and Measurement Area in Profile and Areal Surface Texture Characterization of As-Built Metal Additive Manufactured Components. *Applied Sciences* 11, 5089. <https://doi.org/10.3390/app11115089>
16. Shukla, S.R. (2019). Evaluation of dimensional stability, surface roughness, colour, flexural properties and decay resistance of thermally modified *Acacia auriculiformis*. *Maderas. Ciencia y tecnología* 21, 433–446. <https://doi.org/10.4067/S0718-221X2019005000401>
17. STN EN ISO 21920-3:, 2022. STN EN ISO 21920-3:2021 - Geometrical product specifications (GPS) - Surface Texture: Profile - Part 3: Specification Operators.
18. Wei, W., Cong, R., Xue, T., Abraham, A.D., Yang, C. (2021). Surface roughness and chip morphology of wood-plastic composites manufactured via high-speed milling. *BioRes* 16, 5733–5745. <https://doi.org/10.15376/biores.16.3.5733-5745>



USE OF AREAL SURFACE TEXTURE PARAMETERS FOR QUANTIFICATION OF POROSITY OF PARTICLEBOARDS IN THE EVALUATION OF THEIR DENSITY

Lukáš Adamčík – Richard Kminiak – Anna Darabošová – Iveta Čabalová

Abstract

Nowadays, three-layer particleboard is considered to be an innovative material. For research and development of these composites, there is important to monitor their physical, mechanical, and chemical properties. Chips layering, pressing conditions significantly affect these properties. One of the most important properties of particleboard is density, which is also associated with porosity. The presented paper was intended to use the methodology of measuring areal surface texture parameters to quantify porosity in outer and inner (core) layers. The methodology was based on the hypothesis that with increasing density, the porosity and thus the irregularities of the surface are lower. The methodology was evaluated as suitable for the quantification of pores and at the same time for the identification of possible errors in the formation of particleboard.

Key words: wood-plastic composites, density, porosity, digital microscope, areal surface texture parameters

INTRODUCTION

Due to the high demand for raw materials for the particleboard industry and the reduction in the supply of wood from forests due to environmental protection, it is essential to look for alternative materials (Tabarsa, 2011). Three-layer particleboard with plastic and rubber waste in the inner (core) layer is a material in which wood particles are combined with plastic or rubber granulate to improve certain properties of the boards, such as strength, moisture resistance or environmental sustainability. When evaluating these boards, it is important to consider their physical properties – especially the density of the pressed boards. This also has a significant impact on the other properties of the particleboard (Maraghi et al., 2018). By increasing the density, the other properties of the particleboard are also improved (Eslah et al., 2012; Lias et al., 2014). Three-layer particleboards are characterized by the distribution of density over thickness, the so-called density profile. The density profile is influenced by several properties such as the structure of the mat, pressing conditions (press closing speed, temperature, pressure) and moisture content and its distribution. The unevenness of the density profile in the direction of the board thickness is already created in the process of hot pressing (Nemli and Demirel, 2007). The basis for the creation of the density profile are also the different sizes of chips used to produce particleboards and their stratification. While in the inner (core), thicker chips of 0.25 to 4.0 mm are used for this plastic granulate boards, in the outer layers it is finer chips of 0.25 to

1.0 mm. This ensures that the outer layers are thickened during pressing, which creates a smoother surface of the boards (Özlısoylu, 2023). This is important for downstream technological operations, such as covering panels with foils or veneers. The density and thus the subsequent surface roughness play a key role in this case. According to measurements (Korai, 2022) the density of the outer layers as well as the outer part of the inner (core) layer also has a very significant impact on the increase of MOR as a mechanical property. By (Nemli and Demirel, 2007) higher density in these layers also improves MOE. On the other hand, the inner (core) layer has a lower density, which creates a characteristic U-shaped profile (Wong et al., 1999). Also from measurements (Korai, 2022) An X-ray densitometer shows that the inner (core) layers of particleboard with chips of about 4 mm are characterized by a lower density compared to outer layers with chips up to 1 mm in size. However, the very low density of the inner (core) layer results in increased porosity, water diffusion, and absorption (Akbulut, 1995). Conversely, increasing the density of the inner layer improves internal bond strength and improves thickness swelling.

For the reasons mentioned above, it is therefore important to control the density of the particleboard after pressing. One method is the gravimetric density measurement method, in which the length, width, and thickness of a sample are measured with a caliper and then weighed using precision laboratory balances (Gomes Gonçalves et al., 2018). The second non-destructive method, which is more accurate and allows you to measure and evaluate the density profile, is X-ray densitometry (Martins et al., 2021). In both cases, the density of the boards will be significantly affected by the structure of the board, especially the pores present between each chip. Porosity, which is defined as the ratio of pore volume to total volume, significantly affects the physical, mechanical, acoustic, and thermal properties of particle board (Nazerian et al., 2016). The porosity decreases, the greater the compaction of the chips in the individual layers, because of which the mechanical properties of MOE and MOR are also improved. If the porosity of the boards is high, their density decreases, and the properties of particleboard also deteriorate significantly. From a research point of view, in the absence of X-ray densitometry to evaluate the density profile, it is necessary to quantify the porosity in some way. A possible way is to use digital microscopy, i.e., a combination of a microscope and a profilometer, such as the Keyence VHX-7000 digital microscope.

The aim of this paper was to determine the methodology and its suitability for pore quantification using digital microscopy. Areal surface texture parameters will be used to determine the size of pores as profile dales. Their development will be observed in relation to the measured density of three-layer boards with plastic and rubber waste.

MATERIALS AND METHODS

Preparation of particleboard

In the production of three-layer particleboard (PB) with the addition of waste plastics and rubber from cars and construction waste, wood particles from spruce logs were used, which were processed by the company Kronospan s.r.o. (Zvolen, Slovakia). The particles for the inner (core) layer ranged in size from 0.25 to 4.0 mm and for the outer layer ranged in size from 0.25 to 1.0 mm.

Waste plastic and rubber were cut into smaller parts and cleaned. In the workshops of the Technical University in Zvolen, they were used to produce small particles – granulate, using a plastic shredder from Profing (type DP 11 – 240/350) and a sawdust and chip extractor from Holzmann (type ABS 1080). The plastic granulate with a fraction from 1 mm to 4 mm was separated using an analytical sieving device from Retsch (type AS 200 digit cA). Urea formaldehyde (UF) adhesive Kronores CB 1100 F was used as a binder in composite materials (solid content 67.1%, viscosity 460 mPa·s, condensation time 55 seconds, pH value 8.6). The adhesive mixture contains ammonium nitrate NH_4NO_3 (47%) as a hardener and a paraffin emulsion (30%). The weight composition of the material used for the manufacture of one three-layer particle board is shown in Table 1.

Table 1. Weight composition of three-layer particleboard containing waste plastic granulate from automobiles

Material	Chips [g]	Glue [g]	Paraffin emulsion [g]	Hardener [g]	Granulate [g]
Outer layer	726	113	16	5	0
Inner (core) layer	963	108	18	10	107

The outer and inner (core) layers were prepared by mixing the ingredients in a laboratory coating drum. The surface mixture was applied to the mold, where it was evenly distributed. An inner (core) layer with plastic/rubber granulate was applied to the outer layer and finally the outer layer again. Three-layer particleboards with the following waste plastic and rubber were produced: fuel tanks (FT10), gaskets and mats (SC10), tyres (T10), a combination of tyres and graphite (SC10G10), a combination of gaskets and mats and graphite (SC10G10), with a percentage of filler of 10 % in the central layer and a reference particleboard without filler (PB). Six boards of each condition were produced.

Sample preparation

Samples with a size of 50 × 50 (length × width) were then sawn from the pressed boards, in the number of 6 pieces for each type of particleboard. A total of 36 samples were subjected to density measurements and irregularities scanning and measurement on a digital microscope under laboratory conditions.

Density measurement

In the case of this experiment, density was measured in two ways: gravimetrically and using a solid density measurement set. In the first step, the density was evaluated gravimetrically. Using a digital caliper, the thickness, width, and length of each sample were accurately measured. Subsequently, analytical balances were used to measure the weight and then quantify the density of the samples. In the second step, the KIT 128 solid density measurement set (RADWAG, Kraków, Poland) was used for density measurement. The device works on the principle of Archimedes' law. The immersion of the samples in water in the container of the digital density meter was carried out only after the measurement on a digital microscope, so as not to affect the values of the surface parameters of the irregularities.

Digital microscopy and porosity measurement

The porosity of the samples, as a property directly affecting density, was quantified using the Keyence VHX-7000 digital microscope. In the first step, it was necessary to perform digital scans of the edges of the samples. From the edge area of the particleboard, it is possible to quantify the porosity in both the outer and inner (core) layers. Scans were made from three sides of the 2.5×16 mm samples. The number of sides was chosen to determine the average porosity value more accurately in the outer and inner (core) layers of each type of sample. A total of 18 digital scans were made for each type of particleboard with waste plastic and rubber. Subsequently, the areal surface texture parameters, specifically the parameters Sa and Sv, were evaluated from the scans. This methodology was chosen because the size of the porosity is given by the size of the gaps between the individual pressed chips in the outer and inner (core) layers. The gaps can be understood as surface dales and can therefore be quantified by means of areal surface texture parameters. The parameter Sa (Arithmetical Mean Height) was chosen to evaluate the irregularities on many points below and above the evaluated area. At the same time, it is a relatively stable parameter for measurement. The Sv (Maximum Pit Height) parameter was selected as the parameter defining the greatest depth of pit on the evaluated surface. However, its disadvantage is that it shows lower stability during measurement and, conversely, higher susceptibility to measurement extremes. The evaluated area was a square with a size of 2.5×2.5 mm. On one digital scan, two evaluation surfaces for both outer layers and two surfaces for the inner (core) layers were inserted. The Keyence microscope then averaged the measurements from the surfaces to a single resulting value for the Sa and Sv parameters.

RESULTS AND DISCUSSION

In the first step, the density of three-layer particleboards with plastic and rubber waste was evaluated. The measurement results of the gravimetric method and the solid density measurement kit are presented in Table 2.

Table 2. Values of densities measured by the gravimetric method and the solid density measurement kit (Values in brackets represent standard deviations)

Sample	Density [kg·m ⁻³]	
	Gravimetric	Solid Density Measurement Set
T10	704,11 (3,47)	729,93 (26,13)
T10G10	677,98 (1,07)	717,50 (26,26)
FT10	717,61 (2,68)	760,64 (16,36)
SC10	692,98 (1,96)	725,35 (24,23)
SC10G10	698,53 (2,70)	721,84 (24,23)
PB	702,57 (2,54)	741,07 (23,86)

Table 2 shows that regarding the value of the standard deviation, the gravimetric method is a more accurate measurement method. However, its disadvantage when measuring the density of particleboard is that when calculating the volume, we start from a cuboid-shaped body. However, when samples are manipulated with circular saws, the shape of the sample can be deformed, which then causes inaccuracies in density calculations. On the other hand, a solid density measurement set, which works on the principle of Archimedes' law, shows measurement inaccuracies due to the bubbles that are accumulated on the edge surface (in the pores of the particleboard) during measurement. To some extent, these bubbles lighten the body and cause variations between measurements of individual samples. Even if both above methods show a certain deviation of density values from each other, it is still possible to talk about mutual correlation. At the same time, both methods point to different densities between types of particleboards, even though they have been pressed under the same conditions. We believe that the differences between individual types of particleboards with plastic and rubber waste are due to the different porosity of individual samples, which subsequently directly affects their density. Table 2 also shows that the highest density was measured in the FT10 sample gravimetrically and with a set for measuring the density of solids. The second highest densities were measured with T10 and PB as a reference sample.

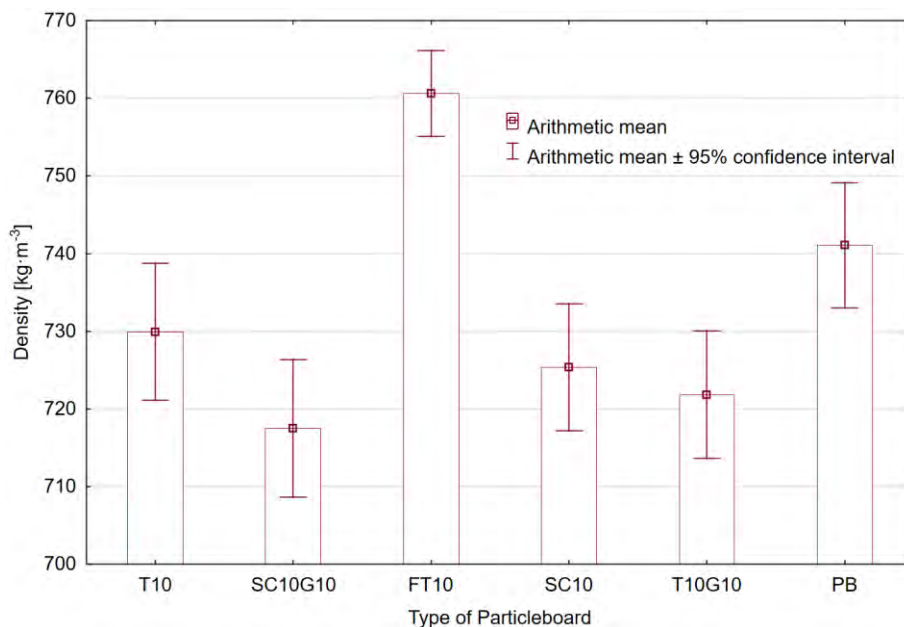


Fig. 1 Graph of measured densities of individual particleboards (vertical clamps represent a 95% confidence interval)

The development of density between individual types of particleboards, which was measured with a set for measuring the density of solids, can be seen in Fig. 1. FT10 samples as well as the reference PB particleboard can be clearly identified as statistically significantly higher densities. In both samples, the porosity is likely to be significantly lower than in the other samples. If we assume that under the same pressing conditions approximately the same density should be achieved, the porosity of the boards should also be the same. However, statistically significant variations in Fig. 1 indicate that denser FT10 and PB samples will contain more compact, compressed outer and inner (core) layers, in

which the profile dales will also be significantly lower. The areal surface texture parameters, which were verified for each type of particleboard in the next step, should also be lower.

Effect of three-layer particleboard on areal surface texture parameters

The samples were then scanned with a digital microscope and the areal surface texture parameters were evaluated. Within the framework of inductive statistics, a two-factor analysis of ANOVA variances was performed to determine the influence of a layer of the particleboard and the type of particleboard on the areal surface texture parameters. Both factors result statistically significantly ($p < 0.05$) on the parameters Sa and Sv, both separately and in mutual interaction.

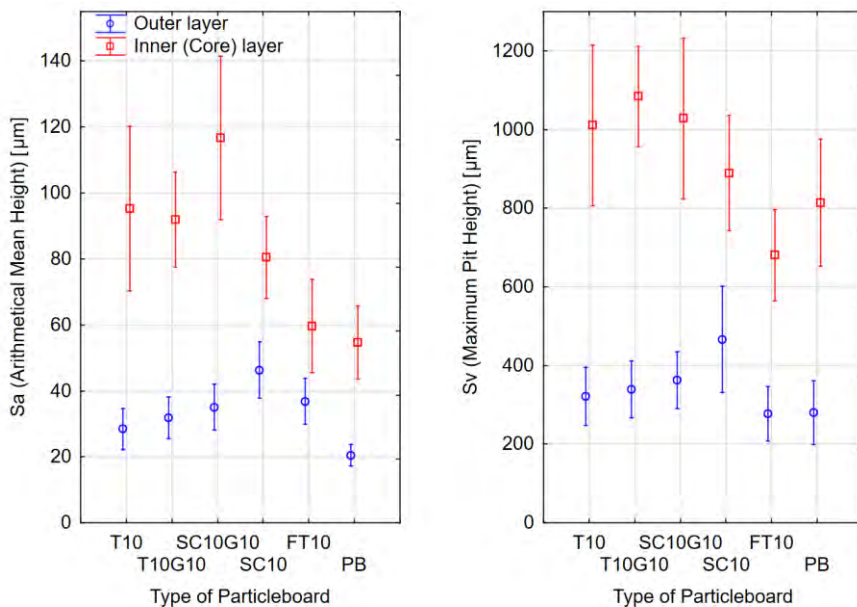


Fig. 2 Graph of irregularities measured in the surface and inner (core) layer of individual particleboards

Fig. 2 shows that lower irregularities around the inner (core) layer was measured in all samples. Thus, it can be argued that with chips with a smaller size, the layers were more compact, which led to a reduction in porosity. At the same time, this measurement correlates with the statements (Korai, 2022) with a higher density in the outer layers of the particleboard. Lower porosity indicates that pressing compressed the pores and therefore the surface had fewer dales (it was "smoother"). At the same time, it can be observed in Fig. 2 that the largest deviations in porosity expressed through surface irregularities were measured at the inner (core) layer of individual types of particleboards. From this point of view, this methodology is suitable for identifying possible defects in the process of producing particleboards with plastic and rubber waste. Significant, statistically significant decreases in irregularities in the inner (core) layer in Fig. 2 may indicate that the chip

layering for the outer and inner (core) layers was not uniform. This created more compact inner (core) layer or, conversely, places with high porosity and thus large dales after compression.

Statistically significant differences were also measured between the individual types of three-layer particleboards. In the outer layers, it was found that the SC10 sample has higher irregularities and thus higher porosity of the outer layers. More interesting results were measured with the inner (core) layers. Statistically significantly lower inequalities were measured in the FT10 sample and the PB reference sample. This means that the inner (core) layer of these particleboards has lower porosity and are more compact. This also probably proves why the highest densities were measured at FT10 and PB. At the same time, the graph of the development of the irregularities of the inner (core) layer correlates to a certain extent with the graph of the development of density (Fig. 1). Thus, where higher sample densities were measured, there were also lower irregularities. Thus, the hypothesis that this methodology (using the Sa parameter) would be able to correctly express the porosity of boards in relation to density development was confirmed. Figure 2 further shows that when comparing the confidence interval, the Sa parameter is a more accurate measurement. Sv as an amplitude parameter, on the other hand, showed wide confidence intervals caused mainly by the measurement extremes (Sv, similarly to the Rv parameter, is defined as the greatest depth of the pit on the evaluated area).

CONCLUSION

The presented experiment shows that the methodology of using areal surface texture parameters to express the porosity of three-layer particleboards is appropriate. Two parameters were used in the experiment, namely Sa and Sv. The established methodology showed that the outer more compact layers have lower porosity and thus irregularities compared to the inner (core) ones. At the same time, the methodology proved to be suitable for identifying possible errors in layering and pressing, that is, in the production of particleboards. The development of porosity expressed through surface irregularities also correlated with density measurements, and thus the hypothesis was confirmed that samples with higher density had more compact layers with less porosity and therefore less surface irregularities. The knowledge gained from this experiment will contribute to further research on three-layer particleboards with plastic and rubber waste. While the methodology does not replace the significant positives of X-ray densitometry, it is a quick way to identify potential pressing problems.

Acknowledgement:

This work was supported by the Slovak Research and Development Agency under the Contract no. APVV-22-0034 (40%), by the Ministry of Education, Research, Development and Youth of the Slovak Republic under the Contract no. VEGA 1/0027/24 (40%) by the research of the project UNIVNET “University Research Association for Waste Recovery, especially from the Automotive Industry” No. 0201/0082/19 funded by the Ministry of Education, Science, Research and Sport of the Slovak Republic (20%). The authors also express their thanks to prof. Ing. Roman Réh, CSc. for his help in setting the pressing parameters of particleboards.

REFERENCES

1. Akbulut, T. (1995). Effects of Some Factors on the Properties of Particleboard. Istanbul University, Istanbul.
2. Eslah, F., Enayati, A., Tajvidi, M., Faezipour, M.M. (2012). Regression models for the prediction of poplar particleboard properties based on urea formaldehyde resin content and board density. *Journal of Agricultural Science and Technology* 14, 1321–1329.
3. Gomes Gonçalves, F., Carlos Costa Lelis, R., Monteiro de Carvalho, A. & T.F. (2018). X-Ray Densitometry in the Evaluation of Density in Particleboard Panel. *Ciência Florestal* 28, 1151–1162.
4. Korai, H. (2022). Effects of Density Profile on Bending Strength of Commercial Particleboard. *Forest Products Journal* 72, 85–91. <https://doi.org/10.13073/FPJ-D-21-00070>
5. Lias, H., Kasim, J., Johari, N.A.N., Mokhtar, I.L.M. (2014). Influence of Board Density and Particle Sizes on the Homogenous Particleboard Properties from Kelempayan (*Neolamarckia cadamba*). *International Journal of Latest Research in Science and Technology* 3, 173–176.
6. Maraghi, M.M.R., Tabei, A., Madanipoor, M., Branch, A. (2018). Effect of Board Density, Resin Percentage and Pressing Temperature on Particleboard Properties Made from Mixing of Poplar Wood Slab, Citrus Branches and Twigs of Beech. *Wood Research* 63.
7. Martins, R.S.F., Gonçalves, F.G., Segundinho, P.G. de A., Lelis, R.C.C., Paes, J.B., Lopez, Y.M., Chaves, I.L.S., Oliveira, R.G.E. de. (2021). Investigation of agro-industrial lignocellulosic wastes in fabrication of particleboard for construction use. *Journal of Building Engineering* 43, 102903. <https://doi.org/10.1016/j.job.2021.102903>
8. Nazerian, M., Beyki, Z., Gargarii, R.M., Kool, F. (2016). The effect of some technological production variables on mechanical and physical properties of particleboard manufactured from cotton (*Gossypium hirsutum*) stalks. *Maderas, Cienc. tecnol.* 0–0. <https://doi.org/10.4067/S0718-221X2016005000017>
9. Nemli, G., Demirel, S. (2007). Relationship Between the Density Profile and the Technological Properties of the Particleboard Composite. *Journal of Composite Materials* 41, 1793–1802. <https://doi.org/10.1177/0021998307069892>
10. Özlüsoylu, I. (2023). The effect of varnish type, glue amount, and density on the surface properties of low density particleboards produced from waste wood bark :: *BioResources*. *BioResources* 18, 7025–7040. <https://doi.org/10.15376/biores.18.4.7025-7040>
11. Tabarsa, T. (2011). Producing Particleboard Using of Mixture of Bagasse and Industrial Wood Particles. *KEM* 471–472, 31–36. <https://doi.org/10.4028/www.scientific.net/KEM.471-472.31>
12. Wong, E.-D., Zhang, M., Wang, Q., Kawai, S. (1999). Formation of the density profile and its effects on the properties of particleboard. *Wood Science and Technology* 33, 327–340. <https://doi.org/10.1007/s002260050119>



BIOCOMPOSITE BASED ON STARCH AND PINE WOOD PARTICLES

Piotr Borysiuk – Radosław Piech – Radosław Auriga

Abstract

As part of the research, biocomposites based on pine wood particles bonded with thermoplastic starch were produced using the flat pressing method. Four variants of biocomposites were produced, three different in terms of starch content (10%, 20% and 30%) and a reference variant bonded with MUF resin. For the produced biocomposites, their mechanical properties (MOR, MOE, IB) and physical properties (density and density profile, thickness swelling, water absorption) were examined. Based on the conducted research, it was shown that thermoplastic starch can be used as a binder for flat-pressed biocomposites, and an increase in the content of thermoplastic starch in the range of 10-30% generally increases their strength properties. Biocomposites bonded with thermoplastic starch are not resistant to water.

Key words: *biocomposites, starch, pine particles, mechanical properties, physical properties*

INTRODUCTION

Biocomposites are materials containing one or more phases of organic origin. Plant fibers (e.g. cotton (Reza *et al.*, 2023), flax (Ibrahim *et al.*, 2014), hemp (Foret *et al.*, 2023), wood fibers (Regazzi *et al.*, 2019; Schutz *et al.*, 2024)) and even by-products of food crops can be used as fillers. Currently, synthetic polymers of fossil origin, such as polyethylene, polypropylene, polystyrene or polyvinyl chloride, are very often used as matrices (Klysov, 2007). It is worth noting, that these may also be polymers from renewable sources, the so-called biopolymers. Biodegradable polymers can be divided into three basic groups (Kuciel *et al.*, 2010):

- polymers produced from plants, e.g. polysaccharides obtained by fractionation (starch produced from potatoes, corn, rice or wheat) or cellulose (cotton, wood, flax, hemp),
- polymers produced by living organisms (e.g. poly (hydroxybutyrate - PHB, poly(hydroxyvalerate) - PHV),
- polymers produced from monomers obtained from biomass (e.g. polylactide - PLA).

Starch is a very common natural polymer. Starch is produced by plants to store chemical energy produced during photosynthesis. Starch can be found primarily in seeds, fruits, tubers and the core of plant stems, corn, wheat, rice, sago and potatoes (Lamaming *et al.*, 2020; Nie *et al.*, 2013).

Due to its biodegradability, easy access, non-toxicity and price competitiveness, starch as a biopolymer is used in many industrial processes (Anugrahwidya *et al.*, 2021; Bangar *et*

Institute of Wood Sciences and Furniture, Warsaw University of Life Sciences – SGGW, 159

Nowoursynowska Str, 02-776 Warsaw, Poland

e-mail: piotr_borysiuk@sggw.edu.pl

al., 2021; Lamaming *et al.*, 2020; Schutz *et al.*, 2024). The structure of starch allows the gelatinization process to be carried out in mild conditions, which creates a coherent polymer matrix (Bangar *et al.*, 2021). Additionally, starch can be subjected to modifications that improve the properties of native starch and increase the possibilities of its use (Hafila *et al.*, 2022). Starches can be used, among others, to produce formaldehyde-free starch-based adhesives, which can be successfully used in the production of formaldehyde free particleboards (Ait Benhamou *et al.*, 2022; Akinyemi *et al.*, 2019; Lamaming *et al.*, 2020).

The aim of this research was to determine the possibility of using pure thermoplastic starch as a binder for pine wood particles constituting a post-production residue. The obtained biocomposites fully fit into the scope of biodegradable and sustainable materials, which are a response to environmental problems related to traditional synthetic plastics.

MATERIALS AND METHODS

Pine particles was obtained as a post-production material, created during the processing of solid boards on a four-sided planer. The moisture content of particles was approximately 7.94%. The granulometric composition of the obtained particles was determined by sieves method. Sieves with mesh sizes: 6mm, 4mm, 2mm, 1.25mm, 1mm, 0.63mm, 0.49mm, 0.315mm and a dust container were used. The amount of raw material used for one test sample was 100g and the sorting time was 30 minutes. A total of 3 tests were performed.

Thermoplastic starch for research purposes was obtained from Grupa Azoty S.A. (Tarnów). The raw material was in the form of powder.

Melamine-urea-formaldehyde resin (Silekol Sp. z o. o., Kędzierzyn-Koźle) was used to produce control variants.

For the purposes of the research, biocomposites were produced with a nominal thickness of 3 mm and an assumed density of 900 kg/m³. In the first stage of production, starch was added in amounts of 10%, 20% and 30%, respectively, in relation to the weight of completely dry sawdust. Homogenization of starch and pine sawdust was performed manually, using a mechanical mixer. In the case of the reference variant glued with MUF glue, the degree of gluing was 12%. The boards were formed using a mold on sheet metal covered with anti-adhesive material.

The composites were pressed at a temperature of 200°C and a maximum unit pressure of 2.5 MPa. The total pressing time was 4 minutes. During pressing after 2 min. the pressure was reduced to 1.25 MPa, and after 3 min. up to approx. 0.625 MPa. After pressing, the boards were air-conditioned for 7 days in laboratory conditions.

For the purposes of research, four variants of composites were produced:

- Variant 0 (W0) – MUF glued reference board (without added starch)
- Variant 1 (W1) – composite with 10% thermoplastic starch
- Variant 2 (W2) – composite with 20% thermoplastic starch
- Variant 3 (W3) – composite with 30% thermoplastic starch

For the manufactured composites, the following was tested:

- Density – in accordance with PN – EN 323:1999.
- Density profile – measurement using a DA-X profilometer (GreCon), measurement every 0.02 mm, measurement speed was 0.05 mm/s.
- MOR and MOE – in accordance with PN-EN 310:1994.
- IB – in accordance with PN-EN 319:1999.
- Thickness swelling and water absorption – after 2 and 24 hours of soaking in water – in accordance with PN-EN 317:1999.

All studies were performed using 10 replicates per study. Statistical analysis was performed in Statistica 13.1 using one-way analysis of variation Anova. The NIR Fisher test was used to determine the significance of differences between the obtained results.

RESULTS

The results of testing the granulometric composition of pine sawdust are shown in Figure 1. In general, it should be stated that the largest percentage is pine sawdust remaining on a sieve with a mesh diameter of 1.25 mm. The lowest percentage was noticed in the case of sawdust remaining on the 0.315 mm sieve. It is worth noting that small particles - dust - have a low percentage in the sawdust mixture (2.94%). This is beneficial in terms of strength, too much dust has a negative impact on the strength parameters of the composites (Thoemen *et al.*, 2010).

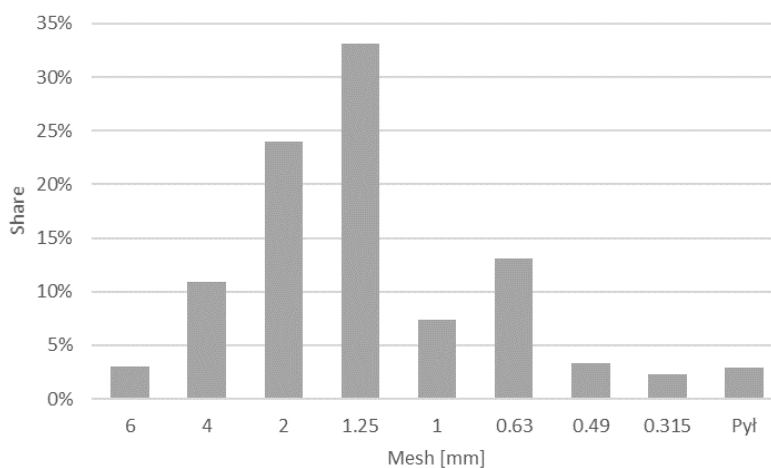


Figure 1. Particle size composition of pine sawdust

The results of the density determination of the composites are shown in Figure 2. In general, it can be stated that the samples with 30% thermoplastic starch have the highest density (W3 - 989kg/m³), and the lowest was obtained by samples with a 10% share of thermoplastic starch (W1 - 878kg/m³). It is worth noting, that the reference variant (W0) and the variant with a 10% share of thermoplastic starch (W1), as well as the variants with a 20% and 30% share of thermoplastic starch (W2 and W3) belong to the same homogeneous groups ("a" and "c" respectively – Figure 2). The difference in density values between the variant with a 10% share of thermoplastic starch (W1) and the variants with 20% and 30% share of thermoplastic starch (W2 and W3) is statistically significant. The increase in the average density of variants containing a higher share of thermoplastic starch is the result of differences in the density of individual components of the composite (pine sawdust and starch). The density of starch is approximately 1350 kg/m³ and is almost twice the density of sawdust. According to Klysov (2007), the density and share of the polymer matrix significantly affect the final density of the composite. Figure 3 shows graphs of the density profiles of the tested biocomposites. Regardless of the share of thermoplastic starch or in the case of the reference variant, the density profile curves do not change significantly

in relation to each other. Generally, it can be stated that the addition of thermoplastic starch does not affect the density profile of biocomposites. Some variation in the course of the density profile curves results from the differences in the thickness of the samples of variants.

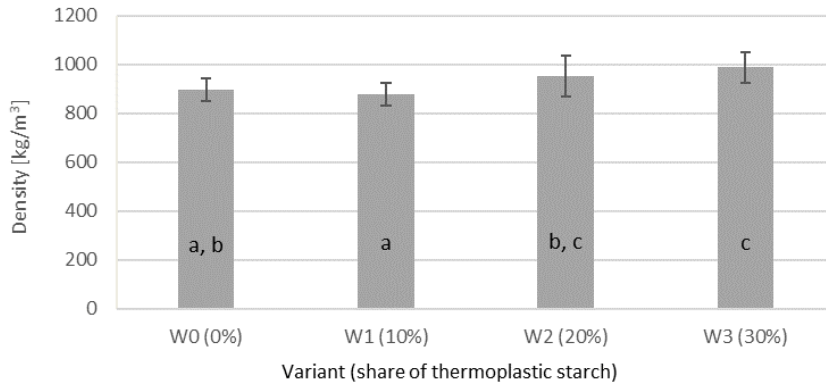


Figure 2. Density values of the tested biocomposites (a, b, c - homogeneous groups)

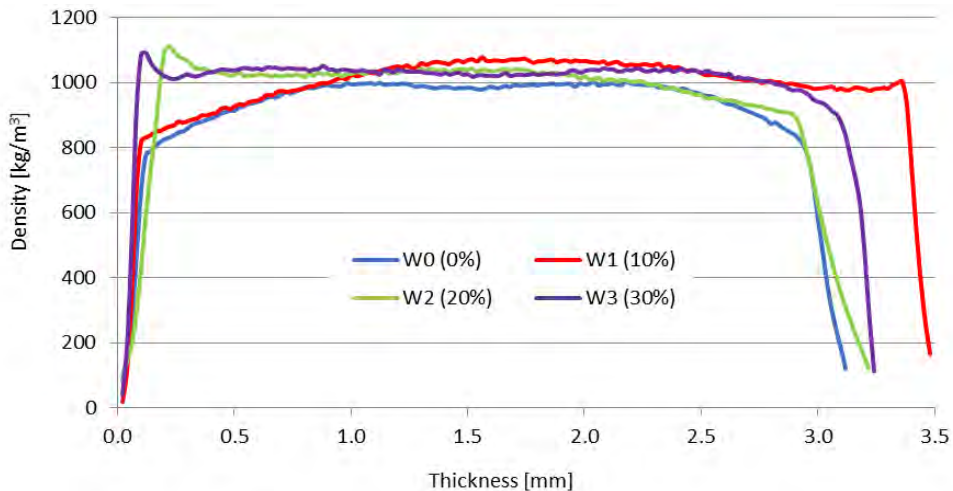


Figure 3. Density profiles of the tested biocomposites

Figure 4 shows the modulus of rupture (MOR) values of biocomposites containing thermoplastic starch in various weight fractions and the reference variant bonded with MUF glue. Analyzing the obtained results, it can be concluded that the highest MOR value was obtained for the reference samples (19.9 N/mm²). Samples with 10% thermoplastic starch (12.7 N/mm²) have the lowest MOR value. Samples with 20% and 30% thermoplastic starch achieved higher strength during the test, but not as high as the reference samples with a gluing degree of 12%. It should be noted that the differences in MOR values between the variant with a 10% share of thermoplastic starch (W1) and the variants with 20% and 30% share of thermoplastic starch (W2 and W3) and the reference variant (W0) are statistically significant (different homogeneous groups a, b, c).

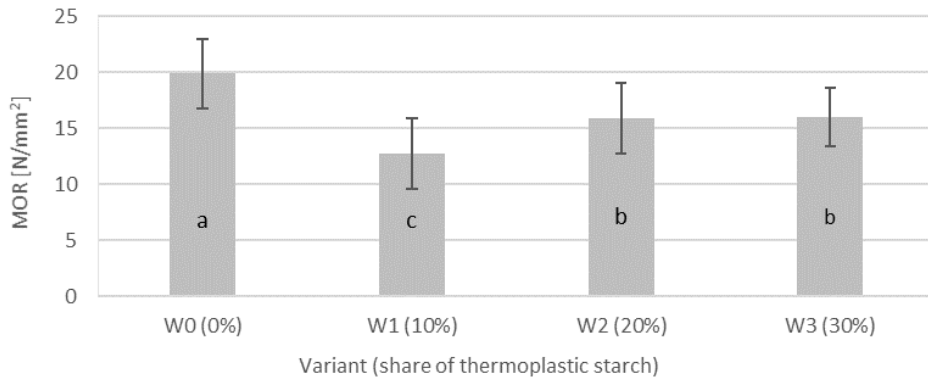


Figure 4. MOR values of the tested biocomposites (a, b, c – homogeneous groups)

The results of the modulus of elasticity (MOE) test are presented in Figure 5. The average MOE value of the reference variant (W0) was 2058 N/mm². The MOE values for the variants with 20% and 30% of thermoplastic starch (W2 and W3) were close to the values for the reference variant, and the differences noted were statistically insignificant (the same homogeneous group "a"). Only the variant with a 10% share of thermoplastic starch (W1) was characterized by statistically significantly lower MOE values.

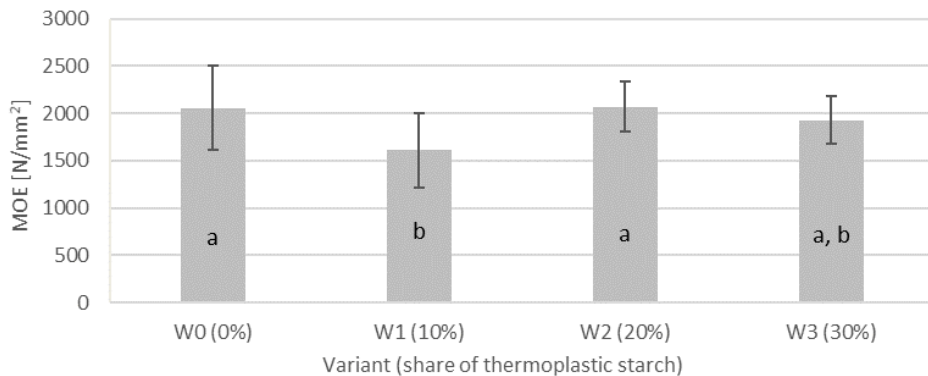


Figure 5. MOE values of the tested biocomposites (a, b – homogeneous groups)

The results of the internal bound strength test (IB) perpendicular to the planes are shown in Figure 6. The highest IB values were noticed for the reference variant (W0 - 1.49 N/mm²) and the variant with a 30% share of thermoplastic starch (W3 - 1.54 N/mm²). The difference between these variants is statistically insignificant (the same homogeneous group "a"). Generally, it should be stated that the increase in the content of thermoplastic starch in the composite resulted in an increase in the IB value. It should be added, that due to the relatively large values of standard deviations, the differences between the variants with 10% and 20% thermoplastic starch content are statistically insignificant (the same homogeneous group "b").

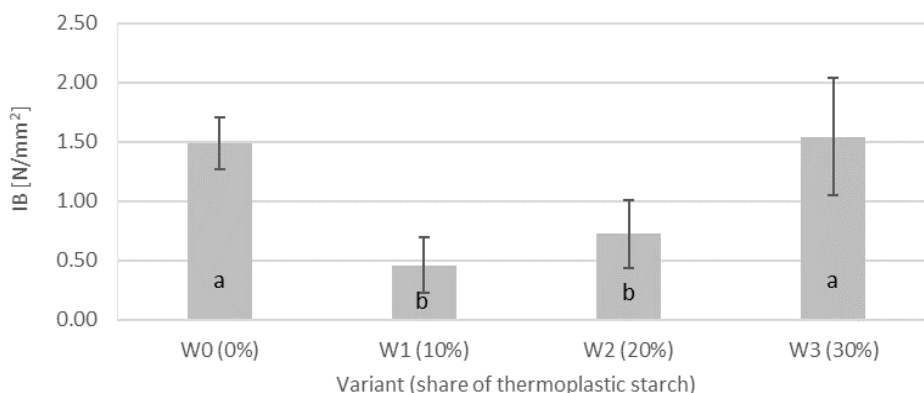


Figure 6. IB values of the tested biocomposites (a, b – homogeneous groups)

The results of thickness swelling and water absorption tests of the composites are presented in Table 1. In general, it can be stated that composites bonded with thermoplastic starch are not resistant to water. During 2 hours of soaking, the biocomposite variants with 20% and 30% of thermoplastic starch (W2 and W3) were destroyed, while the variant with 10% of thermoplastic starch (W1) was characterized by over 100% swelling and nearly 200% water absorption. It should be added, however, that when soaking continued, it was also destroyed. Only the reference variant glued with MUF resin (W0) showed water resistance (full cohesion after 24 hours of soaking). According to Yeh *et al.* (2015), the water resistance of thermoplastic starch can be improved by glutaraldehyde reactions during the gelatinization process.

Table 1. Thickness swelling and water absorption values of the tested biocomposites.

Variant	Thickness swelling				Water absorption			
	2h		24h		2h		24h	
	aver. [%]	SD [%]	aver. [%]	SD [%]	aver. [%]	SD [%]	aver. [%]	SD [%]
W0	22.0	12.4	25.0	9.7	67.0	16.8	80.0	18.6
W1	122.0	48.2	-	-	185.0	45.8	-	-
W2	-	-	-	-	-	-	-	-
W3	-	-	-	-	-	-	-	-

aver. – average, SD – standard deviation.

CONCLUSION

Based on the tests carried out on composites based on pine wood particles bonded with thermoplastic starch, the following conclusions can be drawn:

1. Thermoplastic starch can be used as a binder for flat-pressed biocomposites based on pine wood particles.
2. An increase in the content of thermoplastic starch in the range of 10-30% generally increases the strength properties of biocomposites.
3. The highest values of modulus of rupture (MOR) and modulus of elasticity (MOE) were obtained for biocomposites with 20% and 30% of thermoplastic starch. (differences between the values for these variants are statistically insignificant).

4. The highest values of perpendicular tensile strength were obtained for biocomposites with a 30% share of thermoplastic starch.
5. Flat-pressed biocomposites bonded with thermoplastic starch are not resistant to water.
6. An increase in the content of thermoplastic starch generally results in an increase in the density of biocomposites, however these biocomposites are characterized by a similar density profile.

REFERENCES

1. AIT BENHAMOU, A., BOUSSETTA, A., KASSAB, Z., NADIFIYINE, M., SEHAQUI, H., EL ACHABY, M., MOUBARIK, A., (2022). Elaboration of carboxylated cellulose nanocrystals filled starch-based adhesives for the manufacturing of eco-friendly particleboards. *Constr. Build. Mater.* 348, 128683.
2. AKINYEMI, B.A., OLAMIDE, O., OLUWASOGO, D., (2019). Formaldehyde free particleboards from wood chip wastes using glutaraldehyde modified cassava starch as binder. *Case Stud. Constr. Mater.* 11, e00236.
3. ANUGRAHWIDYA, R., ARMYNAH, B., TAHIR, D., (2021). Bioplastics Starch-Based with Additional Fiber and Nanoparticle: Characteristics and Biodegradation Performance: A Review. *J. Polym. Environ.* 29, 3459–3476.
4. BANGAR, S.P., WHITESIDE, W.S., ASHOGON, A.O., KUMAR, M., (2021). Recent advances in thermoplastic starches for food packaging: A review. *Food Packag. Shelf Life* 30, 100743.
5. FORET, S., MAZIAN, B., BEKAS, V., MARTINS, F.C.B., CAMPANELLA, O.H., PERRÉ, P., AUGUSTO, P.E.D., (2023). Thermoplastic starch biocomposites reinforced with hemp shives obtained via extrusion. *Ind. Crops Prod.* 206, 117707.
6. HAFILA, K.Z., JUMAIDIN, R., ILYAS, R.A., SELAMAT, M.Z., YUSOF, F.A.M., (2022). Effect of palm wax on the mechanical, thermal, and moisture absorption properties of thermoplastic cassava starch composites. *Int. J. Biol. Macromol.* 194, 851–860.
7. IBRAHIM, H., FARAG, M., MEGAHED, H., MEHANNY, S., (2014). Characteristics of starch-based biodegradable composites reinforced with date palm and flax fibers. *Carbohydr. Polym.* 101, 11–19.
8. KLYSOV, A.A., (2007). *Wood-Plastic Composites*. Wiley-Interscience.
9. KUCIEL, S., LIBER-KNEĆ, A., MIKUŁA, J., KUŹNIAR, P., KORNIJEJENKO, K., ŻMUDKA, S., ŁAGAN, S., RYSZKOWSKA, J., GAJEWSKI, J., SAŁASIŃSKI, K., TOMASZEWSKA, J., ZAJCHOWSKA, S., (2010). *Kompozyty polimerowe na podstawie recyklatów z włóknami naturalnymi: praca zbiorowa*. Politechnika Krakowska, Kraków.
10. LAMAMING, J., HENG, N.B., OWODUNNI, A.A., LAMAMING, S.Z., KHADIR, N.K.A., HASHIM, R., SULAIMAN, O., MOHAMAD KASSIM, M.H., HUSSIN, M.H., BUSTAMI, Y., AMINI, M.H.M., HIZIROGLU, S., (2020). Characterization of rubberwood particleboard made using carboxymethyl starch mixed with polyvinyl alcohol as adhesive. *Compos. Part B Eng.* 183, 107731.
11. NIE, Y., TIAN, X., LIU, Y., WU, K., WANG, J., (2013). Research on starch- g -polyvinyl acetate and epoxy resin-modified corn starch adhesive. *Polym. Compos.* 34, 77–87.

12. REGAZZI, A., TEIL, M., DUMONT, P.J.J., HARTHONG, B., IMBAULT, D., PEYROUX, R., PUTAUX, J.L., (2019). Microstructural and mechanical properties of biocomposites made of native starch granules and wood fibers. *Compos. Sci. Technol.* 182, 107755.
13. REZA, M.M., BEGUM, H.A., UDDIN, A.J., (2023). Potentiality of sustainable corn starch-based biocomposites reinforced with cotton filter waste of spinning mill. *Heliyon* 9, e15697.
14. SCHUTZ, G.F., DE ÁVILA GONÇALVES, S., ALVES, R.M.V., VIEIRA, R.P., (2024). A review of starch-based biocomposites reinforced with plant fibers. *Int. J. Biol. Macromol.* 261.
15. THOEMEN, H., IRLE, M., BARBU, M.C., (2010). Wood-based panel technology. An Introduction for Specialists, *Wood-Based Panels - An Introduction for Specialists.* Brunel University Press.
16. YEH, J.T., HOU, Y.J., CHENG, L., WANG, Y.Z., YANG, L., WANG, C.K., (2015). Water proof and strength retention properties of thermoplastic starch based biocomposites modified with glutaraldehyde. *Carbohydr. Polym.* 127, 135–144. DOI: 10.1016/j.carbpol.2015.03.059.



ANALYSIS OF POWER CONSUMPTION DURING MILLING THE WOOD-BASED MATERIALS

Tomáš Čuchor – Peter Koleda – Richard Kminiak

Abstract

The article is devoted to an analysis of power consumption during milling process of wood-based materials. The energy demand of the changed technical-technological parameters was tested on experimental samples of MDF and Particleboard wood. The input parameters are the revolutions of the cutter (14 000, 16000 and 18 000 rpm). Subsequently, the electricity consumption of the machining centre during the milling process was statistically evaluated using ANOVA method. Analysing factor ANOVAs are robust to light violations to the homogeneity of variances assumption. From the investigated technical-technological parameters, the revolutions of cutter have the most statistically significant effect on energy consumption and thus have the most energetic impact on the production process. Material did not show statistically significant change in power consumption.

Key words: *Power consumption, Milling, MDF, Particleboard,*

INTRODUCTION

Manufacturing is energy intensive process. Materials that are machined have different energy requirements due to their structure. Unlike metals wood-based materials are non-homogeneous that means their structure is not always the same as in cases of metal. Wood is one of most used materials. As we manufacture new wood compounds their properties change from original. Engineered sheet material on wood bases are better suited for their increased toughness, resistance to heat etc. Power required for their machining differ from materials that they are made from. In next part will be measuring and analysing medium density fiberboard and particleboard. Manufacturing from these materials in terms of energy required for turning them into final product.

Particleboard (PB) is product made from wood chips and a suitable binder most common synthetic resin. Its advantage is that's cheaper and denser than regular plywood. It's a good substitute for plywood when overall cost is more important than strength.

Manufacturing of particleboards is done by mixing particles or flakes of wood or jute-stick together with a resin and forming the mixture into a sheet. Production process involves other chemicals including wax, dyes, wetting agents and release agents, in order to make material more resistant.

Particles of wood are dried, and resin is sprayed as a fine mist onto the particles.

Particles pass through a sufficient amount to coat all surfaces; next they are layered into a continuous carpet. This carpet is going to be cut into sheets. The formed sheets are cold

compressed to reduce thickness and make them easier to transport. Later, they are compressed again, under pressures between 2 and 3 MPa and temperatures between 140 and 220 °C to set and harden the glue. The boards are then cooled, trimmed and sanded. Process is controlled to ensure the correct size, density and consistency of the board. As mentioned by Nemli (2007) with increase of press time and amount of resin the surface quality, physical and mechanical properties of particleboards, significantly improved.

Medium-density fibreboard (MDF) is product made from broken down wood residuals, wood fibres, wax and resin. It's made from material formed into panels by applying high temperature and pressure. Its density is higher than regular plywood which makes it excellent building material. Typical material required for production of MDF consist of 82 % wood fibre, 9 % urea-formaldehyde resin glue, 8% water, and 1% paraffin wax (Kozłowski and Helwig, 1996). Typical density of MDF is between 500 and 1,000 kg/m³. Akbulut and Koç (2004) investigated the effects of fibreboard density, panel temperature, and cutter sharpness on the roughness of surface.

Davim et al (2008), based on experimental results obtained in milling, showed important role of spindle speed on the evolution of the surface roughness as a function of material removal rate (MRR). The advantage of using high cutting speed in milling this material are evident. (Davim 2008)

Fibres of MDF are evenly distributes fibre into a uniform mat. Mat is pre-compressed and either sent straight to a continuous hot press or cut into large sheets. The hot press activates the bonding resin and sets the strength and density profile. The pressing cycle operates in stages, with the mat thickness being first compressed to around 1.5 times of the finished board thickness, then compressed further in stages and held for a short period. This gives a board profile with zones of increased density, thus mechanical strength, near the two faces of the board and a less dense core.

After pressing, MDF is cooled in a dryer or cooling carousel, trimmed, and sanded. In certain applications, boards are also laminated.

The name MDF derives from the distinction in densities of fibreboard. Its production in Europe and North America began in the year 1980. Evolution of MDF types is driven by the needs of market for its purposes.

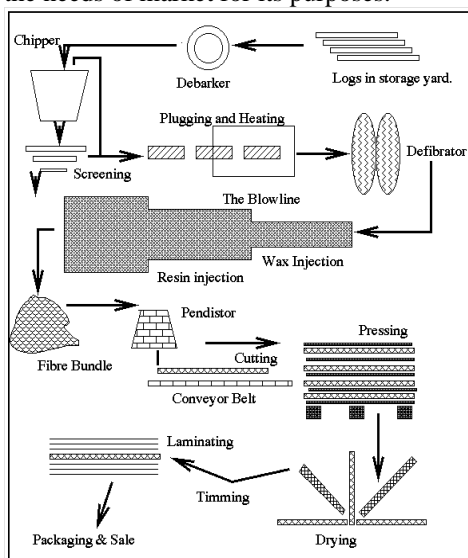


Fig. 1 The Manufacturing Process of Medium Density Fibreboard (Es Shelf, 2017)

MATERIAL AND METHODS

Milling is process of removal of materials. Cutter in milling is usually moved perpendicular to its axis so that cutting occurs on the circumference of the cutter. For purposes of experimentation removal of materials was done by milling tool moving in straight line.

The measurements were realised on an MDF board with dimensions of $500 \times 300 \times 18$ mm and a weight of 1960 g. The experimental samples were sawn from a 2800×2070 mm board. The density of the material was in the range of $720 - 740 \text{ kg}\cdot\text{m}^{-3}$.

The particleboards of the same dimensions have been added as reference samples. The density of particleboard given by the manufacturer was $600 - 640 \text{ kg}\cdot\text{m}^{-3}$. Formaldehyde glue with an admixture of paraffin was used in the production.

Both materials come from Kronospan Ltd. (Zvolen, Slovakia). The manufacturer declared that the material complies with EN 14 322, EN 312-2 and emission class E1 (EN ISO 12460-5) (EN 14322, EN 312-2, EN ISO 12460-5).

The measurement was carried out on the CNC milling centre SCM TECH Z5 from the company SCM – group, Rimini, Italy and was carried out in the laboratories of the Technical University in Zvolen. For process of milling were selected revolutions 14 000, 16 000 and 18 000 rpm.

The power analyser was connected to the electrical power supply of the CNC machining centre (fig. 2). It was connected with the help of current probes and voltage clamps. The voltage clamps were connected to the phase conductors, zero and protective conductor using the installed socket 32 A5P. The current probes were connected in the direction of the current flow, in the case of the opposite connection, the values measured on the terminals would be negative. After the connection of measuring circuit, a test measurement of the signal was realized on the phases.

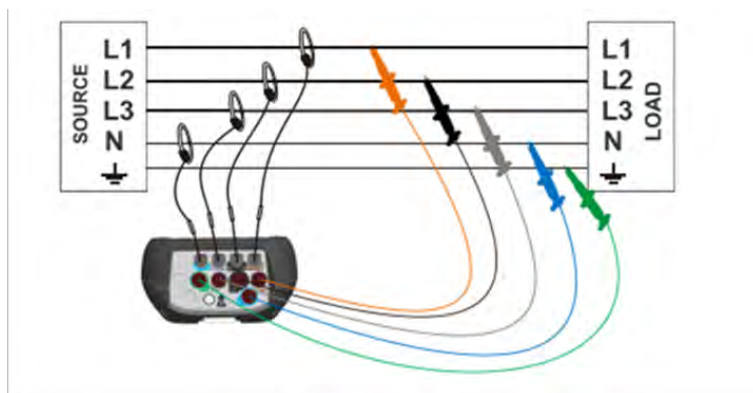


Fig. 2 Connecting the Metrel measuring device

The cutting power was calculated as the difference between the measured power during milling and when the machining center was idle. Statistical method ANOVA was used to evaluate the influence of selected parameters.

RESULTS AND DISCUSSION

The basic statistics of the measured power consumption data are shown in Table 1.

Table 1 Descriptive statistics of cutting power

Parameter	Value	Average P [kW]	St. Dev. [kW]	-95,00% [kW]	95,00% [kW]
Material	Particleboard	3,73	0,45	3,58	3,89
	MDF	3,67	0,4	3,54	3,81
Rpm	14000	3,36	0,23	3,26	3,46
	16000	3,68	0,28	3,56	3,80
	18000	4,07	0,39	3,91	4,24

Fig. 3 shows difference between Particleboard and MDF as materials and their consumption with different revolutions of tool and consumption of power required for milling process.

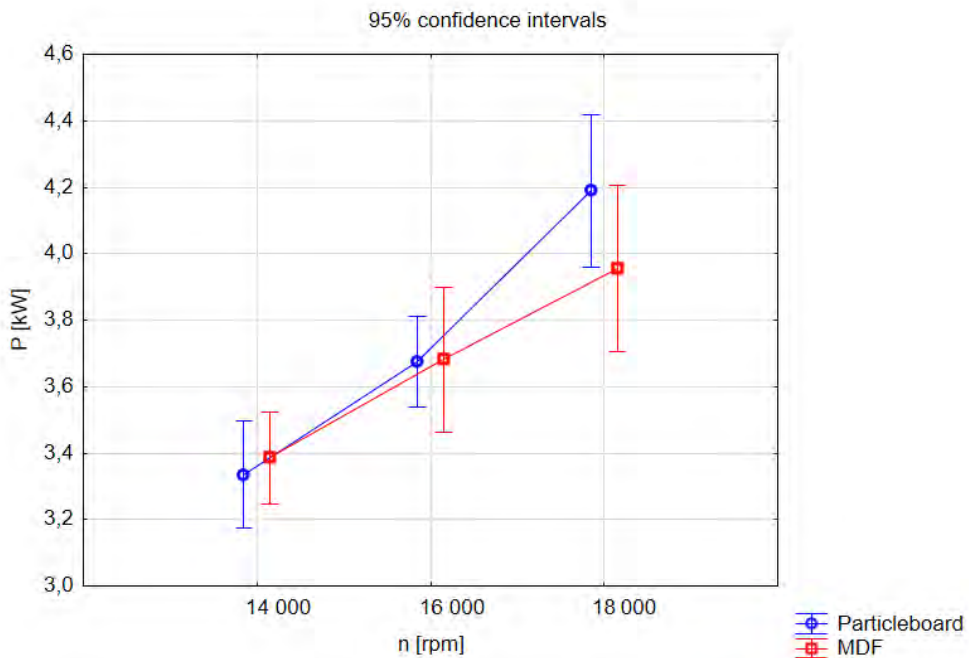


Fig. 3 Analysis of variance of cutting power dependence on revolution and material dependence.

Power requirement for machining was higher during milling particleboard (3,73 kW) than medium density particleboards (3,67 kW) despite of that MDF has higher density than particleboard. However, the difference in power consumption between the material was not statistically significant.

On the basis of the experiments carried out and their evaluation through analysis of dispersion followed by post-hoc test, it can be concluded that with increasing revolutions of spindle of machine centre, the electrical output also increased almost linearly from value of 3,36 kW and speed of 14 000 rpm to the value of 4,07 at speed of 18 000 rpm. This

increase is caused by the increase in the values of currents flowing through the windings of the electric drive for spindle and also by the increased volume of removed material per unit of time. The increase in power required to remove material is also confirmed by the authors (Sedlecký et al. 2017) who examined power consumption during edge milling of MDF and edge-glued panel and also (Barčík et al. 2010) who examined the effect of various feed rates and cutting speed on power consumption during the surface milling of beech wood.

CONCLUSION

Conducted analysis of different materials showed following findings:

1. Difference in power consumption between the material was not statistically significant. Probability of similarity was higher than 5 %, according to Duncan's test it was approximately 30 %.
2. Difference in power consumption between revolutions was statistically significant (probability of similarity was lower than 5 %). With increase in revolution energy demand increases.

These findings will be further expanded and deepened in further research.

ACKNOWLEDGMENT

This research was funded by APVV-20-0403 „FMA analysis of potential signals suitable for adaptive control of nesting strategies for milling wood-based agglomerates“

REFERENCES

- AKBULUT, T., KOÇ, E., 2004, Effects of panel density, panel temperature, and cutter sharpness during edge machining on the roughness of the surface and profiled areas of medium density fiberboard, *Forest Prod J*, 54 (12), pp. 67-70
- BARCÍK, Š., KMINIAK, R., ŘEHÁK, T., KVIETKOVÁ, M. 2010. The influence of selected factors on energy requirements for plain milling of beech wood. *Journal of Forest Science*. 56. 243-250. 10.17221/119/2009-JFS.
- DAVIM J. P., CLEMENTE V. C., SILVA S., 2008, Surface roughness aspects in milling MDF, *International Journal Advance Manufacturing Technology*, pp.49-55
- ES Shelf, 2017. What is MDF? How MDF is made?. Online. Available on <https://www.essshelf.com/what-is-medium-density-fiberboard/>
- KOZŁOWSKI, R., HELWIG, M. ,1996, Critical Look on Cellulose Modification. *Proceedings of the International Symposium on Cellulose Modification*. Honolulu, USA.
- NEMLI, G., AYDIN, I., ZEKOVIÇ, E., 2007, Evaluation of some of the properties of particleboard as function of manufacturing parameters, *Materials & Design*, Volume 28, Issue 4, Pages 1169-1176, ISSN 0261-3069, <https://doi.org/10.1016/j.matdes.2006.01.015>
- SEDLICKÝ, M., GAŠPARÍK, M. 2017. Power consumption during edge milling of medium-density fiberboard and edge-glued panel. *Bioresources*. 12. 7413-7426. 10.15376/biores.12.4.7413-7426.



PYTHAGORAS

INDEWO®



WOOD'N TILES



INOIS®MICRO



SPICA



europlac.sk

europlac 
...das beste aus holz

TO NAJLEPŠIE Z DREVA



COMPUTING THE SPECIFIC HEAT CAPACITIES AND ENERGY CONSUMPTION OF LOGS SUBJECTED TO DEFROSTING

Part 1. Calculating the specific heat capacities of frozen wood

Nencho Deliiski¹ – Ladislav Dzurenda² – Dimitar Angeski¹ – Pavlin Vitchev¹
– Krasimira Atanasova¹

Abstract

An approach for calculating the specific heat capacities of frozen wood subjected to defrosting has been presented. The approach is based on the use of own mathematical descriptions of all four different heat capacities of frozen wood during its thermal treatment, namely: specific heat capacities of frozen and defrosted wet wood itself, and also specific heat capacities of both frozen hygroscopically bound and free water in the wood. These descriptions were entered into Excel software program and with it the change in the average arithmetic values of each of the four heat capacities in the temperature ranges in which they are valid was calculated. The computer simulations were carried out for beech logs with a diameter of 0.4 m, moisture content of 0.4, 0.6, and 0.8 kg·kg⁻¹, and initial wood temperature of -1 °C, -10 °C, -20 °C, -30 °C, and -40 °C at operating temperature of the logs' defrosting medium equal to 80 °C.

Key words: *frozen wood, logs, defrosting, specific heat capacity, energy consumption*

INTRODUCTION

It is well-known that the non-stationary distribution of the temperature in frozen wood during its defrosting and thermal treatment, and also the change in the energy needed for this, can be calculated using the models (Steinhagen 1986, 1991; Khathaby – Steinhagen 1992, 1993; Deliiski 2003, 2011; Câmpean 2005; Dzurenda – Deliiski 2019, Hadjiski et al. 2020; Deliiski et al. 2023; Niemz et al. 2023). The development and solving of such temperature-energy models is carried out using finite differences and requires deep mathematical knowledge.

Of particular interest to the development, study and implementation of science-based energy-saving regimes for thermal treatment would be the availability of a simpler and more accessible engineering approach to calculating the energy for defrosting of wood.

¹ Faculty of Forest Industry, University of Forestry, Kliment Ohridski Bd. 10, 1797 Sofia, Bulgaria
e-mails: deliiski@netbg.com, d.angeski@gmail.com, p_vitchev@abv.bg, k_atanasova@ltu.bg

² Faculty of Wood Sciences and Technology, Technical University of Zvolen, T.G. Masarikova 24, 96053, Zvolen, Slovakia, e-mail: dzurenda@tuzvo.sk

Therefore, the aim of this work is to present an engineering approach for calculating the specific energy required for defrosting of frozen wood.

The approach should include the use of easy-to-apply (manually or with MS Excel) equations to determine the specific heat capacities of frozen wood and also the individual components of mentioned energy, namely: for heating of the frozen and defrosted wood itself above the hygroscopic range, for melting of the frozen part of the bound water, and for melting all the frozen free water in the wood.

MATERIAL AND METHODS

Material for research

This research was conducted over frozen beech (*Fagus sylvatica* L.) logs, which are commonly used in veneer production.

The calculation of the specific heat capacities of frozen wood during its defrosting was carried out for the case of steaming or boiling of frozen logs in equipment operating at atmospheric pressure and at a temperature of the processing medium of 80 °C.

The symbols, units, and values of the main parameters of the studied logs, and also of their defrosting modes, which were involved in the equations of the mathematical models given below, and were used in the computer simulations, are presented in Table 1.

Mathematical description of the effective specific heat capacities of frozen logs

The effective specific heat capacities of the logs above the hygroscopic range during the three ranges of their defrosting process of wood, $c_{w\text{-eff}1,2,3}$, which participate in Equation (1) are equal to the following (Tumbarkova 2019):

$$\text{First range: } c_{w\text{-eff}1} = c_{w\text{-fr}} + c_{ice\text{-bw}} \quad (1)$$

$$\text{Second range: } c_{w\text{-eff}2} = c_{w\text{-nfr}} + c_{ice\text{-fw}} \quad (2)$$

$$\text{Third range: } c_{w\text{-eff}3} = c_{w\text{-nfr}} \quad (3)$$

where $c_{w\text{-fr}}$ and $c_{w\text{-nfr}}$ are the specific heat capacities of frozen and defrosted (non-frozen) wet wood respectively, $\text{J}\cdot\text{kg}^{-1}\cdot\text{K}^{-1}$; $c_{ice\text{-bw}}$ and $c_{ice\text{-fw}}$ – specific heat capacities of frozen bound and free water in the wood respectively, $\text{J}\cdot\text{kg}^{-1}\cdot\text{K}^{-1}$.

In (Deliiski 2003) and (Deliiski et al. 2023) the following equations for calculating the specific heat capacities of the frozen and non-frozen wood above the hygroscopic range, and also of the both frozen bound and free water in the wood:

$$c_{w\text{-fr}} = \left[1.06 + 0.04u + \frac{0.00075(T - 272.15)}{u_{\text{fsp}(272.15\text{K})}} \right] \cdot \frac{526 + 2.95T + 0.0022T^2 + 2261u + 1976u_{\text{fsp}(272.15\text{K})}}{1 + u} \quad (4)$$

at $u > u_{\text{fsp}(272.15\text{K})}$ & $213.15\text{K} \leq T \leq 272.15\text{K}$

$$u_{\text{fsp}(272.15\text{K})} = u_{\text{fsp}(293.15\text{K})} + 0.021 \quad (5)$$

Table 1. Main set parameters of frozen beech logs and their defrosting regimes, which were used during the computer simulations.

№	Parameter name	Symbol	Unit	Value
1.	Diameter of the logs	D	m	0.4
2.	Length of the logs	L	m	2.0
3.	Moisture content of the logs (a – at $u = 0.4$ $\text{kg}\cdot\text{kg}^{-1}$, b – at $u = 0.6$ $\text{kg}\cdot\text{kg}^{-1}$, c – at $u = 0.8$ $\text{kg}\cdot\text{kg}^{-1}$)	u	$\text{kg}\cdot\text{kg}^{-1}$	0.4a 0.6b 0.8c
4.	Fiber saturation point of the wood at 20 °C	$u_{\text{fsp}(293.15\text{K})}$	$\text{kg}\cdot\text{kg}^{-1}$	0.31
5.	Basic density of the beech wood	ρ_b	$\text{kg}\cdot\text{m}^{-3}$	560
6.	Density of the wet wood equal to $\rho_b(1 + u)$	ρ_w	$\text{kg}\cdot\text{m}^{-3}$	784a 896b 1008c
7.	Density of the ice in the wood	ρ_{ice}	$\text{kg}\cdot\text{m}^{-3}$	917
8.	Initial temperature of the wood in the beginning of the logs' defrosting process: (d – at $t_{w0} = -1$ °C, e – at $t_{w0} = -10$ °C, f – at $t_{w0} = -20$ °C, g – at $t_{w0} = -30$ °C, and h – at $t_{w0} = -40$ °C)	t_{w0}	°C	-1d -10e -20f -30g -40h
9.	Temperature of complete melting of frozen part of bound water and start of melting of frozen free water in the wood	$t_{\text{ice-bw-end}}$	°C	-1
10.	Temperature of complete melting of frozen free water	$t_{\text{ice-fw-end}}$	°C	0
11.	Initial temperature of the regimes for logs' defrosting	t_{m0}	°C	10
12.	Temperature of stage $\tau_1 - \tau_2$ of the defrosting regimes	t_{m1}	°C	80
13.	Time constant for exponential increase of t_m from t_{m0} to t_{m1}	τ_e	s	3600
14.	Average mass temperature of the logs at end of their complete defrosting, depending on t_{w0}	$t_{\text{avg-end}}$	°C	48.8d 49.7e 50.6f 51.5g 52.4h
15.	Temperature in the central point of the logs at the end of their complete defrosting	t_{wc}	°C	0

$$c_{\text{ice-bw}} = \left(69.344T + 119.183T \cdot \ln \frac{T}{273.15} \right) \cdot \left(u_{\text{fsp}(272.15\text{K})} - 0.12 \right) \cdot \frac{\exp[0.0567(T - 272.15)]}{1 + u} \quad (6)$$

at $u > u_{\text{fsp}(272.15\text{K})}$ & $213.15\text{K} \leq T \leq 272.15\text{K}$

$$c_{\text{ice-fw}} = 3.34 \cdot 10^5 \frac{u - u_{\text{fsp}(272.15\text{K})}}{1 + u} \quad (7)$$

at $u > u_{\text{fsp}(272.15\text{K})}$ & $272.15\text{K} < T < 273.15\text{K}$

$$c_{w-nfr} = \frac{1}{1+u} (2862u + 2.95T + 5.49u \cdot T + 0.0036T^2 + 555) \quad (8)$$

$$\text{at } u > u_{fsp(272.15K)} \text{ \& } 272.15K < T \leq 413.15K$$

where u is the wood moisture content, $\text{kg} \cdot \text{kg}^{-1}$; $u_{fsp(293.15K)}$ – standardized fiber saturation point of the wood at $T = 293.15 \text{ K}$ (i.e. $t = 20 \text{ }^\circ\text{C}$), $\text{kg} \cdot \text{kg}^{-1}$; $u_{fsp(272.15K)}$ – fiber saturation point of the wood at $T = 272.15 \text{ K}$ (i.e. $t = -1 \text{ }^\circ\text{C}$), $\text{kg} \cdot \text{kg}^{-1}$.

Using Equations (4) – (8), the arithmetic mean values of the individual specific heat capacities in the temperature ranges in which they are valid can be calculated, as follows:

$$c_{w-fr-avg} = \frac{c_{w-fr} \text{ at } T_{w0} + c_{w-fr} \text{ at } 272.15K}{2} \quad (9)$$

$$c_{ice-bw-avg} = \frac{c_{ice-bw} \text{ at } T_{w0} + c_{ice-bw} \text{ at } 272.15K}{2} \quad (10)$$

$$c_{ice-fw-avg} = c_{ice-fw} = 3.34 \cdot 10^5 \frac{u - u_{fsp(272.15K)}}{1+u} \quad (11)$$

$$c_{w-nfr-avg} = \frac{c_{w-nfr} \text{ at } 272.15K + c_{w-nfr} \text{ at } T_{avg-end}}{2} \quad (12)$$

where $T_{avg-end}$ is the average mass temperature of the logs at the end of their defrosting at the time of reaching $0 \text{ }^\circ\text{C}$ in their central point, K . The values of $T_{avg-end}$ are calculated according to an equation given in Part 2 of this work.

RESULTS AND DISCUSSION

A numerical solving of our model of the 1D unsteady temperature distribution along the radius of the logs during their defrosting in order to determine the duration of the regimes for defrosting of beech logs, and also of the temperature $T_{avg-end}$ was carried out with in Visual FORTRAN. It was determined that the average temperature of the logs is equal, as follow: $t_{avg-end} = 48.6 \text{ }^\circ\text{C}$ at $t_{w0} = -1 \text{ }^\circ\text{C}$, $t_{avg-end} = 49.7 \text{ }^\circ\text{C}$ at $t_{w0} = -10 \text{ }^\circ\text{C}$, $t_{avg-end} = 50.6 \text{ }^\circ\text{C}$ at $t_{w0} = -20 \text{ }^\circ\text{C}$, $t_{avg-end} = 51.5 \text{ }^\circ\text{C}$ at $t_{w0} = -30 \text{ }^\circ\text{C}$, and $t_{avg-end} = 52.4 \text{ }^\circ\text{C}$ at $t_{w0} = -30 \text{ }^\circ\text{C}$.

An Excel program has been prepared for joint solving of the Equations (4) – (12). Using this program, the change in the four specific heat capacities of frozen beech logs considered above was investigated for the cases of defrosting at $t_{m1} = 80 \text{ }^\circ\text{C}$ of logs with moisture content of $0.4 \text{ kg} \cdot \text{kg}^{-1}$, $0.6 \text{ kg} \cdot \text{kg}^{-1}$, and $0.8 \text{ kg} \cdot \text{kg}^{-1}$, and initial wood temperature of $-1 \text{ }^\circ\text{C}$, $-10 \text{ }^\circ\text{C}$, $-20 \text{ }^\circ\text{C}$, $-30 \text{ }^\circ\text{C}$, and $-40 \text{ }^\circ\text{C}$. The values of $T_{avg-end}$ pointed above were used for solving of Equation (12).

Figure 1 shows the calculated with Equations (9) and (10) change of the specific heat capacities $c_{w-fr-avg}$ and $c_{ice-bw-avg}$ of the frozen beech logs subjected to defrosting.

Figure 2 presents the calculated with Equations (11) and (12) change of the specific heat capacities c_{ice-fw} and $c_{w-nfr-avg}$ of the frozen beech logs subjected to defrosting.

The analysis of these figures allows the following conclusions to be made about the influence of t_{w0} and u on each of the specific heat capacities that participate in $c_{eff.1,2,3}$ according to equations (1) – (3):

1. The decrease of t_{w0} causes the following almost linear decrease of $c_{w-fr-avg}$:
 - at $u = 0.4 \text{ kg} \cdot \text{kg}^{-1}$: from $2344 \text{ J} \cdot \text{kg}^{-1} \cdot \text{K}^{-1}$ at $t_{w0} = -1 \text{ }^\circ\text{C}$ to $1934 \text{ J} \cdot \text{kg}^{-1} \cdot \text{K}^{-1}$ at $t_{w0} = -40 \text{ }^\circ\text{C}$;
 - at $u = 0.6 \text{ kg} \cdot \text{kg}^{-1}$: from $2373 \text{ J} \cdot \text{kg}^{-1} \cdot \text{K}^{-1}$ at $t_{w0} = -1 \text{ }^\circ\text{C}$ to $1991 \text{ J} \cdot \text{kg}^{-1} \cdot \text{K}^{-1}$ at $t_{w0} = -40 \text{ }^\circ\text{C}$;
 - at $u = 0.8 \text{ kg} \cdot \text{kg}^{-1}$: from $2399 \text{ J} \cdot \text{kg}^{-1} \cdot \text{K}^{-1}$ at $t_{w0} = -1 \text{ }^\circ\text{C}$ to $2040 \text{ J} \cdot \text{kg}^{-1} \cdot \text{K}^{-1}$ at $t_{w0} = -40 \text{ }^\circ\text{C}$.

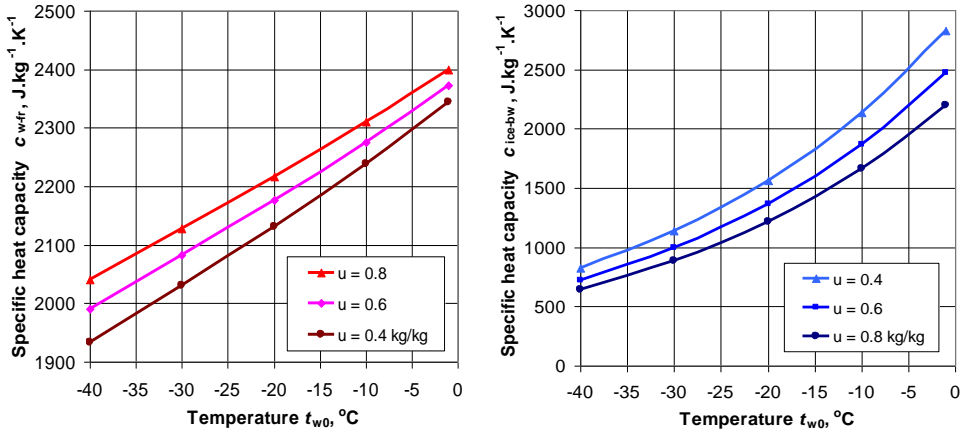


Figure 1. Change in $c_{w-fr-avg}$ (left) and $c_{ice-bw-avg}$ (right) of frozen logs, depending on t_{w0} and u

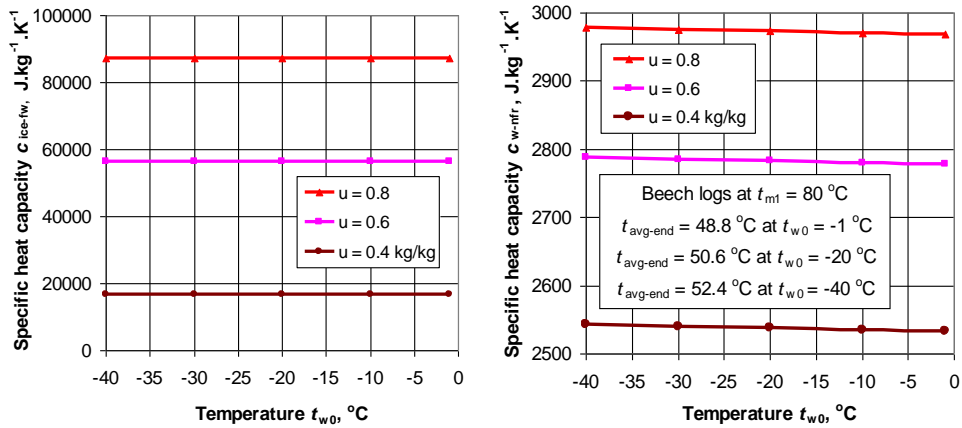


Figure 2. Change in c_{ice-fw} (left) and $c_{w-nfr-avg}$ of frozen logs, depending on t_{w0} and u .

2. The decrease of t_{w0} causes the following exponential decrease in $c_{ice-bw-avg}$:
 - at $u = 0.4 \text{ kg}\cdot\text{kg}^{-1}$: from $2825 \text{ J}\cdot\text{kg}^{-1}\cdot\text{K}^{-1}$ at $t_{w0} = -1 \text{ }^\circ\text{C}$ to $826 \text{ J}\cdot\text{kg}^{-1}\cdot\text{K}^{-1}$ at $t_{w0} = -40 \text{ }^\circ\text{C}$;
 - at $u = 0.6 \text{ kg}\cdot\text{kg}^{-1}$: from $2473 \text{ J}\cdot\text{kg}^{-1}\cdot\text{K}^{-1}$ at $t_{w0} = -1 \text{ }^\circ\text{C}$ to $724 \text{ J}\cdot\text{kg}^{-1}\cdot\text{K}^{-1}$ at $t_{w0} = -40 \text{ }^\circ\text{C}$;
 - at $u = 0.8 \text{ kg}\cdot\text{kg}^{-1}$: from $2198 \text{ J}\cdot\text{kg}^{-1}\cdot\text{K}^{-1}$ at $t_{w0} = -1 \text{ }^\circ\text{C}$ to $643 \text{ J}\cdot\text{kg}^{-1}\cdot\text{K}^{-1}$ at $t_{w0} = -40 \text{ }^\circ\text{C}$.
3. The decrease of t_{w0} does not cause a change in c_{ice-fw} at given value of u . An increase in u causes the following increase in c_{ice-fw} :
 - at $u = 0.4 \text{ kg}\cdot\text{kg}^{-1}$: $c_{ice-fw} = 16700 \text{ J}\cdot\text{kg}^{-1}\cdot\text{K}^{-1}$;
 - at $u = 0.6 \text{ kg}\cdot\text{kg}^{-1}$: $c_{ice-fw} = 56363 \text{ J}\cdot\text{kg}^{-1}\cdot\text{K}^{-1}$;
 - at $u = 0.8 \text{ kg}\cdot\text{kg}^{-1}$: $c_{ice-fw} = 87211 \text{ J}\cdot\text{kg}^{-1}\cdot\text{K}^{-1}$.
4. The decrease of t_{w0} causes the following slight increase in $c_{w-nfr-avg}$, which is the result of the shown in the legend of Fig. 6 slight rise of $t_{avg-end}$ at $t_{wc} = 0 \text{ }^\circ\text{C}$ when t_{w0} decreases:
 - at $u = 0.4 \text{ kg}\cdot\text{kg}^{-1}$: from $2533 \text{ J}\cdot\text{kg}^{-1}\cdot\text{K}^{-1}$ at $t_{w0} = -1 \text{ }^\circ\text{C}$ to $2542 \text{ J}\cdot\text{kg}^{-1}\cdot\text{K}^{-1}$ at $t_{w0} = -40 \text{ }^\circ\text{C}$;
 - at $u = 0.6 \text{ kg}\cdot\text{kg}^{-1}$: from $2777 \text{ J}\cdot\text{kg}^{-1}\cdot\text{K}^{-1}$ at $t_{w0} = -1 \text{ }^\circ\text{C}$ to $2787 \text{ J}\cdot\text{kg}^{-1}\cdot\text{K}^{-1}$ at $t_{w0} = -40 \text{ }^\circ\text{C}$;
 - at $u = 0.8 \text{ kg}\cdot\text{kg}^{-1}$: from $2968 \text{ J}\cdot\text{kg}^{-1}\cdot\text{K}^{-1}$ at $t_{w0} = -1 \text{ }^\circ\text{C}$ to $2978 \text{ J}\cdot\text{kg}^{-1}\cdot\text{K}^{-1}$ at $t_{w0} = -40 \text{ }^\circ\text{C}$.

CONCLUSIONS

It was found that decreasing the initial temperature t_{w0} from -1 °C to -40 °C and the wood moisture content u from 0.8 to 0.4 $\text{kg}\cdot\text{kg}^{-1}$ caused a decrease in $c_{w\text{-fr-avg}}$ from 2399 to 1934 $\text{J}\cdot\text{kg}^{-1}\cdot\text{K}^{-1}$. The same decrease in t_{w0} combined with an increase in u from 0.4 to 0.8 $\text{kg}\cdot\text{kg}^{-1}$ causes a decrease in $c_{\text{ice-bw-avg}}$ from 2825 to 643 $\text{J}\cdot\text{kg}^{-1}\cdot\text{K}^{-1}$.

An increase in u from 0.4 to 0.8 $\text{kg}\cdot\text{kg}^{-1}$ causes a drastic increase in $c_{\text{ice-fw}}$ from 16461 to 87026 $\text{J}\cdot\text{kg}^{-1}\cdot\text{K}^{-1}$ in the range from -1 °C to 0 °C, in which the melting of the frozen free water in the wood takes place. The heat capacity of completely defrosted logs, $c_{w\text{-nfr-avg}}$, at the time of reaching 0 °C in their central point, is almost independent of t_{w0} , but increases from 2533 to 2978 as u increases from 0.4 to 0.8 $\text{J}\cdot\text{kg}^{-1}\cdot\text{K}^{-1}$.

The presented approach could be applied to determine the energy and its components required for defrosting of different frozen wood materials subjected to multiple types of thermal treatment. One such example is shown in the second part of the present work.

REFERENCES

1. CÂMPEAN, M. 2005: Heat Treatments of Wood. Transilvania University of Braşov, Romania 199 p.
2. DELIISKI, N. 2003: Modelling and Technologies for Steaming Wood Materials in Autoclaves. Dissertation for DSc., University of Forestry, Sofia, 358 p. (in Bulgarian).
3. DELIISKI, N. 2011: Transient Heat Conduction in Capillary Porous Bodies. In Convection and Conduction HeatTransfer; Ahsan A., Ed.; InTech Publishing House, Rieka, Croatia, pp. 149–176.
4. DELIISKI, N., NIEMZ, P., DZURENDA, L., VITCHEV, P., ANGELSKI, D. 2023: An Approach for Computing the Thermal Balance and Energy Consumption of Concrete Pits during Boiling of Frozen Logs for Veneer Production. Wood Material Science & Engineering, 18(6): 2153–2163.
5. DZURENDA, L., DELIISKI, N. 2019: Thermal Processes in the Woodworking Technologies. Technical University in Zvolen, Slovakia, 283 p. (in Slovak).
6. HADJISKI, M., DELIISKI, N., TUMBARKOVA, N. 2020: Intelligent Hybrid Control of Thermal Treatment Processes of Wood. In 10th International Conference on Intelligent Systems IS 2020, 26–28 August 2020, Varna, Bulgaria, pp. 482–498.
7. KHATTABI, A., STEINHAGEN, H. P. 1992: Numerical Solution to Two-Dimensional Heating of Logs. Holz als Roh- und Werkstoff, 50(7-8), 308–312.
8. KHATTABI, A., STEINHAGEN, H. P. 1993: Analysis of Transient Non-Linear Heat Conduction in Wood Using Finite-Difference Solutions. Holz als Roh- und Werkstoff, 51(4), 272–278.
9. NIEMZ, P., TEISCHINGER, A., SANDBERG, D. (Eds.). 2023: Springer Handbook for Wood Science and Technology. Springer Nature Switzerland AG, Cham, 2069 p.
10. STEINHAGEN, H. P. 1986: Computerized Finite-Difference Method to Calculate Transient Heat Conduction with Thawing. Wood Fiber Science, 18(3), 460–467.
11. STEINHAGEN, H. P. 1991: Heat Transfer Computation for a Long, Frozen Log Heated in Agitated Water or Steam – a Practical Recipe. Holz als Roh- und Werkstoff, 49(7–8), 287–290.
12. TUMBARKOVA, N. 2019: Modelling of the Freezing and Defrosting Processes of Logs and Their Energy Consumption. Thesis (PhD), University of Forestry, Sofia, 198 p. (in Bulgarian).



COMPUTING THE SPECIFIC HEAT CAPACITIES AND ENERGY CONSUMPTION OF LOGS SUBJECTED TO DEFROSTING

Part 2. Calculating the energy required to defrost logs

Nencho Deliiski¹ – Ladislav Dzurenda² – Dimitar Angeski¹ – Pavlin Vitchev¹ – Krasimira Atanasova¹

Abstract

An approach for computing the energy consumption of frozen logs subjected to defrosting has been presented. The approach includes computer simulations with two own models: one to calculate the 1D unsteady temperature distribution along the radius of the logs during their defrosting and also the connected with it average mass temperature of the logs, and the second – to calculate the energy consumption of the logs and its four components. The influence of all combinations between 3 values of the initial temperature of frozen logs (–10 °C, –20 °C, and –30 °C) and 2 values of their moisture content (0.4 kg·kg⁻¹ and 0.8 kg·kg⁻¹) on the energy required to defrost beech logs with a diameter of 0.4 m at operating temperature of the heating medium of 80 °C was investigated. The results show that this energy changes in the range from 41.5 kWh·m⁻³ (at –10 °C and 0.4 kg·kg⁻¹) to 89.7 kWh·m⁻³ (at –30 °C and 0.8 kg·kg⁻¹)

Key words: *frozen logs, frozen bound water, frozen free water, defrosting, specific heat capacities, energy consumption, simulation study*

INTRODUCTION

It is well-known that the non-stationary distribution of the temperature in frozen wood during its defrosting and thermal treatment, and also the change in the energy needed for this, can be calculated using the models (Steinhagen 1991; Khathaby – Steinhagen 1992, 1993; Deliiski 2003, 2011, 2013; Câmpean 2005; Dzurenda – Deliiski 2019, Tumbarkova 2019; Deliiski et al. 2023; Niemz et al. 2023). The development and solving of such temperature-energy models is carried out using finite differences and requires deep mathematical knowledge.

Of particular interest to the development, study and implementation of science-based energy-saving regimes for thermal treatment would be the availability of a simpler and more accessible engineering approach to calculating the energy for defrosting of wood.

¹ Faculty of Forest Industry, University of Forestry, Kliment Ohridski Bd. 10, 1797 Sofia, Bulgaria
e-mails: deliiski@netbg.com, d.angeski@gmail.com, p_vitchev@abv.bg, k_atanasova@ltu.bg

² Faculty of Wood Sciences and Technology, Technical University of Zvolen, T.G. Masarikova 24, 96053, Zvolen, Slovakia, e-mail: dzurenda@tuzvo.sk

Therefore, the aim of this work is to present an engineering approach for calculating the specific energy required for defrosting of frozen logs.

MATERIAL AND METHODS

Material for research

This research was conducted over frozen beech (*Fagus sylvatica* L.) logs, which are commonly used in veneer production.

The calculation of the specific heat capacities of frozen wood during its defrosting was carried out for the case of steaming or boiling of frozen logs in equipment operating at atmospheric pressure and at a temperature of the heating medium of 80 °C.

The symbols, units, and values of the main parameters of the studied logs, and also of their defrosting modes, which were involved in the equations of the mathematical models given below, and were used in the computer simulations, are presented in Table 1.

Mathematical model of the 1D unsteady temperature change in frozen logs

When the length of the logs, L , is at least four times their diameter, D , the non-stationary temperature distribution along the radius and also their defrosting duration can be determined using the following experimentally verified 1D model (Deliiski 2011):

$$c_{w\text{-eff.1,2,3}} \cdot \rho_w \frac{\partial T(r, \tau)}{\partial \tau} = \text{div} (\lambda_{w\text{-eff.1,2}} \text{ grad } T) \quad (1)$$

$$\text{at} \quad T(r, 0) = T_{w0} \quad (2)$$

and boundary conditions for conductive heat transfer:

$$T(0, \tau) = T_m(\tau), \quad (3)$$

where $c_{w\text{-eff.1,2,3}}$ are the effective specific heat capacities of the frozen wood during 1st, 2nd, and 3rd temperature ranges of its defrosting process [43,44], $\text{J} \cdot \text{kg}^{-1} \cdot \text{K}^{-1}$; $\lambda_{w\text{-eff.1,2}}$ – effective thermal conductivities of the frozen and defrosten wood in radial direction respectively, $\text{W} \cdot \text{m}^{-1} \cdot \text{K}^{-1}$; ρ_w – density of the wet wood, $\text{kg} \cdot \text{m}^{-3}$; r – coordinate along the log's radius: $0 \leq r \leq R$, m; R – radius of the log, m; T – temperature, K; T_{w0} – initial average mass temperature of the log, K; T_m – operating temperature of the defrosting medium, K; τ – time, s.

Mathematical descriptions of $c_{w\text{-eff.1,2,3}}$, $\lambda_{w\text{-eff.1,2}}$, and ρ_w given in (Deliiski 2003, 2011, 2013; Deliiski – Dzurenda 2010) were used in solving model (1) – (3).

During the solving of the model (1) – (3), the average mass temperature of the log, T_{avg}^n , can be calculated according to the following equation (Deliiski et al. 2023)

$$T_{\text{avg}}^n = \frac{1}{R} \int_R T(r, n \cdot \Delta\tau) dR \quad (4)$$

Modelling of the energy consumption of frozen wood subjected to defrosting

The total specific thermal energy consumption of frozen wood subjected to defrosting (in $\text{kWh} \cdot \text{m}^{-3}$), $Q_{w\text{-total}}$, can be expressed by the following model (Deliiski et al. 2023):

Table 1. Main set parameters of frozen beech logs, their defrosting regimes, and average specific heat capacities which were used during the computer simulations.

№	Parameter name	Symbol	Unit	Value
1.	Diameter of the logs	D	m	0.4
2.	Length of the logs	L	m	2.0
3.	Moisture content of the logs (a – at $u = 0.4$ kg·kg ⁻¹ , b – at $u = 0.8$ kg·kg ⁻¹ ,	u	kg·kg ⁻¹	0.4a 0.8b
4.	Fiber saturation point of the wood at 20 °C	$u_{fsp(293.15K)}$	kg·kg ⁻¹	0.31
5.	Basic density of the beech wood	ρ_b	kg·m ⁻³	560
6.	Density of the wet wood equal to $\rho_b \cdot (1 + u)$	ρ_w	kg·m ⁻³	784a 1008b
7.	Density of the ice in the wood	ρ_{ice}	kg·m ⁻³	917
8.	Initial temperature of the wood in the beginning of the logs' defrosting: (c – at $t_{w0} = -10$ °C, d – at $t_{w0} = -20$ °C, e – at $t_{w0} = -30$ °C)	t_{wo}	°C	-10c -20d -30e
9.	Temperature of complete melting of frozen part of bound water in the wood	$t_{ice-bw-end}$	°C	-1
10.	Temperature of complete melting of frozen free water	$t_{ice-fw-end}$	°C	0
11.	Initial temperature of the regimes for defrosting	t_{m0}	°C	10
12.	Constant temperature of the regimes for defrosting of logs	t_{m1}	°C	80
13.	Average mass temperature of the logs at the end of their complete defrosting, depending on t_{w0}	$t_{avg-end}$	°C	49.7c 50.6d 51.5e
14.	Temperature in the central point of the logs at the end of their complete defrosting	t_{wc}	°C	0
15.	Average specific heat capacity of log layers containing frozen bound water at $u = 0.8$ kg·kg ⁻¹ , depending on t_{w0}	$C_{w-fr-avg}$	J·kg ⁻¹ ·K ⁻¹	2310c 2217d 2128e
16.	Average specific heat capacity of completely defrosted layers of logs with $u = 0.8$ kg·kg ⁻¹ , depending on t_{w0}	$C_{w-nfr-avg}$	J·kg ⁻¹ ·K ⁻¹	2971c 2973d 2975e
17.	Average specific heat capacity of the frozen bound water in logs with $u = 0.8$ kg·kg ⁻¹ , depending on t_{w0}	$C_{ice-bw-avg}$	J·kg ⁻¹ ·K ⁻¹	1661c 1214d 885e
18.	Average specific heat capacity of the frozen free water in logs, depending on u	$C_{ice-fw-avg}$	J·kg ⁻¹ ·K ⁻¹	16461a 87026b

$$Q_{w-total} = Q_{w-fr} + Q_{ice-bw} + Q_{ice-fw} + Q_{w-nfr} \quad (5)$$

where Q_{w-fr} is the energy required for the heating of the frozen wood to a condition necessary to melt the frozen bound water in it; Q_{ice-bw} – energy required to melt the frozen bound water in the wood; Q_{ice-fw} – energy required to melt the entire amount of frozen free water in the wood; Q_{w-nfr} – energy required to heat the allready defrosted layers of the wood until reaching 0 °C in the center of materials subjected to defrosting.

The individual components of the energy required for complete defrosting of the frozen wood, $Q_{w-total}$, can be calculated using the following equations (Deliiski et al. 2023):

$$Q_{w-fr} = \frac{\rho_w \cdot c_{w-fr-avg}}{3.6 \cdot 10^6} \cdot (272.15 - T_{w0}) \quad (6)$$

$$Q_{ice-bw} = \frac{\rho_{ice} \cdot c_{ice-bw-avg}}{3.6 \cdot 10^6} \cdot (272.15 - T_{w0}) \quad (7)$$

$$Q_{ice-fw} = \frac{\rho_{ice} \cdot c_{ice-fw-avg}}{3.6 \cdot 10^6} (273.15 - 272.15) \quad (8)$$

$$Q_{w-nfr} = \frac{\rho_w \cdot c_{w-nfr-avg}}{3.6 \cdot 10^6} \cdot (T_{avg-end} - 272.15) \quad (9)$$

where $c_{w-fr-avg}$ and $c_{w-nfr-avg}$ are the arithmetic mean values of the specific heat capacities of frozen and defrosted (non-frozen) wet wood respectively, $J \cdot kg^{-1} \cdot K^{-1}$; $c_{ice-bw-avg}$ and $c_{ice-fw-avg}$ – arithmetic mean values of the specific heat capacities of frozen bound and free water in the wood respectively, $J \cdot kg^{-1} \cdot K^{-1}$; T_{w0} – initial average mass temperature of the log, K; $T_{avg-end}$ – average mass temperature of the logs at the end of their defrosting, which is calculated with Equation (4) upon reaching 0 °C in the central point of the fully defrosted logs, K;

The arithmetic mean values of the mentioned above specific heat capacities are calculated according to the equations given in the Part 1 of this work.

RESULTS AND DISCUSSION

The solving of the model (1) – (3) in order to determine the duration of the regimes for defrosting of beech logs, and also of the average mass temperature, $T_{avg-end}$, was carried out with the help of own software in Visual FORTRAN Professional. It was determined that this average mass temperature of the studied logs is equal, as follow: $t_{avg-end} = 49.7$ °C at $t_{w0} = -10$ °C, $t_{avg-end} = 50.6$ °C at $t_{w0} = -20$ °C, and $t_{avg-end} = 51.5$ °C at $t_{w0} = -30$ °C.

An Excel program has been prepared for joint solving of the Equations (5) – (9) and also the equations for calculating the specific heat capacities of frozen logs given in Part 1 of this work. Using this program, the change in the energy $Q_{w-total}$ and its four components was investigated for the cases of defrosting at $t_{m1} = 80$ °C of beech logs with moisture content of $0.4 \text{ kg} \cdot \text{kg}^{-1}$, $0.6 \text{ kg} \cdot \text{kg}^{-1}$, and $0.8 \text{ kg} \cdot \text{kg}^{-1}$ and initial temperature of -10 °C, -20 °C, and -30 °C. The values of $T_{avg-end}$ pointed above were used for solving of Equation (9).

Figure 1 presents with Excel graphs the change in the energy $Q_{w-total}$ (in $\text{kWh} \cdot \text{m}^{-3}$) required for defrosting the beech logs with $u = 0.4 \text{ kg} \cdot \text{kg}^{-1}$ and $u = 0.8 \text{ kg} \cdot \text{kg}^{-1}$, and also the change in all four components of this energy, depending on t_{w0} . Figure 2 also with Excel graphs shows the change in the individual components of the energy $Q_{w-total}$ in % to its total value for logs with the studied two values of u , depending on t_{w0} .

In Figure 1 it can be seen that when expressing the energy $Q_{w-total}$ and its components in $\text{kWh} \cdot \text{m}^{-3}$, a decrease in t_{w0} from -10 °C to -30 °C causes an increase in this energy and also in its components Q_{ice-bw} , Q_{w-fr} , and Q_{w-nfr} , but the component Q_{ice-fw} does not change.

In this case, the total energy $Q_{w-total}$ increases from $41.5 \text{ kWh} \cdot \text{m}^{-3}$ to $54.5 \text{ kWh} \cdot \text{m}^{-3}$ at $u = 0.4 \text{ kg} \cdot \text{kg}^{-1}$ and from $74.0 \text{ kWh} \cdot \text{m}^{-3}$ to $89.7 \text{ kWh} \cdot \text{m}^{-3}$ at $u = 0.8 \text{ kg} \cdot \text{kg}^{-1}$ while the individual components of this energy change as follows:

▪ Q_{ice-bw} increases from 4.9 kWh·m⁻³ to 8.4 kWh·m⁻³ at $u = 0.4$ kg·kg⁻¹ and from 3.8 kWh·m⁻³ to 6.5 kWh·m⁻³ at $u = 0.8$ kg·kg⁻¹. The reason for this is the increase in the difference $272.15 - T_{w0}$ given in parentheses in the right-hand part of Equation (7) with the decrease in temperature T_{w0} ;

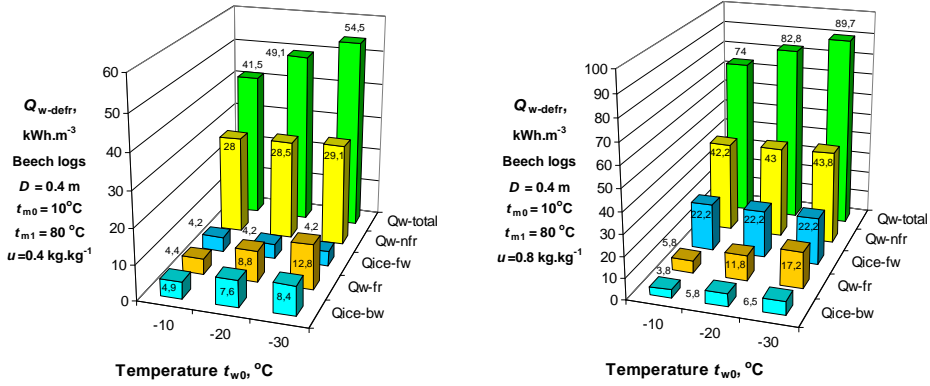


Figure 1. Change in the energy $Q_{w-total}$ (in kWh·m⁻³) and its components required for defrosting of logs with $u = 0.4$ kg·kg⁻¹ (left) and $u = 0.8$ kg·kg⁻¹ (right), depending on t_{w0} .

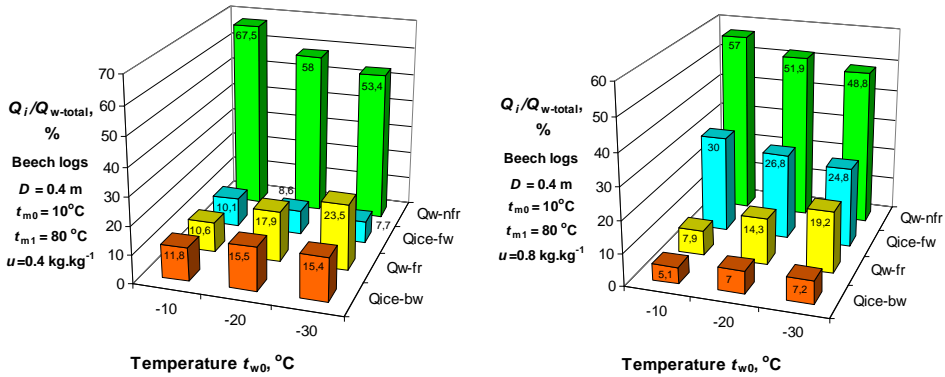


Figure 2. Change in the components of energy $Q_{w-total}$ at $u = 0.4$ kg·kg⁻¹ (left) and $u = 0.8$ kg·kg⁻¹ (right) in % to its total value required for defrosting of the logs, depending on t_{w0} .

▪ Q_{w-fr} increases from 4.4 kWh·m⁻³ to 12.8 kWh·m⁻³ at $u = 0.4$ kg·kg⁻¹ and from 5.8 kWh·m⁻³ to 17.2 kWh·m⁻³ at $u = 0.8$ kg·kg⁻¹ due to the same reason that caused the increase in Q_{ice-bw} (see Equation (6));

▪ Q_{ice-fw} remains unchanged for given wood moisture content with a value of 4.2 kWh·m⁻³ at $u = 0.4$ kg·kg⁻¹ and of 22.2 kWh·m⁻³ at $u = 0.8$ kg·kg⁻¹;

▪ Q_{w-nfr} increases from 28.0 kWh·m⁻³ to 29.1 kWh·m⁻³ at $u = 0.4$ kg·kg⁻¹ and from 42.2 kWh·m⁻³ to 43.8 kWh·m⁻³ at $u = 0.8$ kg·kg⁻¹ due to the insignificant increase in $t_{avg-end}$ of the logs (refer to item 14 in Table 1).

When expressing the components of the energy $Q_{w-total}$ in % to its total value, a decrease in t_{w0} from -10 °C to -30 °C causes the following change in fraction of each component:

- Q_{ice-bw} increases from 11.8% to 15.4% at 0.4 and from 7.4% to 10.1% at 0.8 kg·kg⁻¹;
- Q_{w-fr} increases from 10.6% to 23.5% at 0.4 and from 8.6% to 20.5% at 0.8 kg·kg⁻¹;
- Q_{ice-fw} decreases from 10.1% to 7.7% at 0.4 and from 24.3% to 19.6% at 0.8 kg·kg⁻¹;
- Q_{w-nfr} decreases from 67.5% to 53.4% at 0.4 and from 59.7% to 49.8% at 0.8 kg·kg⁻¹.

CONCLUSIONS

It was found that decreasing the initial wood temperature t_{w0} from $-10\text{ }^{\circ}\text{C}$ to $-30\text{ }^{\circ}\text{C}$ causes an increase in the energy $Q_{w\text{-total}}$ required for defrosting of beech logs with a diameter of 0.4 m at $t_m = 80\text{ }^{\circ}\text{C}$ from $41.5\text{ kWh}\cdot\text{m}^{-3}$ to $54.5\text{ kWh}\cdot\text{m}^{-3}$ at $u = 0.4\text{ kg}\cdot\text{kg}^{-1}$ and from $74.0\text{ kWh}\cdot\text{m}^{-3}$ to $89.7\text{ kWh}\cdot\text{m}^{-3}$ at $u = 0.8\text{ kg}\cdot\text{kg}^{-1}$.

When lowering the initial temperature of the logs from $-10\text{ }^{\circ}\text{C}$ to $-30\text{ }^{\circ}\text{C}$, the sum of the energies $Q_{w\text{-fr}}$ and $Q_{\text{ice-bw}}$ required to melt the frozen bound water in them increases from 9.3 to $21.2\text{ kWh}\cdot\text{m}^{-3}$ at $u = 0.4\text{ kg}\cdot\text{kg}^{-1}$ and from 9.6 to $23.7\text{ kWh}\cdot\text{m}^{-3}$ at $u = 0.8\text{ kg}\cdot\text{kg}^{-1}$.

An increase in u from 0.4 to $0.8\text{ kg}\cdot\text{kg}^{-1}$ causes a drastic increase in the energy required to melt the entire amount of frozen free water in the logs $Q_{\text{ice-fw}}$ from 4.2 to $22.2\text{ kWh}\cdot\text{m}^{-3}$ due to the very large increase of the specific heat capacity $c_{\text{ice-fw}}$ (refer to item 19 in Table 1) in the range from $-1\text{ }^{\circ}\text{C}$ to $0\text{ }^{\circ}\text{C}$, in which the melting of this water in the wood takes place.

The energy $Q_{w\text{-nfr}}$ required to heat the already defrosted layers of the logs until reaching $0\text{ }^{\circ}\text{C}$ in their central point increases from 28.0 to $29.1\text{ kWh}\cdot\text{m}^{-3}$ at $u = 0.4\text{ kg}\cdot\text{kg}^{-1}$ and from 42.2 to $43.8\text{ kWh}\cdot\text{m}^{-3}$ at $u = 0.8\text{ kg}\cdot\text{kg}^{-1}$ when the initial temperature of the logs decreases from $-10\text{ }^{\circ}\text{C}$ to $-30\text{ }^{\circ}\text{C}$.

In conclusion, it can be noted that the approach presented in this work could be applied to determine the energy and its components required for defrosting of different frozen capillary-porous materials subjected to multiple types of thermal treatment.

REFERENCES

1. CÂMPEAN, M. 2005: Heat Treatments of Wood. Transilvania University of Braşov, Romania 199 p.
2. DELIISKI, N. 2003: Modelling and Technologies for Steaming Wood Materials in Autoclaves. Dissertation for DSc., University of Forestry, Sofia, 358 p. (in Bulgarian).
3. DELIISKI, N. 2011: Transient Heat Conduction in Capillary Porous Bodies. In Convection and Conduction Heat Transfer; Ahsan A., Ed.; InTech Publishing House, Rijeka, Croatia, pp. 149–176.
4. DELIISKI, N. 2013: Modelling of the Energy Needed for Heating of Capillary Porous Bodies in Frozen and Non-Frozen States; Lambert Academic Publishing, Scholars' Press: Saarbrücken, Germany, 106 p.
5. DELIISKI, N., NIEMZ, P., DZURENDA, L., VITCHEV, P., ANGELSKI, D. 2023: An Approach for Computing the Thermal Balance and Energy Consumption of Concrete Pits during Boiling of Frozen Logs for Veneer Production. Wood Material Science & Engineering, 18(6): 2153–2163.
6. DZURENDA, L., DELIISKI, N. 2019: Thermal Processes in the Woodworking Technologies. Technical University in Zvolen, Slovakia, 283 p. (in Slovak).
7. KHATTABI, A., STEINHAGEN, H. P. 1992: Numerical Solution to Two-Dimensional Heating of Logs. Holz als Roh- und Werkstoff, 50(7-8), 308–312.
8. KHATTABI, A., STEINHAGEN, H. P. 1993: Analysis of Transient Non-Linear Heat Conduction in Wood Using Finite-Difference Solutions. Holz als Roh- und Werkstoff, 51(4), 272–278
9. NIEMZ, P., TEISCHINGER, A., SANDBERG, D. (Eds.). 2023: Springer Handbook for Wood Science and Technology. Springer Nature Switzerland AG, Cham, 2069 p.

10. STEINHAGEN, H. P. 1991: Heat Transfer Computation for a Long, Frozen Log Heated in Agitated Water or Steam – a Practical Recipe. *Holz als Roh- und Werkstoff*, 49(7–8), 287–290.
11. TUMBARKOVA, N. 2019: Modelling of the Freezing and Defrosting Processes of Logs and Their Energy Consumption. Thesis (PhD), University of Forestry, Sofia, 198 p. (in Bulgarian).

Našu ponuku nájdete na:
www.areko.sk





ACIDITY OF STEAMED BEECH SAPWOOD AND FALSE HEARTWOOD

Michal Dudiak – Adrián Banski

Abstract

The work evaluates the changes in the acidity of beech sapwood and wood with false heartwood in the process of steaming wood with saturated steam. The beech wood of the individual zones was steamed at a temperature of $t = 125 \pm 2.5$ °C for $\tau \leq 24$ hours. Wood pH was measured using a pH-meter pH7110 with a Sen Tix Sur surface electrode on dried wood with a moisture content of $w = 10 \pm 2\%$. By statistical processing of the measured results, the polynomial dependence of pH on time τ was plotted and calculated. The correlation between the acidity of beech wood in individual zones and the time τ of wood exposure to modification was described using mathematical equations: $pH_{\text{sapwood}} = 6.5 - 1.3043 \cdot \tau + 0.1357 \cdot \tau^2$; $pH_{\text{false heartwood}} = 6.02 - 0.8029 \cdot \tau + 0.0571 \cdot \tau^2$, which can be used to control the wood steaming process.

Key words: *beech wood, sapwood, false heartwood, acidity, saturated water steam.*

INTRODUCTION

Beech wood belongs to the scattered-porous coreless woods with the possibility of forming a false heartwood. Sapwood and mature beech wood is medium heavy, flexible, easily split. It has good mechanical properties, it is plasticized, bent and machined very well. Thanks to its high permeability, it is well impregnated, stained and dyed. Beech wood is used for the production of furniture, floors, sports equipment, toys and small household items. White and mature beech wood has a light white-gray color with a yellow tinge. Beech wood is used for the production of furniture, floors, sports equipment, toys and small household items.

A false heartwood beech is a growth defect that results from air-wood reactions in the mature wood zone. The primary cause of a false heartwood is injury to the tree trunk or branches, which allows air to enter the tree trunk. The oxygen contained in the air will cause the oxidation of soluble carbohydrates and starch (contained in living or partially dead parenchymal cells), resulting in brown-colored polyphenolic compounds that penetrate into the neighboring tissues and color them Bauch and Koch (2001), Račko and Čunderlík (2010). In comparison to sapwood and mature wood, the wood of the false heartwood has a lower moisture content in the growing tree, and according to the work of Babiak *et al.* (1990) lower fluid permeability.

The pH value is a measure of the concentration of H^+ ions in a solution and is used to determine the acidic, neutral, or basic behavior of a chemical reaction. pH values are very

important physiological parameters for plants, humans and animals. In production processes, the change in acidity is used to control technological processes.

In the lumens of the cells of wet wood there is a diluted aqueous solution of sugars, organic acids and salts of calcium, magnesium, potassium, sodium of inorganic acids, which are transported to the living tree by the root system (Čudinov 1968; Blažej *et al.* 1975; Zevenhoven 2001, Pňakovič and Dzurenda 2015), as a result of which this solution has a certain acidity. Wood acidity of deciduous, scattered-porous woods with moisture above the fiber saturation point (BNV) is in the range of pH = 5.5 – 4.8 (Sandermann and Rothkamm 1956; Irlle 2012; Solár 2014; Geffert *et al.* 2019).

By applying heat to wet wood, chemical changes in the wood are also initiated. The first chemical reactions include the partial hydrolysis of hemicelluloses and the extraction of water-soluble substances (Fengel and Weneger 1989; Bučko 1995; Laurova *et al.* 2004; Solár 2005; Sundqvist *et al.* 2006; Samešova *et al.* 2018).

The pH value is a parameter that can be measured quickly and easily and is therefore advantageously used for control and management of technological processes. Several measurement methods have been developed for the direct measurement of wood pH, presented in the contributions of the authors Geffert *et al.* (2019), Dudiak (2022).

The processes of thermal treatment of wood, in addition to targeted physical-mechanical changes used in the production of veneers, plywood, bent furniture, or pressed wood, are also accompanied by a change in color (Kollmann and Gote 1968; Trebula 1986; Molnár and Tolvaj 2002; Dzurenda 2013; Dzurenda *et al.* 2020; Dudiak 2021; Dzurenda and Dudiak 2021).

The aim of the work is to determine the acidity of dried, steamed beech sapwood and wood with a false core for moisture $w \approx 10\%$, using a direct pH measurement method - SenTix Sur surface electrode.

MATERIALS AND METHODS

Blanks with dimensions of $32 \times 50 \times 800$ mm were made by longitudinal and transverse sawing from the middle lumber of thickness $h = 32$ mm of beech wood with a false heartwood. 75 sapwood blanks and 75 false heartwood blanks were randomly selected. The blanks were divided into 5 groups so that each group contained 15 sapwood blanks and 15 false heartwood blanks. The blanks of the 1st group were not steamed. Other blanks were steamed with saturated steam at a temperature of $t_{II} \approx 125 \pm 2.5$ °C. Individual cages with steamed wood were removed from the steaming autoclave after steaming $\tau = 6$ h, $\tau = 12$ h, $\tau = 18$ h and $\tau = 24$ h. Steaming of wood was carried out in a pressure autoclave APDZ 240 (Himmasch AD, Haskovo, Bulgaria) installed at Sundermann s.r.o. Banská Štiavnica (Slovakia). The steaming conditions saturated water steam of beech wood with a false heartwood, with marked time intervals of sampling during treatment v are shown in the diagram in Fig. 1.

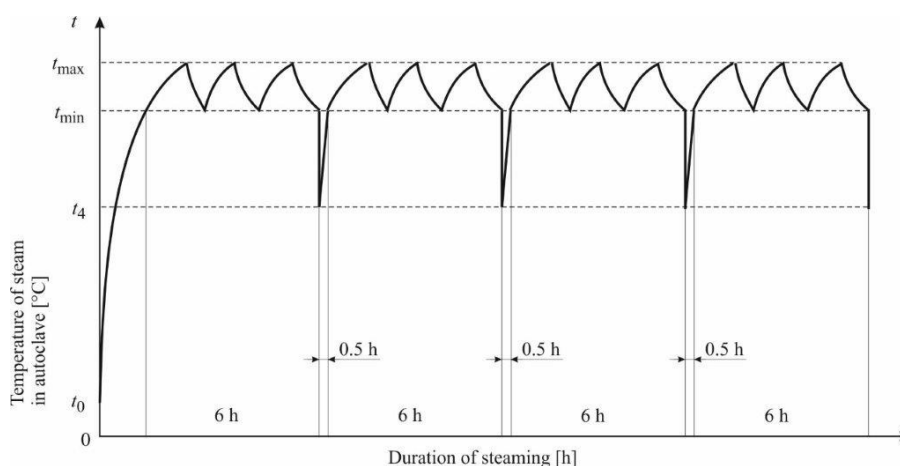


Fig. 1 Diagram of the steaming process of beech wood in a pressure autoclave.

Table 1. Beech wood steaming mode

Mode	Saturated steam temperature [°C]			Steaming time [h]			
	t_{max}	t_{min}	t_4	τ_1	τ_2	τ_3	τ_4
125 °C	122.5	127.5	100	6 h*	12 h*	18 h*	24 h

Note: * Taking a group of steamed blanks from the autoclave at planned intervals took 0.5 h. The actual steaming time compared to the planned steaming time was extended by the time of technological breaks.

The moisture content of the wood was determined before entering the technological process itself by randomly selecting 5 sapwood blanks and 5 blanks with a false heartwood, from which samples were sawn to determine the wood moisture content. The moisture content of the dried blanks was also determined, where 5 sapwood blanks and 5 blanks with a false heartwood were randomly selected from which samples were sawn to determine the wood moisture content. The moisture content of wet and dried wood was determined by the gravimetric method according to STN EN 13183-1 (2003).

Unsteamed and steamed samples of beech sapwood and wood with a false heartwood were dried in a hot air oven according to the Dzurenda (2022) mode in order to preserve the original color of the wood achieved by the technological process of steaming. The bedding surfaces of the dried lumber were machined on a FS 200 horizontal plane milling machine.

Measurement of the acidity of dried native and steamed beech sapwood and false heartwood was performed on a planed surface using a pH-meter pH7110 with a SenTix Sur surface electrode (Dudiak and Dzurenda 2020).

Measuring the acidity of beech wood consists in applying the surface electrode of the SenTix Sur pH-meter type: pH7110 to the surface of the wood. The acidity value was read after the pH value stabilized on the pH-meter display. At the point of measuring the pH of dry wood with a SenTix Sur surface electrode, first one drop of distilled water was dripped onto the surface of the wood using a dropper, and then the surface contact electrode was pressed against the surface of the wood in the place of the dropped drop, thereby creating

contact between the electrode and the surface of the wood. The pH value was read after approx. 180 to 240 seconds of stabilization of the electrode on the pH-meter pH7110. The record of the measurement of the acidity of dry beech wood is shown in Fig. 2.

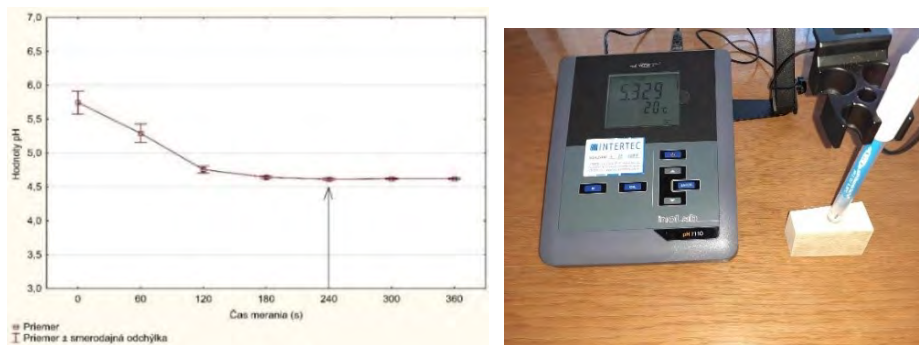


Fig. 2 Measurement of pH on the surface of beech wood after moistening it with a drop of distilled water.

The measured values of moisture content and acidity of sapwood beech and false heartwood are given in the form of notation, $x = \bar{x} \pm s_x$ i.e. average measured value and standard deviation.

RESULTS AND DISCUSSION

The average moisture of sapwood beech determined by the gravimetric method before entering the steaming process was $58.6 \pm 5.2\%$, the moisture of the false heartwood before the steaming process was $48.1 \pm 4.5\%$. After modification, all blanks were dried in a chamber hot air dryer to a moisture content of $10.0 \pm 2\%$.

From the measured results of wood moisture, it follows that the wood was sufficiently wet, while the moisture requirement was met, that the wood before entering the pressure steaming process must contain moisture higher than BNV $w \geq 30\%$ in order to achieve the desired effect of color modification.

The acidity before the steaming process of dry native sapwood was at the level of $\text{pH} = 5.4 \pm 0.18$ and of the false heartwood $\text{pH} = 5.3 \pm 0.1$.

Acidity values of dry beech wood in the zone of the sapwood and false heartwood measured by the contact method of measuring pH with a SenTix Sur surface electrode in the steaming process are shown in Table 2 and Table 3.

Table 2 Measured average pH values of sapwood beech in the steaming process

Mode	Time of the steaming process of sapwood beech				
	0h - native	6 h	12 h	18 h	24h
	pH [-]	pH [-]	pH [-]	pH [-]	pH [-]
Mode $t = 125^\circ\text{C}$	5.4 ± 0.2	4.3 ± 0.2	3.8 ± 0.2	3.6 ± 0.1	3.3 ± 0.1

Table 3 Measured average pH values of false heartwood beech in the steaming process

Mode	Time of the steaming process of false heartwood beech				
	0h - native	6 h	12 h	18 h	24h
	pH [-]	pH [-]	pH [-]	pH [-]	pH [-]
Mode $t = 125\text{ }^{\circ}\text{C}$	5.3 ± 0.1	4.6 ± 0.1	4.1 ± 0.2	3.8 ± 0.1	3.4 ± 0.1

As a result of the chemical reactions taking place in the wood during the heat treatment process, the color of the wood changes, while the pH value of the wood decreases. It follows from the decline in the acidity of beech wood that the temperature factor is more significant than the time factor.

From the experimentally measured pH values of beech wood during heat treatment of wood with saturated water steam at temperature $t = 125\text{ }^{\circ}\text{C}$ for time $\tau = 6 - 24\text{ h}$, a graphical dependence of the change in acidity on temperature and time was determined (Fig. 3).

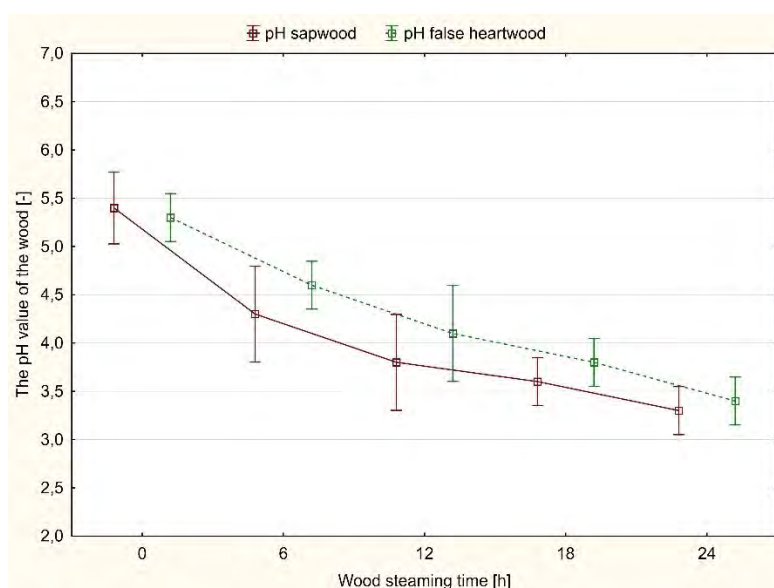


Fig. 3 Correlation of the pH value of wet beech wood and the temperature of saturated water steam t and the time τ .

Changes in acidity values of dry sapwood beech and false heartwood at the temperature of saturated water steam at temperature $t = 125\text{ }^{\circ}\text{C}$ and time $\tau = 6 - 24\text{ h}$ they state mathematical equations in the form:

$$\text{pH}_{\text{sapwood}} = 6.5 - 1.3043 \cdot \tau + 0.1357 \cdot \tau^2 \quad (1)$$

$$\text{pH}_{\text{false heartwood}} = 6.02 - 0.8029 \cdot \tau + 0.0571 \cdot \tau^2 \quad (2)$$

Where: τ – time wood is exposed to steaming in hours.

CONCLUSION

The paper presents the measured acidity values with the SenTix Sur touch electrode of steamed and unsteamed sapwood beech and false heartwood at the temperature: $t = 125 \pm 2.5$ °C during $\tau = 24$ h dried in a chamber dryer to a moisture content of $w = 10$ %.

The acidity of sapwood beech wood changed from $\text{pH} = 5.4$ to $\text{pH} = 3.3$ during the steaming process, the acidity of the false heartwood from $\text{pH} = 5.3$ to $\text{pH} = 3.4$.

The correlation between the acidity of beech wood in individual zones during the steaming process depending on the time τ of wood exposure to modification was described using mathematical equations: $\text{pH}_{\text{sapwood}} = 6.5 - 1.3043 \cdot \tau + 0.1357 \cdot \tau^2$; $\text{pH}_{\text{false heartwood}} = 6.02 - 0.8029 \cdot \tau + 0.0571 \cdot \tau^2$, which can be used to control the wood steaming process.

The pH value is a parameter that can be measured quickly and easily and is therefore advantageously used for the control and management of technological processes.

Acknowledgement:

This research was supported by the Research and Development Support Agency, project number APVV 21-0051, and at the same time, the contribution is the result of the grant scientific project VEGA 1/0256/23 - Research on the sapwood and the false heartwood of beech for the purpose of eliminating the differences in the color of the wood by steaming with saturated water steam.

REFERENCES

1. Babiak, M., Kubovský, I., Mamoňová, M. (2004). "Farebný priestor vybraných domácich drevín," In: Interaction of wood with various Forms of Energy, Technical University in Zvolen, Zvolen, Slovakia, pp. 113-117.
2. Bauch, J., Koch, G. (2001). Biologische und Chemische Untersuchungen über Holzverfärbungen der Rotbuche (*Fagus sylvatica* L.) und Möglichkeiten Vorbeugender Maßnahmen; Abschlussbericht; Bundesforschungsanstalt für Forst- und Holzwirtschaft, Universität Hamburg:Hamburg, Germany, 2001.
3. Blažej, A., Šutý, L., Košík, M., Krkoška, P. Golis, E. (1975): *Chémia dreva*. ALFA, Bratislava. 221 p.
4. Bučko, J. (1995). Hydrolyzné procesy [Hydrolysis Processes], Technical University in Zvolen, Zvolen, Slovakia.
5. Čudinov, B. S., Stepanov, V. L. (1968): Phasenzusammensetzung der Wassers in gefrorenem Holz. In: *Holztechnologie*, 9(1): 14-18 pp.
6. Dudiak, M., Dzurenda, L. (2020). Acidita (pH) termicky a hydrotermicky upravovaného bukového dreva. In: *Trieskové a beztrieskové obrábanie dreva 2020: vedecký časopis*. Zvolen: Technická univerzita vo Zvolene, 2020, s. 37-40.
7. Dudiak, M. (2021). Modification of maple wood colour during the process of thermal treatment with saturated water steam. *Acta Fac. Xylogiae Zvolen* 2021, 63, 25-34.
8. Dudiak, M. (2022). Acidita (pH) nepravého jadra a bele bukového dreva pred a po procese sušenia. *Nábytok a výrobky z dreva 2022*, Medzinárodný vedecko-odborný seminár 24. November. Technická univerzita vo Zvolene ISBN 978-80-228-3341-7
9. Dzurenda L. (2013): Modification of wood colour of *Fagus sylvatica* L. to a brown-pink shade caused by thermal treatment. *Wood research* [58] 3:475-482.

10. Dzurenda, L.; Geffert, A.; Geffertová, J.; Dudiak, M. (2020). Evaluation of the process thermal treatment of maple wood saturated water steam in terms of change of pH and color of wood. *Bioresources* 2020, 15, 2550–2559.
11. Dzurenda, L., Dudiak, M. (2021). Cross-correlation of color and acidity of wet beech wood in the process of thermal treatment with saturated steam. *Wood Res.* 2021, 66, 105–116.
12. Dzurenda, L. (2022). Mode for hot air drying of steamed beech blanks while keeping the colors acquired in the steaming process. *Acta Fac. Xylogologiae Zvolen* 2022, 64, 81–88.
13. Fengel, D., and Wegener, G. (1989). *Wood- Chemistry, Ultrastructure, Reactions*, Walter de Gruyte, Berlin, Germany.
14. Geffert, A., Geffertová, J., Dudiak, M. (2019). Direct Method of Measuring the pH Value of Wood. In: *Forests* 10(10), 852.
15. Hon, D.S.N. (2001). *Weathering and Photochemistry in Wood*. In *Wood and Cellulosic Chemistry*, 2nd ed.; Hon D.S.N., Shiraishi, N., Eds.; Marcel Dekker: New York, NY, USA, 2001; pp. 513–546.
16. Irle, M. (2012): pH and why you need to know it. *Wood Based Panels International* Available online: <http://www.wbpionline.com/features/ph-and-why-you-need-to-know-it/>.
17. Kollmann, F., and Gote, W. A. (1968). *Principles of Wood Sciences and Technology. Vol. 1. Solid Wood*, Springer Verlag, Berlin, Germany.
18. Laurova, M., Mamonova, M., Kučerova, V. (2004): Proces parciálnej hydrolyzy bukového dreva (*Fagus sylvatica* L.) parením a varením. Zvolen: TU Zvolen. 58 s.
19. Molnar, S., Tolvaj, L. (2002): Colour homogenisation of different wood species by steaming. In: *Interaction of wood with various Forms of Energy*. Technical university in Zvolen, p. 119–122.
20. Pňakovič, L., Dzurenda, L. (2015): Combustion characteristics of fallen fall leaves from ornamental trees in city and forest parks. *BioResources*, 10(3): 5563-5572. DOI: 10.15376/biores.10.3.5563-5572.
21. Račko, V., Čunderlík, I. (2010). Mature wood as a limiting factor in the formation of a false heartwood beech (*Fagus sylvatica* L.). *Acta Fac. Xylogologiae Zvolen*, 2010, 52 (1):15 – 24.
22. Samešová, D., Dzurenda, L., Jurkovič, P. (2018): Kontaminácia kondenzátu produktmi hydrolyzy a extrakcie v termickom procese farebnej modifikácie roztrúsenopórovitých listnatých drevín. In: *Trieskové a beztrieskové obrábanie dreva*, 11(1): 235–239. ISSN 2453-904X
23. Sanderman, W., Rothkamm, M. (1959): The determination of pH values of woods and their practical importance In: *Holz Roh- Werkstoff*, 17: 433-441.
24. Solár, R. (2004): *Chémia dreva*, Technická univerzita vo Zvolene, Zvolen. 102 s.
25. Sundqvist, B., Karlsson, O., Westremark, U. (2006): Determination of formic-acid and acid concentrations formed during hydrothermal treatment of birch wood and its relation to color, strength and hardness, In: *Wood Sci Technol* 40(7):549-561.
26. Trebula, P. (1986). Sušenie a hydrotermická úprava dreva [Drying and hydrothermal treatment of wood]. Zvolen: TU Zvolen, 255 p.
27. Zevenhoven, M. (2001): *Ash-forming matter in biomass fuels*. Åbo Akademi University. 88 s. ISBN 952-12-0813-9.



THE EFFECT OF STEAMING ALDER WOOD ON THE QUALITY OF THE MILLED WOOD SURFACE

Michal Dudiak – Richard Kminiak – Adrián Banski

Abstract

*The work presents the effect of steaming alder wood on the final quality of the milled wood surface. The process of steaming the investigated wood results in a targeted change in the color of the wood, which changes from the original light white-grey-orange color to fine reddish-brown to dark brown more or less saturated color shades depending on the modification temperature. The achieved color changes during the modification process were identified using coordinates in the CIE color space $L^*a^*b^*$ and described by the overall color difference ΔE^* . It has been proven that the wood steaming process reduces the roughness of the wood surface depending on the steaming temperature, which means that the quality of the wood surface increases. The reduction in the roughness of steamed alder compared to unsteamed wood was at the temperature of saturated water steam $t_I = 105 \pm 2.5$ °C by $Ra = 4.4\%$, at $t_{II} = 125 \pm 2.5$ °C by $Ra = 5.9\%$, at $t_{III} = 135 \pm 2.5$ °C by $Ra = 16.2\%$. It has been proven that by reducing the density of wood due to the temperature of saturated water vapor in the steaming process, the roughness of the wood surface decreases, which means that the milled surface is less rough compared to native wood. It was also proven by measurements that the resulting wood roughness profile is negatively affected by both the material removal parameter and the feed speed.*

Key words: alder wood, wood steaming, wood color, wood density, wood surface roughness profile.

INTRODUCTION

The quality of the machined surface is an important factor that is influenced by both technical and technological parameters of machines and tools used for cutting and machining Karagoz *et al.* (2011), Kminiak (2014), Kvietkova *et al.* (2015), Ispas *et al.* (2016), Vančo *et al.* (2017), Kaplan *et al.* (2018), Vitchev (2019), Atanasov (2021), as well as by the properties of the processed material (type of wood, wood moisture, macro-, micro-, sub-micro-structure) Rubén *et al.* (2017), Kúdela *et al.* (2018), Paridah *et al.* (2019), Chun-Won *et al.* (2023) and, last but not least, the quality of the surface also affects the marketability of the product Zhong *et al.* (2013), Sedliačiková and Moresova (2022). Authors Sandak and Negri (2005) define surface quality as a set of specific surface properties defined by ridges (peaks) and depressions. These features can also be named as surface topography. Kminiak (2014) characterizes the quality of the machined wood surface by the roughness and waviness of the surface, as well as possible damage to the wood surface by torn fibers, tool grooves, which are generally considered to be unevenness

and the result of technological operations in which the integrity of the wood is violated due to machining. The STN EN ISO 21920-2:2021 standard evaluates the surface quality parameters of materials as the difference between the unevenness of the surface (estimated from the primary profile), the roughness (estimated from the roughness profile) and the waviness (estimated from the waviness profile). According to the mentioned standard, we can define the real surface of the wood as the surface that borders the given body and separates it from the surrounding environment. In practice, to define the quality of the surface of the wood, the mean arithmetic deviation of the roughness, denoted Ra, is most often used.

According to the works of the authors Bekhta and Niemz (2003), Brischke *et al.* (2007), Esteves and Pereira (2009), González-Peña and Hale (2009), Karagoz *et al.* (2011), Barcik *et al.* (2015), Baranski *et al.* (2017), (Kučerka and Očkajová 2018), Očkajová (2019), Dudiak and Dzurenda (2021) thermal or hydrothermal treatment of wood, such as steaming, drying, or thermo-wood production technologies, also affects the quality of the treated wood surface.

The process of steaming wood with saturated moist air or saturated water vapor temporarily changes the physical and mechanical properties of wood used in its division, shaping or densification. The action of heat initiates chemical reactions in wet wood, such as: extraction of water-soluble substances, degradation of polysaccharides, cleavage of free radicals and phenolic hydroxyl groups in lignin resulting in the formation of new chromophoric groups causing a change in the color of the wood (Bučko 1995; Geffert *et al.* 2020). The steaming process and the aforementioned chemical changes create permanent physical-mechanical changes in wood properties, such as a decrease in density, a weakening of strength and an increase in wood fragility, affecting the machining process and the quality of the surface of the machined wood (Barcik *et al.* 2015; Kúdela *et al.* 2018).

Recently, the attention of research in the field of thermal treatment of wood is focused on steaming with saturated water steam for the purpose of targeted wood color to non-traditional wood shades of deciduous trees Tolvaj *et al.* (2009), Dzurenda (2014), Hadjiski and Deliiski 2016; Dzurenda *et al.* (2020), Dzurenda and Dudiak (2021), which creates a wider space for designers and constructors to use the excellent mechanical properties of the wood of deciduous trees in other non-traditional colors.

The aim of the article is to analyze the influence of *Alnus glutinosa* wood steaming regimes on the final quality of the created surface (roughness Ra) under specified cutting conditions, feed speed and amount of material removal.

MATERIALS AND METHODS

Material

Alder wood (*Alnus glutinosa*) was harvested in the research from the Kremnické vrchy locality (Slovakia). Radial blanks with the dimensions $h = 40 \text{ mm} \times \text{width } w = 80 \text{ mm} \times \text{length } l = 600 \text{ mm}$ in the number of 120 were used for the research. The blanks were divided into 4 groups, which represented 30 pieces of blanks for one group. The blanks of the 1st group were untreated (native wood). The blanks of the 2nd group were modified by the steaming process in mode I., the blanks of the 3rd group were modified by the steaming process II. and blanks of the 4th group were modified by the steaming process III.

Steaming and drying of blanks

The technological process of wood vaporization of individual wood species was carried out in a pressure autoclave APDZ 240 at a higher pressure of saturated water steam than atmospheric pressure. Temperatures of saturated water steam in individual treatment modes are shown in Table 1. Temperatures t_{\max} and t_{\min} are the temperature range in which saturated water steam is supplied to the autoclave for the implementation of the technological process. Temperature t_4 is the temperature of the saturated water steam in the autoclave after reducing the pressure of the water steam in the autoclave to atmospheric pressure, enabling the safe opening of the pressure device and the selection of samples after the specified modification time.

Table 1. Modes of modification of blanks saturated water steam.

Modes	Saturated steam temperature [°C]			Technological operation time [h]		
	t_{\min}	t_{\max}	t_4	τ_1 - phase	τ_2 - phase	Total time
Mode I	102.5	107.5	100			
Mode II	122.5	127.5	100	1.5	7.5	9.0
Mode III	132.5	137.5	100			

Native as well as steamed wood saturated water steam was dried to the final moisture content $w = 12 \pm 0.5\%$. The drying technology was realized by the low-temperature drying mode of Dzurenda (2022) with emphasis on preserving the obtained color in the steaming process.

Color measurement of modified alder wood

Identification of the color of modified wood by steaming of individual wood species, as well as unsteamed wood in the CIE $L^*a^*b^*$ color space, was determined using a Color Reader CR-10 colorimeter (Konica Minolta, Japan). The measurement was carried out on the bearing surfaces at a distance of 50 mm from the face of the blanks. A D65 light source with an illuminated area of 8 mm was used. The color was evaluated based on changes in the CIE color space $L^*a^*b^*$ on the lightness coordinate L^* and color coordinates: red color a^* , yellow color b^* .

The value of the total color difference was calculated according to the above mathematical equation in accordance with the ISO 11 664-4 standard:

$$\Delta E^* = \sqrt{(L_2^* - L_1^*)^2 + (a_2^* - a_1^*)^2 + (b_2^* - b_1^*)^2} \quad (1)$$

Where: L_{1}^* , a_{1}^* , b_{1}^* values on the coordinates of the color space of the surface of dried milled native wood,

L_{2}^* , a_{2}^* , b_{2}^* values on the coordinates of the color space of the surface of dried milled modified wood.

Density measurement of unsteamed and steamed alder wood

The density of wood in an absolutely dry state was determined according to STN 49 0108: 1993 Wood – Determination of density. For the production of samples to determine the density of unsteamed and steamed alder wood, milled blanks were used separately for each level of the wood steaming regime. 30 test bodies were randomly selected from individual groups of unsteamed and steamed blanks for each group with dimensions: thickness $h = 15$ mm; width $w = 40$ mm; length $l = 100$ mm. The produced test bodies were dried in a

laboratory oven (MEMMERT UM110m) at a temperature of $t = 103 \pm 2$ °C to a constant weight. After drying, the samples were placed in a desiccator, and then, after cooling, the wood density was measured. Measurement of the density of unsteamed and steamed alder wood by individual modes in an absolutely dry state was carried out using a digital density meter: Set for determining the density of solid substances KIT 128 from the company RADWAG (Poland) working on the principle of Archimedes' law. The density of unsteamed and steamed alder wood specimens was calculated from the equation:

$$\rho_0 = \frac{m_0}{V_0} = \frac{m_0}{\frac{m_0 - m_0^*}{\rho_{H_2O} \cdot g}} = \left(\frac{m_0}{m_0 - m_0^*} \right) \cdot (\rho_{H_2O} \cdot g) \quad [\text{kg} \cdot \text{m}^{-3}] \quad (2)$$

Where: m_0 – mass of dry sample [kg],

V_0 – volume of dry sample [m^3].

m_0^* – mass of dry sample immersed in distilled water [kg],

ρ_{H_2O} – density of distilled water at atmospheric pressure and temperature $t = 14.5$ °C,

$g = 9.81 \text{ m} \cdot \text{s}^{-2}$, the gravitational acceleration of the Earth.

Milling of blanks

Unsteamed and steamed blanks were milled on a CNC 5-axis center SCM Tech Z5 from the manufacturer SCM Group, Italy. For milling, we used the spiral milling cutter, which has the type designation F193 – 16061 from the manufacturer IGM tools and machines from the Czech Republic. It is a tool with three cutting edges with the diameter of the working surface $D = 16\text{mm}$, with the length of the working surface $B = 55\text{mm}$, the diameter of the clamping surface $d = 16\text{mm}$ and the total length $L = 110\text{mm}$. We installed the mentioned cutter in a SOBO 302680291 GM 300 HSK 63F hydraulic clamp, manufactured by Gühring KG, Germany. We oriented the samples in the CNC machining center: in the direction of the "X" axis - length, in the direction of the "Y" axis - width and in the direction of the "Z" axis - thickness. The feed velocity vector coincided with the "X" axis and the removal was within the "Y" axis.



Fig. 1 CNC 5-axis center SCM Tech Z5.

Table 2 Parameters of the wood milling process.

Parameter	Value
Feed rate (v_f)	$2 \text{ m} \cdot \text{min}^{-1}$
	$4 \text{ m} \cdot \text{min}^{-1}$
	$6 \text{ m} \cdot \text{min}^{-1}$
Depth of cut (e)	1 mm
	3 mm
	5 mm
Tool rotates (n)	18 000 rpm

Measuring the surface roughness of milled wood

We carried out non-contact measurement of surface unevenness on processed test samples using the laser profilometer LPM – 4, which was constructed at the Department of Woodworking TU in Zvolen in cooperation with the company KVANT Ltd. The LPM-4 profilometer works on the principle of triangulation laser profilometry. The Marlin F131B digital camera captures an image of the laser line at a certain angle, and based on the captured image, the cross-sectional profile of the object is subsequently evaluated. The roughness meter shown in Fig. 2. consists of an aluminum structure, which is also the supporting part and is fitted with powerful profilometer components. A horizontal beam is placed on the structure, which enables the positioning of the measuring head, which in turn enables the height adjustment and focusing of the camera (Šustek 2010).

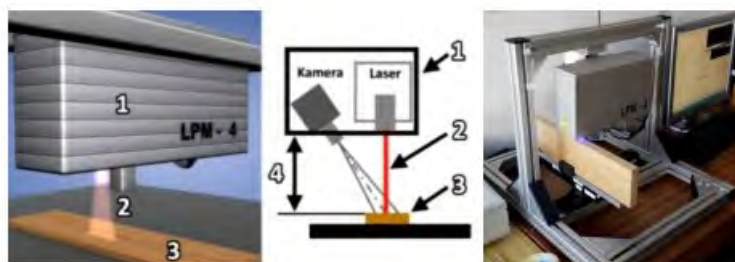


Fig. 2. Operating principle of the LPM – 4.

1 – camera, 2 – laser, 3 – sample, 4 – distance between LPM – 4 and measured object.

Statistical processing of measured data

From the measured data of the total color difference ΔE^* of the wood of the alder wood and the roughness of the wood surface, the graphic dependences $\Delta E^* = f(t)$ and $R_a = f(t)$ in the range of temperatures were determined using the program STA-TISTICA 12 (V12.0 SP2, USA): $t = 105 - 135$ °C and time $\tau = 9$ h. Program processing of the measured results partially eliminated the influence of measurement errors caused by wood heterogeneity. The measured data were processed, and the individual significance of the factors was evaluated using a multifactor analysis.

RESULTS AND DISCUSSION

The process of wood steaming in the mentioned modes changes the color of the wood from a soft pink-brown to the brown color achieved in I. and II. mode up to the dark brownish gray color shades achieved in III. mode. The saturation of wood coloring depends on the temperature of the saturated water vapor in the technological process. The color of the wood in individual steaming modes is declared in Table 2, and the values on the coordinates of the CIE color space L^*a^*b , including the total color difference ΔE^* , are given in Table 3.

Table 3 Changes in the color of the alder wood in the steaming process.


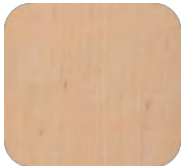
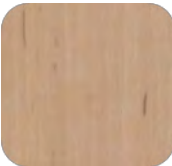

Wood	Native wood	Wood color modification modes		
		Mode I	Mode II	Mode III
Alder				

Table 4 Color of native and modified alder wood.

Wood	Coordinates CIE L*a*b*	Native wood	Wood color modification modes		
			Mode I	Mode II	Mode III
Alder	L*	78.3 ± 2.3	70.5 ± 1.9	61.7 ± 1.1	51.2 ± 1.1
	a*	9.2 ± 1.6	12.2 ± 1.0	12.6 ± 0.6	12.5 ± 0.5
	b*	22.6 ± 1.2	20.8 ± 0.8	18.4 ± 0.6	16.6 ± 0.5
	ΔE*	-	7.8	15.9	26.4

The density in the dry state of unsteamed and steamed wood by individual steaming modes is given in Table 5.

Table 5 Density of unsteamed and steamed absolutely dry alder wood.

Wood	Wood density			
	Native kg.m ⁻³	Mode I kg.m ⁻³	Mode II kg.m ⁻³	Mode III kg.m ⁻³
Alder	519.9 ± 29.9	508.5 ± 24.7	501.9 ± 21.9	498.9 ± 21.1

The results of roughness measurements on the surface of unsteamed and steamed wood by individual modes of steaming of the studied woods depending on the set parameters such as material removal and feed speed during surface milling are presented in Table 6.

Wood	Depth of cut [mm]	Feed rate [m·min ⁻¹]	Roughness [μm]			
			Native	Mode I	Mode II	Mode III
Alder	1	2	4.8 ± 0.4	4.9 ± 0.2	4.4 ± 0.5	4.1 ± 0.2
		4	5.1 ± 0.6	5.1 ± 0.1	4.9 ± 2.6	4.4 ± 0.7
		6	5.7 ± 0.8	5.4 ± 0.3	5.3 ± 0.2	4.9 ± 0.9
	3	2	6.4 ± 0.3	5.8 ± 0.9	6.1 ± 0.3	5.4 ± 0.2
		4	6.8 ± 0.8	6.6 ± 0.7	6.4 ± 0.4	5.6 ± 0.2
		6	7.2 ± 0.3	7.1 ± 0.4	6.8 ± 0.2	6.1 ± 0.2
	5	2	9.1 ± 0.7	8.9 ± 0.2	8.6 ± 0.8	8.3 ± 0.1
		4	9.2 ± 0.9	9.3 ± 0.6	8.8 ± 0.5	8.5 ± 1.1
		6	9.7 ± 0.5	9.2 ± 1.1	9.1 ± 0.9	8.9 ± 0.3

The presented roughness values of the milled wood surface shown in table 5 are the result of the action of several factors. They take into account both the technical and technological conditions of processing alder wood, as well as changes in the properties of alder wood

caused by the process of steaming with saturated water steam in individual modes. For this reason, the roughness is analyzed from the point of view of:

- a) removal of the chip taken,
- b) feed speed,
- c) changes in physico-chemical properties expressed by the overall color difference,
- d) changes in the density of alder wood in the steaming process.

a) The effect of chip removal on surface roughness Ra:

The average roughness of the surface of unsteamed alder wood with a removal of 5 mm is 1.8 times higher than with a removal of 1 mm. A similar tendency was also noted for steamed alder wood in mode III. where with a removal of 5 mm, the average roughness of the wood surface is 1.9 times higher than with a removal of 1 mm. The measured values confirm the fact that the larger the cut chip, the lower the quality of the wood surface. This phenomenon can be explained by the transformation of the chip formation process. When increasing the removal value, the thickness of the cut layer gradually increases. Within the transition plane (the plane between the old and new surface) there is a significant change in the angle of fiber cutting. At the beginning, the resultant vector of the cutting speed is similar to the inclination of the wood fibers, while at the end it is up to 90 °. The larger this angle is, the more the wood structure is broken below the parting plane (the fibers are "pulled out"). A larger removal also means a larger path of the tool in the cut. The longer this path is, the greater the force ratios are in the section (Adamčík *et al.* 2022). Authors Zhu *et al.* (2022) also proved the opposite with measurements, that the amount of removal can also reduce the roughness.

b) Effect of feed rate on surface roughness Ra:

From the analysis of the impact of removal and sliding speed according to the measured data listed in Table 5 shows that the surface roughness of the milled wood was more influenced by the size of the material removal than by the feed speed. This is confirmed numerically by the data that while the roughness of the surface of unsteamed alder wood at a feed of 6 m.min⁻¹ is Ra = 9.7 μm at a removal of 5 mm, while at a feed of 2 m.min⁻¹ it is Ra = 9.1 μm, which is ΔRa = 0.6 μm less.

A comparison of the average data due to removal on the surface roughness in the interval of removal values 1-5 mm and a sliding speed of 2-6 m.min⁻¹ shows that while the difference in surface roughness of unsteamed alder wood due to removal is ΔRa = 4.1mm, the difference average values of the surface roughness due to the sliding speed is ΔRa ≈ 0.6 mm. When comparing the average data on the effect of removal on surface roughness in the interval of removal values of 1-5 mm and sliding speed of 2-6 m.min⁻¹ for steamed alder wood in individual modes, we can conclude that the temperature of saturated water steam has no effect in terms of sliding speed on surface roughness compared to the values of native wood.

c) The influence of the change in physico-chemical properties expressed by the overall color difference:

From the achieved physico-chemical changes in wood manifested by a change in color to the roughness of the surface due to steaming, it can be said that the roughness Ra of the surface of steamed and milled wood at a higher temperature and a greater degree of darkening and browning is smaller than that of steamed wood or steamed at a lower temperature than declared by Fig. 3.

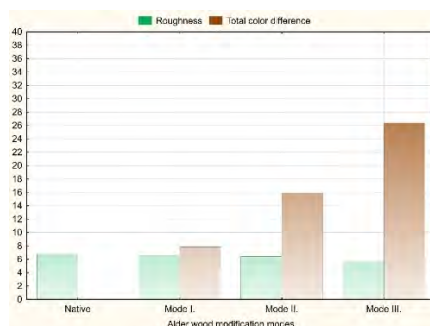


Fig. 3 Graphic representation of the influence of the temperature of saturated water steam on the overall color difference and roughness of the surface of the milled wood at a removal of 3 mm and a feed speed of $4 \text{ m} \cdot \text{min}^{-1}$.

From the average roughness values of the milled surface of alder wood and the change in color of the steamed wood depending on the temperature of the saturated steam used in the steaming process, it clearly follows that the roughness of the milled surface decreases as the temperature increases. If the average roughness of the milled surface of unsteamed alder wood at a removal of 3 mm is $R_a = 6.8 \text{ } \mu\text{m}$, then the roughness of the milled surface of alder wood of a pinkish-brown color acquired by steaming mode I at the temperature of saturated water steam $t_I = 105 \pm 2.5 \text{ } ^\circ\text{C}$ is reduced by $R_a = 4.4\%$, the roughness of brown alder wood acquired by steaming mode II. at $t_{II} = 125 \pm 2.5 \text{ } ^\circ\text{C}$ it decreases by $R_a = 5.9\%$, the roughness of steamed alder wood of a dark brownish gray color acquired during steaming mode III with a temperature of $t_{III} = 135 \pm 2.5 \text{ } ^\circ\text{C}$ decreased by $R_a = 16.2\%$.

The decrease in the roughness of the steamed wood can be attributed to the increased brittleness of the wood due to the loss of amorphous polysaccharides (Esteves and Pereira 2009). The fragility of steamed wood causes the protrusions to break during the cycloidal movement of the tool in the machining process, rather than tearing off the fibers. This fact results in the creation of a milled surface with less roughness. Authors Vančo *et al.* (2017) state that the roughness of thermally treated wood R_a up to the thermal treatment temperature $t = 160 \text{ } ^\circ\text{C}$ is lower than the roughness of native wood. From the thermal treatment temperature above $160 \text{ } ^\circ\text{C}$, it increases, and at a temperature of $210 \text{ } ^\circ\text{C}$, the roughness is even higher than the roughness of native wood.

d) The effect of changing the density of alder wood in the steaming process on the surface roughness R_a :

The average value of the density of unsteamed alder wood in the dry state is $\rho = 519.9 \pm 29.9 \text{ kg} \cdot \text{m}^{-3}$. The value coincides with the density of alder wood reported in the work (Liepiņš *et al.* 2023). The process of steaming wood with saturated steam in the temperature range $t = 105 - 135 \text{ } ^\circ\text{C}$ reduces the density of alder wood by 2.2% in mode I, mode II. by 3.5% and steam mode III. by 4.1% Dudiak and Dzurenda (2021), Liu *et al.* (2022).

From the comparison of the measured values of roughness of alder wood in Table 5 in relation to the density of unsteamed wood and steamed wood by individual modes, it is also possible to analyze the effect of the change in density on the surface roughness of the milled wood, as declared in Fig. 4. In our case, the average roughness of the surface of non-steamed alder wood when removing 3 mm is $R_a = 6.8 \text{ } \mu\text{m}$, which is compared to the roughness of the surface of steamed alder wood by mode I at temperature $t = 105 \pm 2.5 \text{ } ^\circ\text{C}$ with a value of $R_a = 6.5 \text{ } \mu\text{m}$ is lower by 4.4% and for steamed alder wood by mode III.

with temperature $t = 135 \pm 2.5$ °C lower by 16.2%. A similar reduction in the roughness of modified beech, birch and maple wood compared to native wood is also reported by Dudiak *et al.* (2024).

The average moisture of sapwood beech determined by the gravimetric method before entering the steaming process was $58.6 \pm 5.2\%$, the moisture of the false heartwood before the steaming process was $48.1 \pm 4.5\%$. After modification, all blanks were dried in a chamber hot air dryer to a moisture content of $10.0 \pm 2\%$.

From the measured results of wood moisture, it follows that the wood was sufficiently wet, while the moisture requirement was met, that the wood before entering the pressure steaming process must contain moisture higher than $BNV w \geq 30\%$ in order to achieve the desired effect of color modification.

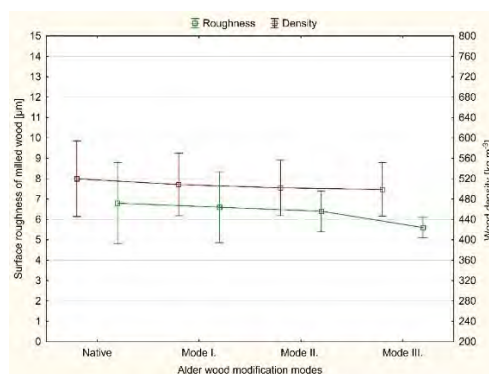


Fig. 4 Dependence of the density and roughness of the milled wood surface at a removal of 3 mm and a feed speed of $4 \text{ m} \cdot \text{min}^{-1}$ on the temperature of saturated water steam.

From the presented values of the roughness R_a of alder wood, it follows that as the density decreases, the surface roughness expressed in the form of the R_a value decreases, as can also be seen in Fig. 4. The stated findings are not in agreement with the works of the authors: Siklienka *et al.* (2008), Paridah *et al.* (2019), Chun-Won *et al.* (2023), who state that surface roughness decreases with increasing wood density. On the contrary, the authors Karagoz *et al.* (2011), Gochev (2017), Atanasov (2021) state that the surface roughness is more influenced by the technical-technological parameters of woodworking, such as: removal and sliding speed of the cutting tool, than the density of the wood.

The comparison of the surface roughness of the individual modified wood species clearly shows that the surface roughness decreases on average in the same way due to wood steaming in all investigated wood species compared to the surface roughness of the native wood, however, a more significant decrease in the surface roughness of the modified wood was recorded in the case of alder wood in the third mode. The process of wood modification with saturated water steam in order to change the color of the wood has a positive effect on the roughness profile of the milled wood surface.

CONCLUSION

The work presents the results of the color change of alder wood in the process of wood modification by steaming with saturated steam at temperatures: $t_I = 105 \pm 2.5$ °C, $t_{II} = 125 \pm 2.5$ °C and $t_{III} = 135 \pm 2.5$ °C during $\tau = 9$ h of steaming. The work also presents the results

of the surface roughness profile of native and modified wood, as well as the influence of material removal parameters and feed speed on the resulting roughness of the wood surface. The technological process of modification by steaming alder wood results in a change in color from the original light white-gray-orange color to fine red-brown to dark brown more or less saturated color shades depending on the modification temperature. The color changes achieved during the modification process are identified using coordinates in the color space CIE L*a*b* and described by the total color difference ΔE^* .

The alder wood steaming process reduces the density and roughness of the wood surface depending on the steaming temperature, which means that the surface quality of the modified wood increases. The reduction in roughness compared to native wood was in the modification process at the temperature of saturated water steam $t_I = 105 \pm 2.5$ °C by $R_a = 4.4\%$, at $t_{II} = 125 \pm 2.5$ °C by $R_a = 5.9\%$, at $t_{III} = 135 \pm 2.5$ °C by $R_a = 16.2\%$. It can be concluded that the roughness decreased due to the loss of amorphous portions of polysaccharides, which ultimately affects the mechanical properties of the wood. The roughness of the milled surface of the native and modified wood of the studied trees is negatively affected by the size of the material removal, as well as the speed of the workpiece, which makes the milled surface of lower quality.

Acknowledgement:

This research was supported by the Research and Development Support Agency, project numbers APVV-17-0456 and APVV-SK-PL-21-0059.

REFERENCES

- 1 Adamčík, L.; Kminiak, R.; Banski, A. 2022. The effect of thermal modification of beech wood on the quality of milled surface. *Acta Fac. Xylologiae Zvolen*, 64(2): 57–67.
- 2 Atanasov, V. 2021. Experimental research on the cutting force during longitudinal milling of solid wood and wood-based composite. *Acta Fac. Xylologiae Zvolen*, 63, 73–84.
- 3 Baranski, J.; Klement, I.; Vilkovská, T.; Konopka, A. 2017. High Temperature Drying Process of Beech Wood (*Fagus sylvatica* L.) with Different Zones of Sapwood and Red False Heartwood. *BioResources*, 12, 1861–1870.
- 4 Barčík, Š.; Gašparík, M. 2014. Effect of tool and milling parameters on the sizedistribution of splinters of planed native and thermally modified beech wood. *BioResources*, 9, 1346–1360.
- 5 Bekhta, P.; Niemz, P. 2003. Effect of High Temperature on the Change in Color, Dimensional Stability and Mechanical Properties of Spruce Wood" *Holzforschung*, vol. 57, no. 5, 539-546.
- 6 Brischke, C.; Welzbacher, C.R.; Brandt, K.; Rapp, A.O. 2007. Quality control of thermally modified timber: Interrelationship between heat treatment intensities and CIE L*a*b* color data on homogenized wood samples. *Holzforschung: international journal of the biology, chemistry, physics and technology of wood* 61, 19–22.
- 7 Bučko, J. 1995. *Hydrolysis Processes*; Technical University in Zvolen: Zvolen, Slovakia.
- 8 Dudiak, M.; Dzurenda, L. 2021. Changes in the Physical and Chemical Properties of Alder Wood in the Process of Thermal Treatment with Saturated Water Steam. *Coatings*, 11, 898.

- 9 Dudiak, M.; Kminiak, R.; Banski, A.; Chuchala, D. 2024. The Effect of Steaming Beech, Birch and Maple Woods on Qualitative Indicators of the Surface. *Coatings*, 14, 117.
- 10 Dzurenda, L. 2014. Colouring of BeechWood during Thermal Treatment using SaturatedWater Steams. *Acta Fac. Xylogologiae Zvolen*, 56, 13–22.
- 11 Dzurenda, L.; Geffert, A.; Geffertová, J.; Dudiak, M. 2020. Evaluation of the Process Thermal Treatment of MapleWood SaturatedWater Steam in Terms of Change of pH and Color ofWood. *BioResources*, 15, 2550–2559.
- 12 Dzurenda, L.; Dudiak, M. 2021. Cross-correlation of color and acidity of wet beech wood in the process of thermal treatment with saturated steam. *Wood Res.* 66, 105–116.
- 13 Dzurenda, L. 2022. Mode for hot air drying of steamed beech blanks while keeping the colours acquired in the steaming process. *Acta Facultatis Xylogologiae Zvolen*, 64, 81–88.
- 14 Esteves, B.; Pereira, H. M. 2009. Wood modification by heat treatment: A review. *BioResources* 4(1), 370-404.
- 15 Geffert, A.; Geffertová, J.; Výbohová, E.; Dudiak, M. 2020. Impact of Steaming Mode on Chemical Characteristics and Colour of Birch Wood. *Forests*, 11, 478.
- 16 Gochev, Z.; Vukov, G.; Vitchev, P.; Atanasov, V.; Kovatchev, G. 2017. Modeling and experimental study of the processes in longitudinal milling of solid wood. *Theme*, 22, 76.
- 17 González-Peña, M. M.; Hale, M. D. 2009. Colour in thermally modified wood of beech, Norway spruce and Scots pine. Part 2: Property predictions from colour changes. *Holzforschung* 63(4):394-401.
- 18 Hadjiski, M.; Deliiski, N. 2016. Advanced Control of theWood Thermal Treatment Processing. *Cybern. Inf. Technol.* 16, 176–197.
- 19 Chun-Won, K.; Kazuharu, H.; Eun-suk, J.; Haradhan, K. 2023. Relationship betweenwood anatomical features and surface roughness characteristics. *Wood Research* 68(3):455-464.
- 20 Ispas, M.; Gurau, L.; Campean, M.; Hacibektasoglu, M.; Racasan, S. 2016. Milling of heat-treated beech wood (*Fagus sylvatica* L.) and analysis of surface quality. *BioRes.* 11(4), 9095-9111.
- 21 Kaplan, L.; Kvietková, M.; Sikora, A.; Sedlecký, M. 2018. Evaluation of the effect of individual paramaters of oak wood machining and their impact on the values of waviness measured by a laser profilometer. *Wood Res.* 63, 127–140.
- 22 Karagoz, U.; Akyildiz, M.H.; Isleyen, O. 2011. Effect of heat treatment on surface roughness of thermal wood machined by CNC. *ProLigno*, 7(4): 50-58.
- 23 Kminiak, R. 2014. Effect of the saw blade construction on the surface quality when transverse sawing spruce lumber on crosscut miter saw. *Acta Fac. Xylogologiae Zvolen* 2014, 56, 87–96.
- 24 Kučerka, M.; Očkajová, A. 2018. Thermowood and granularity of abrasive wood dust. *Acta Fac. Xylogologiae Zvolen*, 60, 43–51.
- 25 Kúdela, J.; Mrenica, L.; Javorek, L'. 2018. The influence of milling and sanding on wood surface morphology. *Acta Fac. Xylogologiae Zvolen*, 60, 71–83.
- 26 Kvietková, M.; Gaff, M.; Gašparík, M.; Kaplan, L. 2015. Barcik, Š. Surface quality of milled birch wood after thermal treatment at various temperatures. *BioResources*, 10, 6512–6521.
- 27 Liepiņš, K.; Liepiņš, J.; Ivanovs, J.; Bārdule, A.; Jansone, L.; Jansons, Ā. V. 2023. Variations in the Basic Density of the Tree Components of Gray Alder and Common Alder. *Forests*, 14, 135.

- 28 Liu, H.; Li, Z.; Zhang, X.; Tang, B.; Wan, C.; Wang, K. 2022. The Effect of Different Moderate Thermal Modification Durations on the Wood Properties of American Alder. *Materials*, 15, 8839.
- 29 Očkajová, A.; Barčík, Š.; Kučerka, M.; Koleda, P.; Korčok, M.; Vyhnáliková, Z. 2019. Wood dust granular analysis in the sanding process of thermally modified wood versus its density. *BioResources*, 14, 8559–8572.
- 30 Paridah, M.T.; Alia-Syahirah, Y.; Hamdan, H.; Anwar, U.M.K.; Nordahlia, A.S.; Lee, S.H. 2019. Effects of anatomical characteristics and wood density on surface roughness and their relation to surface wettability of hardwood. *Journal of Tropical Forest Science (JTFS)*, 31(3), 269–277.
- 31 Rubén, L.; Sanz-Lobera, A.; Villasante, A.; López-Espí, P.; Martínez-Rojas, J.A.; Alpuente, J.; Sánchez-Montero, R.; Vignote, S. 2017. Effect of the anatomical structure, wood properties and machining conditions on surface roughness of wood. *Maderas, Cienc. tecnol.* 19 (2), 203–212.
- 32 Sandak, J.; Negri, M. 2005. Wood surface roughness—What is it? In *Proceedings of the 17th International Wood Machining Seminar (IWMS 17)*, Rosenheim, Germany, 26–28 September 2005; pp. 242–250.
- 33 Sedliačiková, M.; Moresová, M. 2022. Are consumers interested in colored beech wood and furniture products? *Forests*, 13, 1470.
- 34 Siklienka, M.; Šustek, J.; Hajník, I., 2008. Quantification of surface unevenness using a laser profilometer during sawing on a horizontal band saw. In: *Chip and chipless woodworking processes*. Zvolen: Technická univerzita vo Zvolene, 207–212. ISSN 1339-8350.
- 35 STN EN ISO 21920-2:2021; Geometrical Product Specifications (GPS)—Surface Texture: Profile—Part 2: Terms, Definitions and Surface Texture Parameter. International Organization for Standardization: Geneva, Switzerland, 2022.
- 36 Šustek, J. 2010. LPM laser profilometer with horizontal displacement for tracking surface unevenness. In *Chip and Chipless Woodworking Processes*; Technical University in Zvolen: Zvolen, Slovakia, 187–192. ISSN 1339-8350.
- 37 Tolvaj, L.; Nemeth, R.; Varga, D.; Molnar, S. 2009. Colour homogenisation of beech wood by steam treatment. *Drewno*, 181, 5–17.
- 38 Vančo, M.; Mazáň, A.; Barčík, Š.; Rajko, L.; Koleda, P.; Vyhnáliková, Z.; Safin, R. 2017. Impact of Selected Technological, Technical, and Material Factors on the Quality of Machined Surface at Face Milling of Thermally Modified Pine Wood. *BioResources*, 12, 5140–5154.
- 39 Vitchev, P. 2019. Evaluation of the surface quality of the processed wood material depending on the construction of the wood milling tool. *Acta Fac. Xylogologiae Zvolen*, 61, 81–90.
- 40 Zhong, Z.W.; Hizirolu, S.; Chan, C. 2013. Measurement of the surface roughness of wood based materials used in furniture manufacture. *Measurement*, 46, 1482–1487.
- 41 Zhu, Z.; Jin, D.; Wu, Z.; Xu, W.; Yu, Y.; Guo, X.; Wang, A.X., 2022. Assessment of Surface Roughness in Milling of Beech Using a Response Surface Methodology and an Adaptive Network-Based Fuzzy Inference System. *Machines*. 10(567), 567.



HEAT CONSUMPTION FOR THE ELIMINATION OF COLOR DIFFERENCES OF BEECH SAPWOOD AND FALSE HEARTWOOD BY THE STEAMING PROCESS

Ladislav Dzurenda – Michal Dudiak

Abstract

The article presents the results of heat consumption for the steaming process of beech wood for the purpose of eliminating the color differences between sapwood and false heartwood in $h = 40$ mm thick lumber with saturated water steam in the temperature range: $t = 105 - 120$ °C in a pressure autoclave AZ 240 steaming modes I., II. and III.

Normative of heat consumption Q_{TZN} for the steaming process of beech wood by mode I. unifying the color of the wood from sapwood and false heartwood to pale brown with coordinates $L^ = 63.4 \pm 2.3$, $a^* = 13.0 \pm 1.4$; $b^* = 19.1 \pm 1.6$ in the color space CIE $L^*a^*b^*$ is $Q_{TZN-I} = 102.71 \text{ kWh.m}^{-3}$. Normative heat consumption for the process of steaming mode II. to brown color with color space CIE $L^*a^*b^*$ values: $L^* = 59.0 \pm 2.1$; $a^* = 12.9 \pm 1.4$; $b^* = 18.8 \pm 1.7$ is $Q_{TZN-II} = 113.22 \text{ kWh.m}^{-3}$ and for steam mode III. reaching a dark brown-gray color with values on the coordinates of the color space CIE $L^*a^*b^*$: $L^* = 57.5 \pm 2.0$; $a^* = 13.4 \pm 1.2$; $b^* = 18.8 \pm 1.5$ is $Q_{TZN-III} = 116.68 \text{ kWh.m}^{-3}$.*

The dependence of the norm Q_{TZN} of heat consumption on the temperature of saturated water steam in the process of unifying the colors of beech sapwood and false heartwood is described by the equation: $Q_{TZN} = -0,0239.t^2 + 6,3163.t - 296,64$.

Key words: *beech wood, sapwood, false heartwood, color, steaming, saturated water steam, thermal energy consumption standard*

INTRODUCTION

The wood of *Fagus sylvatica* L. belongs to the scattered-porous, coreless woods with the possibility of forming a false heartwood. Some older trees have wood of a different color in the center of the trunk, referred to as false heartwood. The color of beech wood in the zone of sapwood and mature wood is light whitish-grey, or white pink Nečesný (1959), Makovíny (2010), Dzurenda – Dudiak (2022) and in the false heartwood brown-red Nečesný (1959), Dzurenda – Dudiak (2023). Author Dzurenda (2023) numerically documented the visual color differences between the color of beech sapwood and wood with false heartwood through the values on the coordinates of the color space CIE $L^*a^*b^*$ and the total color difference ΔE^* . The sapwood color is white with lightness $L^* = 79.2 \pm 2.4$ and values on the chromatic coordinates $a^* = 8.3 \pm 1.6$, $b^* = 19.1 \pm 1.8$. The color of the false heartwood is described by the following values: $L^* = 65.8 \pm 3.8$, $a^* = 11.6 \pm 1.9$, $b^* = 19.5 \pm 1.5$. The color difference between the color of the wood of the false heartwood and the color of the sapwood, expressed through the total color difference, is $\Delta E^* = 18.1$.

Within the categorization of color difference, the value total color difference $\Delta E^* = 18.1$ belongs to the category of significantly different colors. The difference in the color of the wood of the false heartwood from the color of the sapwood is the reason for the removal of sawmill assortments with a share of wood of the false heartwood from the production of bent furniture, sports tools and partly construction and carpentry products.

Steaming of wood is a technological process in which wet wood with a moisture content of $w \geq 40\%$ is heated by the action of heat in the form of saturated moist air or saturated water steam and changes its physical, mechanical and chemical properties. Temporary physical-mechanical changes are used in the production of veneers, plywood, bent furniture, or pressed wood. Nikolov *et al.* 1980; Sergovskij and Rasev 1987; Lawnniczak 1995; Trebula 1996; Dzurenda – Deliiski (2019). Permanent chemical changes manifested, among other things, by a change in color, are used to change the color of the wood to more or less distinct shades Deliiski (1991), Tolvaj *et al.* (2009), Dzurenda (2014), Milić *et al.* (2015), Geffert *et al.* (2017), Dzurenda – Dudiak (2022).

The aim of this contribution is to determine the heat consumption of the steaming modes for the purpose of unifying the colors of beech wood with sapwood and false heartwood with saturated water steam at temperatures $t_I = 105 \pm 2.5$ °C, $t_{II} = 115 \pm 2.5$ °C and $t_{III} = 120 \pm 2.5$ °C.

MATERIALS AND METHODS

On the basis of experimental research aimed at analyzing the influence of temperature and length of steaming time on the unification of the color of beech sapwood and wood of false heartwood presented in the work Dzurenda – Dudiak (2024), 3 modes of steaming beech wood with different darkening of the wood were determined. Due to the technological conditions of steaming, mode I. at the steaming temperature $t_I \approx 105$ °C, beech wood acquires a pale brown color with values on the coordinates of the color space: $L^* = 63.4 \pm 2.3$; $a^* = 13.0 \pm 1.4$; $b^* = 19.1 \pm 1.6$. Mode II. at the steaming temperature $t_{II} \approx 115$ °C, the color of the sapwood and the false heartwood becomes brown with the values on the coordinates: $L^* = 59.0 \pm 2.1$; $a^* = 12.9 \pm 1.4$; $b^* = 18.8 \pm 1.7$. Dark brown-gray color with values on the coordinates: $L^* = 57.5 \pm 2.0$; $a^* = 13.4 \pm 1.2$; $b^* = 18.8 \pm 1.5$ acquired by beech wood through the mode III. steaming process at the vaporization temperature $t_{III} \approx 120$ °C. Color of beech sapwood and false heartwood before steaming fig. 1a) and after steaming with saturated water vapor in individual modes is shown in Fig.1b),1c),1d).

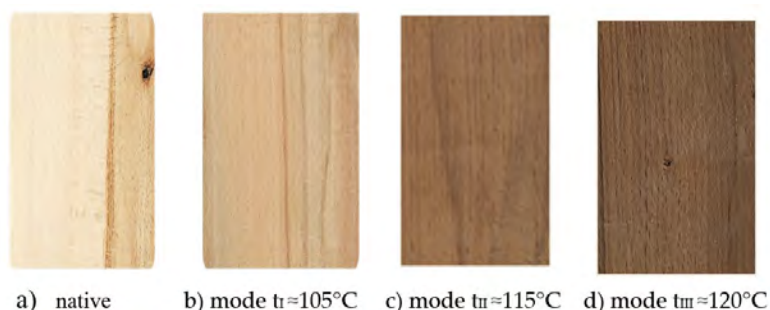


Fig.1 Wood color of steamed beech sapwood and false heartwood under steaming conditions according to individual steaming modes.

Tab. 1. Modes for steaming beech wood with saturated water steam

Modes	Saturated steam temperature [°C]			Steaming time [h]			Total time
	t _{max}	t _{min}	t ₄	τ ₀ heating	τ ₁ steaming	τ ₃ cooling	
Mode I	102.5	107.5	100	3.5	18.0	0.5	22.0
Mode II	112.5	117.5	100	3.5	15.0	0.5	19.0
Mode III	117.5	122.5	100	3.5	9.0	0.5	13.0

To determine the heat consumption in the technological process, the so-called model is applied technically justifiable standard (TZN), which is a specific heat consumption expressing the objectively necessary amount of heat consumed to produce a unit of the product Dzurenda – Deliiski (2008). The standard of the technically justified standard of color homogenization of beech wood is described by the equation:

$$Q_{TZN} = \frac{Q_D + Q_A + Q_I + Q_S + Q_P + Q_K}{V_D}, \quad (1)$$

Where: Q_D – heat required for heating colored homogenized wood, kWh;
 Q_A – heat required to heat the structure of the autoclave material, kWh;
 Q_I – heat required to heat the autoclave insulation, kWh;
 Q_S – heat required to cover heat losses from the surface of the pressure autoclave emitted during the technological process into the atmosphere, kWh;
 Q_P – heat removed by saturated steam after opening the autoclave during its emptying, kWh;
 Q_K – heat removed by condensate from the pressure autoclave, kWh;
 V_D – volume of steamed wood in a pressure autoclave, m³.

The stated balance of heat consumption was processed into the EXCEL program Dzurenda (2016), which in the form of a numerical table based on:

- a) technical parameters of the pressure autoclave,
- b) properties of steamed wood,
- c) parameters of the steaming mode,

provides information on: a) Q_{TZN} - technically feasible consumption standard. of heat per 1 m³ of steamed wood,

- b) Q_i - heat consumption for individual heat items of the technological process.

RESULTS AND DISCUSSION

The heat consumption of individual items of the steaming autoclave AZ 240 for steaming 16 m³ of beech lumber with a moisture content of $W_a \approx 60\%$ with saturated water steam and the Q_{TZN} standard is given in the following Table 3.

Tab. 2 Heat consumption of the process of color homogenization of beech wood sapwood and false heartwood in autoclave AZ 240 and Q_{TZN} standards.

Title of heat consumption item	Symbol	Mode I	Mode II	Mode III
		[kWh]		
Heat for heating steaming wood	Q_D	1 118.47	1 247.50	1 312.83
Heat for heating the construction material of the autoclave	Q_A	158.33	175.00	183.33
Heat for heating the autoclave insulation	Q_I	22.95	25.37	26.57
Heat to cover the heat losses of the pressure autoclave	Q_S	70.86	64.33	35.94
Heat removed by saturated steam after opening the autoclave during its emptying	Q_P	15.26	15.26	15.26
Heat removed by condensate from the pressure autoclave	Q_K	257.53	284.13	292.86
Total heat consumption for steaming wood in an autoclave	Q_i	1 643.41	1 811.58	1 866.80
Technically justifiable standard of heat consumption [kWh.m ⁻³]	Q_{TZN}	102.71	113.22	116.68

The dependence of the increase in heat consumption on the temperature of saturated water steam in the technological process of color homogenization of beech sapwood and false heartwood, is shown in Fig. 2.

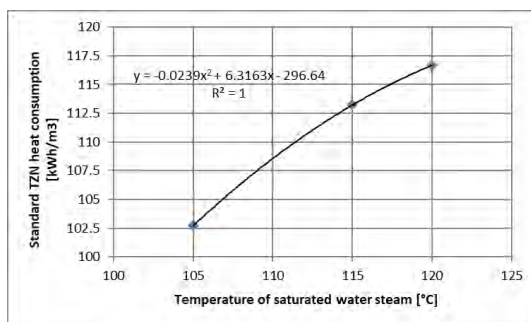


Fig. 2. Dependence of heat consumption on the process of unifying the colors of sapwood and false heartwood beech on temperature

From the analysis of the share of individual items of heat consumption in Table 2, it follows that the largest heat consumption for the color unification of beech lumber with wood with a false heartwood of thickness $h = 40$ mm in the AZ 240 autoclave is heat for heating steamed wood: $Q_D = 1\,226.3$ kWh (69.2% of the total heat consumption). Heat consumption for heating the structure of the steaming autoclave $Q_A + Q_I = 197.2$ kWh (11 % of the total heat consumption) and heat consumption covering heat losses of the pressure autoclave in the form of drained condensate $Q_K = 278.2$ kWh (15.7 % of the total heat consumption). The fact that more than 2/3 of the supplied heat is directly used for the implementation of the technological process testifies to the high efficiency of heat use in the thermal process of color homogenization of wood in pressure autoclaves. The stated

value is 3 times higher than the direct use of heat in wood steaming technologies implemented at atmospheric pressure in steam pits, chambers and bells Lawnniczak (1995), Trebula (1996), Dzurenda – Deliiski (2019).

It follows from the heat consumption balance of individual steaming modes that an increase in the temperature of saturated steam from temperature $t_I = 105\text{ °C}$ to temperature $t_{III} = 120\text{ °C}$, i.e., at $\Delta t = 15\text{ °C}$ despite shortening the time of the technological process by $\tau = 9\text{ h}$ is reflected in the increase in the total heat consumption of the steaming process by mode III. compared to mode I. by 13.6%.

CONCLUSION

The paper presents heat consumption in the form of a technically justifiable Q_{TZN} standard for the steaming process of beech wood, removing the differences in the color of sapwood and false heartwood. Normative of heat consumption Q_{TZN} for the process of color unification of beech wood with saturated water steam in autoclave AZ 240 according to mode I to a pale brown color with values on the coordinates of the color space CIE $L^*a^*b^*$: $L^* = 63.4 \pm 2.3$, $a^* = 13.0 \pm 1.4$; $b^* = 19.1 \pm 1.6$ is $Q_{TZN-I} = 102.73\text{ kWh.m}^{-3}$. Q_{TZN} norm for the process of color homogenization to brown with values on the coordinates of the color space CIE $L^*a^*b^*$: $L^* = 59.0 \pm 2.1$; $a^* = 12.9 \pm 1.4$; $b^* = 18.8 \pm 1.7$ according to mode II is $Q_{TZN-II} = 113.22\text{ kWh.m}^{-3}$ and the Q_{TZN} norm for the process of color unification of sapwood and false heartwood to a dark brown-gray color with values on the color coordinates: $L^* = 57.5 \pm 2.0$; $a^* = 13.4 \pm 1.2$; $b^* = 18.8 \pm 1.5$ according to mode III is $Q_{TZN-III} = 116.68\text{ kWh.m}^{-3}$.

From the analysis of the share of individual items of heat consumption, it follows that the largest heat consumption of the technological process is the heat consumption for heating steamed wood 69.2 %. Other heat consumption for the implementation of the technological process is lower. The heat consumption for heating the structure of the steaming autoclave is 11% and the heat consumption for covering the heat losses of the pressure autoclave in the form of drained condensate is 15.7 %.

The effect of an increase in the temperature of saturated water steam from temperature $t_I = 105\text{ °C}$ to $t_{III} = 120\text{ °C}$, i.e., o $\Delta t = 15\text{ °C}$, despite shortening the time of the steaming process by $\Delta\tau = 9\text{ h}$, it is reflected in an increase in heat consumption in the process of unifying the colors of sapwood and false heartwood from $Q_{TZN-I} = 102.73\text{ kWh.m}^{-3}$ to $Q_{TZN-III} = 116.68\text{ kWh.m}^{-3}$ i.e. by 13.6%.

The dependence of the norm Q_{TZN} of heat consumption on the temperature of saturated water steam in the process of unifying the colors of beech sapwood and false heartwood is described by the equation: $Q_{TZN} = -0.0239.t^2 + 6.3163.t - 296.64$.

Acknowledgement:

This experimental research was prepared within the grant project: APVV-21-0051 “*Research of false heartwood and sapwood of Fagus sylvatica L. wood in order to eliminate color differences by the process of thermal treatment with saturated water steam*” and VEGA 1/0256/23.

REFERENCES

- Deliiski, N. (1991): Metod dlja ocenki stepeni oblagoraživanja bukovych pilomaterialov vo vremja ich proparki. *Current problems and perspectives of beech lumber drying* 1991. ES-VŠLD in Zvolen (Slovakia), 37–44.
- Dzurenda, L., Deliiski, N. (2008): Matematický model pre stanovenie normatívu spotreby tepla na farebnú homogenizáciu bukových prírezov v tlakových autokaroch. In: *Trieskové a beztrieskové obrábanie dreva 2008*, s. 307 – 314.
- Dzurenda, L. (2014): Colouring of Beech Wood during Thermal Treatment using Saturated Water Steam. *Acta Fac. Xylogologiae Zvolen* 2014, 56, 13–22.
- Dzurenda, L. (2016): Numeric model of the normative consumption of heat for the colour homogenisation of wood in pressure autoclaves. In: *AIP Conf Proc.* 1745, 020008
- Dzurenda, L., Deliiski, N. (2019): Tepelné procesy v technológiách spracovania dreva. Zvolen: Vydavateľstvo TU, 283 s. ISBN 978-80-228-3159-5.
- Dzurenda, L. Dudiak, M. (2022): Modifikácia farby dreva v procese parenia sýtou vodnou parou. Zvolen: Vydavateľstvo TU Zvolen, 120 s. ISBN 978-80-228-3318-9.
- Dzurenda, L. (2023): Natural Variability of the Color of Beech Wood in the Color Space CIE L*a*b*. In: *Forests* 14, 1103. doi.org. 10.3390/f14061103.
- Dzurenda, L. Dudiak, M. (2023): Color diversity of beech wood with a false heartwood in the color space CIE L*a*b*. In: *Wood Research* 68(4): 68(4): 792-801 pp.
- Dzurenda, L., Dudiak, M. (2024): Homogenization of the color of beech sapwood and false heartwood by the steaming process. In: *Forests*, 15, 1009. doi.org.10.3390/f15061009.
- Geffert, A., Vybohová, E., Geffertová, J. (2017): Characterization of the changes of colour and some wood components on the surface of steamed beech wood. *Acta Facultatis Xylogologiae Zvolen* 59(1): 49–57.
- Lawniczak, M. (1995): Zarys hydrotermicznej i plastycznej obróbki drewna. Czesc I. – Warzenie i parzenie drewna. Poznan, 149 p.
- Makovíny, I. (2010): Úžitkové vlastnosti a použitie rôznych druhov dreva. Zvolen: TU Zvolen, 104 s.
- Milić, G.; Todorović, N.; Popadić, R., (2015): Influence of steaming on drying quality and colour of beech timber. *Glas. Šumar. Fak.* 2015, 112, 83–96. [CrossRef]
- Nikolov, S., Rajchev, A., Deliiski, N. (1980). *Proparvane na drvesinata*. Sofia: Zemizdat, 174 p.
- Nečesaný, V. (1959): *Jádro buka, štruktúra, vznik a vývoj*. Vydavateľstvo Slovenskej akadémie vied, Bratislava, 256 s.
- Sergovskij, P. S., Rasev, A. I. (1987). *Gidrotermičeskaja obrabotka i konservirovanije drevesiny*. Lesnaja promyšlennost, Moskva, 360 p.
- Tolvaj, L.; Nemeth, R.; Varga, D.; Molnar, S. (2009): Colour homogenisation of beech wood by steam treatment. *Drewno* 2009, 52, 5–17.
- Trebula, P. (1996). *Sušenie a hydrotermická úprava dreva*. Zvolen: TU Zvolen, 255 p.



DUST MONITORING IN URBAN HEATING PLANTS ON FOREST BIOMASS

Miloš Gejdoš – Daniel Tomčík

Abstract

The process of production, storage, handling, and consumption of forest biomass is characterized by a relatively high concentration of dust, consisting mainly of wood dust, dirt on wood, and, during operation, spores of molds and fungi. The aim of the work was to monitor the dustiness of the working environment in the operation of a biomass heating plant and to assess potential health risks for human health. Dust measurement was carried out in the operation of the heating plant before the end of the heating period on 21. 03. 2024. As a reference measurement, it was conducted in the inner city of Zvolen on 26. 03. 2024 under similar weather conditions. The concentration and abundance of dust particles of sizes 2.5 μm and 10 μm were measured. The technical reference value for the risk assessment of dust as a carcinogenic factor was not exceeded during these measurements. However, when assessing the levels of dust concentration according to world health standards, the results showed that the limits for healthy air in the operation of the heating plant were exceeded. In conditions of a normal intravillage without industrial production, up to three times lower dust concentration values were recorded.

Key words: *Dust particles, healthy air, health risks, heating plant, forest biomass storage*

INTRODUCTION

Dust is a mixture of microscopic solid particles in the air. These particles can originate from various sources, such as industry, transport, as well as natural processes like wind erosion or volcanic activity. Dust particles typically range in size from micrometers to several tens of micrometers (Hatina et al. 2006). In various sectors of the economy, the production of dust poses a significant health problem. The impact of dust on human health depends on several factors: the type and method of production, its chemical composition, and other variables. In addition to affecting the respiratory system, dust can also irritate the mucous membranes of the eyes, nose, mouth, and larynx (Bohadana et al. 2000; Douwes et al. 2001). The significant effect of fine dust particles on mucous membranes leads to drying, while dust with higher humidity can foster conditions for fermentation and the formation of chemical reactions between dust particles and biological particles contained within the dust, potentially leading to allergies in the human body (Dolny, 1993). Allergic reactions can also manifest on the skin, presenting symptoms such as redness, blisters, and inflammation (Mahút et al. 1993). Dust can also cause (Očkajová, 2012):

- Dermatoses: caused by mechanical irritation, chemical irritation, and allergic reactions to certain wood components.

- Respiratory problems: influenced by particle size and the type of wood (resulting in inflammation of the mucous membranes and airways).
- Allergic respiratory problems: including allergies to components of wood dust (leading to asthma, bronchitis) and allergies to molds and fungi present in wood.
- Carcinogenic effects of some types of wood.

The greatest danger to respiratory organs is posed by the respirable (alveolar) component, with particles smaller than 10 μm , which penetrate the lungs via the respiratory tract and act as mechanical or chemical irritants. Prolonged exposure to such a dusty environment can lead to pneumonocytosis, also known as dusting of the lungs (Urbánek, 2001).

The process of production, storage, handling, and consumption of forest biomass is also characterized by a relatively high concentration of dust, primarily consisting of wood dust, dirt on wood, and spores of molds and fungi. The highest concentrations are typically observed during the technological process of chipping. There is relatively limited research focused on the dustiness of the working environment in heating plant operations and large-capacity forest biomass warehouses (Magagnotti et al. 2013; Gulci et al. 2018). This scarcity may be attributed to the equipment and time requirements of such studies, as well as various other factors that can influence the results. Additionally, there have been cases where wood dust from wood chips has been identified as the cause of explosions, leading to serious consequences for human health and lives (Diehl, 1998; Hedlund et al. 2014).

The aim of the work was to monitor the dustiness of the working environment in the operation of a biomass heating plant with a large-capacity pile of forest chips and to assess its risk to the health of workers as well as residents of the nearby area.

MATERIAL AND METHODS

The measurement was conducted at a city-type heating plant in the Banská Bystrica self-governing region. Dust measurement took place before the conclusion of the heating period on March 21, 2024, during which there was an approximate volume of 3,000 m^3 of forest chips in the large-capacity pile. For the measurement, CEM DT-9880 dust meter was used to count particles, and Temtop M2000C 2nd generation meter was utilized to measure the dust concentration in the air. These meters were positioned between the large-capacity pile and the building of the heating plant (see Fig. 1).



Fig. 1 Placement of the measurement point for dust meters

The measurement methodology adhered to the provisions of the standards STN EN 689+AC Occupational exposure. Measurement of inhalation exposure to chemical agents. Strategy for testing compliance with occupational exposure limit values, and STN EN 482 Occupational exposure. Procedures for determining the concentration of chemical factors. These standards stipulate a minimum two-hour measurement during a work shift. Dust particles of sizes PM_{2.5} and PM₁₀ were measured. According to the World Health Organization (WHO) and its guidelines from 2021, healthy air is considered to have an average daily concentration of PM_{2.5} particles not exceeding 15 $\mu\text{g}\cdot\text{m}^3$. Conversely, according to the US Environmental Protection Agency (EPA), the air is deemed unhealthy when the concentration of PM_{2.5} dust particles ranges from 55 to 150.4 $\mu\text{g}\cdot\text{m}^3$ on average over 24 hours (Du, Varde, 2016; Pai et al. 2022).

As a reference, dust concentration values were also measured in the classic urban area of the city of Zvolen, outside the industrial operation area, on March 26, 2024. Similar atmospheric conditions prevailed on this day as on the day of measurement in the premises of the heating plant. The software products MS Excel and R-Studio were utilized to process the results.

RESULTS

Figure 2 illustrates the assessment of the basic atmospheric conditions during the measurements at the heating plant on March 21, 2024, and the reference measurement in the inner city of Zvolen on March 26, 2024

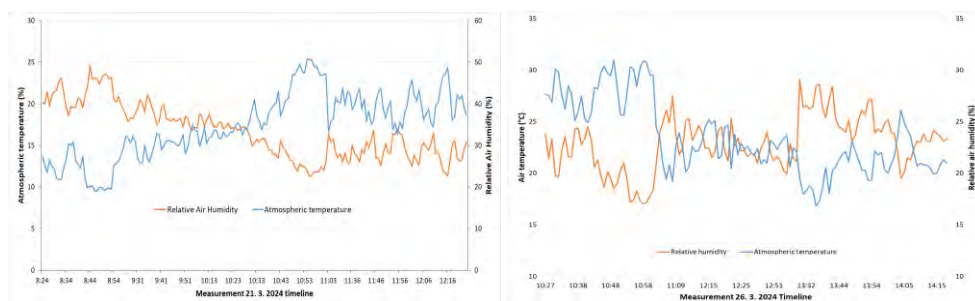


Fig. 2 Atmospheric conditions in the heating plant (21. 3. 2024) and inner city Zvolen (26. 3. 2024)

The measurements of atmospheric conditions reveal that very similar air temperatures prevailed, and the relative air humidity was also at a similar level. The dispersion and spread of dust particles are fundamentally influenced by the wind. It should be noted that wind conditions during both measurement days at both locations were very similar. There were no gusts of wind, and there was a moderate northwesterly breeze with a speed of up to $2 \text{ m}\cdot\text{s}^{-1}$.

Figure 3 presents the evaluation of dust measurements conducted during the operation of the heating plant on March 21, 2024. The concentration of dust particles is measured in $\mu\text{g}\cdot\text{m}^{-3}$, and the number of individual dust particles is assessed. The technical guideline value for risk assessment of dust as a carcinogenic factor is up to $5 \text{ mg}\cdot\text{m}^{-3}$, which was not exceeded. However, when assessing levels according to world health standards (as detailed in the methodology chapter), it can be concluded that the dust levels were extremely high, particularly in the first hour of measurement, surpassing the thresholds for healthy air.

According to WHO standards, air harmful to health persisted throughout the measurement period.

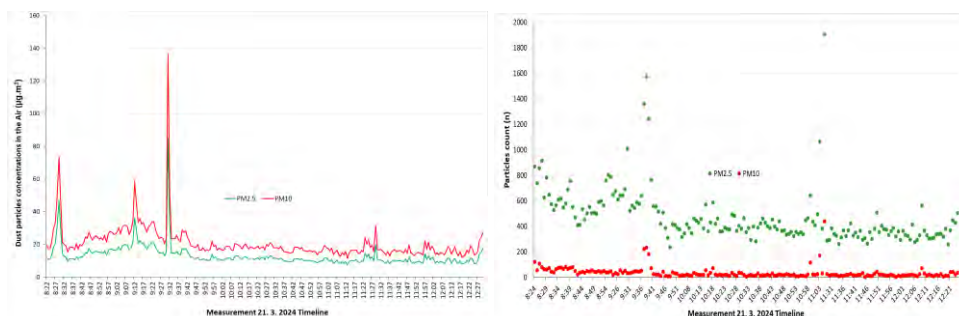


Fig. 3 Measurement in the heating plant on 21. 3. 2024 – Dust concentration in the air and particles count in the air

Figure 4 depicts a reference measurement conducted in the inner city of Zvolen under similar atmospheric conditions. The results indicate that the concentrations of dust in the air throughout the entire measurement period were approximately three times lower than during the measurement taken during the operation of the heating plant. For most of the measurement time, the dust values did not exceed the levels considered healthy according to health standards. Thus, it is possible to confirm the influence of the operation of the heating plant and the storage and handling of biomass on increased concentrations of dust. It is justified to consider such an operation risky from the perspective of human health. Although the obligation of personal protective equipment has not yet been established for these levels, it can be strongly recommended for workers who move around the premises of the operation. The nearby residential zone, located only 20-30 meters from the measurement point, appears to be problematic. The operation of the heating plant and the storage of biomass undoubtedly represent a long-term health risk for these residents.

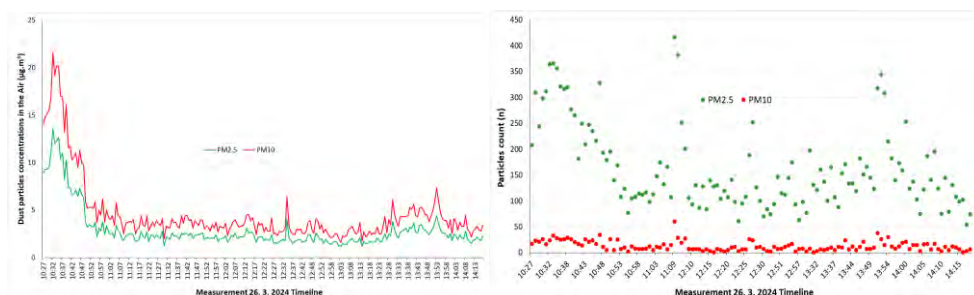


Fig. 4 Reference dust measurement in Zvolen 26. 3. 2024 - Dust concentration in the air and particles count in the air

DISCUSSION AND CONCLUSION

The concentration of dust particles in the operations of biomass heating plants poses a problem from the perspective of the health of workers and residents, especially when the operation is situated in an urban area. The challenge lies in the difficulty of establishing relevant legislation, as the direct and long-term impact of dust on human health remains

problematic to prove. In addition to dust particles of biological origin (such as wood dust, fungal, and mold spores), particles of ash, dirt, flue gas, etc., also accumulate in the air. Barontini et al. (2014) demonstrated that the health risk diminishes only at a distance of approximately 300 meters from the stored pile or operation. Moreover, high concentrations of dust, combined with fuel vapors from operating machinery, can potentially create a flammable and explosive mixture (Hedlund et al., 2014).

Our measurements indicated that operation in a city-type heating plant does not generate dust concentrations that would necessitate assessment for carcinogenic effects according to legislation. However, it was confirmed that dust concentrations are three times higher than in the normal non-industrial environment of the inner city, and from the perspective of international hygiene standards, they constitute an unhealthy working and living environment.

ACKNOWLEDGEMENTS

This publication is the result of the project implementation: APVV-22-0001 “ Optimization of main health and safety risks in the use of forest biomass for energy purposes“; and KEGA 004TU Z-4/2023 „Innovative methods for assessing the quality potential of forest stands“.

REFERENCES

- HATINA, T., KORDOŠOVÁ, M., MATULOVÁ, S., PERICHTOVÁ, B. ŠKVARKOVÁ, V. 2006. Terminologický slovník bezpečnosti a ochrany zdravia pri práci. Inštitút pre výskum práce a rodiny. Bratislava, 2006 (nepublikované).
- BOHADANA, A.B., MASSIN, N., WILD, P., TOAMAIN, J.P., ENGEL, S., GOUTET, P. 2000. Symptoms, airway responsiveness, and exposure to dust in beech and oak wood workers. *Occupational and Environmental Medicine*, Vol. 57(4), p. 268-273. DOI: 10.1136/oem.57.4.268.
- DOUWES, J., MCLEAN, D., SLATER, T., PEARCE, N. 2001. Asthma and other respiratory symptoms in New Zealand pine processing sawmill workers. *American Journal of Industrial Medicine*, Vol. 39(6), p. 608-615. DOI: 10.1002/ajim.1060.
- DOLNY, S. 1993. Transport pneumatyczny i odpylanie w przemyśle drzewnym. VŠ Skriptá, Wydawnictwo akademii rolniczej w Poznaniu, Poznań, p. 214.
- MAHÚT, J., BUČKO, J., ČUNDERLÍK, I., HURDA, B., KRAKOVSKÝ, A., KURJATKO, S., RÉH, R., ŠUPÍN, M. 1993. Menej známe a menej používané tropické dreviny - awoura, ekoune, izombé, kanda, naga, yatandza. *Vedecké a pedagogické aktuality*, 2/1993. Zvolen : Technická univerzita vo Zvolene, 1993. ISBN 80-228-0268-9. pp. 92.
- OČKAJOVÁ, A. 2012. Výroba štiepok a možné riziká vplývajúce na človeka. In: *Biomasa a riziká pri jej spracovaní. Zborník vedeckých prác*. 2012.TU Zvolen, ISBN 978-80-228-2365-4, p. 190-205.
- URBÁNEK, T. 2001. Regenerácia filtračných textílií. *Filtračné textílie*, Vol. 99, Zvolen, TU vo Zvolene, p. 28-32.
- MAGAGNOTTI, N.; NANNICINI, C.; SCIARRA, G.; SPINELLI, R.; VOLPI, D. 2013. Determining the Exposure of Chipper Operators to Inhalable Wood Dust. *Ann. Occup. Hyg.* 2013, 57(6), p. 784-792, DOI: 10.1093/annhyg/mes112.

- GULCI, S.; AKAY, A.E.; SPINELLI, R.; MAGAGNOTTI, N. 2018. Assessing the exposure of chipper operators to wood dust in a roadside landing area. *Fresen. Environ. Bull.* 2018, 27(6), p. 4132-4138.
- DIEHL, S.V. 1998. Respiratory health problems associated with worker exposure to fungi on wood and wood chips. *Tappi J.* 1998, 81(5), 115-118.
- HEDLUND, F.H.; ASTAD, J.; NICHOLS, J. 2014. Inherent hazards, poor reporting and limited learning in the solid biomass energy sector: A case study of a wheel loader igniting wood dust, leading to fatal explosion at wood pellet manufacturer. *Biomass Bioenerg.* 2014, 66,450-459, DOI: <https://doi.org/10.1016/j.biombioe.2014.03.039>.
- STN EN 689+AC Workplace exposure. Measurement of exposure by inhalation to chemical agents. Strategy for testing compliance with occupational exposure limit values; STN EN 482 Workplace exposure. Procedures for the determination of the concentration of chemical agents. Basic performance requirements.
- DU, X.; VARDE, A.S. 2016. Mining PM_{2.5} and Traffic Conditions for Air Quality. In *Proceedings of the 7th International Conference on Information and Communication Systems (ICICS)*, Irbid, Jordan, 5–7 April 2016.
- PAI, S.J.; CARTER, T.S.; HEALD, C.L.; KROLL, J.H. 2022. Updated World Health Organization Air Quality Guidelines Highlight the Importance of Non-antropogenic PM_{2.5}. *Environ. Sci. Technol. Lett.* 2022, 9, 501–506. <https://doi.org/10.1021/acs.estlett.2c00203>.
- BARONTINI, M.; CROGNALE, S.; SCARFONE, A.; GALLO, P.; GALLUCCI, F.; PETRUCCIOLI, M.; PASCIAROLLI, L.; PARI, L. 2014. Airborne fungi in biofuel wood chip storage sites. *Int. Biodeter. Biodegr.* 2014, 90, 17–22. <https://doi.org/10.1016/j.ibiod.2013.12.020>.



EFFECT OF LENS FOCAL LENGTH IN CO₂ LASER ENGRAVING

Zhivko Gochev – Pavlin Vitchev

Abstract

The article presents the results of a study of surface roughness created by CO₂ laser engraving of birch plywood samples. The roughness of the treated surfaces was measured with an electronic profilometer, model SurfTest SJ-210 (Mitutoyo - Japan). A ZnSe lens with a focal length of $F = 50.8$ mm was used for the research; focal position $\Delta F = -4, -6$ and -8 mm above the surface of the material; laser beam power $P = 4.0, 5.6$ and 7.2 W; laser beam scanning speed $v_f = 250, 260$ and 270 mm/s. The experimental results were evaluated using R_a, R_q and R_z parameters and analyzed using specialized Q-StatLab software, ANOVA analysis and interaction diagrams of all parameters, and relevant conclusions and recommendations were drawn.

Key words: CO₂ laser engraving; plywood; roughness of surfaces

INTRODUCTION

Laser technologies based on different types of laser sources are widely used in the modern wood and furniture industry. One of the main directions in which CO₂ lasers are used is for cutting and engraving solid wood and wood-based materials (WBM).

Modern software products, which are part of laser technologies, open wide possibilities for building complex graphic images, type of photography, on solid wood and WBM samples. This opens up new challenges for the furniture industry and not least for the souvenir industry.

Along with the development of laser technology, of particular interest to researchers is the study of the mechanism of interaction of the laser beam with different types of wood and WBM. The main guidelines being worked on are the most appropriate modes to be applied, depending on the objective set and the specific type of material.

The most commonly investigated factors of CO₂ lasers are the power and feed (scan) speed of the laser beam, the focal length of the focusing optics and the position of the focus relative to the surface of the material to be processed, the mode structure of the beam. The object of study are the formation of the slot and its parameters, the modifications that occur in the processed material, the changes in the color of the engraved surfaces as a result of carbonization of the wood material, etc. (Orech and Jůza, 1987; Gotchev *et al.*, 1994; Gochev, 1996; Gochev and Dinkov, 1996; Dinkov *et al.*, 1996; Batov *et al.*, 1997; Pagano *et al.*, 2009; Kubovský *et al.*, 2012; Hernández-Castañeda *et al.*, 2011; Eltawahni *et al.*, 2013; Petutschnigg *et al.*, 2013; Gochev, 2016; Gurau *et al.*, 2017; Martínez-Conde *et al.*, 2017; Vidholdová *et al.*, 2017; Sikora *et al.*, 2018; Jurek and Wagnerová, 2021; Gochev and Vitchev, 2022; Kúdela *et al.*, 2022; Gochev, 2023 and others.).

Information can be found in the literature, from different authors, about the changes that occur in the color of different types of solid wood and WBM when engraving or decorating with a CO₂ laser beam (Petutschnigg *et al.*, 2013; Gurau *et al.*, 2017; Vidholdová *et al.*, 2017; Sikora *et al.*, 2018; Jurek and Wagnerová, 2021; Gochev and Vichev, 2022; Kúdela *et al.*, 2022; Jurek and Wagnerová, 2021 *and others*). The different colour shades, when building complex graphic images, stand out best when engraving with a laser beam on homogeneous solid wood and WBM. A number of authors have also investigated the influence that the roughness of the carbonized material has on the quality of graphic images (Gurau *et al.*, 2017; Kúdela *et al.*, 2022; Li *et al.*, 2022; Kúdela *et al.*, 2023 *and others*). The aim of the present work is to investigate the surface roughness obtained during CO₂ laser engraving of birch plywood samples and the influence of the different position of the focusing lens over the material surface at different powers and scanning speeds of the CO₂ laser beam, as well as to formulate relevant conclusions and recommendations.

MATERIALS AND METHODS

The experimental studies were conducted using a FormaTec laser engraving and cutting machine, model K40 with 40 W power (Fig. 1).



Fig. 1 CO₂ laser engraving and cutting machine

For the purpose of the experiment plywood samples were used - common birch (*Betula pendula* Roth.) with dimensions 200 x 200 x 3 mm, density $\rho = 400 \text{ kg/m}^3$ and humidity $W = 6\%$. Birch plywood is manufactured from developed birch veneer and is characterized by high strength and dimensional stability. Birch is a hard broad-leaved wood species with a light, smooth, even surface and a homogeneous, fine structure and is a suitable material for CO₂ laser engraving.

A test was performed on plywood samples to examine the change in color of the surface layer when varying the laser beam power (P , W); scan speed (v_f , mm/s) and focal length of a ZnSe lens, $F = 50.8 \text{ mm}$. The focal position, for each matrix series of the planned experiment, was above the material surface: $\Delta F = -4 \text{ mm}$; $\Delta F = -6 \text{ mm}$ and $\Delta F = -8 \text{ mm}$ (Fig. 2).

The values of the variable factors - laser beam power (P , W) and laser beam scan (feed) speed (v_f , mm/s) in open and coded form are given in Table 1.

A high-precision roughness profilometer, model SurfTest SJ-210 (Mitutoyo - Japan), was used to measure the roughness changes in the surface layer color of the birch plywood samples (Fig. 3).

The matrix of the planned two-factor experiment is shown in Table 2.

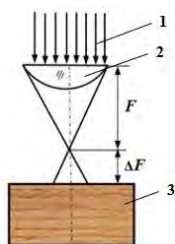


Fig. 2 Position of the focal plane of the focusing lens above the surface of the material:
 1 – laser beam; 2 – focusing lens; 3 – processed material

Table 1 Variable factor values

Variable factors	Minimum value		Average value		Maximum value	
	open form	coded form	open form	coded form	open form	coded form
$X_1 = P, W$	4,0	-1	5,6	0	7,2	+1
$X_2 = v_f, \text{mm/s}$	250	-1	260	0	270	+1

Tab. 2 Matrix of the planned two-factor experiment

№ of the experiment	Variable factors			
	$X_1 = P, W$		$X_2 = v_f, \text{mm/s}$	
1.	-1	4.0	-1	250
2.	+1	7.2	-1	250
3.	-1	4.0	+1	270
4.	+1	7.2	+1	270
5.	-1	4.0	0	260
6.	+1	7.2	0	260
7.	0	5.6	-1	250
8.	0	5.6	+1	270
9.	0	5.6	0	260
Experiments in the middle of the factor space				
10.	0	5.6	0	260
11.	0	5.6	0	260
12.	0	5.6	0	260

RESULTS AND DISCUSSION

The results of the test conducted on the color change of the surface layer of the plywood samples, according to the matrix of the planned two-factor experiment, are shown in Figure 4, for different focus positions ΔF above the material surface. The arrangement of the samples was made vertically, in four rows, according to the experiment matrix of Table 2.

On the surface of the samples shown in Fig. 4 is an engraved system of isolated areas with different colors from dark brown to light, approaching the natural color of birch plywood. Specialized software was used to conduct this test „Inkscape“ (<https://wikibgbg.top/wiki/Inkscape>; <https://paradacreativa.es/bg/que-es-inkscape-y-como-funciona/>). For each experience of the planned experiment matrix (Table 2), the laser beam power was varied from 100% to 5% with a step of 5%.



Fig. 3 Roughness profilometer, model SurfTest SJ-210, Mitutoyo - Japan

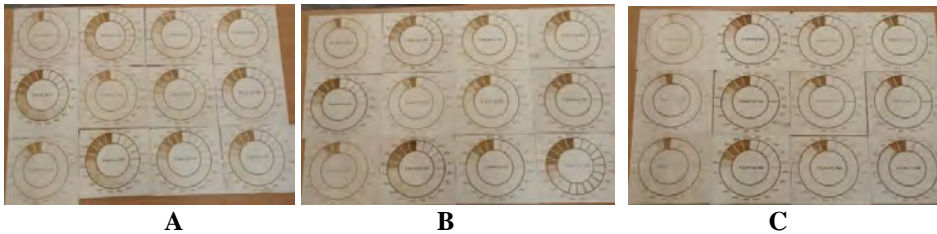


Fig. 4 Test for colour change in the surface layer of birch plywood at: A – $\Delta F = -4$ mm; B – $\Delta F = -6$ mm; C – $\Delta F = -8$ mm

Since the volume of roughness measurements, for each effect zone, is very large, as can be seen in Figures 3 and 4, only the results of the areas affected with the laser beam at 100% power are presented here, according to the experiment matrix in Table 2.

The values of R_a (the absolute mean difference between the peak and valley of the irregularities, within the reference length l), R_q (the root mean square deviation of the evaluated profile from the mean line within the reference length l) and R_z (the absolute arithmetic mean sum of the five largest peaks and the five largest valleys, within the reference length l) were used to evaluate the roughness of the surface irradiated by the laser beam (BDS EN ISO 4287:2006). Each measurement was carried out in the area of influence, repeating the measurements three times in different directions to obtain averaged values (Table 3, 4 and 5).

Table 3 Surface roughness parameters at $\Delta F = -4$ mm

№ of the experiment	Variable factors		Output factors		
	$X_1 = P, W$	$X_2 = v_f, \text{mm/s}$	$Y = R_a, \mu\text{m}$	$Y = R_q, \mu\text{m}$	$Y = R_z, \mu\text{m}$
1.	4.0	250	9.47	12.12	59.01
2.	7.2	250	24.59	29.65	119.98
3.	4.0	270	14.42	17.29	83.09
4.	7.2	270	21.59	26.05	106.29
5.	4.0	260	13.72	17.74	84.66
6.	7.2	260	21.33	26.03	106.83
7.	5.6	250	19.06	23.59	98.84
8.	5.6	270	17.32	21.45	94.48
9.	5.6	260	20.66	25.59	111.19
Experiments in the middle of the factor space					
10.	5.6	260	24.69	30.34	128.69
11.	5.6	260	19.03	23.36	98.71
12.	5.6	260	16.88	21.32	94.68

Table 4 Surface roughness parameters at $\Delta F = -6$ mm

№ of the experiment	Variable factors		Output factors		
	$X_1 = P, W$	$X_2 = v_f, \text{mm/s}$	$Y = Ra, \mu\text{m}$	$Y = Rq, \mu\text{m}$	$Y = Rz, \mu\text{m}$
1.	4.0	250	7.00	9.27	49.31
2.	7.2	250	19.44	23.91	97.84
3.	4.0	270	10.37	13.67	69.51
4.	7.2	270	18.03	22.19	94.67
5.	4.0	260	7.80	10.42	55.64
6.	7.2	260	13.04	16.39	73.99
7.	5.6	250	16.46	20.60	91.07
8.	5.6	270	17.42	21.55	93.48
9.	5.6	260	20.32	24.69	105.85
Experiments in the middle of the factor space					
10.	5.6	260	16.49	20.48	90.09
11.	5.6	260	15.92	19.61	83.20
12.	5.6	260	19.05	23.26	98.06

Table 5 Surface roughness parameters at $\Delta F = -8$ mm

№ of the experiment	Variable factors		Output factors		
	$X_1 = P, W$	$X_2 = v_f, \text{mm/s}$	$Y = Ra, \mu\text{m}$	$Y = Rq, \mu\text{m}$	$Y = Rz, \mu\text{m}$
1.	4.0	250	5.62	7.33	38.32
2.	7.2	250	11.15	20.68	89.85
3.	4.0	270	5.42	7.35	27.30
4.	7.2	270	17.49	21.71	67.55
5.	4.0	260	8.84	11.51	54.94
6.	7.2	260	16.96	20.48	85.00
7.	5.6	250	11.22	19.86	88.58
8.	5.6	270	14.12	17.42	76.31
9.	5.6	260	14.55	18.60	86.52
Experiments in the middle of the factor space					
10.	5.6	260	13.06	16.95	78.12
11.	5.6	260	13.16	16.73	76.20
12.	5.6	260	17.51	21.71	90.62

In North America the most commonly used surface roughness parameter is Ra , while in Europe the more common roughness parameter is Rz .

The Ra parameter is statistically stable and repeatable, but it does not distinguish between peaks and valleys of the profile.

The Rz parameter averages only the five highest peaks and the five deepest valleys - therefore the extreme values have a much greater influence on the final result.

The Rq parameter is more sensitive to peaks and valleys than Ra and is commonly used in research and statistical control of very smooth surfaces (Kalimanova *et al.*, 2012).

Which parameter to use to evaluate the surface roughness Rz or Ra depends on the manufacturer and the customer. It is recommended as a safe conversion to use a ratio range for Rz to $Ra = 4:1$ to $7:1$ (<https://www.productionmachining.com/articles/the-difference-between-ra-and-rz>, Kovács *et al.*, 2012), but this is still an example of not good engineering practice.

Because using Ra alone may cause some points, such as single convexities, to be neglected, it is better to use Ra and Rz together. In this study, to obtain a more complete picture, results are also given for the parameter Rq .

Figure 5 shows a roughness profile from the surface of a birch plywood sample not treated with CO₂ laser beam, and Figures 6, 7 and 8 after laser beam treatment at the position of the focus above the material surface ($\Delta F = -4$ mm, $\Delta F = -6$ mm and $\Delta F = -8$ mm). The roughness profiles in Fig. 5 were obtained for variable factor parameters corresponding to No. 10 in Table 2.

It can be seen from all the above figures that:

- the CO₂ laser-treated surfaces of the birch plywood samples have a greater roughness than the untreated ones, and for the parameter R_a the variation is from 2 to 4 times, and for R_z from 2.2 to 3.9 times;
- the largest roughness of the CO₂ laser treated surfaces is obtained at the focal position $\Delta F = -4$ mm above the material surface and the smallest at $\Delta F = -8$ mm, an intermediate position for the surface roughness is obtained at $\Delta F = -6$ mm;
- съотношението между $\Delta F = -4$ mm към $\Delta F = -6$ mm, към $\Delta F = -8$ mm за R_a е 2.0:1.7:1.2, а за R_z е 1.8:1.5:1.2;
- the main reason for the different roughness of the CO₂ laser treated surfaces at different focus positions over the material surface is the different power density of the laser beam (Fig. 2);
- at all three focus positions an unfocused laser beam falls on the plywood samples, but at $\Delta F = -4$ mm the spot diameter is the smallest and the power density is the largest, while at $\Delta F = -8$ mm the spot diameter is the largest and the power density is the smallest;
- greater beam power density leads to a greater amount of absorbed heat and increased surface roughness.

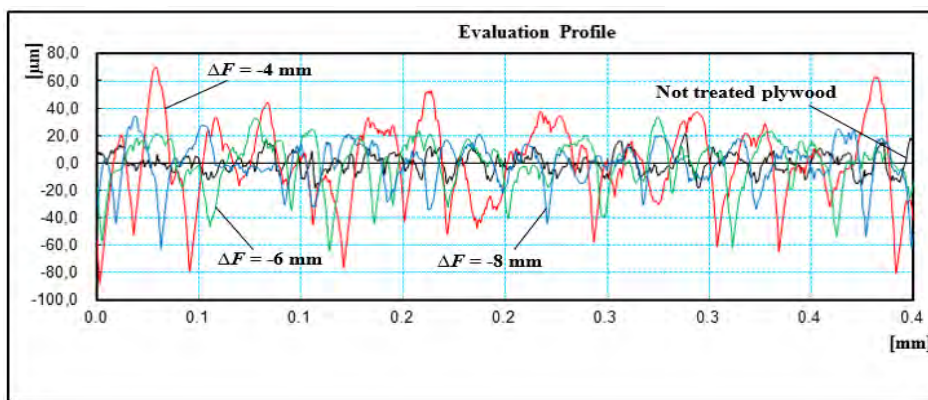


Fig. 5 Various machined surface roughness profiles

The results of the experimental studies were processed mathematically with specialized Q-StatLab software and regression equations were derived for the roughness parameters R_a and R_z at different focal positions on the material surface:

- Regression equation for R_a at $\Delta F = -4$ mm

$$Y_1 = 19.98 + 4.98X_1 - 0.035X_2 + 1.74X_1^2 - 1.078X_2^2 - 1.98X_1X_2 \quad (1)$$

- Regression equation for R_a at $\Delta F = -6$ mm

$$Y_1 = 17.22 + 4.22X_1 - 0.49X_2 + 5.38X_1^2 - 1.14X_2^2 - 1.19X_1X_2 \quad (2)$$

- Regression equation for R_a at $\Delta F = -8$ mm

$$Y_1 = 14.75 + 4.29X_1 - 1.51X_2 + 2.21X_1^2 - 2.44X_2^2 - 1.63X_1X_2 \quad (3)$$

- Regression equation for R_z at $\Delta F = -4$ mm

$$Y_2 = 106.98 + 17.72X_1 - 1.005X_2 + 8.57X_1^2 - 7.655X_2^2 - 9.44X_1X_2 \quad (4)$$

- Regression equation for Rz at $\Delta F = -6$ mm

$$Y_2 = 91.79 + 15.34X_1 - 3.24X_2 + 21.96X_1^2 - 5.496X_2^2 - 5.842X_1X_2 \quad (5)$$

- Regression equation for Rz at $\Delta F = -8$ mm

$$Y_2 = 85.164 + 20.306X_1 - 7.598X_2 + 19.792X_1^2 - 7.317X_2^2 - 0.61X_1X_2 \quad (6)$$

It can be seen from the equations that it is the coefficient in front of X_1 corresponding to the cutting power (P) that will have the greatest influence, and to a greater extent than feed rate (v_f), on the roughness of the surfaces. The sign in front of the coefficient is „plus“, i.e. as P increases, Ra and Rz will increase. The coefficient in front of X_2 has a negative sign, i.e. with increasing feed rate (scanning) Ra and Rz will decrease. The sign in front of the coefficient of double interactions X_{12} is negative, indicating the divergent influence of laser beam power (P) and feed rate (v_f) on the surface roughness.

CONCLUSION

Based on the research conducted, the following more important conclusions and recommendations can be drawn:

1. The largest values of the roughness parameters of the CO_2 laser treated surfaces are obtained at the focal position $\Delta F = -4$ mm above the material surface and the smallest at $\Delta F = -8$ mm, an intermediate position for the surface roughness is obtained at $\Delta F = -6$ mm.
2. At a focus position above the material surface of $\Delta F = -4$ mm, the loss of wood mass is greater than at focus positions of $\Delta F = -6$ mm and $\Delta F = -8$ mm. In the first case, the diameter of the unfocused laser beam is smaller, the power density is greater and the amount of vaporized material is greater than at $\Delta F = -6$ mm and $\Delta F = -8$ mm, which is also reflected in larger values of the parameters Ra , Rz and Rq .
3. As the laser beam power (P) increases, the values of the parameters Ra and Rz , i.e. the roughness of the machined surfaces, will also increase.
4. Increasing the feed rate (scanning) of the laser beam, the values of the roughness parameters Ra and Rz decrease, as the time of the laser beam impact on the material decreases, leading to a decrease in the degree of carbonization of the surface layer, and hence to a decrease in its roughness.
5. The ratio of $\Delta F = -4$ mm to $\Delta F = -6$ mm and to $\Delta F = -8$ mm for Ra is 2.0:1.7:1.2, and for Rz is 1.8:1.5:1.2.
6. The CO_2 laser-treated surfaces of the birch plywood specimens have a greater roughness than the untreated ones, with a variation of 2 to 4 times for the Ra parameter and 2.2 to 3.9 times for Rz .
7. Depending on the effect to be achieved when building complex graphic images with the help of a laser beam, modes can be developed in which a certain shade is achieved between darkening of the surface layer of the material and its roughness.

Acknowledgement:

We would like to thank the Research Sector of the University of Forestry, Sofia, Bulgaria, with whose support, through Contract No. NIS-B-1284/19.10.2023 and Contract No. № NIS-B-1298/11.12.2023, this research was carried out.

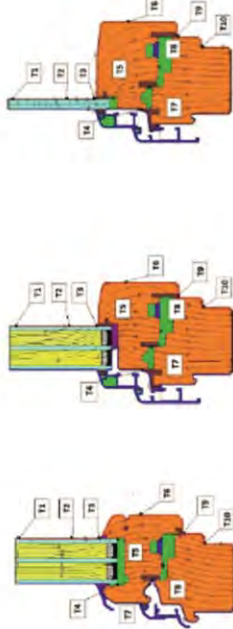
REFERENCES

- 1 Batov I., Gotchev Zh., Dinkov B., Janic Z., 1997, Study on the head field and the structural changes during the interactions between CO₂ laser beam and wood material, The 3rd International Conference on the Development of Forestry and Wood Science/Technology, Volume II, Belgrade, pp. 560-568, ISBN 86-7299-048-x.
- 2 BDS EN ISO 4287:2006.
- 3 Dinkov B., Gochev Zh., Barnekov V., 1996. Optimization of the Influence of the Main Notch Formation Factors in Laser Beam Interaction with Wood and Wood Materials, Proceedings of the International Scientific Conference „Mechanical Technology of Wood”, 21-23 November 1996, Sofia, University of Forestry Publishing House, pp. 305-311 (in Bulgarian).
- 4 Eltawahni H., Rossini N., Dassisti M., Alrashed K., Aldaham T., Benyounis K., Olabi A., 2013. Evaluation and optimization of laser cutting parameters for plywood materials. *Opt. Lasers Eng.*, 51(9):1029-1043, ISSN: 0143-8166.
- 5 Gotchev J., Barnekov V., Dinkov B., 1994. Modeling the Laser Cutting of Particleboard, 2nd International Conference on Automated Lumber Processing Systems and Laser Machining of Wood and Composites, Michigan State University, East Lansing, Michigan, USA, pp. 71-81.
- 6 Gochev Zh., 1996. Investigation of the process of laser cutting of furniture parts made of particle board, PhD Thesis, University of Forestry, Sofia, p. 200 (in Bulgarian).
- 7 Gochev Zh., Dinkov B., 1996. Specific Cutting Energy at Laser Beam Interaction with Wood and Wood Materials, Proceedings of International Scientific Conference, University of Forestry, Section: Mechanical Technology of Wood, Sofia, pp. 298-304 (in Bulgarian).
- 8 Gochev Zh., 2016. Laser wood cutting and modification in its structure, IInd International Furniture Congress: proceedings of papers, 13-15 October, Muğla Sitki Koçman University Faculty of Technology Department of Wood Product Industrial Engineering, Turkey, pp. 210-215.
- 9 Gochev Zh., Vichev P., 2022. Color modifications in plywood by different mode of CO₂ laser engraving, *Scientific journal Acta Facultatis Xylologiae*, Zvolen, 64(2), DOI: 10.17423/afx.2022.64.2.08, pp. 77-86, ISSN 1336-3824.
- 10 Gochev Zh., 2023. Real Parameters of a Focused CO₂ Laser Beam and its Determination when Using Lenses with Different Focal Lengths, 32nd International Conference on Wood Science and Technology – ICWST 2023, Unleashing the Potential of Wood-Based Materials, proceeding of papers, 7-8 December, Zagreb, pp. 67-74, ISBN 978-953-292-083-3.
- 11 Gurau L., A. Petru, A. Varodi, M. Timar, 2017. The Influence of CO₂ Laser Beam Power Output and Scanning Speed on Surface Roughness and Colour Changes of Beech (*Fagus sylvatica*), *BioResources* 12(4):7395-7412, ISSN: 1930-2126, doi: 10.15376/biores.12.4.7395-7412.
- 12 Hernández-Castañeda J., H. Kursad, L. Li, 2011. The effect of moisture content in fibre laser cutting of pine wood. *Opt. Lasers Eng.*, 49(9-10):1139–1152, ISSN: 0143-8166.
- 13 Jurek M., R. Wagnerová, 2021, Laser beam calibration for wood surface colour treatment, *European Journal of Wood and Wood Products*, 79(5):1097–1107, ISSN: 1436736X.
- 14 Kalimanova I., D. Teodosiev, D. Diakov, H. Nikolova, 2012. Study of the influence of the glass-carbon coating on the micro-topography of the articulating surfaces of ceramic implants, Proceedings of the XXII National Scientific Symposium with „Metrology

- and Metrological Assurance 2012“, September 10-14, 2012, Sozopol, Bulgaria, pp. 147-153, ISSN: 1313-9126 (in Bulgarian).
- 15 Kovács B., S. Sipos, Á. Czifra, 2012. Interpretation of „Rz = 4×Ra“ and other roughness parameters in the evaluation of machined surfaces, ICT-2012, In Proceedings of the 13th International Conference on Tools 27-28 March 2012, Miskolc, Hungary, pp. 237-242, ISBN: 978-963-9988-35-4.
 - 16 Kubovský I., M. Babiak, Š. Cipka, 2012. A determination of specific wood mass removal energy in machining by CO₂ laser, Acta Facultatis Xylogologiae Zvolen, 54(2): 31–37, 2012, Zvolen, Technická univerzita vo Zvolene, ISSN: 13363824.
 - 17 Kúdela J., I. Kubovský, M. Andrejko, 2022. Influence of Irradiation Parameters on Structure and Properties of Oak Wood Surface Engraved with a CO₂ Laser, Materials, Vol. 15, Iss. 23, p. 21, ISSN: 1996-1944.
 - 18 Kúdela J., M. Andrejko, I. Kubovský, 2023. The Effect of CO₂ Laser Engraving on the Surface Structure and Properties of Spruce Wood, Coatings, Vol. 13, Iss. 12, p. 17, ISSN: 2079-6412.
 - 19 Li R. C. He, W. Xu, X. Wang, 2022. Prediction of Surface Roughness of CO₂ Laser Modified PoplarWood Via Response Surface Methodology. Maderas. Ciencia y Tecnología 2022, Vol. 24, pp. 1-12, on-line ISSN: 0718-221X.
 - 20 Martinez-Conde A., T. Krenke, S. Frybort, U. Müller, 2017. Review: Comparative analysis of CO₂ laser and conventional sawing for cutting of lumber and wood-based materials. Wood Sci. Technol., 51: 943–966, ISSN: 1432-5225.
 - 21 Orech, J., F. Jůza, 1987. Měrná energie úběru a její určení při interakci laserového záření se dřevem. Drevársky výskum, Číslo 114, stránky 29-40, ISSN: 0012-6136.
 - 22 Pagano N., S. Genna, C. Leone, V. Lopresto, 2009. Wood Laser machining using CO₂ 30W laser in CW and pulse regime, In book: Innovative production machines and systems. LAPT, Napoli, pp. 145-150, ISBN-10:1849950067.
 - 23 Petutschnigg A., M. Stöckler, F. Steinwendner, J. Schnepps, H. Güttler, J. Blinzer, H. Holzer, Th. Schnabel, 2013. Laser Treatment of Wood Surfaces for Ski Cores: An Experimental Parameter Study, Advances in Materials Science and Engineering, Volume 2013(11), Article ID 123085, pp 1-7, ISSN: 1687-8434 (Print), ISSN: 1687-8442 (Online).
 - 24 Sikora A., F. Kačík, M. Gaff, V. Vondrová, T. Bubeníková, I. Kubovský, 2018. Impact of thermal modification on color and chemical changes of spruce and oak wood, Journal of Wood Science, Volume 64, pp. 406-416, ISSN: 1611-4663.
 - 25 Vuchkov I., S. Stoyanov, 1986. Mathematical modeling and optimization of technological objects, SPH Tehnika, Sofia, p. 341 (in Bulgarian).
 - 26 Vidholdová Z., L. Reinprecht, R. Igaz, 2017. The Impact of Laser Surface Modification of Beech Wood on its Color and Occurrence of Molds, 12(2):7395-7412, ISSN: 1930-2126.
 - 27 <https://wikibgbg.top/wiki/Inkscape>; <https://paradacreativa.es/bg/que-es-inkscape-y-como-funciona/>.
 - 28 <https://www.productionmachining.com/articles/the-difference-between-ra-and-rz>.



Spoločnosť AREKO, s.r.o. a Technická univerzita vo Zvolene majú dlhodobú spoluprácu v rámci dodávania záznamových a meracích prístrojov, senzorov, softvéru a kalibrácií. V rámci drevárskej fakulty sa prístroje využívajú napr. na katedre drevených stavieb pre výskum vlhkosťnych a tepelných vlastností drevených konštrukcií, tepelno-technických vlastností okien na báze dreva, energetickej náročnosti stavieb a kvality vnútorného prostredia drevostavieb.



Využívané sú prístroje ako ALMEMO typ MA 5690 – 1, snímač teploty, vlhkosti a tlaku vzduchu FHAD46CO, snímač koncentrácie CO2 FYA600CO2, snímač koncentrácie formaldehydu vo vzduchu FYA600CH2O, ALMEMO METEO-MULTISENZOR FMD760, ALMEMO 202 a iné. Pomocou prístrojového vybavenia Areko bol zrealizovaný napr. aj výskum vplyvu konštrukcie drevených a drevo-hliníkových okien na povrchové teploty.

V súčasnosti prebiehajú v dlhodobom horizonte výskumy vlhkosťnych a tepelných vlastností obalových konštrukcií na báze dreva v referenčnom výskumnom objekte v areáli TU vo Zvolene, ako aj na reálnych obývaných stavbách. Taktiež dôležitým prebiehajúcim výskumom je aj **mapovanie parametrov obytnej vnútornej klímy ako teplota, vlhkosť, stav CO2 a formaldehydu.**

tzv. syndróm chorých budov





TOOL COATINGS AND THEIR EFFECT ON CUTTING FORCE REDUCTION IN CNC MDF MILLING

Lud'ka Hanincová – Vít Novák – Jiří Procházka – Radek Matrosz

Abstract

Tool coatings play a crucial role in the performance and service life of cutting tools. This study evaluates the impact of various tool coatings on cutting forces during CNC milling of Medium Density Fiberboard (MDF). Five different tool coatings were tested: lapped surface, Hyperlox, TripleSi, DLC (Diamond-Like Carbon), and an uncoated reference tool. The experiments were conducted under different cutting speeds (8; 10; 12 m/s) and feed rates (0.1; 0.2; 0.3 mm) for both types of milling (conventional and climb) on CNC machine SCM Morbidelli m100. The results indicate that lapped surfaces and TripleSi coatings significantly reduce values of total active cutting force compared to the reference tool and DLC coating. The findings provide insights into optimizing tool selection for increasing in the woodworking industry.

Key words: CNC machining, cutting force, coating, MDF

INTRODUCTION

Cutting tools undergo continuous development, leading to increasingly sophisticated shapes (Häusler et al. 2020) and material solutions (Berger et al. 2010). In machining tough materials, the primary challenge is the high friction during chip formation, which causes excessive tool heating (Horman et al. 2014). This issue is exacerbated in machining wood-based materials, which are typically thermal insulators, causing heat to accumulate in the tool (Igaz et al. 2018). A common solution is reducing the tool's friction coefficient with appropriate coatings, which improves the friction between the tool body and the material and facilitates easier chip removal from the cut. Today, a wide range of hard coatings based on carbides and nitrides (Berger et al. 2010) are available on the market, applied in microscopic layers on the tool surface. These coatings are applied using chemical vapor deposition (CVD) and newer physical vapor deposition (PVD) methods, each with various extensions depending on the coating material (Raheem, 2019). These methods are often used to apply a thin layer of carbon in its hardest sp³ structure (Deutchman and Partyka, 1990), known as Diamond-Like Carbon (DLC) (Folea et al. 2010). Since its inception in the 1970s, the technology has been continually improved (Ghadai et al. 2018), achieving up to 90% tetrahedral structure with sp³ bonds, resulting in an exceptionally high-quality tool surface with hardness up to 90 GPa (TetrabondTM, 2021). DLC coatings, however, do not have high thermal resistance, similar to PCD, with manufacturers stating a limit of 500 – 700 °C (Folea et al. 2010; Meng et al. 2015). Nevertheless, due to the significantly reduced friction coefficient (Swisher, 2020), the risk of critical temperature during machining is

minimized. DLC coatings appear to be a potential universal solution for machining wood-based materials, including solid wood (Pancielejko et al. 2012), but this hypothesis needs to be tested by comparing the cutting parameters of different tool materials on various workpiece materials.

The aim of this research is to evaluate the suitability of tool coatings in terms of cutting force during open milling of MDF boards on a CNC machining center.

MATERIAL AND METHODS

For the experiment, Medium Density Fiberboard (MDF) with a thickness of 18 mm was chosen for its homogeneity. The boards used in the experiment had a density of 770 kg/m³ and a moisture content of 7.5 %, with dimensions before milling of 300 × 155 × 18 mm.

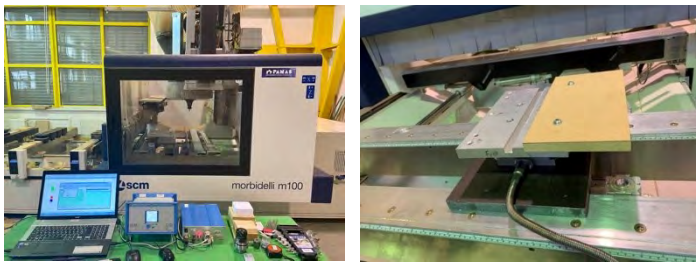


Figure 1: Kistler measuring system and CNC machine; Clamped MDF sample on Kistler measuring equipment

A CNC machining center SCM Morbidelli m100 (SCM, Italy) was used for the experiment. The tools included five single-flute cutters (Vydoná, Czech Republic) with different coatings:

- **Lapped surface:** Provides a very smooth surface that minimizes friction.
- **Hyperlox:** Known for its hardness and wear resistance.
- **TripleSi:** Combines hardness and temperature resistance.
- **DLC (Diamond-Like Carbon):** Very hard coating with a low friction coefficient.
- **Reference tool:** Served as a control sample for comparison with coated cutters. Since it has the same tool geometry as the other cutters, it allows isolating and quantifying the effect of the coating on machining results.

Tools with a straight edge were chosen to eliminate the effect of force acting in the Z-axis.

Table 1: Tool parameters

Tool diameter	10 mm	
Tool length	80 mm	
Number of teeth	1	
Tool geometry	Radial groove angle: 5° positive (i.e., -0.436 before the center)	
	Axial rake angle: 0° / straight tooth	
	Radial rake angle: F1 30° / 1 mm, F2 40° with radial lead 0.5° / 270°	
	Axial rake angle on the tool face: F1 15° / 1 mm, F2 20° / axial undercut 210°	

Both climb and conventional milling were chosen. Material removal was 1 mm, with varying cutting conditions (cutting speed, feed per tooth, and tool coatings). The tool machined the front face of the workpiece first by conventional milling and then by climb

milling at different feed rates per tooth (0.1, 0.2, and 0.3 mm) and cutting speeds (8, 10, and 12 m/s).

A Kistler measuring system was used to measure cutting forces, consisting of a Kistler 9257B dynamometer, DAQ type 5697A data acquisition unit, 5070A data amplifier, and DynoWare evaluation software. This system allows precise measurement of forces in the X, Y, and Z axes. The dynamic analysis of milling is based on the Ernst-Merchant force diagram (Fig. 2).

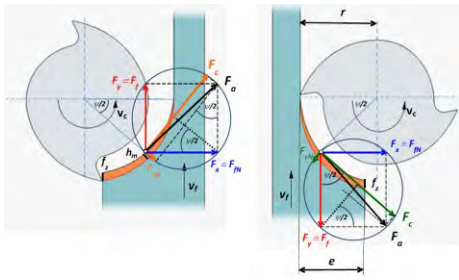


Figure 2: Ernst-Merchant force diagram

Due to the use of a straight-edged cutter, the axial force component in the Z direction is zero. The total active cutting force (F_a) is calculated using the Pythagorean theorem from the measured forces in the X and Y directions. F_x is perpendicular to the feed direction, and F_y is equal to the force in the feed direction (Kopecký et al. 2019):

$$F_a = \sqrt{F_x^2 + F_y^2} \quad [\text{N}] \quad (1)$$

RESULTS AND DISCUSSION

The graphs represent the total active cutting force during conventional and climb milling of MDF boards for different tool coatings at different cutting speeds and feed rates per tooth.

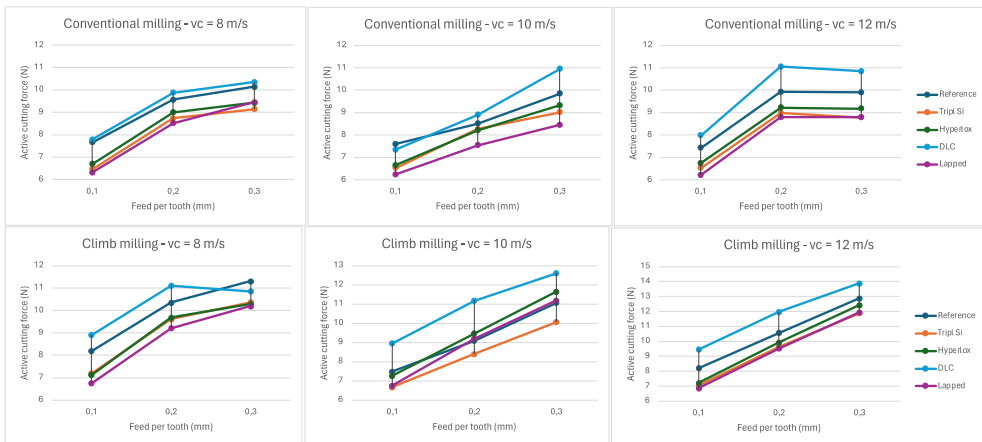


Figure 3: The total active cutting force (N) during conventional and climb milling

Regardless of the type of coating and cutting speed, the total active cutting force increases with higher feed per tooth. This trend is consistent in all cases except for conventional milling at $v_c = 12$ m/s. Koch (1964), Heisel et al. (2007), Kminiak and Kubš (2016), Moradpour et al. (2016) claim that the cutting force increases with feed speed (or feed force).

At higher cutting speeds (10 m/s and 12 m/s), the total active cutting force is higher than at 8 m/s. This increase is evident for all coatings. Nasir and Cool (2018) claim that contradictory results have been reported for the effect of cutting speed on cutting force and power. Moradpour et al. (2016) presented that higher cutting speed corresponds to efficient cutting, indicated by a reduction in parallel and normal cutting forces. On the other hand, cutting speed has been linked to an increase in cutting force (Axelsson et al. 1993, Porankiewicz et al. 2007, 2011). Franz (1958), and Eyma et al. (2005) state that cutting speed has no effect on cutting force values.

DLC exhibits the highest total active cutting force in all cases. This trend is consistent at all feed rates per tooth and cutting speeds. The lapped surface exhibits the lowest total active cutting force among all tested coatings. This trend is clear at all cutting speeds and feed rates per tooth except for climb milling at $v_c = 10$ m/s. The graphs indicate that the lapped surface is the most effective coating for reducing total active cutting forces when milling MDF boards. TriplSi and Hyperlox coatings also show good results and are significantly better than DLC or the reference tool. In most cases, the DLC coating has the highest total active cutting force values, even higher than the reference tool, indicating its lower efficiency under these experimental conditions. Optimizing coatings can significantly contribute to reducing cutting forces, thereby increasing the efficiency of the machining process.

Tables 2 and 3 provide a detailed comparison of the total active cutting force for different tool coatings at various cutting speeds (v_c) and feed rates per tooth (f_z). Average values and percentage comparisons relative to the reference tool are provided.

Table 2: Comparison of the total active cutting force for different tool coatings – conventional milling

v_c [m/s]	8			10			12			Percentage comparison	
	0,1	0,2	0,3	0,1	0,2	0,3	0,1	0,2	0,3		
Reference	7,66	9,56	10,14	7,6	8,51	9,85	7,43	9,92	9,9	8,95	0 %
Tripl Si	6,47	8,74	9,14	6,52	8,27	9,01	6,53	8,98	8,78	8,05	-10 %
Hyperlox	6,7	9	9,43	6,65	8,21	9,32	6,75	9,22	9,18	8,27	-8 %
DLC	7,79	9,88	10,35	7,34	8,9	10,95	7,98	11,05	10,85	9,45	6 %
Lapped	6,32	8,52	9,45	6,24	7,54	8,45	6,21	8,8	8,79	7,81	-13 %
	6,99	9,14	9,70	6,87	8,29	9,52	6,98	9,59	9,50	Average values	

For reducing total active cutting force, it is recommended to use tools with a lapped surface or TriplSi coating. These coatings show the lowest average total active cutting force values in all tested conditions.

Table 3: Comparison of the total active cutting force for different tool coatings – climb milling

v_c [m/s]	8			10			12				
f_z [mm]	0,1	0,2	0,3	0,1	0,2	0,3	0,1	0,2	0,3		Percentage comparison
Reference	8,19	10,35	11,3	7,49	9,09	11,06	8,21	10,56	12,88	9,90	0 %
Tripl Si	7,19	9,61	10,36	6,68	8,4	10,07	7,04	9,63	11,89	8,99	-9 %
Hyperlox	7,12	9,68	10,29	7,27	9,47	11,64	7,21	9,92	12,43	9,45	-5 %
DLC	8,91	11,11	10,85	8,96	11,17	12,6	9,45	11,98	13,88	10,99	11 %
Lapped	6,75	9,21	10,19	6,76	9,2	11,19	6,86	9,52	11,94	9,07	-8 %
	7,63	9,99	10,60	7,43	9,47	11,31	7,75	10,32	12,60	Average values	

TriplSi consistently shows the lowest total active cutting force values in all tested conditions. DLC exhibits the highest total active cutting forces, indicating its lower efficiency.

Conventional milling generally shows lower total active cutting force values than climb milling. This means that during conventional milling, the tool experiences less stress and potentially better surface quality. Using a climb cutting mode, where the tool and the workpiece move in the same direction, requires more cutting power than conventional cutting (Nasir and Cool 2018).

Lapped surface and TriplSi are the most effective coatings for reducing total active cutting forces in both types of milling, but they perform better in conventional milling. Due to the properties of the lapped surface, the time-consuming manufacturing process, and the fact that polishing does not improve the tool's hardness, a tool with a lapped surface may have a shorter lifespan. Therefore, a tool with TriplSi coating is a more suitable choice.

Hyperlox also provides good results but is less effective than TriplSi and the lapped surface.

DLC coating exhibits the highest total active cutting forces in both types of milling, indicating its lower efficiency compared to other coatings. This phenomenon may be due to the material being milled during the experiment. DLC-coated tools are more suitable for working with hard and exotic woods and woods with high resin content. Also, it would be very interesting to further test the long-time machining effect of each coating type, where it might be expected better performance of DLC relatively to its properties.

The reference tool shows higher total active cutting forces than coated tools, confirming the benefits of coatings for reducing total active cutting forces.

CONCLUSION

The correct choice of tool coating is a crucial factor for effective CNC machining of MDF boards. Coatings such as TriplSi and lapped surface offer significant advantages in reducing total active cutting forces, increasing tool life, and improving surface quality. Although the DLC coating shows higher total active cutting force values, it may be useful in applications where its specific properties, such as extreme hardness and low friction coefficient, are required. These findings are essential for optimizing manufacturing processes and increasing efficiency in the woodworking industry.

REFERENCES

1. Axelsson, B. O., Lundberg, Å.S., Grönlund, J. A. Studies of the main cutting force at and near a cutting edge. *European Journal of Wood and Wood Products*, 1993, 51(2), 43–48.
2. Berger, C.; Scheerer, H.; Ellermeier, J. Modern materials for forming and cutting tools – overview. *Materialwissenschaft und Werkstofftechnik* 2010, 41, 5–16.
3. Deutchman, A.H.; Partyka, R.J. The Deposition of Diamond Films on Steel. *JOM* 1990, 42, 58–58.
4. Eyma, F., Méausoone, P. J., Larricq, P., Marchal, R. Utilization of a dynamometric pendulum to estimate cutting forces involved during routing. comparison with actual calculated values. *Annals of Forest Science*, 2005, 62(5), 441–447.
5. Folea, M.; Roman, A.; Lupulescu, N.-B. An Overview of DLC Coatings on Cutting Tools Performance. *Academic Journal of Manufacturing Engineering* 2010, 8, 30–36.
6. Franz, N. C. An Analysis of the Wood-Cutting Process. 1958, Dissertation, University of Michigan, Ann Arbor, MI.
7. Ghadai, R.K.; Kalita, K.; Mondal, S.C.; Swain, B.P. PECVD Process Parameter Optimization: Towards Increased Hardness of Diamond-like Carbon Thin Films. *Materials and Manufacturing Processes* 2018, 33, 1905–1913, doi:10.1080/10426914.2018.1512114.
8. Häusler, A.; Werkle, K.; Maier, W.; Moehring, H.-C. Design of Lightweight Cutting Tools. *International Journal of Automation Technology* 2020, 14, 326–335, doi:10.20965/ijat.2020.p0326.
9. Heisel, U., Martynenko, S., Schneider, M. Influence of chip space filling on cutting forces in high-speed milling of wood and derived timber products. 2007, Proceedings of the 3rd
10. Horman, I.; Busuladžić, I.; Azemović, E. Temperature Influence on Wear Characteristics and Blunting of the Tool in Continuous Wood Cutting Process. *Procedia Engineering* 2014, 69, 133–140, doi:10.1016/j.proeng.2014.02.213.
11. Igaz, R.; Kminiak, R.; Krišťák, L.; Němec, M.; Gergel, T. Methodology of Temperature Monitoring in the Process of CNC Machining of Solid Wood. *Sustainability* 2018, 11, 95, doi:10.3390/su11010095.
12. Kminiak, R., Kubš, J. Cutting power during cross-cutting of selected wood species with a circular saw. *BioResources*, 2016, 11(4), 10528–10539.
13. Koch, P. (1964) *Wood Machining Processes* (New York: Ronald Press Co.).
14. Kopecký, Z., Hlášková, L.; Solař, A.; Nesázal, P. Cutting forces in quasi-orthogonal cnc milling. *Wood research*. 2019(5), 879–889. ISSN 1336-4561.
15. Meng, D.; Yue, W.; Lin, F.; Wang, C.; Wu, Z. Thermal Stability of Ultrahard Polycrystalline Diamond Composite Materials. 2015, 37, 6.
16. Moradpour, P., Scholz, F., Doosthoseini, K., Tarmian, A. Measurement of wood cutting forces during bandsawing using piezoelectric dynamometer. *Drvna Industrija*, 2016, 67(1), 79–84.
17. Nasir, V., Cool, J. A review on wood machining: characterization, optimization, and monitoring of the sawing process, *Wood Material Science & Engineering*, 2018. 15(1), pp. 1–16. doi: 10.1080/17480272.2018.1465465.
18. Pancielejko, M.; Czyżniewski, A.; Gilewicz, A.; Zavaleyev, V.; Szymański, W. The Cutting Properties and Wear of the Knives with DLC and W-DLC Coatings, Deposited by PVD Methods, Applied for Wood and Wood-Based Materials Machining. *Archives of Materials Science and Engineering* 2012, 58, 10.
19. Porankiewicz, B., Axelsson, B., Grönlund, A.A., Marklund, B. Main and normal cutting forces by machining wood of *Pinus sylvestris*. *BioResources*, 2011, 6(4), 3687–3713.

20. Porankiewicz, B., Bermudez E, J. C., Tanaka, C. Cutting forces by peripheral cutting of low density wood species. *BioResources*, 2007, 2(4), 671–681.
21. Raheem, Z. [Arthur A. Tracton] *Coatings Technology Handbook*; 2019;
22. Swisher, M.M. A Molecular Dynamics Study of the Tribological Properties of Diamond like Carbon. Thesis, Massachusetts Institute of Technology, 2020.
23. Tetrabond™ Technology Ionbond Available online: <https://www.ionbond.com/technology/tetrabondtm/> (accessed on 28 September 2021).

ACKNOWLEDGEMENTS

The research was supported by the Specific University Research Fund MENDELU IGA-LDF-22-TP-004: „Advanced tool materials and their influence on the parameters of CNC machining of wood-based materials“



SURFACE AND ADHESIVE PROPERTIES OF BEECH WOOD TREATED BY LOW TEMPERATURE PLASMA AND SATURATED WATER STEAM

Peter Jurkovič¹ – Igor Novák² – Ján Matyašovský¹ – Angela Kleinová²
– Matej Mičušík² – Ján Sedliačik³

Abstract

Saturated water steam treatment causes changes in the surface properties of wood, the surface becomes hydrophobic, which can cause serious problems when gluing or coating. In this study, the radio-frequency (RF) discharge plasma in air was used to increase the hydrophilicity of the steam-modified wood due to the formation of various polar groups. The increased surface polarity improves the wood hydrophilicity due to oxidation reactions.

Keywords: *beech wood, hydrophilicity, FTIR, RF plasma, water steam treatment*

INTRODUCTION

Discharge plasma in air itself significantly increases the hydrophilicity of wood because various polar groups are formed, and the wood macromolecules are also cross-linked, which leads to an increase in scratch resistance and an improvement in the barrier properties of the wood material (Hünnekens et al. 2018). and also increases the adhesion between adhesive and wood substrate (Acda et al. 2012, Novák et al. 2016). The discharge plasma significantly increases the hydrophilicity of wood due to the formation of various polar groups (Abbasipour et al. 2012). The application of discharge plasma improves the strength of joints polymeric adhesives- wood substrates. A radio-frequency plasma is a mixture of various excited particles, such as ions, atoms, electrons, and radicals, that have sufficient energy to break chemical bonds in wood substrates (Odraskova et al. 2008). The effects of the discharge plasma treatment of wood are limited to a nanometers and do not affect the bulk properties of wood (Novak et al. 2012). The increase in surface polarity due to oxidation reactions induced during the modification of wood by RF plasma improves the wettability and hydrophilicity of wood (Muller et al. 2009).

The treatment with water steam represents an hydrothermal method of modification that results in chemical changes influencing its hydrophilicity. The steam degradation (modification) of wood alters its chemical and physical properties. The effect and mechanisms of the water steam regarding to changes in the chemical structure have not been in details understood (Dzurenda and Dudiak 2020).

¹ Peter Jurkovič, Ján Matyašovský, VIPO, a.s., Slovak Republic

² Igor Novák, Angela Kleinová, Matej Mičušík, Polymer Institute SAS, Slovak Republic

³ Technical University in Zvolen, T. G. Masaryka 24, 960 01 Zvolen

e-mail: pjurkovic@vipo.sk

This paper summarized the results of surface, adhesive and chemical changes investigation in beech wood as well as beech wood treated by water steam and radio-frequency discharge plasma.

EXPERIMENTAL

Materials

Beech wood (*Fagus sylvatica* L.) was thermally modified with saturated water steam at a temperature of 135 ± 2 °C during a period of 9 hours.

Radio-frequency discharge (RFD) plasma treatment

The RF plasma treatment of thermally modified wood was performed in a laboratory plasma reactor. The RF plasma reactor has a voltage of 2 kV, a frequency of 13.56 MHz and a maximum current intensity of 0.6 mA.

Methods used

Hydrophilicity of steam-treated beech wood before/after plasma treatment was evaluated by the determination of contact angle (CA, θ) with a water-free 99.5% glycerol as the testing liquid. The 5 μ l drops of testing liquid were placed on the wood surface with a micropipette. Glycerol CA measurements were taken using a professional Surface Energy Evaluation (SEE) System device coupled to a web camera and the required PC software.

The Fourier Transform Infrared Spectroscopy - Attenuated Total Reflection (FTIR-ATR) spectrum of wood is basically a mixed spectrum of cellulose and lignin with characteristic peaks of both OH bonds and in the fingerprint wave numbers, which are particularly low for C–O–C, CH₂ and COO bonds, typical for polysaccharides. Spectra of beech wood samples were recorded by the ATR technique in the mid-infrared region (4000–650 cm⁻¹) using a germanium crystal on a NICOLET 8700™ instrument.

Adhesion measurements were carried out with determination of the tensile strength of adhesive lap joints for native and steam-modified beech wood before/after plasma treatment. Adhesive strength was determined according to EN 204 durability class D4 under conditioning sequences: dry (7 days in standard atmosphere); boiled (7 days in standard atmosphere, 6 hours in boiling and 2 hours in cold water), and soaked (7 days in standard atmosphere, 4 days in cold water).

X-ray photoelectron spectroscopy (XPS) data were recorded using a Thermo Scientific K-Alpha XPS system (Thermo Fisher Scientific, UK) equipped with a micro-focused, monochromatic Al K α X-ray source (1486.6 eV). An X-ray beam with a spot size of 400 μ m size was used at 6 mA x 12 kV.

RESULTS AND DISCUSSION

For hydrophilicity determination the contact angles (CA) of glycerol were carried out and were repeated 8 times. The arithmetic mean and standard deviation of the measurements were analysed (Table 1).

Table 1. Contact angles of native and water steam-modified beech wood treated subsequently by radio-frequency discharge plasma

Sample	CA [°] 0 s	CA [°] after 60 s	CA [°] after 120 s
Beech wood – native	61.5 (2.8)	51.5 (2.2)	26.2 (1.8)
Beech wood – native + plasma	46.6 (2.2)	36.1 (2.2)	18.8 (1.6)
Beech wood – steam-modified	65.5 (2.6)	54.8 (2.2)	32.2 (2.0)
Beech wood – steam-modified + plasma	48.2 (2.0)	38.8 (2.0)	26.2 (2.5)

Standard deviations are in parentheses

The CA on steam-modified beech wood are higher in comparison with native wood. With the time duration after plasma treatment, the CA values decreased in all cases. After plasma treatment, the CA values were lower than those of non-treated wood. The CA on native beech wood reached a value of 61.5°. The CA on beech wood treated with plasma reached a lower value of 46.6° compared to unmodified wood. With the time that passed since the plasma modification the CA value decreased in both cases. After plasma treatment, the CA values of steamed wood were lower than those of non-steamed wood, they decreased after 60s and 120s.

Adhesive properties

The results of the strength of adhesive lap joints measurements were carried out for native and steam-modified beech wood before/after plasma treatment (Table 2). It was found that the tensile strength of lap adhesive joints prepared from native and steam-modified beech wood is equal. RF plasma-treated samples have a higher tensile strength when compared to samples without plasma treatment, approximately up to 10 %.

Table 2. Strength of adhesive lap joints after D4 according to EN 205

Sample	dry [MPa]	boiled [MPa]	soaked [MPa]
Beech wood – native	15.5 (2.21)	3.1 (0.63)	3.6 (0.53)
Beech wood – native + plasma	15.8 (2.64)	3.6 (0.86)	3.8 (0.85)
Beech wood – steam-modified	15.7 (2.76)	2.9 (0.64)	3.7 (0.59)
Beech wood – steam-modified + plasma	15.7 (2.24)	3.4 (0.66)	4.0 (0.65)

standard deviations are in parentheses

FTIR-ATR

A visual comparison of FTIR-ATR spectra of beech wood samples were found that there are few differences between the individual spectra in the whole infrared range (Figure 1). The biggest differences were observed in FTIR-ATR spectra of steamed wood before and after plasma treatment, while the spectra of steamed wood after plasma treatment were more noisy in the range of wavenumbers 1800-1300 cm⁻¹ than untreated ones. This phenomenon is probably related to a greater susceptibility to roughening of the surface of the steamed wood after plasma application to the steamed wood.

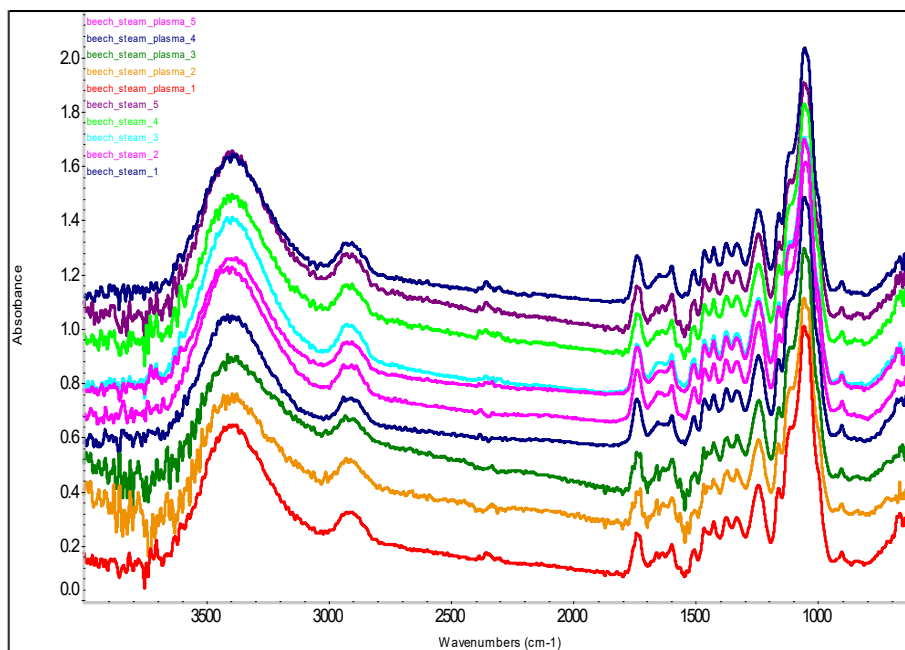


Figure 1. Spectra of beech-steamed vs beech-steamed plasma in the whole IR range.

Figure 2A and Figure 2B represent the XPS spectra of beech wood modified by RF plasma. Figure 2A and Figure 2B compare the carbon C1s peaks of untreated beech wood (Figure 2A) and a plasma-treated (120s) sample (Figure 2B) obtained from XPS measurements. The spectrum of the untreated beech wood shows two basic peaks, one attributed to C–C bonds at ~ 284.9 eV and the other associated with C–O bonds at ~ 286.5 eV; additionally, some minor peaks assigned to C=O at ~ 288.1 eV and COOH at ~ 289.1 eV bonds can be observed. After plasma treatment, there was an increase in the intensity of peaks corresponding to carbon-oxygen groups, especially those assigned to C=O and COOH groups.

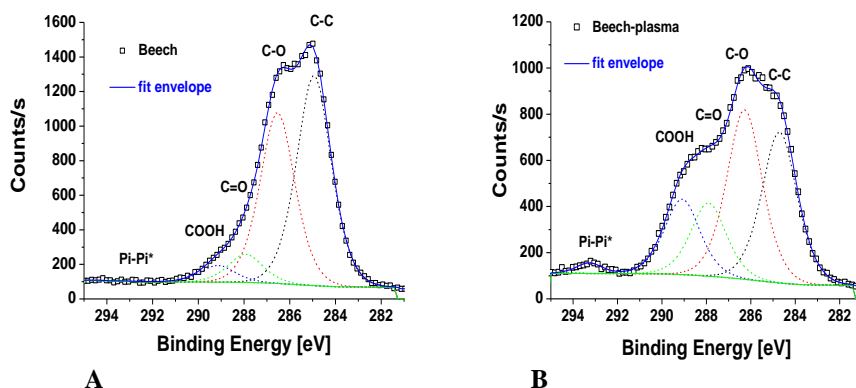


Figure 2. XPS spectra of beech wood: A – carbon C1s peak of native beech wood, B – carbon C1s peak of RF plasma-treated (120 s) beech wood

Table 3. Apparent surface chemical composition of beech wood modified by RF plasma for 120s as determined by XPS

Beech wood	Surface chemical composition [at.%]				
	O1s	C1s fit		N1s	Ca2p
		C-C, C-O, C=O, COOH, $\pi \rightarrow \pi^*$			
Native	26.1	72.8±0.5		0.9	0.3
	±0.6			±0.2	±0.1
	52.9±3.5, 37.6.0±2.4, 6.2±0.4, 2.9±1.0, 0.3±0.1				
Plasma-treated	38.2	58.1±2.9		2.5	1.2
	±2.4			±0.3	±0.3
	37.0±4.8, 34.4±1.7, 14.1±1.1, 13.4±2.2, 1.1±0.5				

Another reason is the greater stability of the C–O bond compared with that of the C–N bond and thus the greater stability of the C=O bond versus the C=N bond (Table 3). The concentration of oxygen on the beech wood surface after 120 s of plasma treatment increased from 26.1 to 38.2 at.%, and the amount of nitrogen increased from 0.9 to only 2.5 at.%. The amount of carbon during the plasma treatment of the beech wood conversely decreased from 72.8 to 58.1 at.%.

CONCLUSION

RF plasma treatment proved its efficiency, plasma-treated samples reached significantly lower contact angles values in comparison with plasma non-treated samples. The biggest differences were observed in the spectra of steamed wood before and after plasma treatment, while the spectra of steamed wood after plasma treatment were more noisy in the range of wavenumbers 1800 - 1300 cm^{-1} than untreated ones. After RF plasma treatment an increase was observed in the intensity of peaks corresponding to carbon-oxygen groups, especially those assigned to C=O and COOH groups. Better hydrophilicity was confirmed by the higher strength of lap adhesive joints after different conditioning sequences.

Acknowledgement

This work was supported by the Slovak Research and Development Agency under the contracts APVV-20-0593, APVV-20-0159 and APVV-21-0051;

REFERENCES

- Abbasipour Ma., Salem M.K., Sari A.H., Abbasipour Mi., 2012: Wood surface functionalization by means of low-pressure air plasma. *Radiation Effects and Defects in Solids*, vol. 167(11), p. 814-825.
- Acda MN, Devera EE, Cabangon RJ, Ramos HJ (2012) Effects of Plasma Modification on Adhesion Properties of Wood. *International Journal of Adhesion and Adhesives* 32: 70-75.

Dzurenda, L., Dudiak, M., 2020: The effect of the temperature of saturated water steam on the colour change of wood *Acer pseudoplatanus* L. *Acta Facultatis Xylogiae Zvolen* 62(1): 19, p. 28.

Hünnekens B, Avramidis G, Ohms G, Krause A, Viöl W, Militz H (2018) Impact of plasma treatment under atmospheric pressure on surface chemistry and surface morphology of extruded and injection-molded wood-polymer composites (WPC). *Applied Surface Science* 441: 564-574.

Muller G., Schopper C., Vos H., Kharazipour A., Polle A., 2009. FTIR-ATR spectroscopic analyses of changes in wood properties during particle- and fibreboard production of hard- and softwood trees. *BioResources*, vol. 4(1), p. 49-71.

Novák I., Popelka A., Krupa I., Chodák I., Janigová I., Nedelčev T., Špírková M., Kleinová A. 2012: High-density polyethylene functionalized by cold plasma and silanes. *Vacuum*, vol. 86(12), p. 2089-2094.

Novák I, Sedliačik J, Gajtanská M, Schmidtová J, Popelka A, Bekhta P, Krystofiak T, Proszyk S, Žigo O (2016) Effect of Barrier Plasma Pre-Treatment on Polyester Films and their Adhesive Properties on Oak Wood. *BioResources* 11(3): 6335-6345.

Odrášková M., Ráhel J., Záhoranová A., Tiňo R., Černák M., 2008: Plasma Activation of Wood Surface by Diffuse Coplanar Surface Barrier Discharge. *Plasma Chemistry and Plasma Processing*, vol. 28(2), p. 203-211.



CUPPING DEFORMATION DURING DRYING OF BEECH WOOD (*FAGUS SYLVATICA* L.)

Ivan Klement – Tatiana Vilkovská – Peter Vilkovský – Aleksandra Suchta
– Jacek Barański

Abstract

Wood drying does not only consist in removing its moisture: the quality of the dried product is the main requirement for the industrial process. Because wood shrinks during drying, deformations and stresses develops than can lead to unusable product. When developing drying technologies and methods, the aim is to achieve the shortest possible drying times. The most common defects in wood after drying include cross warping (cup), which significantly affects the efficiency of processing the raw material into products. The research was focused on the effect of different drying conditions (temperature, drying gradient) on the size of the cross warping. Despite very intensive drying and large moisture gradients at the end of drying, the values of cross-peeling in beech samples after high-temperature drying were small and the positive effect of high temperatures on the amount of drying of the wood was confirmed. A reduction in the size of the cross warping can also be achieved by effective loading of the samples in combination with a more precise control of the high temperature drying process so that smaller values of the moisture gradients of the samples at the end of the drying process are achieved.

Key words: *deformations, cup, beech wood, high temperature drying, drying intensity, drying gradient.*

INTRODUCTION

Wood, being a natural hygroscopic material, the interaction between wood and moisture plays a crucial role in wood processing and utilization. Drying shrinkage is a common phenomenon during the processing and utilization of wood induced by moisture loss (Fu *et al.* 2022; Ormarsson 1999). The moisture content of a growing tree is high, and it is normally needed to dry the timber before using it for construction purposes. During drying of wood, it is important to avoid excessive deformation of the sawn timber. The deformation process is affected by differences of the moisture and temperature conditions. To minimize unfavorable deformations, such as cup, twist, crook, bow (Fig. 1), one may optimize the environmental conditions during the drying process as well. Characteristic of wood is that its behavior is strongly orthotropic due to the internal structure of the material and exact dependent on moisture and temperature (Miyoshi *et al.* 2018). In addition, the material is characterized by a strong variation of the properties in the radial direction. Furthermore, the behavior of wood is strongly affected by variations in the environmental conditions, especial when the trees is exposed to stress.

This anisotropy affects many of the wood species characteristics such as strength, shrinkage, swelling, thermal and electrical conductivity. As a representative example, wood exhibits different levels of shrinkage among tangential, radial, longitudinal directions.

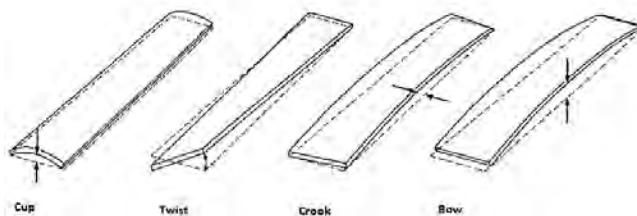


Fig. 1 Different forms of deformation of wood (Bond, Espinoza 2016)

This anisotropy affects many of the wood species characteristics such as strength, shrinkage, swelling, thermal and electrical conductivity (Fig.1). As a representative example, wood exhibits different levels of shrinkage among tangential, radial, longitudinal directions. Commonly, the tangential shrinkage is the greatest, around 6–12%, followed by radial shrinkage at 3–6%, and longitudinal shrinkage being less than 0.1–0.2% (Glass, Zelinka 2021; Nocetti *et al.* 2015). The loss of moisture leads to different drying shrinkage in different grain directions of wood, and thus shrinkage anisotropy of wood is one of the reasons for the drying stresses. Additionally, due to in reliabilities of moisture content between the surface and core layers during the drying process of wood, as well as differences in material properties between heartwood and sapwood, or earlywood and latewood, there will be uneven distribution of moisture content. The uneven distribution of wood moisture will produce moisture gradient stress, which forms an additional source of drying stresses in wood. Therefore, the shrinkage anisotropy stress and moisture gradient stress, are the two principal catalysts of drying stresses in wood (Fu *et al.* 2015). One type of deformation is cup, which is defined as a distortion of a board in which there is deviation from flatness across the width of the board (Simpson 1991, Vilkovský *et al.* 2023).

The main objective of the present paper is to characterize and analyze one of the most common wood defects after drying, namely cross warping, which significantly affects the efficiency with which the raw material can be processed into products. Therefore, the article is designed to evaluate the effect of temperature on the size of the cupping deformation during high-temperature drying and warm-air drying.

MATERIAL AND METHODS

The testing tree species was beech (*Fagus sylvatica* L.), which is the most economically important tree species in the forests of Slovakia. Logs with a diameter at the thinner end of 50 to 56 cm and a length of 4 metres were used. The logs were harvested in the forests of the University Forestry Enterprise in the locality of Hronská Breznica. The logs were sawed by cant sawing pattern. Subsequently, the prisms were cut into 25 mm thick sawn timber. The dimensions of the samples were 25 × 120 × 1000 mm. Specimens were cut from the centre of the lumber so that their net dimension was 1000 mm. Samples were cut at the edge of the specimen for moisture content and moisture gradient (Figure 2). Specimens with annual circles with a slope of 0 to 30° tangential sawn timber were selected for test specimens. At regular time intervals, the selected samples were weighed. Based on this moisture content, the drying process was controlled.

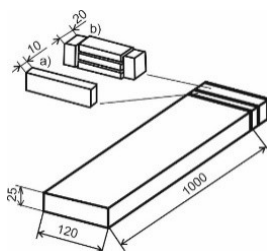


Fig. 2 Samples for determination a) moisture content b) moisture gradient

Drying mode

Two drying modes were used. High-temperature and warm-air drying. Drying of the samples was done in the drying kiln in the drying laboratory at the Department of Wood Technology, Technical University of Zvolen. For warm-air drying, a low-temperature drying mode with constant drying environment parameters was used. For high temperature drying (HT), two drying modes were used, which differed in the maximum temperature used in the last mo stage (130 and 150 °C). The parameters of the drying modes are given in Table 1. The samples were dried to a final moisture content of 10 ± 1 %.

Table 1 Parameters of used drying modes

Moisture content [%]		High temperature drying process						Warm - air drying process					
		t_s [°C]	Δt [°C]	U [-]		t_s [°C]	Δt [°C]	U [-]		t_s [°C]	Δt [°C]	U [-]	
above	60	100	4		5.82	100	4		5.82	40	5		5.82
60	40	100	4	5.82	3.88	100	4	5.82	3.88			4.8	3.2
40	30	100	6	4.44	3.33	100	6	4.44	3.33			3.2	2.4
30	25	100	6	3.33	2.78	100	6	3.33	2.78			2.4	2
25	20	115		5.68	4.55	115		5.68	4.55			2	1.6
20	15	130		10	7.5	130		10	7.5			1.6	1.2
15	10	130		7.5	5	150		21.43	14.29			1.2	0.8

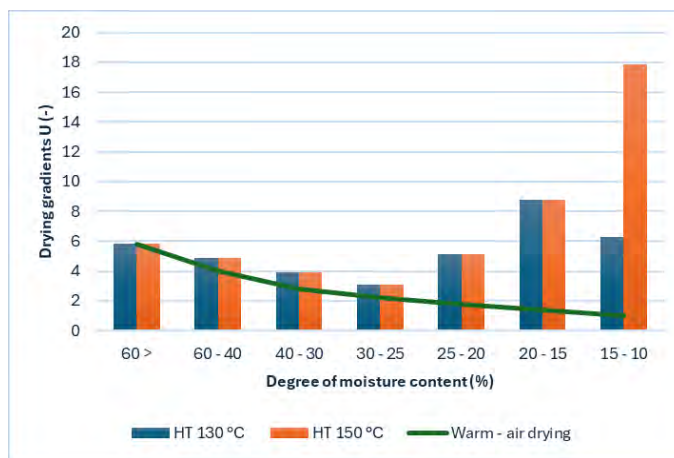


Fig. 3 Average values of drying gradient U in moisture levels and drying modes

A graphical representation of the average values of the drying gradients for the moisture stages and for each drying mode is shown in Figure 3. The drying gradient characterises the drying intensity and is the ratio between the actual wood moisture content w and the equilibrium moisture content w_r .

Moisture measurement was carried out by the weight method according to *EN 49 0103*. During drying, the drying samples were weighed at regular time intervals to determine the actual moisture content of the wood.

The moisture gradient characterises the distribution of moisture in the cross-section of the wood. The samples for the determination of the moisture gradient were processed as shown in Figure 4.

Determination of the moisture contents of the individual layers was carried out by the weighting method. The level of the moisture gradient was calculated according to the equation:

$$\Delta w = w_c - w_p \quad [\%] \quad (1)$$

where: w_c – moisture content middle layer of wood [%], w_p - moisture content surface layer of wood [%].

Cross warping

The value of the level of the cross warping was expressed using the so-called relative warping. The relative warping is the ratio of the maximum deflection f to the width of the sawn timber b (Fig. 4) and is expressed as a percentage.

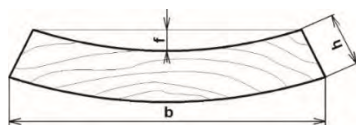


Fig. 4 Measurement of cross warping

Due to the small volume of the dried samples in the dryer, their relative loading was small and did not affect the size of the measured cross warping.

The values of cross warping K were calculated according to Eq. (2):

$$K = \frac{f \cdot 100}{b} \quad [\%] \quad (2)$$

Where: f - maximum deflection [mm], b - width of timber [mm].

RESULTS AND DISCUSSION

The average values of the moisture contents of the samples, the drying times and rates, and the densities of the samples in the dry state are given in Table 3. The moisture loss of the samples as a function of time is shown graphically in Figure 5.

Tab. 3 Basic drying characteristics for individual modes

Type of drying	Maximal drying temperature [°C]	Moisture content [%]		Drying time [h]	Drying rate [%·h ⁻¹]	Density [kg·m ⁻³]
		initial	final			
High temperature drying (HT)	130	69,1	12,6	30,0	1,9	702,0
	150	69,0	10,0	30,0	2,0	717,0
Warm-air drying	40	73,8	10,1	288,0	0,2	709,0

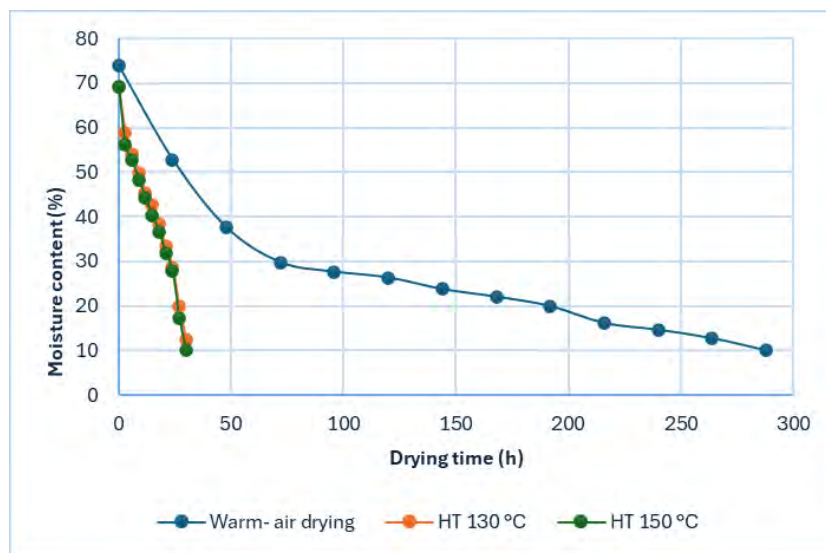


Fig. 5 Drying curves of beech samples in high-temperature and hot-air drying

The initial moisture contents of the samples ranged from 68 to 74,2 % and the final moisture contents ranged from 9,4 to 12,8 %. With high temperature drying and a drying temperature of 130 °C, the final moisture content was higher than originally planned, averaging 12 %. The shape of the drying curves also varied. In the high temperature drying, the curves were linear. This means that the moisture loss was directly proportional to the drying time. The average drying time was 30 hours, and this corresponds to the drying rate, which was slightly higher when a temperature of 150 °C was used.

The resulting drying times are very short compared with low-temperature warm-air drying of this wood, which is due to the high drying intensity around removal of bound water. In warm-air drying, the drying time was 288 hours, and the drying rate was ten times lower compared to high-temperature drying. This corresponds to the values of the drying gradients for the drying modes used. All modes started with the same drying gradient value (5.82) and gradually the drying gradient decreased.

For high temperature drying from an average moisture content of 25 %, the drying gradient increased up to a value of 8,5. At a drying temperature of 150 °C, at the last moisture content stage, it reached a value of almost 18. For warm-air drying, in the evaporation section of the water bound from the samples (below 25%), the drying gradient values decreased and at the last moisture content stage the drying gradient value was 1.

Moisture gradients were measured at three-hour intervals for both high-temperature drying methods. In the warm-air drying, the moisture gradient was measured at the beginning and at the end of the drying process. The average calculated values are shown in Figure 6.

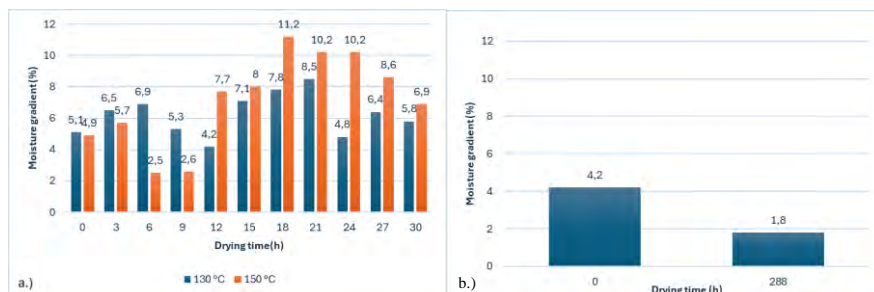


Fig. 6 Average values of moisture gradients of samples (a) high-temperature drying (b) warm-air drying

For high temperature drying, the moisture gradients were higher at a drying temperature of 130 °C in the first part of the drying process (up to an average moisture content of 40 %). Subsequently, until the final stage of drying, higher values of moisture gradients were measured at a drying temperature of 150 °C. If only the drying section where a drying temperature above 100 °C was used is analysed, the effect of the drying temperature has a marked effect on the size of the moisture gradients. At an average wood moisture content of 30 %, the moisture gradient in the drying where the maximum drying temperature of 130 °C was used was 7,8 %, but at a drying temperature of 150 °C it was 11,2 %. At the final stage of drying, the values of the moisture gradients for the different drying temperatures were within one percentage point of each other, being 6,9 % at the drying temperature of 150 °C and 5,8 % at the drying temperature of 130 °C. These values are significantly higher, and it can be concluded that ending the drying process based on the average measured moisture content of the wood is not ideal. It is advisable to take account of the high dynamics of the drying process and to move the finishing of the process later stage.

During warm-air drying using the low-temperature mode, the drying gradients at the beginning of the drying process were comparable to those of the high-temperature drying samples. The average final value for this drying method was 1.8%, indicating that the drying was very slow and mild.

The absolute value of the cross warping (f) was measured at the centre of the samples with a mechanical device and was then converted according to relation (2) to the relative warping (K), considering the width of the samples. The converted mean values and their basic statistical characteristics are shown in Table 4.

Tab. 4 Mean values and basic statistical characteristics of the cross-sectional grading of the samples

Drying mode	Max drying temperature (°C)	Relative cross warping K (%)			variance standard	deviation standard	standard error	coefficient of variation	number of samples
		average	minimum	maximum					
High-temperature drying	130	2,8	1,5	4,0	0,789	0,888	0,256	32,3	30
	150	2,3	1,1	3,9	0,918	0,958	0,277	41,3	30
Warm-air drying	40	1,4	0,6	1,5	0,245	0,495	0,143	28,1	30

The changes in the shape of the samples were small for both drying methods. The average values of relative cross-warping ranged from 1.4 to 2.8 % (Table 4). The lower values were for the low-temperature warm-air drying. Statistical analysis of the measured values showed that drying temperature or drying method was a moderately significant factor affecting the size of the cross warping. As also shown in research Xiang *et al.* (2012) cupping happens because shrinkage parallel is greater than that perpendicular to the growth rings. In other words, cupping is the result of tangential shrinkage of wood being greater than radial shrinkage, and the greater the difference, the more severe the degree. Between drying temperatures of 130 and 150 °C, there was a statistically non-significant effect on cross-warping. Longitudinal warping was also observed on the samples, which was reflected by longitudinal bowing and twisting. Overall, it can be concluded that the values of cross-warping for both drying methods are positive, even because it was not possible for technical reasons to load the samples during drying, which would have eliminated the cross-warping further. Based on the citate work Miyoshi (2014) it was revealed that the mechanical properties of wood in the lateral direction were significantly affected not only by the density but also by the structural features such as deformation of cell shapes, arrangement of ray or vessels, and the degree of the transition from the earlywood to the latewood.

CONCLUSIONS

When developing drying technology and methods, the aim is to achieve the shortest possible drying times. One way this can be achieved is by increasing the temperature of the drying environment. However, it is important that the dried wood is not damaged. One of the most common defects in wood after drying is cross-warping, which considerably affects the efficiency with which the raw material can be processed into products. The following conclusions can be made from the measured results of the research:

- High-temperature drying is a very rapid drying method and compared to the low-temperature drying method, the resulting drying times are on average 10 to 15%, which corresponds to a drying rate that is approximately ten times higher.
- The drying curves for both modes of high temperature drying were very rapid and linear. When a temperature of 150 °C was used in the last moisture level, the final moisture content of the samples was achieved more precisely.
- The values of moisture gradients at the end of the high-temperature drying process were large (5.8-6.9%), which had a negative effect on the size of the cross-warping of the samples.
This is an indication that the control of the drying process based on achieving the average required moisture content is not optimal. For the warm air drying, the moisture gradient was 1.8%.
- The average values of the cross warping were lower in the warm-air drying. The differences between the high-temperature drying modes (130 and 150°C) were minimal and the statistics were not significant.
- Despite very intensive drying and large moisture gradients at the end of drying, the values of cross warping of beech samples after high-temperature drying were small and the positive effect of high temperatures on the size of shrinkage was confirmed.

- Reducing the size of the warping is also possible by efficient loading of the samples in combination with more precise control of the high temperature drying process so that smaller values of moisture gradients of the samples at the end of the drying process are achieved.

Research into the effect of drying conditions on the size of wood warping is important to increase the efficiency of processing raw material into products.

ACKNOWLEDGEMENTS

This work was supported by the Slovak Research and Development Agency under contract no. APVV-21-0049. This work was supported by the Scientific Grant Agency of the Ministry of Education, Science, Research and Sport of the Slovak Republic and the Slovak Academy of Sciences—project VEGA no. 1/0063/22.

LITERATURE

1. Fu, Z.; Wang, H.; Li, J.; Lu, Y. Determination of Moisture Content and Shrinkage Strain during Wood Water Loss with Electro-chemical Method. *Polymers* 2022, 14, 778.
2. Glass, S.; Zelinka, S. Moisture relations and physical properties of wood. In Chapter 4 in FPL-GTR-282; U.S. Department of Agriculture Forest Service: Washington, DC, USA, 2021.
3. Fu, Z.; Zhao, J.; Huan, S.; Sun, X.; Cai, Y. The variation of tangential rheological properties caused by shrinkage anisotropy and moisture content gradient in white birch disks. *Holzforschung* 2015, 69, 573–579. Review on Wood Deformation and Cracking during Moisture Loss.
4. Simpson, W. T. (1991). Dry Kiln Operator's Manual, USDA Forest Service, Agricultural Handbook 188.
5. Ormarsson, S., Dahlblom, O. Petersson, H. A numerical study of the shape stability of sawn timber subjected to moisture variation Part 2: Simulation of drying board. *Wood Science and Technology* 33, 407–423 (1999). <https://doi.org/10.1007/s002260050126>
6. Nocetti, M., Brunetti, M., Bacher, M. Effect of moisture content on the flexural properties and dynamic modulus of elasticity of dimension chestnut timber. *Eur. J. Wood Prod.* 73, 51–60 (2015). <https://doi.org/10.1007/s00107-014-0861-1>
7. Miyoshi, Y., Kojiro, K. & Furuta, Y. Effects of density and anatomical feature on mechanical properties of various wood species in lateral tension. *J Wood Sci* 64, 509–514 (2018). <https://doi.org/10.1007/s10086-018-1730-z>
8. Miyoshi Y, Kojiro K, Furuta Y (2014) Deformation properties of wood in lateral tension effect of tensile direction to the annual rings, moisture, and temperature on lateral tensile deformation of hinoki (*Chamaecyparis obtusa*) (in Japanese). *Mokuzai Gakkaishi* 60:241–248
9. Xiang, Z., Peralta, P., Peszlen, I. (2012). Lumber drying stresses and mitigation of cross-sectional deformation. *Wood and Fiber Science*, 44(1), 94-102
10. Bond, B.H., Espinoza, O. A Decade of Improved Lumber Drying Technology. *Curr Forestry Rep* 2, 106–118 (2016). <https://doi.org/10.1007/s40725-016-0034-z>
11. Vilkovský, P., Klement, I., and Vilkovská, T. (2023). “The impact of the log-sawing patterns on the quantitative and qualitative yield of beech timber (*Fagus sylvatica L.*)” *Applied Sciences* 13(14), 8262. DOI: 10.3390/app13148262



CHIP COLOR ANALYSIS USING THE PROGRAM MATLAB

Pavol Koleda

Abstract

*The aim of the research was to describe the possibility of detecting the color of particles using the Matlab program. first, the loaded image with measured sawdust is converted into black and white. this is done using the Otsu method. In this binarization, the sawdust is represented by white areas, the background is black. Subsequently, individual sawdust is analyzed using the regionprops function. It is used to find all the pixels belonging to each separate sawdust, along with their positions. In these found pixels, the RGB color components are subsequently identified. From the color components of all pixels, an average value representing the color of each separate sawdust is calculated. For practical comparison, the found RGB components are converted to other color space such as CIE $L^*a^*b^*$ and CIE XYZ. The color values in all three spaces are saved in an Excel file for further processing.*

Key words: *Color, Lightness, Matlab, RGB.*

INTRODUCTION

Wood is an important natural renewable material (Dos Santos et al. 2016), and the possibilities for its use are tremendous. It is as important a building material for the interior as it is for the exterior. Wood is used in the furniture industry, and it is an important raw material in the paper industry as well as the power industry. As a natural material, wood is a chemical compound of mostly organic substances. It is mainly composed of organic macromolecular substances: cellulose (35 % to 50 %), hemicelluloses (20 % to 35 %), and lignin (15 % to 35 %) (Geffert 2013). All together, these components make up 90 % to 97 % of the absolute weight of dry wood. Furthermore, wood also contains extractive substances: carbohydrates, starch, and oils; proteins, inorganic salts, waxes, tanstuffs, and resins; and turpentine, ethereal oils, and colorants, as well as others that influence the wood color (Geffert 2013).

The color of wood is an important component of its appearance (Babiak et al. 2004), and therefore it figures crucially in the final decision of a customer (Sahin et al. 2011; Jankowska and Kozakiewicz 2014; Kubovský and Igaz 2014; Barcík et al. 2015). Color is one of wood's basic physical properties (Čunderlík 2009; Dzurenda 2018). The color is determined by the chemical components of wood. Besides genetic factors, the color of the wood is influenced by the environmental conditions (the humidity, solar radiation, pollution, and wind) where the tree and the wood grew (Čunderlík 2009; Valverde and Moya 2013). The color is also one of the parameters of the quality of the surface assessment.

MATERIALS AND METHODS

Particleboard blanks samples with dimensions: thickness $t = 18$ mm, width $w = 300$ mm, and length $l = 500$ mm, were used in the experiment. The specimens were milled with the diamond shank milling cutter with the following technological parameters: constant depth of cut $e = 4$ mm; rotation speed of spindle with cutting tool $n = 18.000$ rpm, and feed speed $v_f = 6$ m.min⁻¹. For each combination of parameters, six specimens in total were collected. The conventional milling (up-milling) method was used for carried experiment. The obtained sawdust is placed on a base with a contrasting color, in this case was the black color base used (figure 1).



Figure 1 Obtained sawdust placed on a black contrasting base

To determine the color of individual sawdust, it is necessary to find out where these particles are located in the image. For this purpose, first the original image is converted to grayscale using the function *im2gray(I)*. This function converts the specified truecolor image RGB to a grayscale intensity image I . The *im2gray* function converts RGB values to grayscale values by forming a weighted sum of the R, G, and B components. The coefficients used to calculate grayscale values in the *im2gray* function are identical to those used to calculate luminance ($E'y$) in Rec.ITU-R BT.601-7 after rounding to three decimal places. Rec.ITU-R BT.601-7 calculates $E'y$ using this formula:

$$0.299 * R + 0.587 * G + 0.114 * B \quad (1)$$

The image modified in this way is then thresholded using the function *imbinarize(bw)*. Function *imbinarize(bw)* creates a binary image from 2-D or 3-D grayscale image bw by replacing all values above a globally determined threshold with 1 and setting all other values to 0. By default, *imbinarize* uses global Otsu's method, which chooses the threshold value to minimize the intraclass variance of the thresholded black and white pixels (Otsu, 1979). *Imbinarize* uses a 256-bin image histogram to compute Otsu's threshold. The result of this step is an image in which white spots are represented by sawdust on a black background (figure 2).

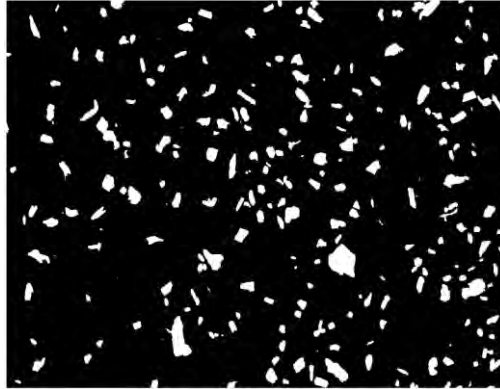


Figure 2

In such a binary image, the individual sawdust is subsequently identified using the function $regionprops(bw, 'PixelList')$. This function finds unique objects in binary image bw using 8-connected neighborhoods for 2-D images and maximal connectivity for higher dimension images. Property $'PixelList'$ return a location of pixels in every found sawdust and their XY coordinates in the image. Subsequently, the color of the pixels in the RGB color space is determined for each sawdust using the function:

$$impixel(I, x_i, y_i) \quad (2)$$

who: I – original loaded image with sawdust,
 x_i, y_i – the coordinates of the i -th point in image.

The color is not determined in the binary image, but in the original unmodified one. For each particle, the average color value in RGB components is calculated. Subsequently, this value is also converted into XYZ and CIA Lab color spaces. The conversion of color components into XYZ is done using coefficients that depend on the angle of incidence of daylight and reference white point, specified as a 1-by-3 vector or one of the CIE standard illuminants. In our experiment, conversion constants during midday daylight with a correlated color temperature of 6504 K were used. The conversion of components from RGB to XYZ color space is given by the relation:

$$\begin{bmatrix} X \\ Y \\ Z \end{bmatrix} = \begin{bmatrix} 0.4124564 & 0.3575761 & 0.1804375 \\ 0.2126729 & 0.7151522 & 0.0721750 \\ 0.0193339 & 0.1191920 & 0.9503041 \end{bmatrix} \begin{bmatrix} R \\ G \\ B \end{bmatrix} \quad (3)$$

The next conversion of components from XYZ to CIE LAB color space is given by the relation:

$$\begin{aligned} L^* &= 116 \cdot f\left(\frac{Y}{Y_n}\right) - 16 \\ a^* &= 500 \left(f\left(\frac{X}{X_n}\right) - f\left(\frac{Y}{Y_n}\right) \right) \\ b^* &= 200 \left(f\left(\frac{Y}{Y_n}\right) - f\left(\frac{Z}{Z_n}\right) \right) \end{aligned} \quad (4)$$

Where t is X/X_n , Y/Y_n , or Z/Z_n :

$$f(t) = \begin{cases} \sqrt[3]{t} & \text{if } t > \delta^3 \\ \frac{1}{3}t\delta^{-2} + \frac{4}{29} & \text{otherwise} \end{cases} \quad \delta = \frac{6}{29}$$

The color values determined in this way are stored in the table editor for possible further data processing, such as statistical analysis in the Statistica program.

RESULTS

Measured values in the CIE Lab color space are shown in the figure 3.

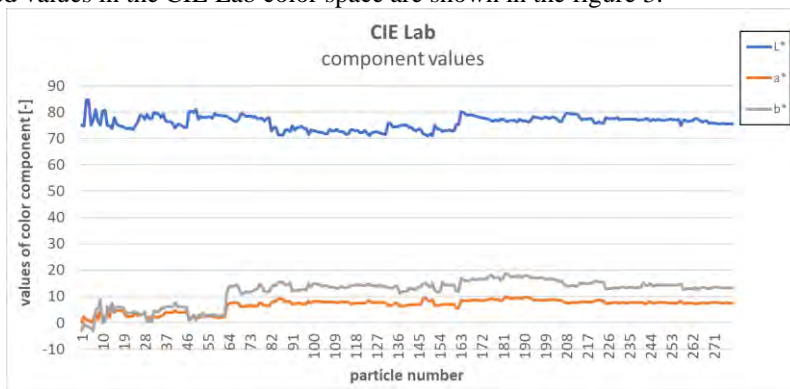


Figure 3 Values of color components in CIE Lab color space

As can be seen in Figure 3, the values of individual sawdust color components are within a narrow range. The color is therefore approximately the same in each particle. The values show that the color of the given sample is in light shades of soft red and yellow. The distribution of the values of the individual components can be determined using a box plot in the figure 4.

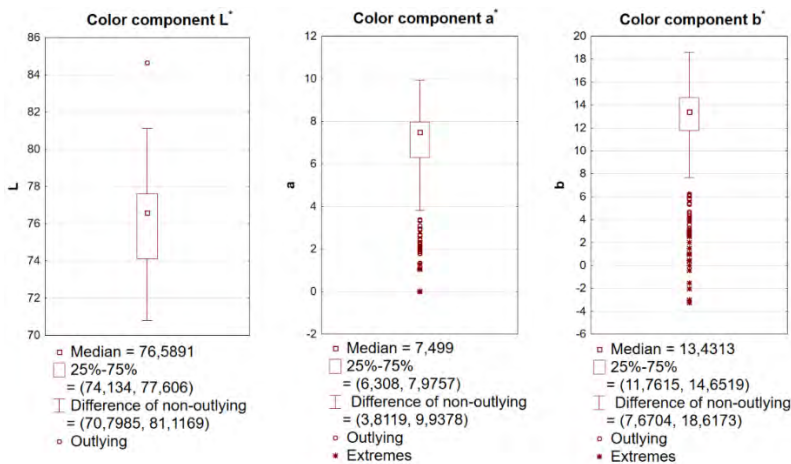


Figure 4 Distribution of color components values

Statistical analysis of the studied sample was done using descriptive statistics in the statistics program Statistica (table 1). Here can be analyzed a given sample using various statistical parameters like mean, median, modus, variance and standard deviation.

Table 1 Statistical analysis of color component values

Variable	N of valid	Average	Median	Modus	Modus frequency	Minimum	Maximum	Variance	Standard deviation
L	279	76,06148	76,58908	75,57136	3	70,79851	84,65494	6,05798	2,461297
a	279	6,62236	7,49902	7,515987	3	0,00350	9,93784	5,18724	2,277551
b	279	11,87001	13,43130	13,16604	3	-3,23685	18,61732	24,07567	4,906696

CONCLUSION

The article describes the possibility of detecting the colors of sawdust or other particles in a digital image using the Matlab program. In this sawdust, the color of every single sawdust is detected, so it is possible to analyze the color changes in each particle. Color components can be converted to different color spaces such as RGB, XYZ or CIE Lab. The measured values can be further analyzed directly in the Matlab program, or the data can be exported to an Excel spreadsheet for further processing, such as statistical analysis in the Statistica program.

ACKNOWLEDGMENTS

The paper was written with the support of project APVV-20-0403, “FMA analysis of potential signals suitable for adaptive control of nesting strategies for milling wood-based agglomerates“ and thanks to support under the Operational Program Integrated Infrastructure for the project: National infrastructure for supporting technology transfer in Slovakia II – NITT SK II, co-financed by the European Regional Development Fund.

REFERENCES

- Babiak, M., Kubovský, I., Mamoňová, M. 2004 . Color space of the selected domestic species. In: *Interaction of Wood with Various Forms of Energy*, Technical University of Zvolen, Zvolen, Slovakia, pp. 113-117.
- Barčík, Š., Gašparík, M., Razumov, E. Y. 2015. Effect of temperature on the color changes of wood during thermal modification. In: *Cell. Chem. Technol.* 49(9-10), 789-798.
- Čunderlík, I. 2009. *Štruktúra dreva*. Technical University in Zvolen, Zvolen, Slovakia.
- Dzurenda, L. 2013. Modification of wood colour of *Fagus sylvatica* L. to a brown-pink shade caused by thermal treatment. In: *Wood Research* 58(3), 475-481.
- Dzurenda, L. 2018. The shades of color of *Quercus robur* L. wood obtained through the processes of thermal treatment with saturated water vapor. In: *BioResources* 13(1), 1525-1533. DOI: 10.15376/biores.13.1.1525-1533
- Geffert, A. 2013. *Chemické technológie dreva*. Technical University in Zvolen, Zvolen, Slovakia.
- Hrčka, R. 2008. Identification of discoloration of beech wood in CieLab space. In: *Wood Res- Slovakia* 53(1), 119-124.

- Jankowska, A., Kozakiewicz, P. 2014. Influence of thermal modification of Scots pine wood (*Pinus sylvestris* L.) on color changes. In: *Annals of Warsaw University of Life Sciences – SGGW. Forestry and Wood Technology* 88(2014), 92-96.
- KOLEDA, P.; BARCÍK, S.; KORČOK, M.; JAMBEROVÁ, Z.; CHAYEUSKI, V. Effect of Technological Parameters on Energetic Efficiency When Planar Milling Heat-treated Oak Wood. *Bioresources* 2021, 16, 515–528. DOI: 10.15376/biores.16.1.515-528
- KORČOK, M., KOLEDA, P., BARCÍK, Š., VANČO, M. 2018. Effects of Technical and Technological Parameters on the Surface Quality when Milling Thermally Modified European Oak Wood. In: *BioResources*, 13(4): 8569-8577.
- KOS, A., BELJO-LUČIĆ, R., ŠEGA, K., RAPP, A. O. 2004. Influence of woodworking machine cutting parameters on the surrounding air dustiness. In *Holz als Roh-und Werkstoff* 62(3): 169-176. DOI:10.1007/s00107-004-0473-2.
- Kubovský, I., Igaz, R. 2014. Utilization of CO2 laser as an unconventional instrument to wood colour changes. In: *Acta Facultatis Technicae*. 19(1), 79-88.
- KUČERKA, M., OČKAJOVÁ, A., KMINIAK, R., PEŹDIK, M., ROGOZINSKI, T. 2022. The Effect of the Granulometric Composition of Beech Chips from a CNC Machining Center on the Environmental Separation Technique. In: *Acta Facultatis Xylogiae*. Zvolen, 2022. vol. 64(1), P 87-97. DOI: 10.17423/afx.2022.64.1.08.
- INTERNATIONAL AGENCY FOR RESEARCH ON CANCER. 1995. Monographs on the Evaluation of Carcinogenic Risks to Humans: Volume 62 Wood Dust and Formaldehyde. Lyon, France. 1995. ISBN 92 832 1262 2.
- OTSU, N., 1979. A Threshold Selection Method from Gray-Level Histograms. In: *IEEE Transactions on Systems, Man, and Cybernetics*. Vol. 9, No. 1, 1979, pp. 62–66.
- REZAEI, H., LIM, C. J., LAU, A., SOKHANSANJ, S. 2016. Size, Shape and Flow Characterization of Ground Wood Chip and Ground Wood Pellet Particles. In: *Powder Technology*. Vol. 301. P. 737-746. DOI: 10.1016/j.powtec.2016.07.016.
- SVOREŇ, J. et al. 2022. Influence of circular saw blade design on reducing energy consumption of a circular saw in the cutting process. In: *Applied sciences*. Vol. 12(3), 2022, 15 p. ISSN 2076-3417.
- Valverde, J. C., and Moya, R. 2013. Correlation and modeling between color variation and quality of the surface between accelerated and natural tropical weathering in *Acacia mangium*, *Cedrela odorata*, and *Tectona grandis* wood with two coatings. In: *Color Research & Application*, 39(5), 519-529. DOI: 10.1002/col.21826.



EXPERIMENTAL ANALYSIS OF PARAMETERS INFLUENCE OF WOODBASED MATERIALS MILLING ON VIBRATIONS AMPLITUDE

Peter Koleda – Áron Hortobágyi – Richard Kminiak

Abstract

The research of the wood-based material processing parameters is currently devoted to their influence on the suitability of indirect analysis of this process from the point of view of adaptive control and prediction. The article describes the method of measuring vibration evaluation using an accelerometer attached to the suction cups of a woodworking center during milling of medium density fibreboards and particle boards. Spiral mill HW 16×42×16 RH and razor cutter with two razors were used as tools, with feed rate of 2, 6, 10 m.s⁻¹ and spindle rotations of 10,000 and 20,000 min⁻¹. The effects of the tool, material and speed on the vibration amplitude were evaluated, and it was shown that the change of these parameters has a statistically significant effect on this amplitude. It is therefore possible to consider the use of vibration measurement also for a certain method of adaptive control of the machining process.

Key words: milling, clamping, vibrations, amplitudes

INTRODUCTION

Wood milling is a well-known manufacturing process, which is the subject of many research in terms of technical-technological parameters. During cutting process in a milling machine, vibration is frequent problem which affects dimensional accuracy of the parts being machined, surface finish and tool life. Vibrations are induced due to machine faults, cutting parameters, cutting tool, work piece deformation, etc. Vibrations are generally measured using accelerometers by mounting on various machine elements (Kusuma et al. 2014). A relation was found for steel machining, that feed rate is the most dominating parameter affecting surface finish, whereas cutting speed is the major factor effecting tool vibration (Bhagal et al. 2015). Similar results were found for aluminum (Asilturk 2011). Singular spectrum analysis was considered as a viable method for analyzing vibration signals applied to the on-line monitoring of surface roughness (Plaza et al. 2017), as well as prediction of surface roughness in CNC turning by model-assisted response surface method (Misaka et al. 2020).

Another factor affecting vibrations is clamping. Vacuum clamping systems, such as used in this study, are predominantly used for machining particle boards on woodworking machining centers. The quality of the particle board edges is reduced, and a high noise level is induced by these vibrations (Hesselbach et al. 2010). However, all the above could be measured by other non-intrusive methods, such as vibro-acoustic analysis (Melnik et al.

2018, Nahorny et al. 2022, Iskra et al. 2015), or by means of energy consumption tests (Pantaleo et al. 2014, Licow et al. 2020).

The aim of the contribution is to analyze the influence of the milled material and the speed on the amplitude of vibrations arising during the milling of MDF and particle boards and to assess the suitability of their measurement for adaptive control.

MATERIAL AND METHODS

Medium density fiberboards cut to 500x300x18mm with weight 1960g were used as samples. The density of these samples was $720 \text{ kg}\cdot\text{m}^{-3}$ – $740 \text{ kg}\cdot\text{m}^{-3}$. Particleboards of same dimensions were added as reference samples. Both originated from Kronospan Ltd., Zvolen, Slovakia. The density of particleboards given by the manufacturer is $600 \text{ kg}\cdot\text{m}^{-3}$ – $640 \text{ kg}\cdot\text{m}^{-3}$ (deciduous 10 %, coniferous 90 %), and urea formaldehyde glue with paraffin admixture is used. The manufacturer declares that the material complies with the EN 14322 standard, EN 312-2, and emission class E1 (EN ISO 12460-5).

Samples were clamped to four pneumatic grippers, each with surface $120 \times 120 \text{ mm}$ and clamping force $16 \text{ kg}\cdot\text{m}^{-2}$. Each cut had depth of 19mm, so whole thickness of material was machined in one run. To emulate conditions of nesting milling, tool trajectory cut through middle of sample. Spiral mill HW $16\times 42\times 16 \text{ RH}$ and razor cutter with two razors were used as tools, with feed rate varying 2, 6, $10 \text{ m}\cdot\text{s}^{-1}$ and spindle rotations 10 000 and 20 000 min^{-1} . Cutting was repeated 3 times for each parameter. Both experimental layout and cutting parameters are shown in Figure 1 (Hortobágyi et al. 2022).

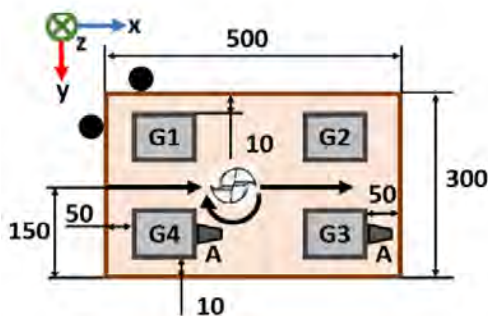


Figure 1 Experiment layout. (a) Sample placement and tool path on CNC. G – pneumatic gripper, A – accelerometer, x,y,z – orientation of accelerometer axes, (b) cutting parameters of experiment and used tools (Hortobágyi et al. 2022)

Data was then processed in MATLAB (MathWorks, Inc., USA). Initial signal was cut so only milling part would be assessed and measured voltage was converted to acceleration (Picotech). Pre spektrálnu analýzu meraného signálu bola použitá Fast Fourier Transform (FFT).

RESULTS AND DISCUSSION

Fast Fourier transform brought several results. First were dominant frequencies. First peaks were observed at 165,93 Hz – 166,13 Hz. Next peaks were 332,26 Hz and 498,2 Hz. These, with rest of peaks present multiples of first value. However, these were still present, but with maxima smaller than 0,5 and were filtered out. Similar results were observed through use of all parameters. Therefore, it seems the main vibrations were caused by rotating tool.

Descriptive statistics of filtered dominant amplitudes (peak > 0,5) of vibration acceleration are shown in Table 1.

Table 1 Descriptive statistics of amplitudes

Parameter	Average	Std. dev.	-95 %	+ 95%
Spiral milling tool	1,80	1,98	1,65	1,95
Razor milling tool	3,59	5,75	3,23	3,95
10 000	2,55	4,54	2,26	2,83
20 000	3,32	4,83	2,95	3,69
MDF	3,28	5,05	2,92	3,64
DTD	2,49	4,28	2,20	2,78

In Figure 2, results show the spindle speed has effect on amplitude overall, with values in range (2,28 – 2,85) for $n = 10\,000\text{ min}^{-1}$ and (2,95 – 3,7) for $n = 20\,000\text{ min}^{-1}$. Significance of this result is shown in Table 2. When different material is also considered, results are similar – amplitude ranges are higher with higher cutting speed. Ranges are overall smaller with PTB, when compared to MDF.

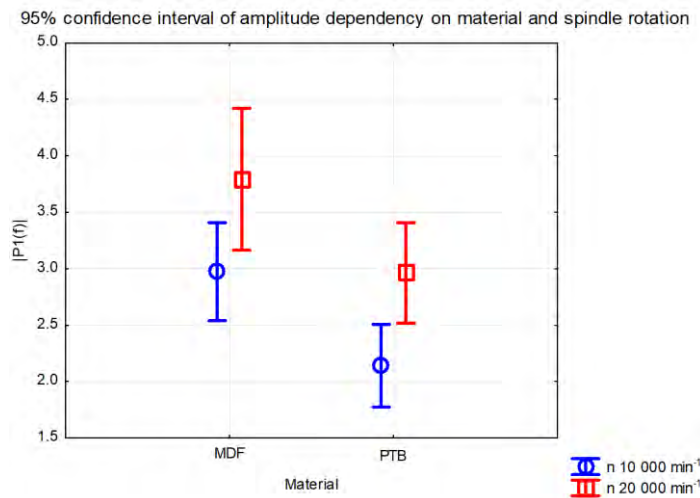


Figure 2 Box plot of 95 % confidence interval of amplitude dependency on material and spindle rotation.

Tables 2 to 4 show the testing of the statistical significance of the influence of individual parameters: revolutions, tool and milled material. The resulting data sets have a probability of similarity of less than 5 % when the monitored parameter changes, and thus

all the monitored parameters have a statistically significant effect on the amplitude of the resulting vibrations.

Table 2 Duncan test of spindle rotation effect on amplitudes

n [min⁻¹]	2,5486	3,3197
10000		0.000842
20000	0.000842	

Table 3 Duncan test of tool effect on amplitudes

tool	1,8031	3,5918
spiral		0.000009
razor	0.000009	

Table 4 Duncan test of material effect on amplitudes

material	3,27	2,49
MDF		0.000540
PTB	0.000540	

CONCLUSION

Main goal of research was to determine, whether vibration monitoring on gripper could be used for adaptive control, and therefore, if changes during milling process would be detectable. To answer this question, tests were conducted to find, if changes of parameters would produce differing measurements. Fast Fourier transform was used to process measured signals.

Dominant frequencies seem to origin from tool cutting into material. When single sided spectrum maxima were compared, tool, spindle rotation and feed rate seemed to affect the result. Variance analysis showed significant effect of investigated factors: material and spindle rotations.

Overall, vibrations measured at pneumatic gripper processed with Fast Fourier analysis seem to be sufficient as a potential signal for adaptive control during milling, similarly to (Plaza et al. 2017). As in (Misaka et al. 2020), roughness of samples should be measured and paired with vibrations in further study, to provide data for adaptive control model.

Finally, the use of vibration measurement, or acoustic emission can be considered as a data source for creating a model using AI, for example artificial neural network, decision trees or support vector machines.

ACKNOWLEDGMENT

This research was funded by APVV-20-0403 „FMA analysis of potential signals suitable for adaptive control of nesting strategies for milling wood-based agglomerates“

REFERENCES

- Kusuma, N.; Agrawal, M.; Shashikumar, P. V. Investigation on the influence of cutting parameters on Machine tool Vibration & Surface finish using MEMS Accelerometer in high precision CNC milling machine. *AIMTDR* **2014**, *375*, 1-6.
- Bhokal, S. S.; Sindhu, C.; Dhami, S. S.; Pabla, B. S. Minimization of surface roughness and tool vibration in CNC milling operation. *Journal of Optimization* **2015**.
- Asilturk, I. On-line surface roughness recognition system by vibration monitoring in CNC turning using adaptive neuro-fuzzy inference system (ANFIS). *International Journal of the Physical Sciences* **2011**, *6*, 5353-5360.
- Plaza, E. G.; López, P. N. Surface roughness monitoring by singular spectrum analysis of vibration signals. *Mechanical systems and signal processing* **2017**, *84*, 516-530.
- Misaka, T.; Herwan, J.; Ryabov, O.; Kano, S.; Sawada, H.; Kasashima, N.; Furukawa, Y. Prediction of surface roughness in CNC turning by model-assisted response surface method. *Precision Engineering* **2020**, *62*, 196-203.
- Hesselbach, J.; Hoffmeister, H. W.; Schuller, B. C.; Loeis, K. Development of an active clamping system for noise and vibration reduction. *CIRP annals* **2010**, *59*, 395-398.
- Melnik, Y. A.; et al. On adaptive control for electrical discharge machining using vibroacoustic emission. *Technologies*, **2018**, *6*, 96.
- Nahorny, V.; et al. Method of Using the Correlation between the Surface Roughness of Metallic Materials and the Sound Generated during the Controlled Machining Process. *Materials*, **2022**, *15*, 823.
- Iskra, P.; Tanaka, C. The influence of wood fiber direction, feed rate, and cutting width on sound intensity during routing. *European Journal of Wood and Wood Products*, **2005**, *63*, 167-172.
- Pantaleo, A.; Pellerano, A. Assessment of wood particleboards milling by means of energy consumption tests. *Wood Material Science & Engineering* **2014**, *9*, 193-201.
- Licow, R.; et al. Effect of pine impregnation and feed speed on sound level and cutting power in wood sawing. *Journal of Cleaner Production*, **2020**, *272*, 122833.
- EN 14322; Wood-Based Panels-Melamine Faced Board for Interior Uses—Definition, Requirements and Classification. European Committee for Standardization: Brussels, Belgium, 2017.
- EN 312-2; Particleboards-Specifications-Part 2: Requirements for General Purpose Boards for Use in Dry Conditions. European Committee for Standardization: Brussels, Belgium, 1996.
- EN ISO 12460-5; Determination of Formaldehyde Release-Part 5: Extraction Method (Called the Perforator Method). European Committee for Standardization: Brussels, Belgium, 2016.
- Hortobágyi, Á.; Koleda, P.; Kminiak, R. Workpiece gripper vibration measurement for nesting milling. *Trieskové a beztrieskové obrábanie dreva* **2022**, *13*, 19-24.
- Picotech. Three Axis Accelerometer Kit - Quick Start Guide. Available online: <https://www.picotech.com/download/manuals/ThreeAxisAccelerometerKitQSG.pdf> (accessed on 28 02 2023).



INFLUENCE OF V-BELT TYPE ON THE VIBRATION OF A WOODWORKING MILLING MACHINE AT IDLE

Georgi Kovatchev

Abstract

This study presents how V-belt type influences over vibrations of the cutting mechanism on a woodworking shaper with bottom position of the spindle at idle. In order to drive the cutting mechanism V-belts with sections Z and SPZ are used. During the experiment, the vibration speed was measured by changing the type of V-belt. Measurements are made at four points in the radial direction. Two of them are located in the upper bearing, housing the other two in the lower bearing. The measurements were performed at three different rotation frequencies 4000 min^{-1} , 6000 min^{-1} and 8000 min^{-1} . The specified rotation frequencies are often used in the various milling processes of wood and wood-based materials. The study is aimed at improving the reliability and efficiency of a wood shaper machine, as well as to ensure the accuracy and quality of products.

Key words : *wood shaper, cutting mechanism, V-belts, vibrations;*

INTRODUCTION

Belt gears have simple construction, low cost and easy service. This makes them the preferred gears for driving various mechanisms in general engineering. Woodworking and furniture machines are no exception to this trend. Belt gears are widely used to drive the various types of mechanisms in woodworking machines. Various types of belts are available on the market, from the classic flat belts to ribbed and timing belts. The variety of constructions is very large. The shape, the construction, the rubber compound from which the belts are made are constantly being improved. All this is done with the aim of improving the qualities of the belt, and hence improving the operation of mechanisms and machines. Manufacturers of belts and rubber products offer various systems, devices and software for calculating, designing and controlling the operation of belt drives. V-belts are one of the most commonly used in practice. Their new modifications and designs also find great use in general engineering (SOKOLOVSKI 2007, Continental-industry.com). Modern universal milling machines are widely used in the woodworking and furniture industries. They allow working with high cutting speeds, which can reach up to 90 m/s (OBRESHKOV 1997). This inevitably is associated with the machinery resources to work at different rotational speed. High rotation frequencies are one of the reasons for the occurrence of intense vibrations at idle. Their reduction is essential for the operation of the cutting mechanism of the machine both at idle and in working mode. In this way, no significant mistakes are made on the details of the exact shape, dimensions, roughness class, which correspond to the permissible deviations laid down in the technical documentation (KORCOK *etal.* 2018, KMINIAK *etal.* 2018, SYDOR *etal.* 2021).

The aim of the present work is to measure and analyze the vibration speed at idle on a universal wood shaper with bottom location of the working shaft. The cutting mechanism of the machine was driven by two different types of V-belts. The cross-section of the belts is the same but with different wedge sizes. The analysis of the obtained results can be aimed at improving the drive the cutting mechanisms of various woodworking machines and for reducing the vibration levels both at idle and at working mode.

MATERIAL AND METHODS

In the present paper, all experimental studies are made on a woodworking shaper with bottom position of the spindle. The machine can be seen in Fig.1. The design of the cutting mechanism consists of an asynchronous electric motor with a power of 3 kW and a rotation frequency of 2880min^{-1} , a belt drive and a main shaft on which the cutting tools are put. The working frequencies of the machine are 4000min^{-1} , 6000min^{-1} and 8000min^{-1} . They allow high technological results to be achieved for realizing different cutting speeds by using cutting tools with different diameters.



Fig 1. Wood shaper with bottom position of the spindle

The specified rotation frequencies are realized with special belt pulleys, which are mounted on the electric motor and the working shaft of wood shaper. V-belts with different wedge sizes are used to drive the cutting mechanism. During the experiment, the cutting mechanism was driven by two classic V-belts with a Z section, as well as with two SPZ section V-belts. Fig.2 shows classic V-belt size with a Z section.



Fig 2.Classic V-belt size with a Z section

Classic V-belts are widely used to drive various types of machines, including woodworking machines. Realizing the gear is simple and quick. The ratio of the width ($W = 10$ mm) to the height ($T_0 = 6$ mm) of the wedge in classic V-belts is approximately 1.6 (SOKOLOVSKI 2007). Fig.3 shows V-belt size with cross-section SPZ.

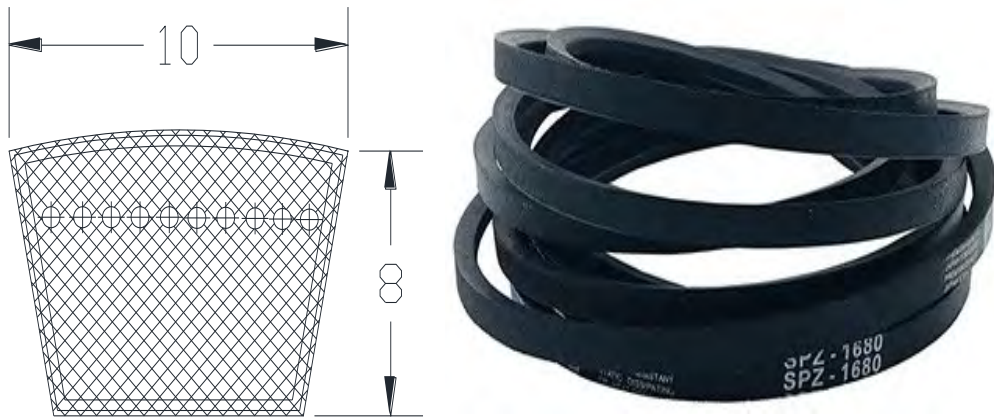


Fig 3.V-belt size with a SPZ section

Narrow SP V-belts are increasingly used in practice. In addition to the automotive industry, this type of belt is used to drive metalworking, woodworking and other types of machines. Compared to classic V-belts, they have a higher pulling capacity and opportunity to work at higher speeds. The ratio of the width ($W = 10$ mm) to the height ($T_0 = 8$ mm) of the wedge in narrow SP V-belts is approximately 1.2 (SOKOLOVSKI 2007).

The intensity of the vibrations is assessed on the basis of the root mean square value of the vibration speed (V mm/s(r.m.s.)). The measurements have been performed at four measuring points located on the bearing house. Two of them are located near the upper bearing next to the cutting tool. The other two are located near the lower bearing next to

the belt pulley. The measurement points are located mutually perpendicular, radial to the main shaft of the machine Fig.4 (БДС ISO 10816 – 2002).

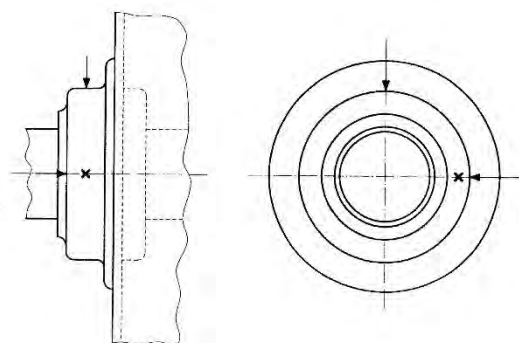


Fig4. *Measurement points*

Root mean square value of vibration speed V mm/s (r.m.s.) is measured using a specialized device model Bruel&KjaerVibrotest 60 Fig.5. The sensor which measures the intensity of the vibrations is attached to the bearing house with a magnet Fig.6 (Bkvibro.com). The vibration speed was measured while the machine was at idle. A groove cutter with diameter $D = 140$ mm is put on the machine.



Fig 5. *Bruel&KjaerVibrotest 60*



Fig 6. *Measuring sensor*

RESULTS AND DISCUSSION

All measurements were carried out at idle. In this way we tracked out which type of V-belt has a lower vibration speed. The measurement points near the upper bearing are respectively: A_x – radial direction parallel to the feed direction, A_y – radial direction perpendicular to the feed direction.

The measurement points near the lower bearing are respectively: B_x – radial direction parallel to the feed direction, B_y – radial direction perpendicular to the feed direction.

Fig.7 and Fig.8 show the variation of the vibration speed measured at a rotation frequency 4000 min^{-1} . To drive the cutting mechanism two belts with section Z and two belts with section SPZ are used.

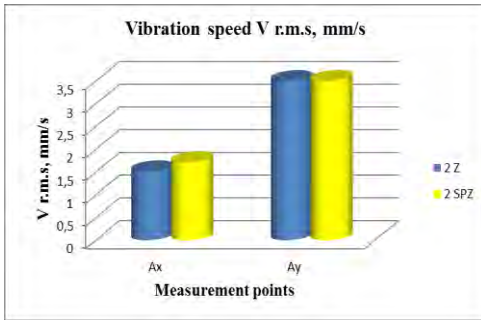


Fig 7. Variation of the vibration speed near the upper bearing, rotation frequency 4000 min⁻¹

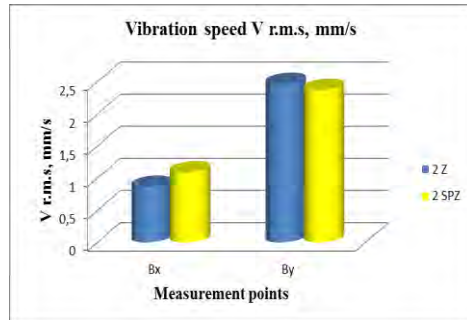


Fig 8. Variation of the vibration speed near the lower bearing, rotation frequency 4000 min⁻¹

From Fig.7 it can be seen that at point Ax and Ay the vibration speed is not affected by the type of V-belt. The measured values are almost equal with minimal changes which do not have a significant impact. The same trend is observed in the measurements performed near the lower bearing shown in Fig.8.

Variation of the vibration speed at a rotation frequency of 6000 min⁻¹ is shown in Fig.9 and Fig.10.

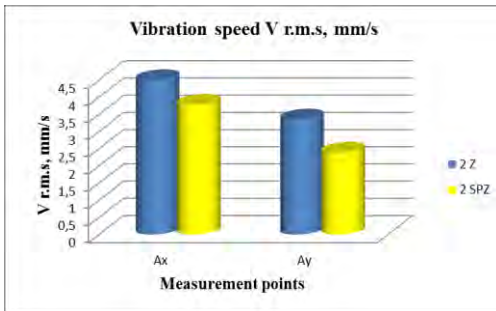


Fig 9. Variation of the vibration speed near the upper bearing, rotation frequency 6000 min⁻¹

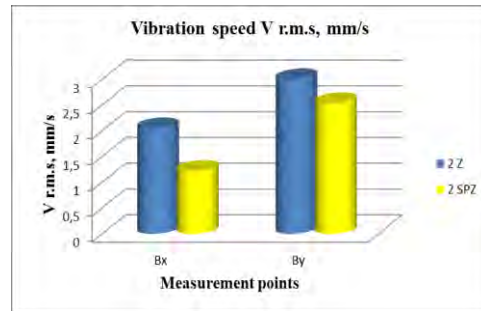


Fig 10. Variation of the vibration speed near the lower bearing, rotation frequency 6000 min⁻¹

Fig.9 shows the vibration speed in the upper bearing depending on the type of V-belt. At both measurement points, the vibration speed is lower when using an SPZ V-belt. The differences in the measured values reach up to 1 mm/s. The variation of the measured vibration speed in the lower bearing Fig.10 is the same as in the upper bearing. From the measurements it can be observed that at a rotation frequency of 6000 min⁻¹, the vibration speed at all four measurement points is lower when V-belts with a cross-section SPZ are used.

Fig.11 and Fig.12 show the variation of the vibration speed measured at a rotation frequency 8000 min⁻¹. At point Ax Fig.11 an increase in the vibration speed up to 13.6 mm/s can be observed no matter which belt drives the cutting mechanism. This result can be explained by an operating mode close to the resonance zone without completely entering it. At point Ay the values of the vibration speed are almost equal. At points B_x and B_y, the vibration speed is lower when using SPZ belts Fig.12.

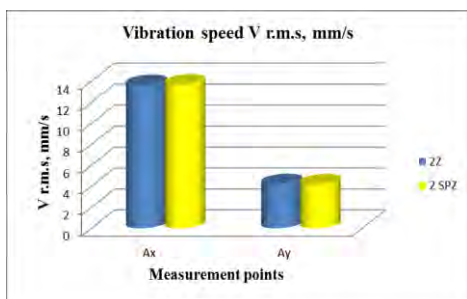


Fig 11. Variation of the vibration speed near the upper bearing, rotation frequency 8000 min^{-1}

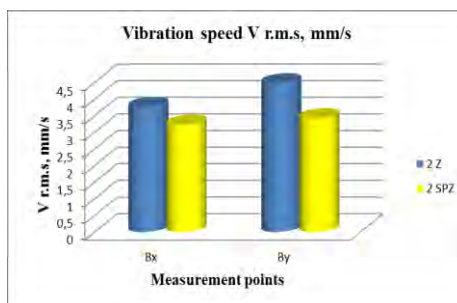


Fig 12. Variation of the vibration speed near the lower bearing, rotation frequency 8000 min^{-1}

CONCLUSION

As a result of research and data analysis, the following conclusion can be made:

The type of V-belt has no influence on the vibration speed at a rotation frequency of 4000 min^{-1} at all four measurement points. At a rotation frequency of 6000 min^{-1} , SPZ belts operate more smoothly than classic V-belts at all measurement points. The low levels of the measured vibration are a direct prerequisite for a higher quality of the processed details (KOVATCHEV et al. 2022). At the highest rotation frequency of 8000 min^{-1} in one of the measuring point Ax, the vibration speed levels were higher for both types of belts, unlike point Ay where they are almost equal. The measured vibration values in the lower bearing show that SPZ belts run more smoothly.

REFERENCES

- KMINIAK, R., SIKLIENKA, M., SUSTEK, J. 2018. Influence of the thickness of removed layer on the quality of created surface when milling oak blanks on the CNC machining center. *Chip and Chipless Woodworking Processes* 11 (1): 79-86, Zvolen, ISSN 2453-904X (print), ISSN 1339-8350 (online).
- KORCOK, M., VANCO, M., BARCIK, S., GOGLIA, V. 2018. Influence of tool angular geometry on surface quality after milling of thermally modified oak wood. *Chip and Chipless Woodworking Processes* 11 (1): 87-96, Zvolen, ISSN 2453-904X (print), ISSN 1339-8350 (online).
- KOVATCHEV, G., V. ATANASOV, I. RADKOVA (2022), Influence of mechanical oscillations on the accuracy of making grooves in solid wood, "Chip and Chipless Woodworking Processes", Tatranska Lomnica, TU-Zvolen, ISSN 2453-904X (print) ISSN 1339-8350 (online), pp. 65 – 71.
- OBRESHKOV P. 1997. *Woodworking Machines*, Sofia. 182 p. (in Bulgarian)
- SOKOLOVSKI, S. 2007. *Machine elements*, Sofia, ISBN 978-954-332-044-38, 318 p. (in Bulgarian)
- SYDOR, M., R. MIRSKI, K. STUPER-SZABLEWSKA, T. ROGOZINSKI (2021), Efficiency of Machine Sanding of Wood, *Applied Sciences*, Volume 11 – Issue 6 /2860/ March 2 2021, ISSN 2076 – 3417, <https://doi.org/10.3390/app11062860>
- БДС ISO10816-1:2002, Evaluation Of Machine Vibration By Measurement On Non – Rotating Parts – Part 1: General Guidelines, 25 p.
- Bruel&Kjaer Vibro – www.bkvibro.com
- Continental Belts and Components the Product Range – www.continental-industry.com



COMPARISON OF PARTICLES FROM THE SANDING PROCESS OF SPRUCE AND OAK ON A NARROW BELT SANDER

Martin Kučerka – Lukáš Adamčík – Martin Júda – Richard Kminiak
– Alena Očkajová

Abstract

The paper deals with the microscopic analysis and comparison of particles from the sanding process of spruce and oak on a narrow belt sander. The values of all sizes obtained from the microscope measurements ranged over a wide range of all sizes between 3-1000 μm . Chips with sizes $< 100.0-10.0 \mu\text{m}$ were the most prevalent, accounting for 50% and 47% of the total sizes present in the oak and spruce samples, respectively. The presence of chips $< 10.0 \mu\text{m}$ in size was present in oak samples 37% and in spruce samples 33% of the total number of chips. Chips of larger sizes were present in 13 % of the oak samples and 20 % of the spruce samples. The study of sizes below $< 10.0 \mu\text{m}$ showed that, based on medians, the most frequently occurring splinter size was 5.43 μm diameter for both species equally. In both samples, the sizes ranged from 3.43 to 9.71 μm . The study of dimensions below $< 100.0-10.0 \mu\text{m}$ showed that the most frequently occurring dimensions based on medians were chips with a diameter of approximately 30 μm for oak and chips with a diameter of approximately 28 μm for spruce.

Key words: oak, spruce, microscopic analysis, sanding process, narrow belt sander

INTRODUCTION

Sanding wood is a seemingly simple process, but there is a complex science behind it. It involves interesting processes that lead to the formation of chips and dust, which also affects the final surface of the wood (ČistěDrevo.sk 2023). When wood is sanded, abrasive particles are used to remove material from the surface of the wood. These particles on the sanding belt move across the surface of the wood to cut away small pieces of wood (Sydor et al. 2021). The size of these fragments depends on the type of abrasive material, its grain size and the force of pressure exerted on the abrasive tool. Splinters are larger fragments of wood that are produced when sanding with coarser grits or when too much pressure is applied. They can vary in shape and size from small flakes to coarser-grained wood particles. Wood sanding dust is made up of fine wood particles that are removed from the surface (Chuchala et al. 2024). Its volume and composition depend on the type of wood, the sanding material and the grain size. Dust can pose a health hazard, so it is important to use personal protective equipment when sanding.

Wood sanding is a widely used process in the woodworking industry, employed to smooth out the surface of wood and prepare it for finishing, painting, or other applications. Despite its widespread use, the mechanics of wood sanding remain not fully understood, and the optimization of this process is still an active area of research. The quality of the finished surface produced by sanding is heavily dependent on a complex interplay of factors, including the type and grit of sandpaper used, the pressure and speed of sanding, and the properties of the wood itself (Meraj 2023; Jenkins 2023). Recent studies have shown that the properties of wood can play a significant role in determining the effectiveness of sanding (Adamčík et al. 2023). For example, woods with higher densities tend to be more resistant to abrasion and require more aggressive sanding techniques (Čunderlík 2009). Additionally, the presence of defects such as knots or splits can significantly affect the sanding process and impact the quality of the finished surface (Gaff et al. 2015; Barčík et al. 2014). Despite these challenges, advancements in sanding technology have led to significant improvements in efficiency and quality (Sydor et al. 2021; Rogoziński 2018; Rogoziński a Dolny 2004). The development of new types of sandpaper, such as diamond-coated and ceramic-coated papers, has enabled more effective removal of wood fibers and improved surface finish (Warguła et al. 2023). Furthermore, advances in robotics and automation have enabled more precise control over the sanding process, allowing for improved consistency and reduced waste (Jenkins 2023).

Sanding is basically the work of several cutting wedges (sanding grains) working in a groove. The basic strength properties of the wood involved in chip formation are bending strength (when the chip is bent by the cutting wedge face), tension along the grain (on the inside of the chip - facing the cutting wedge face) and pressure along the grain (on the outside of the chip), tension perpendicular to the grain in front of the cutting edge in the case of longitudinal cutting (sanding), and shear strength is also involved in some way.

Many authors are focused on parameters that influence granularity and shape of created particles. They point out particles smaller than 0.1 mm - hazardous for working environment, particles smaller than 0.01 mm - hazardous for working staff. Among the observed parameters belong processed material - hard and soft wood (Dzurenda a Očkajová 2003; Očkajová et al. 2006), juvenile wood, thermally modified wood (Dzurenda et al. 2010), frozen and unfrozen wood, way of machining - sawing, planing, sanding (Porankiewicz et al. 2010), cutting conditions, feed speed, tool geometry (Očkajová et al. 2006), cutting direction (Dzurenda et al. 2008).

In this paper, we analyzed and compared particles by microscopic analysis from the sanding process of coniferous (spruce) and deciduous (oak) wood on a narrow belt sander. We found that chips with sizes $<100.0-10.0 \mu\text{m}$ were the most prevalent, accounting for 50% and 47% of the total sizes present in the oak and spruce samples, respectively. The presence of chips with size $<10.0 \mu\text{m}$ was present in oak samples 37% and in spruce samples 33% of the total number of chips. The study of sizes below $<10.0 \mu\text{m}$ showed that, based on medians, the most frequently occurring size of splinters was $5.43 \mu\text{m}$ diameter equally for both tree species. In both samples, the sizes ranged from 3.43 to $9.71 \mu\text{m}$. The study of dimensions below $<100.0-10.0 \mu\text{m}$ showed that the most frequently occurring dimensions based on medians were chips with a diameter of approximately $30 \mu\text{m}$ for oak and chips with a diameter of approximately $28 \mu\text{m}$ for spruce. The final objective is to evaluate the results obtained in terms of the sanding on the narrow belt sander and the type of wood species.

MATERIAL AND METHODOLOGY

Experimental samples

For analyzing the dimensions of dust particles, two species of wood were used - Norway spruce (*Picea abies* L.) and summer/winter oak (*Quercus petraea*) with an equilibrium moisture content of 8 to 10%. The dust particles were taken from the sanding process with a belt sander with P80 grit. The fraction was subsequently subjected to particle size analysis.

Machinery

Narrow belt sander JET JSG-96, cutting speed $10 \text{ m}\cdot\text{s}^{-1}$, sanding belt HIOLIT XO P80 sanding belt grit 80, individual pressure of the wood sample on the sanding belt, laboratory experiments. A sharp sanding belt was used for each wood species.

Digital particle analysis

Dust particles from the collected fraction were analyzed by optical method on a Keyence VHX-7000 digital microscope. The particles were uniformly deposited on a slide that can be placed in XY θ a motorized stage in the microscope. The uniformity of particle deposition was achieved by applying the particles with a laboratory double-sided spoon to a sieve that was placed over the slide and then passing them through a $125 \mu\text{m}$ mesh. This methodology avoided coagulation of the small dust particles during their deposition on the glass (the coalescence of the particles under the microscope would have made it impossible to analyse the particles individually). Subsequently, a $10 \times 10 \text{ mm}$ area was scanned at $100\times$ objective magnification. The analysis on the VHX-7000 microscope works on the principle of illuminating the slide with dust particles using a high-intensity bottom illumination. The size of the particles and their area is then digitally calculated based on the different brightness of the particle (dark, opaque, casting a shadow across the objective, which is recorded by the digital camera) and the surroundings (transparent glass). Two main particle dimensions were determined as part of the analysis: the maximum diameter (the largest dimension of the particle in two-dimensional XY space) and the minimum diameter (the smallest dimension of the particle in two-dimensional XY space). In addition, particle area, circumference and circularity were also analyzed. These data were then processed with the statistical software STATISTICA 14 (TIBCO Software Inc., Palo Alto, California), using descriptive statistics (arithmetic mean, standard deviation, maximum and minimum values). The total number of scans for oak and spruce wood was 30. A total of more than 62 000 pieces of dust particles were analyzed.

RESULTS AND DISCUSSION

In the first step, the outliers of the measurement were removed, and the measurement was repeated. Subsequently, descriptive statistics were performed, in which the following data were determined: average maximum diameter, average minimum diameter and slimmness ratio as the ratio between the maximum diameter and the minimum diameter. Tab. 1 shows that the spruce chips were larger in sample. The slimmness ratio also indicates that the spruce chip has a more elongated shape, i.e., the maximum diameter (length) is larger.

Table 1 Average dimensions and slinness ratio for oak and spruce chips. The data in parentheses represent the standard deviation

Type of Wood	Average Max. Diameter [μm]	Average Min. Diameter [μm]	Slinness Ratio
Oak	41,07 (55,02)	22,20 (30,4)	1,85
Spruce	56,19 (73,47)	25,90 (35,3)	2,17

The analysis of individual dust particles was then carried out using a digital microscope. Based on the established methodology, the microscope divided the particles into fractions over 100 micrometers, under 100 micrometers and under 10 micrometers. For each fraction, the average values of the maximum diameter and the minimum diameter as well as the slinness ratio were again measured (Tab. 2). The table shows that the length of the chip (expressed by the maximum diameter) is greater in each fraction for spruce wood. At the same time, the slinness ratio within the individual fractions is again proof that spruce chips are longer than oak chips.

Table 2 Average dimensions and slinness ratio for oak and spruce chips in individual sieved fractions. The data in parentheses represent the standard deviation

Type of Wood	Size range [μm]	Average Max. Diameter [μm]	Average Min. Diameter [μm]	Slinness Ratio
Oak	>100.0	157,25 (63,60)	85,22 (33,6)	1,85
Oak	<100.0	38,06 (25,36)	20,85 (16,2)	1,82
Oak	<10.0	5,54 (1,89)	2,53 (1,1)	2,19
Spruce	>100.0	178,73 (72,02)	79,62 (40,2)	2,24
Spruce	<100.0	39,06 (27,13)	19,26 (17,3)	2,03
Spruce	<10.0	5,65 (1,91)	2,51 (1,1)	2,26

Analyzing data of sizes for normality with the Shapiro-Wilk test showed a non-normal distribution. Due to the non-homogeneity of variance, the standard parametric ANOVA tests cannot be used. Thus, the nonparametric analysis of variances Kruskal-Wallis one-way ANOVA was used. The presented numbers were calculated based on the confidence factor of 95%. The presented results were calculated with the statistic software STATISTICA 14 (TIBCO Software Inc., Palo Alto, California).

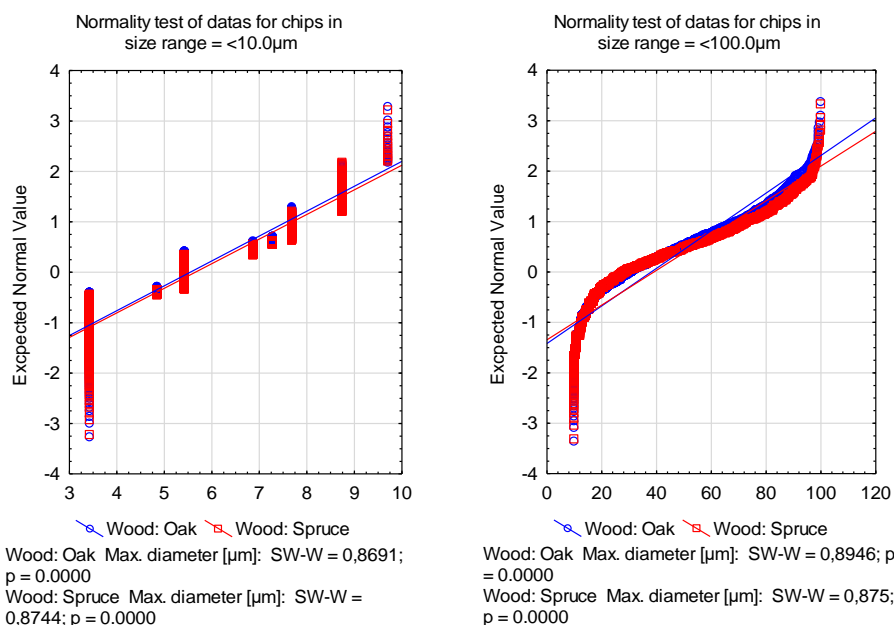


Fig. 1 Test for normality of dates for sizes in size range <10µm and <100µm for Oak and Spruce samples

Obtained values of all sizes from automatic measurement by microscope ranged widely across all sizes in between 3-1000µm. For easier interpretation and fitting to article aims here we used size ranges by <10.0µm, by <100.0µm, and by size range >100.0µm. Size range <10.0µm representing all sizes between <10.0-0.0µm, <100.0-10.0µm representing all sizes below <100.0-10.0µm and size range >100.0µm represents all chip sizes above this size limit. This chip size range distribution is shown in a histogram, which represents size ranges and their percentual distribution by numerical observed chip sizes obtained by digital automatic microscope measuring.

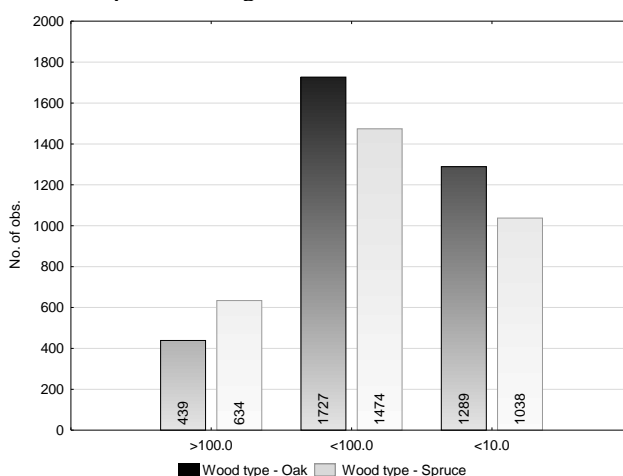


Fig. 2 Chip size distribution by size ranges with respect to total present amounts of sizes

Histogram is showing the observed number in analyzed screen of sizes. Based on observed results the most distributed chips were in sizes $<100.0-10.0\mu\text{m}$, which for Oak samples presented by 50% and in Spruce samples by 47% of the total present sizes. The presence of chips in sizes $<10.0\mu\text{m}$ were present in Oak samples by 37% and in Spruce samples by 33% from the total chip sizes. The chips of higher sizes were found by 13% in Oak samples and by 20% in Spruce samples. Comparing those percentual results based on post-hoc test showed differences on p level for $<10.0\mu\text{m}$ ($p=0.3$) and for $<100.0\mu\text{m}$ ($p=0.7$). These results pointing on difference, but without significant differences and thus, based on obtained results samples showed there is no significant difference between the content of chips in sizes $<100.0\mu\text{m}$ and $<10.0\mu\text{m}$ between Oak and Spruce wood.

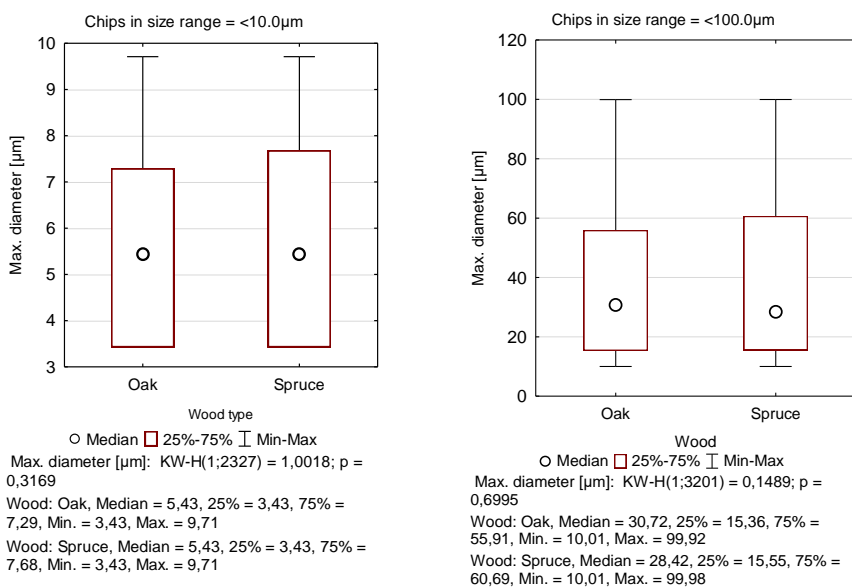


Fig. 3 Difference in amounts of chips in size $<100.0-10.0\mu\text{m}$ and $<10.0-0.0\mu\text{m}$ for oak and spruce

Studying the sizes below $<10.0\mu\text{m}$ showed that based on medians most occurring size of chips is diameter size $5,43\mu\text{m}$ equally for both materials. In both samples the sizes ranged from $3,43-9,71\mu\text{m}$. Studying the sizes below $<100.0-10.0\mu\text{m}$ showed that most occurring size based on medians were chips for Oak wood in approximately diameter of size $30\mu\text{m}$ and for Spruce wood chips approximately in diameter of size $28\mu\text{m}$.

CONCLUSION

The results show that microscopic analysis of particles from the sanding process of spruce and oak wood on a narrow belt sander yielded interesting findings. The particle size values obtained ranged over a wide range from 3 to $1000\mu\text{m}$. Particle sizes $<100.0-10.0\mu\text{m}$ were the most frequent, accounting for 50 % and 47 % of the total sizes present in the oak and spruce samples, respectively. Splinters smaller than $10.0\mu\text{m}$ accounted for 37 % of oak samples and 33 % of spruce samples. Larger chips were present in 13 % of the oak samples and 20 % of the spruce samples. The average size of chips below $10.0\mu\text{m}$ was the same for

both species, 5.43 μm . Dimensional analysis below $<100.0\text{-}10.0$ μm showed that the most common sizes were approximately 30 μm for oak and 28 μm for spruce.

Acknowledgments: This experimental research was carried out under the grant project VEGA 1/0323/23 "Vplyv vybraných faktorov na kvalitatívno-kvantitatívne charakteristiky drevného prachu v pracovnom ovzduší pri opracovaní dreva elektrickým ručným náradím “

LITERATURE

ADAMČÍK, Lukáš, Richard KMINIAK, Michal DUDIÁK a Adrian BANSKI, 2023. The Impact of Abrasive Grit Size on Roughness of Sanded Beech Wood Surface. *Annals of WULS, Forestry and Wood Technology* [online]. 2023, roč. 121, s. 51–60 [cit. 15.7.2024]. ISSN 1898-5912, 2719-6518. Dostupné na: doi:10.5604/01.3001.0053.8636

BARCÍK, Š., M. GAŠPARÍK, A. HOUSKA, E. RAZUMOV a M. SEDLECKÝ, 2014. Vliv technologických faktorů na kvalitu opracování povrchu při frézování termicky modifikovaného dřeva. V: *Chip and Chipless woodworking processes: Trieskové a beztrieskové obrábanie dreva*. Zvolen: Technická univerzita vo Zvolene, s. 11–22. ISBN 978-80-228-2658-7.

ČISTÉDREVO.SK, 2023. Ako na správne brúsenie dreva | ČistéDrevo.sk. *cistedrevo.sk* [online] [cit. 15.7.2024]. Dostupné na: <https://www.cistedrevo.sk/navody/ako-na-spravne-brusenie-dreva/>

ČUNDERLÍK, Igor, 2009. Štruktúra dreva [online]: Zvolen: Technická univerzita vo Zvolene [cit. 19.10.2021]. ISBN 978-80-228-2061-5. Dostupné na: https://www.library.sk/arl-sldk/sk/detail-sldk_un_cat-0038328-struktura-dreva/

DZURENDA, L., M. KUČERKA a A. BANSKI, 2008. Vplyv techniky na kvalitu deleného a obrábaného dreva. 1. vyd. Zvolen: Technická univerzita vo Zvolene. 2/2008/B. ISBN 978-80-228-1923-7.

DZURENDA, Ladislav a Alena OČKAJOVÁ, 2003. Rozmerová analýza drevného prachu smreka, borovice a duba z procesu rovinného brúsenia. V: *Obrábanie a spájanie dreva*. Zvolen: ES TU, s. 53–57. ISBN 80-228-1270-6.

DZURENDA, Ladislav, Kazimierz A. ORLOWSKI a M. GRZESKIEWICZ, 2010. Effect of Thermal Modification of Oak Wood on Sawdust Granularity. *Drvna Industrija* [online]. 2010, roč. 61, č. 2, s. 89–94 [cit. 15.7.2024]. Dostupné na: <https://drvnaindustrija.com/archive/volume-2010-issue-2/effect-of-thermal-modification-of-oak-wood-on-sawdust-granularity/>

GAFF, M., M. KVIETKOVA, M. GASPARIK, L. KAPLAN a Š. BARCÍK, 2015. Effect of Selected Parameters on the Surface Waviness in Plane Milling of Thermally Modified Birch Wood. *Bioresources*. 2015, roč. 10, č. 4, s. 7618–7626. ISSN 1930-2126.

CHUCHALA, Daniel, Tomasz ROGOZIŃSKI, Kazimierz A. ORLOWSKI, Marta PĘDZIK, Luďka HANINCOVÁ a Olafur EGGERTSSON, 2024. Granulometric characterization of Arctic driftwood sawdust from frame sawing process. *Industrial Crops and Products* [online]. 2024, roč. 213, s. 118448 [cit. 4.4.2024]. ISSN 09266690. Dostupné na: doi:10.1016/j.indcrop.2024.118448

JENKINS, Steve, 2023. Sanding wood: What you need to know to get the best finish. *Homebuilding & Renovating* [online] [cit. 15.7.2024]. Dostupné na: <https://www.homebuilding.co.uk/advice/sanding-wood>

MERAJ, Md, 2023. How to Sand Wood: Expert Tips for Perfect Finish. Wood Working Advisor [online] [cit. 15.7.2024]. Dostupné na: <https://woodworkingadvisor.com/how-to-sand-wood/>

OČKAJOVÁ, Alena, 1999. Sand belt running time and its wear. 1999, s. 9–13.

OČKAJOVÁ, Alena, Adrián BANSKI a Ján RONČKA, ed., 2006. Dust in Woodworking Plants and Possibilities of its Reducing. V: Alena OČKAJOVÁ, Adrián BANSKI a Ján RONČKA, ed. Jubilee Scientific Conference: Manufacturing Engineering in Time of Information Society. Gdansk: Gdansk University of Technology, s. 255–260. ISBN 83-88579-61-4.

OČKAJOVÁ, Alena, Martin KUČERKA, Richard KMINIAK, Luboš KRIŠŤÁK, Rastislav IGAZ a Roman RÉH, 2020. Occupational Exposure to Dust Produced when Milling Thermally Modified Wood. International Journal of Environmental Research and Public Health [online]. 2020, roč. 17, č. 5, s. 1478 [cit. 11.4.2021]. ISSN 1660-4601. Dostupné na: [doi:10.3390/ijerph17051478](https://doi.org/10.3390/ijerph17051478)

OČKAJOVÁ, Alena, Mikuláš SIKLIENKA a Štefan BARCÍK, 1999. Physico-mechanical phenomenons in sanding process of natural and modified wood. V: Proceedings of the 14 th International Wood Machining Seminar Paris, Epinal, Cluny. s. 691–700. 12-19. September. ISBN 978-2-87614-362-3.

PORANKIEWICZ, Boleslaw, Adrian BANSKI a Grzegorz WIELOCH, 2010. Specific resistance and specific intensity of belt sanding of wood. BioResources [online]. 2010, roč. 5, č. 3, s. 1626–1660 [cit. 19.10.2021]. ISSN 1930-2126. Dostupné na: https://ojs.cnr.ncsu.edu/index.php/BioRes/article/view/BioRes_05_3_1626_Porankiewicz_BW_Spec_Resist_Belt_Sanding

ROGOZINSKI, T. a S. DOLNY, 2004. Influence of moisture content on the apparent densities of dust from sanding of alder wood. V: Trieskové a beztrieskové obrábanie dreva '04. Zborník prednášok z MVK. s. 205–208.

ROGOZIŃSKI, Tomasz, 2018. Pilot-scale study on the influence of wood dust type on pressure drop during filtration in a pulse-jet baghouse. Process Safety and Environmental Protection [online]. 2018, roč. 119, s. 58–64 [cit. 19.10.2021]. ISSN 0957-5820. Dostupné na: [doi:10.1016/j.psep.2018.07.016](https://doi.org/10.1016/j.psep.2018.07.016)

SYDOR, Maciej, Radosław MIRSKI, Kinga STUPER-SZABLEWSKA a Tomasz ROGOZIŃSKI, 2021. Efficiency of Machine Sanding of Wood. Applied Sciences [online]. 2021, roč. 11, č. 6, s. 2860 [cit. 15.7.2024]. ISSN 2076-3417. Dostupné na: [doi:10.3390/app11062860](https://doi.org/10.3390/app11062860)

WARGUŁA, Łukasz, Dominik WILCZYŃSKI, Bartosz WIECZOREK, Teijo PALANDER, Łukasz GIERZ, Carla NATI a Maciej SYDOR, 2023. Characterizing Sawdust Fractional Composition from Oak Parquet Woodworking for Briquette and Pellet Production. Advances in Science and Technology. Research Journal [online]. 2023, roč. 17, č. 5, s. 236–247. ISSN 2080-4075, 2299-8624. Dostupné na: [doi:10.12913/22998624/172534](https://doi.org/10.12913/22998624/172534)



EFFICIENCY OF INTEGRATED TECHNOLOGICAL MODULES IN MASS PRODUCTION PROCESSES OF WOODEN DOOR FRAMES

Zdzisław Kwidziński – Marta Pędzik – Adam Wilczyński –
Tomasz Rogoziński – Marcin Drewczyński

Abstract

Low-waste technologies and technological lines aimed at reducing costs and increasing efficiency in the production of construction products ensure the achievement of savings, which is linked to an intelligent production management system. The developed original way of controlling the technological line allows for optimizing the consumption of materials for door frame production, especially in producing a short series of products with highly customized parameters. The production line based on PortaFRAME technology receives information about the processing parameters of semi-finished products directly from the intelligent control system. The development work carried out in the area of production construction products such as wooden door frames for technical doors allows intelligent scheduling and flexible control of door frames' production efficiency, consequently lowering their unit costs.

Keywords: *production efficiency, takt time, technical door frames, mass customization, internet of things, industry 4.0*

INTRODUCTION

The product catalog of today's wooden door frame companies is characterized by enormous complexity and variability. To cope with the unpredictable and changing demands of consumers, companies are moving from mass production to mass customization (Jain et al., 2023). On a large scale, customization is possible thanks to the dynamic development of production technology. This is possible thanks to the introduction and development of the Industry 4.0 concept, which integrates advanced information technology and automation into production processes (Espinoza Pérez et al., 2022). In addition, the automation of production lines and the implementation of advanced IT solutions make it possible to make changes to improve the visual qualities of products freely (Kwidziński et al., 2021). What is especially important, the processing time is reduced, and this allows to increase the efficiency of the entire technological line (Tarigan et al., 2019). In Industry 4.0, equipment and machines in an automated production line require the use of precision machining tools to ensure high precision and quality machining of the product. The use of such tools has benefits such as the minimization of excess material for processing, resulting in financial benefits and better material utilization. The industry's involvement in process innovation and developed technologies also provides

beneficial results for the bioeconomy. (Wieruszewski et al., 2023). This is key to maintaining a competitive edge in the market, and the process itself becomes more technically and economically efficient, which is in line with sustainability development (Pędzik et al., 2020). Automated systems connect the central planning level directly to production, where parameterized orders are transmission to specific machines (Kwidziński et al., 2021). The integration of information systems allows for the collection and analysis of large amounts of data, monitoring and optimization in real time (Haddouche and Ilinca, 2022). The systems detect potential problems and enable steps to be taken to resolve them quickly without disrupting production. As a result, companies can better manage resources, plan productions and respond to changing market conditions and customer needs with more efficiency.

The work of the integrated information systems was decided to verify by carrying out a study of the impact of product customization on the achieved efficiency of the integrated modules of the automated technology for the processing of PortaFRAME wooden door frames. The PortaFRAME technology consists of two main processing sections: one built from modules provided by Kraft and the second by Bacci. Accordingly, this study aims to determine the effect of selected technical door frame construction on the achieved efficiency of automated technology for processing wooden door frames. The research production technology is parameterized online in real time by implementing advanced IT systems using the IoT (internet of things) concept. Thus making it possible to explore the previously unknown potential of machines and implement them into complex product processes.

MATERIAL AND METHODS

Designed and implemented technology to automate the production process of technical door frames using a new system, integrating core ERP software, Siemens NX® intranet, TeamCenter® with the pilot line control process (ProductionBase API). A set of data (parametric models) from the 3D product configurator was developed, describing all possible custom features of technical door frames. On this basis, information containing parameters for the control of PortaFRAME technology characterized by flexible automation, the possibility of using high-density materials and product customization was prepared. At the stage of verification of the control model and its adequacy from the selected technical solutions implemented in the modules, the work of testing the established format of data communication to individual processing sections of the line was carried out. The designed data transmission process is graphically shown in Figure 1.

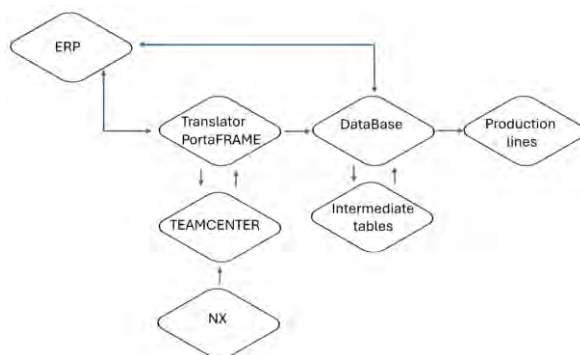


Fig. 1. Structure of connections of the IT system PortaFRAME technology

The transfer of information on the PortaFRAME line begins when the customer places an order. Based on these orders, virtual models are created in the Siemens NX system using previously stored technological and design data in the "Orders" databases. The developed order is transferred to the repository, where it is stored. When a decision is made to send a given order to production, the virtual model is described as orders from the ERP system and control parameters of all machines in the production system are assigned on this basis, using the "Translator" system. From the "Translator" system, the data is transferred to the "Infoprod" database and, through the application optimizing the scheduling process, is transferred to the appropriate technological machine systems for execution. This ensures maximization of the efficiency achieved and proper use of the available machinery. Subsequent orders are grouped into pallets and forwarded for processing with already assigned barcodes identifying each product individually.

On the Kraft section, a schematic of which is shown in Figure 2, data was collected during technology testing using the PORTAFrame intelligent technology information system. The data that was obtained is in the form of a Microsoft Excel spreadsheet. The data sample includes information identifying the product and most important information about the processing time of various parts of the product.

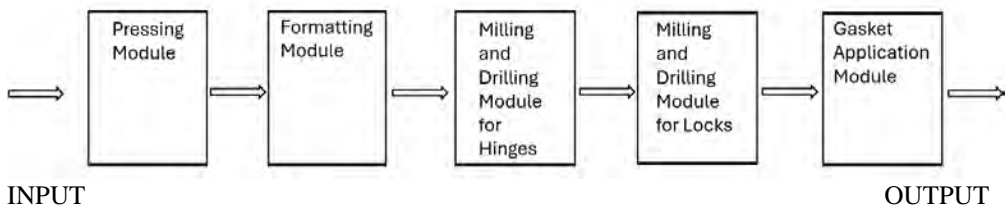


Fig. 2. Kraft technological section.

Analysis of this data allows to calculate the efficiency of the PortaFRAME line modules provided by Kraft. In addition, it allows you to analyze the possible course of efficiency variation during the interval time and the possible difference in efficiency about the form of processed products - door frames from the Porta SYSTEM group, the designs of which are shown in Figure 3.

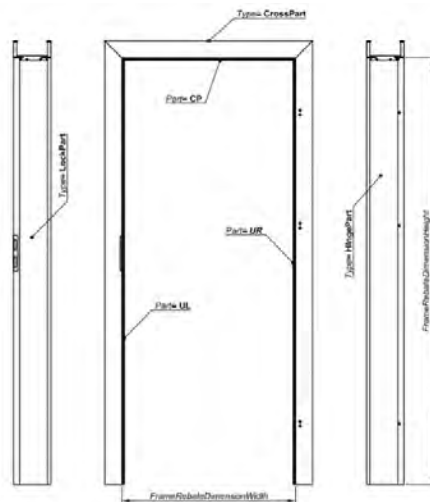


Fig. 3. Construction of the Porta SYSTEM reference frame

To determine the impact of the construction, measurements were also taken for the second type of technical doorframe, i.e. Porta ELEGANCE - non-rebate. The two types of technical door frames were then measured on a Bacci technology module. The Bacci module is dedicated primarily to the production of complicated investment products, but importantly, it also allows the production of reference frames, a schematic of which is shown in Figure 4. The total number of Porta SYSTEM and Porta ELEGANCE doorframes produced during the research was 2344 pieces and 3118 pieces, respectively.

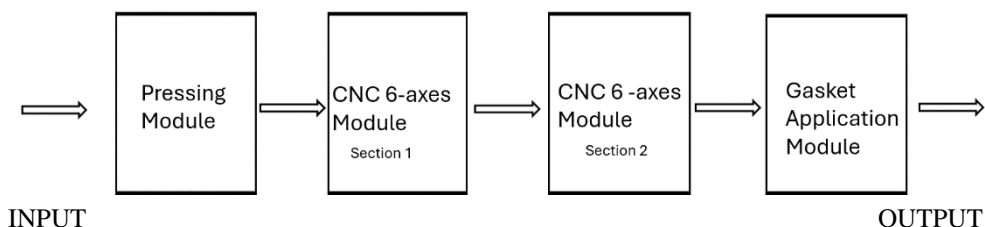


Fig. 4. Bacci technological section.

RESULTS AND DISCUSSION

Figure 5 shows a table with the calculated takt and filtered dimensional range corresponding to the reference configuration of the Porta SYSTEM rebated adjustable frame. In addition, to reject interval times or changes of employees during the day, a filter was made to check only values below the specified time; this is the limit takt time.

	FrameID	Part	StartTime	EndTime	Takt	Takt with filter gct	PosNoOufeed	State	ArcWidth	Board Width	PartLength	Colour
30892	1,3E+08	CP	30-01-2024 13:31:37	30-01-2024 13:34:30	00-01-1900 00:00:20	00-01-1900 00:00:20	8000	1	80.5	147	826	SCM
30889	1,3E+08	CP2	30-01-2024 13:30:59	30-01-2024 13:34:10	00-01-1900 00:00:19	00-01-1900 00:00:19	8000	1	80.5	147	826	SCM
30886	1,3E+08	CP	30-01-2024 13:30:59	30-01-2024 13:33:51	00-01-1900 00:00:20	00-01-1900 00:00:20	8000	1	80.5	147	826	SCM
30883	1,3E+08	CP	30-01-2024 13:31:08	30-01-2024 13:33:31	00-01-1900 00:00:20	00-01-1900 00:00:20	8000	1	80.5	147	826	SCM
30879	1,3E+08	CP2	30-01-2024 13:29:42	30-01-2024 13:33:11	00-01-1900 00:00:20	00-01-1900 00:00:20	8000	1	80.5	147	826	SCM
30876	1,3E+08	CP	30-01-2024 13:29:42	30-01-2024 13:32:51	00-01-1900 00:00:20	00-01-1900 00:00:20	8000	1	80.5	147	826	SCM
30873	1,3E+08	CP	30-01-2024 13:29:35	30-01-2024 13:32:31	00-01-1900 00:00:20	00-01-1900 00:00:20	8000	1	80.5	147	826	SCM
30870	1,3E+08	CP2	30-01-2024 13:28:49	30-01-2024 13:32:11	00-01-1900 00:00:20	00-01-1900 00:00:20	8000	1	80.5	147	826	SCM
30867	1,3E+08	CP	30-01-2024 13:28:49	30-01-2024 13:31:51	00-01-1900 00:00:20	00-01-1900 00:00:20	8000	1	80.5	147	826	SCM
30864	1,3E+08	CP2	30-01-2024 13:28:00	30-01-2024 13:31:31	00-01-1900 00:00:22	00-01-1900 00:00:22	8000	1	80.5	127	826	SCM
30861	1,3E+08	CP	30-01-2024 13:28:00	30-01-2024 13:31:09	00-01-1900 00:00:23	00-01-1900 00:00:23	8000	1	80.5	127	826	SCM
30858	1,3E+08	CP	30-01-2024 13:27:49	30-01-2024 13:30:46	00-01-1900 00:00:22	00-01-1900 00:00:22	8000	1	80.5	127	826	SCM
30855	1,3E+08	CP2	30-01-2024 13:26:15	30-01-2024 13:30:24	00-01-1900 00:00:21	00-01-1900 00:00:21	8000	1	80.5	127	826	SCM
30852	1,3E+08	CP	30-01-2024 13:26:15	30-01-2024 13:30:03	00-01-1900 00:00:23	00-01-1900 00:00:23	8000	1	80.5	127	826	SCM
30849	1,3E+08	CP	30-01-2024 13:25:58	30-01-2024 13:29:40	00-01-1900 00:00:23	00-01-1900 00:00:23	8000	1	80.5	127	730	IDQ
30846	1,3E+08	CP2	30-01-2024 13:24:54	30-01-2024 13:29:17	00-01-1900 00:00:26	00-01-1900 00:00:26	8000	1	80.5	127	730	IDQ
30840	1,3E+08	CP2	30-01-2024 13:24:25	30-01-2024 13:28:31	00-01-1900 00:00:23	00-01-1900 00:00:23	8000	1	80.5	127	730	IDQ
30836	1,3E+08	CP	30-01-2024 13:24:25	30-01-2024 13:28:08	00-01-1900 00:00:23	00-01-1900 00:00:23	8000	1	80.5	127	730	IDQ
30833	1,3E+08	CP2	30-01-2024 13:23:52	30-01-2024 13:27:45	00-01-1900 00:02:13	00-01-1900 00:00:00	8000	1	80.5	127	730	IDQ

Fig. 5. Data takt from the Kraft module database

An analysis of the KRAFT machine test report was carried out in relation to the processing times of reference frames. Initial analysis of the time data obtained during performance tests of the PortaFRAME line modules supplied by Kraft involved sorting them. From the file containing data from the entire test, only those times relating to the Porta SYSTEM series of doorframes were isolated. In turn, the end of each working takt was taken as the time when each successive lintel assembly produced left the line, which is marked in the "Part" column as CP, or CP2. For preliminary calculations, it was assumed to exclude all situations in which the takt would be more than 30 s. Such time means downtime for lines associated with maintenance or setting activities. The obtained results of both calculated and measured takt and maximum efficiency of Kraft line modules are shown in Table 1.

Table 1. Takt and efficiency values for door frames from the Kraft module.

Parameter	Door frame series	
	Porta SYSTEM, rebated	Porta ELEGANCE, non-rebated
Calculated takt time [s]	20	30
Average takt time [s]	21	30
Efficiency [pcs/min]	2.86	2.00
Door frames [pcs]	2344	3118

The average takt time for a rebated frame is 21 seconds, which is 9 seconds less than for a non-rebated frame. As a result, it is possible to obtain an efficiency of 2.86 pcs/min per section of Kraft modules, without taking into account the additional Bacci technology modules included in the PortaFRAME technology under study. These results give confidence in obtaining an efficiency of 3 pcs/min on the line during the operation of both modules. This can also be seen in Figure 6, which summarizes the calculation of the takt of each module for both door frame constructions. This is essentially the maximum value that a given line module can reach.

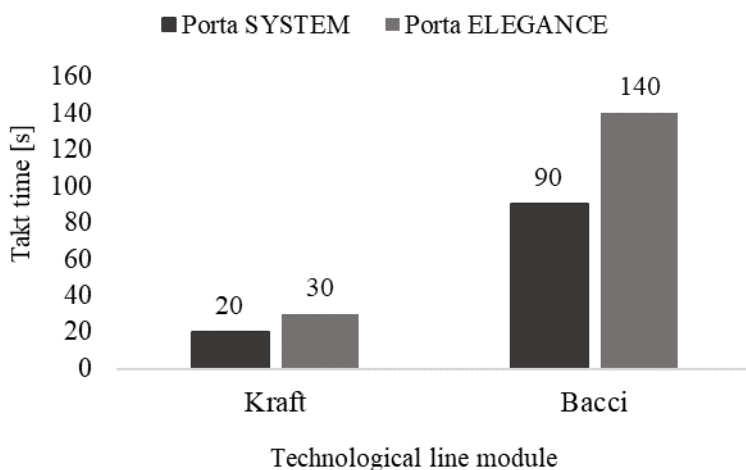


Fig. 6. Calculated takt time of the various technological line modules.

CONCLUSION

Thanks to the integration of individual processing modules dedicated to successive technological stages of PortaFRAME door frame manufacturing, the optimization of the line's operating parameters in terms of quality and efficiency, and the use of an innovative parametric control system, it is possible to achieve an efficiency of more than 3 pieces/minute. At the same time, the fundamental impact of the construction on the efficiency of the technology is confirmed. As a result of the application of the technological process control system according to PORTA's idea, it is possible to flexibly control the time of the production process of technical door frames, especially at the stage of design, introduction of programs to individual processing stations and by minimizing changeover time. The developed and implemented performance model has made it possible to

continuously achieve high production efficiency thanks to the use of algorithms analyzing processing times for individual customized door frame constructions and parametric control of the production process in "just in time" mode.

REFERENCES

- Espinoza Pérez, A.T., Rossit, D.A., Tohmé, F., Vásquez, Ó.C., 2022. Mass customized/personalized manufacturing in Industry 4.0 and blockchain: Research challenges, main problems, and the design of an information architecture. *Information Fusion* 79, 44–57. <https://doi.org/10.1016/j.inffus.2021.09.021>
- Haddouche, M., Ilinca, A., 2022. Energy Efficiency and Industry 4.0 in Wood Industry: A Review and Comparison to Other Industries. *Energies (Basel)* 15, 2384. <https://doi.org/10.3390/en15072384>
- Jain, P., Garg, S., Kansal, G., 2023. Issues and challenges of mass customization. *Mater Today Proc.* <https://doi.org/10.1016/j.matpr.2023.03.408>
- Kwidziński, Z., Bednarz, J., Pędzik, M., Sankiewicz, Ł., Szarowski, P., Knitowski, B., Rogoziński, T., 2021. Innovative line for door production technoporta—technological and economic aspects of application of wood-based materials. *Applied Sciences (Switzerland)* 11. <https://doi.org/10.3390/app11104502>
- Kwidziński, Zdzisław, Bednarz, J., Sankiewicz, Ł., Pędzik, M., Rogoziński, T., 2021. TechnoPORTA intelligent, customized technological line for the automated production of technical doors - selected technical and economic indicators. *Annals of WULS Forestry and Wood Technology* 96–100.
- Pędzik, M., Bednarz, J., Kwidziński, Z., Rogoziński, T., Smardzewski, J., 2020. The idea of mass customization in the door industry using the example of the company porta KMI Poland. *Sustainability (Switzerland)* 12. <https://doi.org/10.3390/su12093788>
- Tarigan, U., Tarigan, U.P.P., Sukirman, V., 2019. Integration of Lean Manufacturing and Group Technology Layout to increase production speed in the Manufacture of Furniture. *IOP Conf Ser Mater Sci Eng* 528, 012058. <https://doi.org/10.1088/1757-899X/528/1/012058>
- Wieruszewski, M., Turbański, W., Mydlarz, K., Sydor, M., 2023. Economic Efficiency of Pine Wood Processing in Furniture Production. *Forests* 14, 688. <https://doi.org/10.3390/f14040688>



KERATIN AS ENVIRONMENTALLY FRIENDLY FORMALDEHYDE SCAVENGERS FROM WOOD-BASED PANELS

Ján Matyašovský¹ – Ján Sedliačik² – Igor Novák³ – Peter Jurkovič¹
– Peter Duchovič¹

Abstract

Currently, polycondensation urea-formaldehyde (UF) resins are the most used wood gluing adhesives in the woodworking industry. Their use in the woodworking and furniture industry is widespread due to their relatively low price, high reactivity, availability of raw materials, ease of use, after curing they provide a transparent brittle joint, but their main disadvantage is the intensive emission of formaldehyde. In this study, the naturally occurring biopolymer keratin and the amino acid cysteine prepared from sheep wool were selected and tested as potential agents in reducing formaldehyde emissions from urea-formaldehyde (UF) adhesives.

X-Ray photoelectron spectroscopy (XPS) was used for qualitative and quantitative determination of basic elements prepared samples from biopolymers keratin and presence of sulphur groups was proved for all keratin samples. The differences between the spectra of the keratin samples are for all elements and for sulfur also in the ratio of sulfur in its reduced form C-S (S2p signal at ~ 163 eV) and in the oxidized form SO₃ (S2p signal at ~ 168 eV). The antioxidant activity of the samples was determined in a suspension of polyethylene glycol SLOVAPEG-600 and the Berthelot-Hood temperature function was chosen to estimate the stability. The highest antioxidant stability was achieved by modification amino acid cysteine with MOD-I (glutaraldehyde PROTECTOL GA-50 + urea). Formaldehyde emissions were assessed according to JIS A 1460 (2001): "Building boards. Determination of formaldehyde emissions. Desiccator method". The most significant reduction of formaldehyde emission by up to 44.0% was achieved by applying 99% UF + 1% (MOD I + cysteine) - to the UF adhesive standard. The gluing quality has been assessed according to standards EN 314-1 and EN 314-2 and the tested plywood meet the requirements of the standard for Class 1 – suitable for application in the interior. Samples prepared for this study might therefore have a great potential for application as environmentally friendly formaldehyde scavengers.

Key words: keratin, urea-formaldehyde resin, plywood, formaldehyde, emission, scavenger

INTRODUCTION

Annual European production of UF adhesives achieves about 4.8 million tons, of which 60 % is consumed for production of particleboard, 30 % for production of medium density fiberboards (MDF), and 10 % for adhesive bonding in production of furniture, interior doors, and plywood (Maminski et al. 2006). The disadvantages of this type of adhesives are low moisture resistance and low water resistance and subsequent releasing of formaldehyde from finished products, which causes the environmental burden by formaldehyde

¹ VIPO, a.s., Partizánske, Slovak Republic

² Technical University in Zvolen, T. G. Masaryka 24, 960 01 Zvolen

³ Polymer Institute, Slovak Academy of Sciences, Bratislava, Slovakia

e-mail: jmatyasovsky@vipo.sk

emissions. Many previous works have described the emission of formaldehyde mainly from three sources: residual formaldehyde present in the resin, formaldehyde formed by polycondensation reaction between hydroxymethyl groups, and formaldehyde released by hydrolytic degradation of the cured adhesive – especially under conditions of increased humidity and increased temperature. Glutaraldehyde (GA) is a chemical that is often tested to modify urea-formaldehyde adhesives. (Maminski et al. 2006) modified the melamine-urea-formaldehyde adhesive (MUF) by adding glutaraldehyde to the hardener in the form of a 50% aqueous solution. The shear strength of birch samples bonded with the modified adhesive was significantly higher compared to the reference sample. Formaldehyde adversely affects the respiratory system, eyes, skin, genetic material, reproductive organs, and has a strong effect on the central nervous system (Příhoda 1988).

Formaldehyde is categorized as a dangerous substance causing serious health problems; and therefore, testing of formaldehyde content and testing of formaldehyde emission have become an indispensable part of testing of glued materials parameters. Formaldehyde emissions and the harmful effects of formaldehyde have become a problem, especially in indoor products. Formaldehyde is toxic, has strong antiseptic properties with adverse biological effects on living organisms and destroys most microorganisms, including spores. Research of modification of adhesives for woodworking industry is aimed on natural non-toxic, biologically degradable, and cheap biopolymers. Market offers large number of biopolymers e.g., collagen and keratin, waste from food and leather productions and polymer polyphenolic molecules of vegetable tannins, which can be used as modifiers of adhesives for woodworking industry. Possibilities of effective processing and applications of leather tanned and non-tanned waste for different products are described in (Pünterer 1995, Buljan *et al.*, Matyašovský et al. 2011, Matyašovský 2008). Controlled enzymatic hydrolysis of leather waste has the advantage of lower energy consumption, especially when using commercially available commercial proteases of microbial origin (Kolomazník et al. 1999, Kolomazník et al. 2000, Sun and Zhong 2000). The advantage of this procedure may be the control of the average molecular weight of the hydrolysate by selecting the reaction time of the enzymatic hydrolysis. Proteins of amino-acids with peptide bond are the source of large number of amino-groups $-NH_2$, which are reactive with formaldehyde. Fibril character of collagen presents similar analogy with cellulose fibers and its structure can be stabilized with chemical bond e.g., formaldehyde, glutaraldehyde etc. Another advantage of biopolymers is their non-toxicity and biodegradation ability to basic structural elements (Matyašovský et al. 2001).

Thermo-oxidative stability of different materials and biopolymers was tested by differential scanning calorimetry (DSC). The method is based on determination of the end of induction period, or the beginning of the main oxidation process (Šimon et al. 2001, Šimon et al. 2006).

Experimental research was aimed on preparation of adhesive mixtures and testing their influence on formaldehyde emission and strength of glued joint. The aim of the study was to reduce the release of formaldehyde from wood materials by developing and testing new more effective keratin-based environmental modifiers that bind formaldehyde and form more stable methylene bonds and their effect on the bond strength of wood-based panels.

EXPERIMENTAL

Materials and chemicals

Modification of urea-formaldehyde adhesives was solved by preparation and application of four samples of keratin hydrolysates and amino acid cysteine, which were prepared from

sheep wool 'Merino' of the following composition: nitrogen 12.15 %, ash 2.53 %, sulfur 2.21 %, fat 7.16 %. The wool was separated, washed, defatted, and dried at room temperature.

The increase of stability and efficiency of the amino acid cysteine was solved by its modification with the additive MOD-I which was prepared by condensation of glutaraldehyde PROTECTOL GA-50 and urea.

Description and labeling of prepared samples No:

1. Keratin K-1 – prepared by acid hydrolysis and neutralized with NaOH solution,
2. K-2 - keratin – prepared by oxidative hydrolysis,
6. Cysteine – prepared from sheep wool which was modified with glutaraldehyde PROTECTOL GA-50 and urea – (MOD-I),
9. K-9 - keratin – prepared by alkaline hydrolysis and neutralized with HCl solution,
11. K-11 - keratin – prepared by alkaline-oxidative hydrolysis.

Adhesive compositions were prepared by applying the urea-formaldehyde adhesive Protodur 303.0 in the form of a powder diluted with water and condensed at 100 °C for 20 minutes.

Adhesive mixtures for modification UF resin were prepared according to following scheme:

0. 100% UF adhesive PROTODUR 303.0 - reference sample mixing ratio with water (2:1), Keratin K-1 – prepared by acid hydrolysis and neutralized with NaOH solution.

1. 99.5% UF + 0.5% Keratin K-1
 2. 99% UF + 1.0% Keratin K-1
 3. 97% UF + 3.0 % Keratin K-1
- K-2 - keratin – prepared by oxidative hydrolysis.

4. 99.5% UF+ 0.5% Keratin K-2
5. 99% UF + 1.0% Keratin K-2
6. 97% UF + 3.0 % Keratin K-2

Cysteine – prepared from sheep wool which was modified with glutaraldehyde PROTECTOL GA-50 and urea - (MOD -I).

7. 99.5% UF + 0.5% Cysteine + (MOD -I)
8. 99% UF + 1.0% Cysteine + (MOD -I)
9. 97% UF + 3.0% Cysteine + (MOD -I)

Keratin K-9 – prepared by alkaline hydrolysis.

10. 99.5% UF + 0.5% Keratin K-9
11. 99% UF + 1.0% Keratin K-9
12. 97% UF + 3.0% Keratin K-9

Keratin K-11 – prepared by alkaline-oxidative hydrolysis.

13. 99.5% UF + 0.5% Keratin K-11
14. 99% UF + 1.0% Keratin K-11
15. 97% UF + 3.0% Keratin K-11

The samples were characterized by XPS spectroscopy, thermo-oxidative stability was studied by differential scanning calorimetry (DSC), formaldehyde was tested according JIS A 1460 by Desiccator method and quality according to standards EN 314-1 and EN 314-2

Methods of testing

X-Ray photoelectron spectroscopy (XPS) signals were recorded following a previously described procedure (Stach et al. 2011) using a Thermo Scientific K-Alpha XPS system

(Thermo Fisher Scientific, UK) equipped with a micro-focused, monochromatic Al K α X-ray source (1486.6 eV). An X-ray beam of 400 μm size was used at 6 mA \times 12 kV. The spectra were acquired in the constant analyzer energy mode with pass energy of 200 eV for the survey. Narrow regions were collected using the snapshot acquisition mode (150 eV pass energy), enabling rapid collection of data (5 s per region).

DSC calorimeter Perkin-Elmer DSC7

Thermo-oxidative stability of the samples was studied by power-compensated calorimeter Perkin-Elmer DSC-7 equipped with a high-pressure DSC cell. Temperature calibration was carried out until the melting point of indium and the enthalpy calibration was carried out up to the heat of fusion of In. Samples of 2–4 mg were placed in standard open aluminum pans. The measurements were performed in oxygen atmosphere; oxygen pressure was set to 10 bar and the samples were heated in the temperature range of 50–250°C with heating rates of 1, 3, 5, 7 and 10°C/min.

Plywood strength testing

These tests were performed following a previously described methodology (Bekhta et al. 2019). Quality of gluing was tested according to standards EN 314-1 and EN 314-2. Three-layer plywood of beech wood (*fagus sylvatica*) veneer was prepared for determination of physical and mechanical properties at following conditions: pressing (laboratory hydraulic press FONTIJNE) pressure 1.8 MPa, temperature 105 °C, time 5 resp. 6 min. Plywood were conditioned at the temperature of 20 ± 2 °C and relative humidity 65 ± 5 %. Tested pieces were pre-treated for the class 1:

- immersion in water 20 °C for 24 hours,
- constant rate loading,
- disruption after 30 ± 10 seconds,
- accuracy of 1 N.

Formaldehyde emissions

Formaldehyde emissions from five-layer beech wood plywood were tested according to the test method JIS A 1460 “Building boards. Determination of formaldehyde emission. Desiccator method” according to following conditions:

- volume of desiccator: 9-11 dm³,
- loading coefficient: 1800 cm²,
- temperature of 20 ± 0.5 °C,
- test duration 24 h,

The concentration of formaldehyde absorbed in distilled water was evaluated by acetyl-acetone method with spectrophotometric evaluation using the ultraviolet spectrophotometer UviLine SI 5000 at 412 nm wavelength.

RESULTS AND DISCUSSION

X-Ray photoelectron spectroscopy (XPS) was used for qualitative and quantitative determination of basic elements prepared samples of biopolymers keratin. Analysis of sample surfaces determined by X-Ray photoelectron spectroscopy can be seen on the Table 1.

Table 1: Apparent surface chemical composition samples of keratin as determined by XPS.

Surface chemical composition of samples prepared from keratin [%]						
Sample No.	C1s	O1s	N1s	S2p - sulfide(C-S)/SO ₃	Cl2p	Na1s
1. Keratin K-1	65.8	15.8	13.5	3.0 – 89.2/10.8	1.3	0.6
2. Keratin K-2	82.2	10.5	4.5	1.3 – 14.9/85.1	0.5	0.0
6. Cysteine modified (MOD-I)	63.4	14.4	20.7	0.7 – 100.0/0.0	0.5	0.2
9. Keratin K-9	53.5	18.3	13.6	2.3 – 78.0/22.0	6.7	5.5
11. Keratin K-11	57.2	21.4	12.0	1.9 – 44.4/55.6	0.9	6.6

The differences between the spectra of prepared samples are visible mainly in the amount of sulfur and in the ratio of the reduced state C-S (signal S2p at -163 eV) and the oxidized state SO₃ (signal S2p at 168 eV). In the sample of keratin K-2 prepared by oxidative hydrolysis, there were a significant decrease nitrogen to 4.5% (N1s signal at ~ 400 eV) and oxygen to 10.5% (O1s signal at ~ 532 eV). Total amount of sulfur is 1.3% and its oxidative form increased to 85.1% (S2p signal at ~ 163 eV). Sample No. 6 has the highest nitrogen content to 20.7 % (N1s signal at ~ 400 eV) and the lowest total content of sulfur is only 0.7% but only in the reduced state as sulfide.

Antioxidation activity samples prepared from biopolymer keratin.

Perkin-Elmer DSC7 calorimeter with a high-pressure measuring head was used to study the thermo-oxidative stability of the prepared samples. The stabilizing effect of antioxidants depends on the matrix where they are dispersed.

The antioxidant effects of prepared samples were determined in a suspension with polyethylene glycol SLOVAPEG-600 (Slovchema, Slovakia). The mixtures of PEG and prepared samples were ultrasonicated for 5 min. Keratin hydrolysates swelled in polyethylene glycol (PEG) resulting in a suspension. Composition of the suspensions is shown in Table 2.

Tab. 2 Mass of components of the suspensions of PEG with tested biopolymers No.

parameter	PEG [®] + 1 ^(a)	PEG [®] + 2 ^(b)	PEG [®] + 6 ^(c)	PEG [®] + 9 ^(d)	PEG [®] + 11 ^(e)
<i>m</i> (tested sample)/g	0,0994	0,1027	0,1049	0,1045	0,0991
<i>m</i> (PEG [®])/g	4,1994	4,2300	4,1999	4,2232	4,2100
<i>X</i>	2,367	2,428	2,498	2,474	2,354

PEG[®] polyethylene glycol - reference, ^(a) Keratin K-1, ^(b) Keratin K-2, ^(c) Cysteine-modified with Glutareldehyde and urea MOD -I, ^(d) Keratin K-9, ^(e) Keratin K-11

Concentration of the sample is expressed as parts of the sample per hundred parts of PEG (phr) and is marked as X. In fact, X is the relative mass fraction of the sample in PEG.

Oxidation onset values depending on the heating rate were obtained from DSC records. The values of oxidation onset temperature (OOT) as a function of heating rate are.

Table 3: Dependence of the oxidation onset temperature (OOT) on the heating rate (β)

$\beta/^\circ\text{C}\cdot\text{min}^{-1}$	OOT/ $^\circ\text{C}$					
	PEG [®] pristine	PEG [®] + 1 ^(a)	PEG [®] + 2 ^(b)	PEG [®] + 6 ^(c)	PEG [®] + 9 ^(d)	PEG [®] + 11 ^(e)
1	117,6	119,6	126,6	165,7	139,1	121,9
3	129,6	126,9	138,2	182,5	152	132
5	135	130,6	148	188,2	158,8	141
7	140,8	133,8	152,9	191,8	160,8	145,1
10	147	138,4	157,9	197,1	163,6	151

[®] PEG pristine – reference, ^(a) Keratin K-1, ^(b) Keratin K-2, ^(c) Sample-6 – cysteine modified with methyl-ol pre-condensate - MOD-I, ^(d) Keratin K-9, ^(e) Keratin K-11.

The kinetic parameters A and D have been obtained by the non-linear least-square method using the program ORIGIN. Their values with standard deviations are listed in Table 4.

Table 4: Kinetic parameters describing the induction period of PEG thermo-oxidation

Sample	$\ln(A/\text{min}) \pm \text{SD}$	$D (\text{K}^{-1}) \pm \text{SD}$
PEG pristine	33,8±2,2	0,0803±0,0056
PEG + sample No.1	51,8±4,1	0,127±0,010
PEG + sample No.2	31,4±1,9	0,0723±0,0048
PEG + sample No.6	35,4±1,4	0,0745±0,0031
PEG + sample No.9	40,3±2,4	0,0919±0,0057
PEG + sample No.11	33,6±2,5	0,0790±0,0063

The kinetic parameters obtained enable us to model the length of induction period for any temperature regime. For constant temperature, the length of induction period (i.e., OIT) was determined using (Šimon et al. 2008, Šimon et al. 2009).

The stabilizing effect can be better illustrated by the employment of the value of protection factor, (PF). PF is defined as the ratio OIT for PEG with the addition of stabilizer and the pristine PEG (Cibulková et al. 2005).

Antioxidant efficiency then does not depend on the antioxidant concentration in the matrix (valid exactly for low concentrations) and can be employed for the comparison of antioxidants. Antioxidant efficiency of individual antioxidants in the PEG matrix as a function of temperature is depicted in Figure 1.

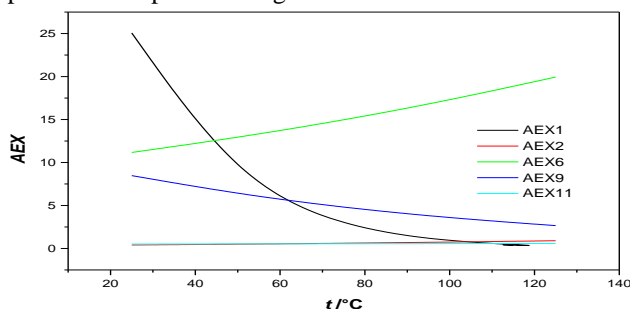


Figure 1. Antioxidant efficiency of antioxidants under study in PEG matrix.

Figure 1. shows that the antioxidant efficiency of the samples No. 2, 9 and 11 is of the order only in units. Better results were obtained at lower temperatures for sample No.1 K-1 where the antioxidant efficiency is in the order from units to tens. The best result was obtained for sample No.6 – (amino acid cysteine prepared from keratin modified by glutaraldehyde and urea). Thus, according to the AEX value, study samples prepared from keratin biopolymer can be characterized as weak antioxidants for the selected temperature range and matrix. Cysteine modified with glutaraldehyde and urea) shows slightly better stabilizing efficiency as a mildly strong antioxidant. However, compared to conventional industrial antioxidants, which have hundreds of AEX values at high temperatures, samples prepared from sheep's wool do not achieve comparable antioxidant activity. Nevertheless, these results show the potential for the use of secondary - waste natural materials to develop new antioxidants.

Formaldehyde emission and shear strength from wood-based panels

Keratin hydrolysates K-1, K-2, Sample No.6-(cysteine modified with MOD-I), K-9 and K-11 were tested to determine their influence on release of formaldehyde and quality of gluing from wood-based panel bonded with UF resins.

Results evaluation of the influence of modifications on the release formaldehyde and shear strength of the plywood test pieces are shown in Table 5.

Table 5: Test results – plywood properties ^(a,b)

Sample No. 1 – Keratin K-1	Formaldehyde concentration [mg/L]	Shear strength [MPa]
100% UF resin + UF resin Protodur 303.3 – reference	0.44	1.82
1 – 99.5% UF resin + 0.5% Keratin K-1	0.37	1.8
2 – 99.0% UF resin + 1.0% Keratin K-1	0.33	1.92
3 – 97.0% UF resin + 3.0% Keratin K-1	0.27	1.52
Sample No. 2 – Keratin K-2		
100% UF resin + UF resin Protodur 303.3 – reference	0.44	1.82
4 – 99.5% UF resin + 0.5% Keratin K-2	0.42	1.77
5 – 99.0% UF resin + 1.0% Keratin K-2	0.39	1.65
6 – 97.0% UF resin + 3.0% Keratin K-2	0.32	1.69
Sample No. 6 – cysteine modified – MOD -I		
100% UF resin + UF resin Protodur 303.3 – reference	0.44	1.82
7 – 99.5% UF resin + 0.5% Sample No. 6	0.30	1.87
8 – 99.0% UF resin + 1.0% Sample No. 6	0.27	2.24
9 – 97.0% UF resin + 3.0% Sample No. 6	0.19	2.05
Sample No. 9 – Keratin K-9		
100% UF resin + UF resin Protodur 303.3 – reference	0.44	1.82
10 – 99.5% UF resin + 0.5% Keratin K-9	0.33	1.85
11 – 99.0% UF resin + 1.0% Keratin K-9	0.31	2.02
12 – 97.0% UF resin + 3.0% Keratin K-9	0.25	1.93
Sample No. 11 – Keratin K-11		
100% UF resin + UF resin Protodur 303.3 – reference	0.44	1.82
13 – 99.5% UF resin + 0.5% Keratin K-11	0.38	1.76
14 – 99.0% UF resin + 1.0% Keratin K-11	0.35	1.51
15 – 97.0% UF resin + 3.0% Keratin K-11	0.30	1.23

^(a) Standard JIS 233 requires for the best formaldehyde evaluation F^{☆☆☆☆} average value of 0.30 at maximum value 0.40 [mg/L]. ^(b) Standard EN 314-2 requires the value of shear strength to be 1.0 MPa.

Reduction of formaldehyde emission - Formaldehyde emissions were tested from five-layer plywood according to the test method JIS A 1460. The results and evaluation of the effect of the presented modifications on formaldehyde emissions from wood-based boards - plywood glued with UF adhesives shown in Figure 2.

Shear strength of plywood panels - Quality of gluing was tested from three-layer plywood according to standards EN 314-1 and EN 314-2. The results and evaluation of the effect of the presented modifications on the shear strength from wood-based boards - plywood glued with UF adhesives expressed in percentages are graphically shown in Figure 3.

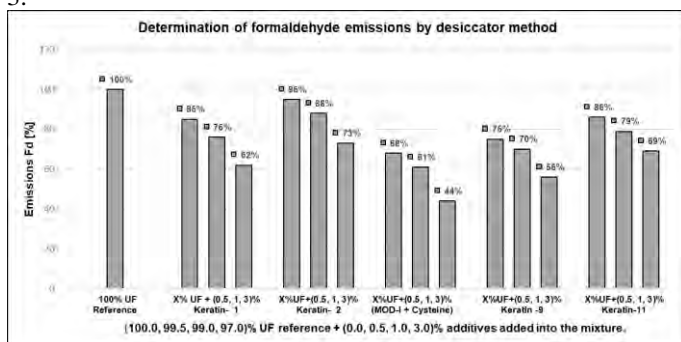


Figure 2. Results of formaldehyde emission by desiccator method

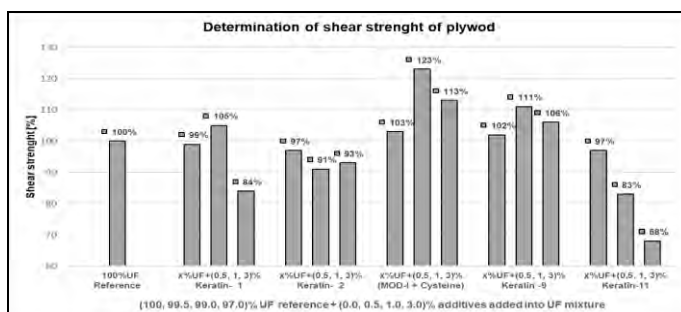


Figure 3. Influence of modifications UF adhesive PROTODUR 303.0 by additives prepared from keratin on shear strength of plywood.

Measured values of extinctions of tested samples of UF glue PROTODUR 303.0 confirmed the lowering of formaldehyde emissions for each concentration of additives prepared from biopolymer keratin in comparison with the reference sample.

The most significant decrease of formaldehyde from wood-based panels up to 44% was achieved with the modification of sample No. 6 - 97% UF + 3% cysteine (prepared from sheep wool) +MOD I (prepared by modification glutaraldehyde with urea).

Tested samples might have a great potential for application as environmentally friendly formaldehyde scavengers.

Tested plywood fulfils requirement of the standard for class of gluing 1 – they are suitable on application in normal interior environment. European standard EN 314-2 requires the value of shear strength above 1.0 MPa.

The highest shear strength 2.24 MPa was obtained for sample No. 6 – 99% UF adhesive PROTODUR 303.0 +1% (MOD-I prepared by modification glutaraldehyde with urea +

cysteine prepared from sheep wool), which corresponds to an increase in shear strength of 123% compared to the reference UF sample. The shear strength of the plywood test pieces decreases slightly with increasing concentration of biopolymers in the mixture of UF adhesives.

CONCLUSIONS

This investigation has focused on modifications of natural biopolymer keratin and possibilities its modification directed mainly to cleavage of the disulfide bonds.

The differences between the XPS spectra of prepared samples are visible mainly in the amount of sulfur and in the ratio of the reduced state C-S (signal S2p at -163 eV) and the oxidized state SO₃ (signal S2p at 168 eV). The sample of keratin K-2 prepared by oxidative hydrolyses, there were a significant decrease in nitrogen from 12,5% to 4.5% (N1s signal at ~ 400 eV). Sample No. 6 has the highest nitrogen content to 20.7 % (N1s signal at ~ 400 eV) and the lowest total content of sulfur is only 0.7% but in the reduced state as sulfide.

The antioxidant activity of the samples was determined in the suspension of polyethylene glycol SLOVAPEG-600 and the test sample. The best result was obtained for sample 6 – (amino acid cysteine prepared from keratin modified by glutaraldehyde and urea). Thus, according to the AEX value, cysteine modified with glutaraldehyde and urea, shows slightly better stabilizing efficiency as a mildly strong antioxidant. The efficiency of the Keratin K-1 sample is moderate at room temperature and negligible at higher temperatures.

The addition of keratin and cysteine prepared from wool sheep into (UF) urea-formaldehyde adhesives for possibilities of lowering formaldehyde emission from wood-based panels was another aim of this study. It was confirmed that sample No. 6, amino acid cysteine modified MOD-I with the highest antioxidant effect has also achieves the highest decrease formaldehyde emissions and the highest strength compared to the reference UF sample. Samples prepared for this study might therefore have a great potential for its application as environmentally friendly formaldehyde scavengers.

Acknowledgements: The authors are grateful for financial support to the Slovak Research and Development Agency projects No. APVV-17-0456, APVV-18-0378 and APVV-22-0238.

REFERENCES

1. MAMINSKI M.L., PAWLICKI J., PARZUCHOWSKI P. 2006. Improved water resistance and adhesive performance of a commercial UF resin blended with glutaraldehyde. In the Journal of Adhesion. 2006, 82, p. 629-641
2. CIBULKOVÁ, Z., ŠIMON, P., LEHOCKÝ, P. AND BALKO J.; Antioxidant Activity of p-Phenylenediamines Studied by DSC. *Polymer Degradation and Stability*, **87**, 479-486, 2005.
3. PŘÍHODA, P., JECH, L. 1988. Hygienické aspekty problematiky formaldehydu unikajícího z výrobků dřevozpracujícího průmyslu. In Systema – Chemizace dřeva průmyslu. Dom techniky ČSVTS Brno. 1988, p. 45-53.
4. PÜNTERER A., 1995: The Ecological Challenge of Producing Leather. Journal of the American Leather Chemists Association 90, 206-215.

5. BULJAN J., REICH G., LUDVÍK J., 1997: Mass Balance in Leather Processing. In: Centenary Congress of the IULCS, London, 138-156.
6. MATYAŠOVSKÝ J., SEDLIAČIK J., JURKOVIČ P., KOPNÝ J., DUCHOVIČ P., 2011: De-chroming of chromium shavings without oxidation to hazardous Cr⁶⁺. In: Journal of the American Leather Chemists Association 106, 8-17.
7. MATYAŠOVSKÝ J., 2008: Applications of collagen from secondary raw materials in the wood composite. Dissertation thesis. TU Zvolen. p. 33-36.
8. KOLOMAZNÍK K. et al., 1999: Application of protein hydrolysate for manufacturing of biodegradable plastics. In Environmentally Degradable Plastics, Smolenice. p. 100-102.
9. KOLOMAZNÍK K. at al., 2000: Experiences in Industrial Practice of Enzymatic Dechromation Shavings. Journal of the American Leather Chemists Association 95, 55-63.
10. SUN S., ZHONG Z., 2000: Adhesives from modified soy proteins. In: Wood Adhesives 2000. Extended Abstracts. Nevada: Forest Products Society, p. 5-6.
11. MATYAŠOVSKÝ J., KOPNÝ J., MELUŠ P., SEDLIAČIK J., SEDLIAČIK M., 2001: Modifikácia polykondenzačných lepidiel bielkovinami. In: Pokroky vo výrobe a použití lepidiel v drevopriemysle. TU Zvolen, s. 37-42.
12. ŠIMON, P., et al. 2001: DSC study of oxidation induction periods. *Journal of Thermal Analysis and Calorimetry* 64, 813-820.
13. ŠIMON, P., et al. 2006: Induction periods – theory and applications. *Journal of Thermal Analysis and Calorimetry* 84, 263-270.
14. ŠIMON, P., HYNEK, D., MALÍKOVÁ, M. AND CIBULKOVÁ Z.; Extrapolation of Accelerated Thermooxidative Tests to Lower Temperatures Applying non-Arrhenius Temperature Functions. *Journal of Thermal Analysis and Calorimetry*, **93**, 817-821, 2008.
15. ŠIMON, P.; Material Stability Predictions Applying a New non-Arrhenian Temperature Function. *Journal of Thermal Analysis and Calorimetry*, **97**, 391-396, 2009.
16. STACH, M., KRONEKOVÁ, Z., KASÁK, P., KOLLÁR, J., PENTRÁK, M., CHORVÁT JR., D., NUNNEY, T. S. AND LACÍK, I.; Polysulfobetaine Films Prepared by Electrografting Technique for Reduction of Biofouling on Electroconductive Surfaces. *Applied Surface Science*, **257**, 10795-10801, 2011.
17. BEKHTA, P., SEDLIAČIK, J., KAČÍK, F., NOSHCHENKO, G. AND KLEINOVÁ, A.; Lignocellulosic Waste Fibers and Their Application as a component of Urea-formaldehyde Adhesive Composition in the Manufacture of Plywood. *European Journal of Wood and Wood Products*, **77**, 495-508, 2019.



EXAMPLES OF SAFETY AND HEALTH RISK FACTORS IN WOODWORKING INDUSTRY IN SLOVAK REPUBLIC

Alena Očkajová¹ – Adrián Banski² – Martin Kučerka¹ – Zuzana Vyhnáliková²

Abstract

In the article, we want to point out the still existing safety and health risks in woodworking operations, the essence of which lies in processing of non-homogeneous materials such as wood, with anisotropic properties and the occurrence of natural wood defects, manual feed of the workpiece into the cut, tools with a large number of cutting edges and high cutting speeds, manual handling of loads, but also in many cases in the irresponsible approach of the employees or employers themselves to the OHS. Failure to address or avoid these risks leads not only to injuries, but long-term work in this environment to occupational diseases, especially hearing loss, diseases of the musculoskeletal system, etc. Although the legislation covers all areas in terms of OSH, its implementation in practice is lengthy and not always adequate. The basis for characterizing the existing safety and health risks was the manual "Risk Assessment Basics - Good for You, Good for Your Company", Check list for Woodworking. Based on the description, it is obvious that the safety risks in woodworking are known, but in many operations they tolerate, and due to health risks, minimal attention is paid to manual handling of loads and ergonomics, the neglect of which contributes significantly to diseases of the musculoskeletal system.

Key words: *woodworking, safety and health risks, OHS*

INTRODUCTION

The woodworking industry is one of the high-risk industries and although our legislation covers all areas in terms of occupational health and safety (Acts of OHS), we often come across reports of workplace accidents (usually severe) as a result of non-compliance with, or a breach of, OSH regulations from the perspective of the affected employee, or even inadequate workplace security on the part of the employer. The problem in question is more frequent in small and medium-sized companies, which include woodworking operations. This situation is mainly caused by:

- the disintegration of large state-owned companies into small, private, or family-owned companies, where OSH issues are not given much attention,
- equipment with outdated technology, which in many cases does not meet safety criteria,
- the low professionalism of the owners, who are not always specialists in their field, let alone in the area of possible risks at work, because in many cases they do not know about them or do not want to know, in other cases they consider the area of

¹ Matej Bel University in Banská Bystrica, Banská Bystrica 97401, Slovakia
e-mail: alena.ockajova@umb.sk; martin.kucerka@umb.sk

² Technical University in Zvolen, T.G. Masaryka 24, Zvolen 96001, Slovakia
e-mail: banski@tuzvo.sk, vyhnalikova@tuzvo.sk

occupational safety and health more as a burden and unnecessarily invested money, which does not bring the effect immediately,

- low awareness of employees themselves, who approach the issue only through the prism of OSH training but do not implement in practice the acquired knowledge of occupational safety and health, which implies an obligation for each individual to comply with all safety regulations, to protect their own health as well as the health of their co-workers,
- the use of machinery and equipment characterized by high speeds, high noise levels, dangerous tools with many cutting edges,
- strenuous physical work carried out mainly in hazardous environments,
- the phenomenon that many people and experts think of wood as a healthy, natural material, a renewable resource, without taking into account certain negative characteristics that arise from the various technological processes involved in its processing (e.g. wood dust during sanding, free formaldehyde in the production of particleboard and fibreboard, medium density fibreboard (MDF), fungi and moulds in landfills, etc.).

A suitable solution was found to eliminate the risk in the first place, if this is not possible, it must at least be reduced to an acceptable level by complying with the relevant limit values [1]. This is difficult and there is not always the will to do so in smaller and family-run companies. As the situation in various woodworking operations is not only problematic in Slovakia, international health and safety institutions (e.g. the European Agency for Safety and Health at Work) try to help employers with a number of brochures with specific instructions and examples on how to deal with selected situations directly in practice. Although many of the procedures may seem tedious at first sight, if the right system is set up and the issue is approached in a targeted and regular manner, the desired objective will certainly be achieved.

The aim of the presented paper is to highlight examples of safety and health risk factors in woodworking operations (woodworking) that can very quickly become hazardous if they are not controlled or the limit values specified in the legislative regulations are not respected, as there is a high probability not only of a cumulative effect of risk factors in long-term exposure but also of a synergistic effect of several simultaneously acting factors in the working environment, which is common in woodworking operations.

MATERIAL AND METHODOLOGY

From a range of risk assessment materials, we have selected the handbook „Risk Assessment Basics - Good for You, Good for Your Company, part Woodworking“ [2,3] which will be used to characterize selected risk factors for the woodworking industry, with specific examples, to give an idea of their multitude and diversity. It is by characterizing these hazards that we want to emphasize that the risk here cannot be said to be small, perhaps medium, but in most cases large, and that this is then matched by the likelihood and severity of damage to health, whether it is a severe accident or a gradually emerging occupational disease. In addition to the general checklist of hazards or dangers given in this manual, there are also lists of hazards or dangers for selected operations, and for woodworking, the manual gives the following checklist of hazards or dangers:

Work tools, equipment

- Are all machines fitted with covers?

- Are instructions available regarding hazardous work practices?
- Are employees trained to operate the machinery?
- Are regular inspections and tests of work tools provided?
- Do employees use suitable means to guide short or narrow pieces of material through the saw?
- Can employees' clothing be drawn between moving parts of machinery and cause damage to their health?

Electrical hazards

- Are electrical machines earthed?
- Are electrical cables and wiring harnesses maintained in a safe condition?
- Are outlets, connections, switches, and fittings covered?
- Is the environment in the area specified in terms of enclosure?

Air quality

- Do woodworking machines have an automatically activated exhaustion system when in use?
- Do you check the exhaust equipment regularly?
- Do you clean and wipe the dust from ceilings, wall partitions, and cable ducts?
- Do you assess the air quality in your workshop?
- Do employees use respirators if they work in paint booths?

Chemicals

- Are employees who come into contact with hazardous chemicals adequately trained?
- Do employees use personal protective equipment (gloves, goggles, face shields, respirators) when working with chemicals?
- Are chemicals kept well away from sources of fire?

Noise and vibration

- Do you assess the noise level in the workplace?
- Do employees exposed to high noise levels use hearing protection?
- Do you avoid vibrations that can be transmitted from machinery through work pieces to employees' hands?

Health risk

- Do you organize health checks for employees?
- Are employees exposed to high noise levels regularly sent for audiometric examinations?
- Are employees appropriately trained on working with loads?
- Do you try to meet the special needs of employees when designing the workplace (ergonomics)?

On the basis of our own practical experience and numerous visits to woodworking enterprises, as well as experimental measurements we have carried out in them and in the framework of our own research, we present selected examples, in particular for the following areas: Work tools, Equipment; Air quality; Noise and vibration; Health risk.

RESULTS AND DISCUSSION

Safety risks

Work tools, equipment

➤ **Are all machines fitted with covers?**

The woodworking industry is characterized by the presence of tools with a large number of cutting edges that operate at high speeds, e.g. circular sawblades (approx. 7000 min⁻¹), bottom spindle moulder (approx. 8300 min⁻¹), top spindle moulder (up to 30000 min⁻¹), and it is therefore very important to provide them with covers, [4]. Modern woodworking machines are equipped with perfect protection for all moving and rotating parts and tool guards that uncover themselves during the working operation. When changing tools or carrying out maintenance work, the tool cover is only opened when the power supply is switched off.

Of course, all machines are fitted with covers from the manufacturer, but we often encounter unprotected rotating spindles in joint-carpentry and furniture workshops, e.g. (in bottom spindle moulder) in individual production, it is sometimes necessary to change the tool many times per change due to production requirements (customer needs) and this seems to be very tedious for the operator if he should always fix the tool and the cover, which is also part of the exhaust, together with the protective grid, for finger stop. In this case, the danger or hazard is multiplied by the manual feed of the workpiece into the cut. If the work is carried out without a cover, e.g. with a bottom spindle moulder that also includes a finger protection unit, the operator can very quickly come into contact with dangerous moving parts of the tool.

The danger of working on woodworking machines when manually feeding material into the cut is also increased by the very characteristics of the material being machined, such as its anisotropy, the occurrence of knots, and other growth defects. A very dangerous situation can arise especially during planing (thickness and surface planer), and sawing. The knots distort the structure of the wood, have a higher density (2 to 3 times higher than the surrounding wood, [5]), and are often the cause of material kickback, and the operator does not always react promptly to the situation, which can result in the hand slipping off the workpiece being moved. The knots are also dangerous if they are not perfectly bonded to the surrounding wood (unsound knots) – loose knots, knots affected by rot, and they come loose on contact with the cutting edge of the tool and can strike the operator.

➤ **Can employees' clothing be caught between the moving parts of the machinery and cause damage to their health?**

It is the perfectly designed machine covering that should prevent clothing from being drawn between the moving parts of the machinery and thus damage the health of the employees. As mentioned above, if the cover is out of action for any reason and the machine is being worked on, then there is a high probability of employees' clothing being pulled between moving and rotating machine parts, or undressed hair or hanging items - bracelets, chains, etc. being pulled in.

Risk factor – working without a cover and the manual feed of material (wood) into the cut. This activity (manual feed) should certainly be included in the checklist of hazards or dangers for woodworking, the hazards of which are determined by the species, the anisotropy itself (the difference in physical and mechanical properties in three mutually

perpendicular directions) and the occurrence of natural defects in the wood, such as knots, ruptures, defects in the structure of the wood, etc., which essentially distinguish the machining of this material from other materials with a homogeneous texture.

➤ **Do employees use appropriate means to guide short or narrow pieces of material through the saw?**

In most cases, yes, because employees are aware of the dangers of this action, especially when sawing and milling. Rather, a problem can arise when larger chips or dropped knots are on the saw table or bottom spindle moulder and the operator tries to remove them by this means and can very quickly stumble against the moving tool.

➤ **Are there instructions available on dangerous working practices?**

Operating manuals for all machinery and equipment, as well as instructions on hazardous work practices, are available at woodworking facilities.

➤ **Are employees trained to operate the machinery?**

Of course, employees in most operations are trained to operate machinery and certainly warned about unsafe working practices, but the human factor does not always act in accordance with the regulations and instructions. Two risk groups of employees in terms of age need to be highlighted and drawn attention to. While young employees may not yet appreciate the potential risk of not following all the rules for working on woodworking machines, older employees are also aware of the risks involved, but their routine in operating the machines means that they try to 'improve and speed up' certain activities, which often results in the use of unsafe working practices, [6].

Risk factor – age of the employee

Air quality

➤ **Do woodworking machines have an automatically activated exhaust system when they are in use?**

➤ **Do you check the exhaust equipment regularly?**

➤ **Do you clean and wipe the dust from ceilings, wall partitions, and cable ducts?**

The answer to these three questions is yes, every machine in operation is always equipped with an exhaust system, very typical in the case of little-used stands are mobile exhaust units, with high efficiency. It is also ensured that pipelines are checked, as this is the first prerequisite for the spread of dust into the working environment. The problem arises when the employees themselves disable the suction from the machine, as in the case of the bottom milling machines, and thus cause a permanent load on the environment, especially with fine dust, which floats in the environment, does not settle or settles very slowly, and is stirred up again by any movement.

Wood dust dispersed in the working environment are airborne dust particles, with a diameter of less than 100 µm [7,8,9], which pose a health risk to operating personnel because they cause respiratory problems in addition, beech and oak hardwood dust are classified as Category 1 carcinogens, which means a proven chemical carcinogen [10]. In woodworking operations, where dried wood is already handled, that a large number of dust particles with a particle size diameter of fewer than 100 µm are produced and about 80 % of such dust particles are produced during the sanding operation [11,12,13].

Fine coating of dust can often be seen on various structures, walls, sloping surfaces, power lines, and on the exhaust pipeline itself, which is less regularly cleaned (vacuumed) and is swirling again by any activity. Our experiments have confirmed that the smaller the dust particles are, the higher their cohesion and adhesion to the surface and they are able to stick even on "steep surfaces" [14]. The floors are cleaned of dust regularly, but sometimes with compressed air "because it's faster". Another problem in terms of settled dust is the stacked material near the machines (in smaller operations) that will be processed, and it is not possible to clean this area well on a regular basis. It should be in the interest of the employer but also of the employees themselves, in the wood processing industry, to protect their respiratory system and to wear suitable PPE [15].

Risk factor – inadequate cleaning of settled dust

➤ Do employees wear respirators if they work in paint booths?

It certainly is, and it should be pointed out that paint manufacturers are now trying to develop eco-friendly coatings, where harmful chemicals are replaced by less harmful ones or new systems without harmful additives, [1]. But certainly, the use of respirators is important, and this also depends on the type of coating equipment. The dispersion of these substances into the air is different when spraying (the largest), and it would be different when dipping, roller coating, or painting. As spraying is the predominant coating method in smaller operations, the use of respiratory protective PPE should be a matter of course.

➤ Are you assessing the air quality in your workshop?

To ensure the air quality in the workshop, the limit values of hazardous factors in the working environment set by the standards should be respected and employers should take care to professionally monitor and measure these hazardous factors in the workplace, (whether it is dust, free formaldehyde, noise).

Noise and vibration

➤ Are you assessing noise levels in the workplace?

➤ Do employees exposed to high noise levels use hearing protection?

The noise level of the woodworking machines exceeds the limit value of 87 dB [16], (conveyors, main sawing machines – frame saws, trunk band saws, circular saws, sorting lines, planers, moulders etc.), which greatly reduces the quality of the environment in which the operating personnel moves throughout the working shift. The prolonged exposure to noise causes gradual hearing loss but also other health problems – stress, headaches, insomnia, increased blood pressure, lack of appetite, etc.

Employees have hearing protectors, but if we have worked with them ourselves, we can see that they greatly interfere with our comfort at work, weaken communication between colleagues, make us less aware of our immediate surroundings, and can also reduce our alertness and attentiveness. Very important in such cases to invest in personal protective work equipment that will only eliminate high noise levels, not human speech. It must be stressed that noise increases if tools are blunted, or poorly balanced if the wrong size tool is used (e.g. a larger diameter saw blade than is sufficient to perform the operation), again the material, its anisotropy and the occurrence of natural defects, especially knots, etc. must be emphasized [17]. Employees are very unlikely to rotate if they are trained to work on these machines, because if they work in the same hall it does not matter which machine they operate, as the noise in the working environment is equally high in any location.

Risk factors – noise and using PPE, not of the highest quality**➤ Do you avoid vibrations that can be transmitted from the machines through workpieces to the employees' hands?**

There are a number of woodworking operations where vibration cannot be avoided, e.g. the operation of hand-held electrical machinery and tools, where employees are mainly exposed to vibration transmitted to their hands, which can be reduced by the use of appropriate PPE – anti-vibration gloves, although they do not always meet the stated reduction in vibration values in practice, [18].

Risk factor – vibrations and using PPE, not of the highest quality***Health risks*****➤ Are employees adequately trained to work with loads?**

There is still a great deal of strenuous physical work involved in woodworking, which includes working with loads (e.g. when assembling parts, and packing, but often also when loading and unloading parts into and out of the machine). In this work, aids aren't used a lot to reduce or eliminate this factor. This is heavy physical work, whether dynamic or static. I do not know if employers train their employees on the basic rules of handling loads (horizontal plane rule, vertical plane rule – the center of the gravity of the object as close as possible to the center of the gravity of the operator), the principles of lifting, lowering loads, pulling and pushing (e.g., material handlers – proper use of their own weight), etc. Particularly for the younger age group, training is essential to learn the correct procedures and rules (to learn them), as these activities gradually lead to health problems, especially with the sacral spine [19, 20].

Risk factor – aids aren't used a lot to reduce or eliminate working with loads, working without training (accent on young people)**➤ Do you try to meet the special needs of employees in workplace design (ergonomics)?**

I don't know if it is correct in this case to talk about the special needs of employees when designing a workplace. Here, we should not define it as the special needs of employees, but as the employer's obligation to create the best possible workplace, also from the point of view of ergonomics, the aim of which is to preserve the health of employees at maximum performance. In our operations, the aim is primarily maximum performance, and not enough attention is paid to the health and well-being of employees. However, it is in woodworking that we encounter a great deal of physical strain, whether dynamic or static, and it is precisely by the ergonomic design of the workplace that this strain could be eliminated, at least in part.

Static load, which is a long-term, unilateral, and excessive load on the musculoskeletal system, is encountered in woodworking (especially furniture production, construction, and joinery production, upholstery production) when using any tools, especially hand machines, pneumatic nailers, staplers, drills, etc. when the basic ergonomic principle of a straight wrist is not observed - e.g. when pistol tools are used instead of hanging tools for working horizontal surfaces. By having to twist or bend the wrist, more strain is placed on it, resulting in less force being exerted and progressive health problems [21]. This problem is compounded by the sheer weight of hand tools and implements. And it is up to employers

how they tackle the design of their workplaces so that individual operations can be carried out in the context of basic ergonomic principles.

In most positions when operating conveyors (e.g. checking center slats in large composites, assembling parts) the operator has to be bent over (again the basic ergonomic principle of a straight back is not followed), and the height of the handling plane - i.e. the height of the conveyor is uniform for all employees operating it and we can then observe that tall people have to have their back very bent over the conveyor and short people may have a problem with the operator and have to bend over to pick up individual parts. Rarely are these positions equipped with at least simple swivel chairs for a short rest, perhaps adjustable in height, which would go some way to eliminating the uniform height of the handling plane and at least partly eliminate physiologically unacceptable working positions (bending over, stooping...), [22].

Risk factor – not observed the basic ergonomic principles, physiologically unacceptable working positions

CONCLUSION

Based on the description of possible safety and health risks in wood processing operations, it can be concluded that work in this sector is physically demanding. Among the items that receive minimal attention based on our analysis are:

- work is carried out without a tool covers,
- inadequate cleaning of settled dust,
- absent material handling training,
- PPE not of the highest quality or in line with scientific advances,
- minimal ergonomic design of workplaces (static and dynamic loads, physiologically unacceptable working positions, straight wrists, etc.),
- risks age categories of employees with accent to young workers.

There is an absent item in the list of hazards or risks for wood processing:

- processing of non-homogeneous material such as wood, with anisotropic properties and the occurrence of natural wood defects and
- manual feed of the workpiece into the cut.

Funding: This work was supported by the Grant agency VEGA of the Ministry of Education, Science, Research and Sport of the Slovak Republic [No.1/0323/23].

REFERENCES

- [1] Zákon NR SR č. 124/2006 Z.z. o bezpečnosti a ochrane zdravia pri práci a o zmene a doplnení niektorých zákonov.
- [2] Bezpečnosť a ochrana zdravia pri práci sa týka každého - Dobré pre Vás, Dobré pre vašu spoločnosť, Základy posudzovania rizík, Košice: NIP, 2007.
- [3] Healthy Workplaces Campaigns, [Healthy Workplaces Campaigns | Safety and health at work EU-OSHA \(europa.eu\)](https://www.europa.eu/health-at-work), (accessed 10 June 2023).

- [4] A. Očkajová, Z. Fitoš, Posúdenie nebezpečenstiev pri práci na vybratých drevoobrábачích strojoch. Trendy lesníckej, drevárskej a environmentálnej techniky a jej aplikácie vo výrobnom procese, Zvolen: TU, 2006, 116-122.
- [5] J. Dubovský, A. Rohanová, Analýza tvrdosti dreva. Trieskové a beztrieskové obrábanie dreva, Zvolen: TU, 2006, 97-103.
- [6] Young workers. 2017, <https://oshwiki.osha.europa.eu/en/themes/young-workers> (accessed 11 March 2023).
- [7] STN EN 481 Ovzdušie na pracovisku. Určenie veľkosti frakcií na meranie častíc rozptýlených vo vzduchu. 1998.
- [8] WHO. Hazard prevention and control in the work environment: Airborne dust. WHO/SDE/OEH/99.14), World Health Organization, 1999 Geneva.
- [9] L. Dzurenda, Sypká drewná hmota, vzduchotechnická doprava a odlučovanie, Zvolen: TU, 2007.
- [10] Nariadenie vlády Slovenskej republiky č. 356/2006 Z.z. o ochrane zdravia zamestnancov pred rizikami súvisiacimi s expozíciou karcinogénnym a mutagénnym faktorom pri práci.
- [11] A. Očkajová, M. Kučerka, Ľ. Krišťák, R. Igaz, Granulometric analysis of sanding dust from selected wood species, *BioRes.* 13, 4 (2018), 7481-7495. <https://bioresources.cnr.ncsu.edu/issues/vol13-issue4/page/3/>. DOI:10.15376/biores.13.4.7481-7495.
- [12] A. Očkajová, Š. Barčík, M. Kučerka, P. Koleda, M. Korčok, Z. Vyhňáliková, Wood dust granular analysis in the sanding process of thermally modified wood versus its density, *BioRes.* 14, 4 (2019), 8559-8572. <https://bioresources.cnr.ncsu.edu/issues/vol14-issue4/page/7/>. DOI: 10.15376/biores.14.4.8559-8572
- [13] A. Očkajová, M. Kučerka, R. Kminiak, Ľ. Krišťák, R. Igaz, R. Réh, Occupational Exposure to Dust Produced when Milling Thermally Modified Wood. *Int. J. Environ. Res. Public Health.* 2020, 17, 1478. <https://doi.org/10.3390/ijerph17051478>
- [14] A. Očkajová, A. Banski, T. Rogozinski, Tilt angle of wood dust. *Ann, WULS – SGGW, For. and Wood Technol.* 121, (2003) 37-42.
- [15] Drevo výroba a výroba nábytku. Príručka v rámci kampane „Nebezpečné chemické faktory“, Košice: NIP, 2010.
- [16] Nariadenie vlády Slovenskej republiky č. 115/2006 Z.z. o minimálnych zdravotných a bezpečnostných požiadavkách na ochranu zamestnancov pred rizikami súvisiacimi s expozíciou hluku.
- [17] A. Očkajová, J. Stebila, H. Rajnicová, M. Gajtanska, R. Igaz, Ľ. Krišťák, I. Kubovský, L. Pašková, S. Kvočka, M. Rybakowski, Pracovné prostredie a ergonómia, Belianum, Banská Bystrica, 2013.
- [18] V. Goglia, I. Dukič, The vibration transmissibility of gloves – measurement and evaluation, 4 th ISC – Woodworking technique. Prague, Zagreb, 2011, 461-468.
- [19] Nariadenie vlády Slovenskej republiky č. 281/2006 Z.z. o minimálnych bezpečnostných a zdravotných požiadavkách pri ručnej manipulácii s bremenami.
- [20] eTool, Woodworking, [eTool : Woodworking - Packaging/Shipping - Ergonomics | Occupational Safety and Health Administration \(osha.gov\)](https://www.osha-slovakia.gov.sk/eTool/Woodworking-Packaging/Shipping-Ergonomics-Occupational-Safety-and-Health-Administration), (accessed 10 June 2023).
- [21] M. Middlesworth, Fundamental Ergonomic principles, [Fundamental-Ergonomic-Principles-v-2.1.pdf \(ergo-plus.com\)](https://www.ergo-plus.com/fundamental-ergonomic-principles-v-2.1.pdf) (accessed 10 June 2023).
- [22] Vyhláška MZSR č. 542/2007 Z.z. o podrobnostiach o ochrane zdravia pred fyzickou záťažou pri práci, psychickou pracovnou záťažou a senzorickou záťažou pri práci



... dodávateľ najvyššej kvality...
... sme tu pre Vás viac ako 30 rokov...



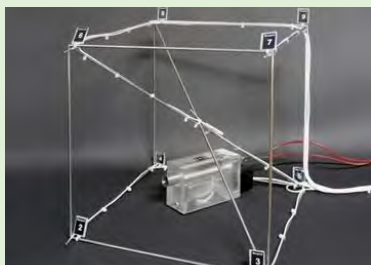
MERACIA TECHNIKA A SNÍMAČE

... univerzálna meracia technika
... presná digitálna technológia snímačov
... spoľahlivé bezkontaktné pyrometre
... bezdrôtové a IoT technológie
... riešenie všetkých meracích aplikácií



ROBOTIKA A PRIEMYSELNÁ AUTOMATIZÁCIA

... riešenia a realizácie „na kľúč“
... vizuálna kontrola kvality
... aplikácie v rôznych priemyselných odvetviach
... odborné poradenstvo a servis
... simulácie a testovanie



AKREDITOVANÉ KALIBRAČNÉ LABORATÓRIUM

... akreditácia podľa normy ISO/IEC 17025:2018
... kalibrované veličiny: teplota, vlhkosť, tlak, objem
... odborné akreditované merania
... validácia skladových priestorov
... kalibrácia klimatických komôr
... odborné poradenstvo a konzultácie



PROTIKORÓZNA OCHRANA

... striekané polyuretánové protikorózne materiály
... viskózne-elastické protikorózne hmoty
... zariadenia na povrchové úpravy potrubí
... plynovody, ropovody, produktovody, armatúry
... rehabilitácia potrubných línií
... poradenstvo v oblasti protikoróznej ochrany



SPECIFIC CUTTING WORK AT DRILLING PARTICLEBOARDS MADE OF AN ALTERNATIVE RAW MATERIAL

Zbigniew Potok – Barbara Pralat – Marta Pędzik – Krzysztof Wiaderek
– Tomasz Rogoziński

Abstract

The study aims to investigate the effect of using alternative lignocellulosic materials in particleboard production on technological properties during drilling by measuring energy consumption and specific cutting work. The object of the research was to compare 3 types of particleboards made from: shredded wood-based panels (PO), energy willow particles (SV) and a mix of raw materials (MIX) when drilling holes for furniture joints. The materials were drilled at a constant revolution of the cutting tools of 6,000 rev/min with variable feed rates of 0.2 and 2 m/min. The boards researched had the same nominal density and met the requirements of EN 312 for P2-type boards. The energy consumption of the drilling process on the Felder Creator 950 CNC machine was tested using a PQ-box 150 energy quality analyzer. Energy consumption for a feed rate of 2.0 m/min is on average three times lower than for a feed rate of 0.2 m/min. The values for energy consumption and specific cutting work indicate that the particleboard material used affects energy consumption during drilling. Energy consumption for drilling one hole is highest for PO boards, and by using 50% of the raw material from shredded boards (MIX), this value can be reduced by 48% and 37% depending on the feed speeds.

Key words: *energy consumption, feed rate, particleboard production, furniture joints*

INTRODUCTION

The furniture industry is subject to ever-increasing demand, and as a result, given the incidence of wood particleboard shortages and high prices, particleboard producers must look for other available sources of raw material. There are many possible raw materials for particleboard production, which, in addition to coniferous species chips and post-consumer wood, can provide a sustainable production process (Reh et al., 2024). When taking up the challenge of enriching production with the use of alternative raw materials, it is important to preserve the quality of the boards and not complicate the machining process. The results of Pędzik et al. (2022) (Pędzik et al., 2022) indicated that forest residues in the form of branches from parts of the tree crown from the harvesting of round pine wood have the same suitability for the production of three-layer particleboards as wood from the most valuable part of the trunk of Scots pine. At the same time, managing waste from the panel industry containing shredded wood particles takes on the challenge of recycling by converting them into value-added products (Aladegboye et al., 2024). These activities are part of the principles of a circular economy. However, it should be considered that material

innovations affect the properties of the produced boards, if only because of the achievable particle size. The size of the particles used and the type of raw material will affect the physical and mechanical properties of the particleboards (Dukarska et al., 2022). Therefore, when using alternative raw materials for particleboard production, it is crucial to maintain not only the quality of the boards determined by mechanical properties (Janiszewska-Latterini and Pizzi, 2023), but also the corresponding constructional and technological properties. Particularly important will be bending strength, mineral particle content and specific cutting work. These properties in practical application will determine the further possibilities and profitability of using particleboards made from alternative raw materials, e.g. for furniture production.

The proper design of case furniture requires, first and foremost, an analysis of the materials used for its structural elements and the selection of appropriate joining systems. The quality of the construction material, the processing methods, and the types of joints used have a significant impact on the durability of the furniture (Langová and Joščák, 2019; Tankut, 2009). Most of the joining solutions for case furniture involve drilling operations in the furniture board panels to create slots or holes for the connectors. Drilling is defined as a cutting process involving the rotational movement of the drill bit and the linear feed movement along the axis of its rotation. One of the parameters characterizing the processing of wood materials is the specific cutting work.

Specific cutting work refers to the amount of work required to convert a unit volume or mass of the cut layer into chips. The value of this parameter depends on the processing parameters and the material being processed. Understanding the influence of these two components is essential for achieving energy efficiency in the cutting process (Rajemi et al., 2010). To determine the specific cutting work, it is necessary to measure the energy consumed during processing. This energy is most often determined based on the forces occurring during cutting. While achieving this is straightforward in laboratory conditions, it is practically impossible in industrial conditions. Therefore, in this study, to obtain information about the amount of energy consumed during cutting, a PQ-box 150 energy quality analyzer was used, allowing for direct measurement of the energy consumption by the machine performing the processing.

The study aims to investigate the effect of using alternative lignocellulosic materials in the production of particleboards on the technological properties during their processing, such as energy consumption and the specific cutting work. In addition, the study determines the effect of feed rate on these parameters. These results will provide the data necessary for the furniture industry to use particleboards from alternative raw materials in the production of products such as furniture.

MATERIAL AND METHOD

The research used 3 variants of particleboards made from alternative lignocellulosic materials. The variants produced included the use of particles and the boards were marked as: PO - particles from shredding wood-based panels such as laminated particleboards and OSB (Oriented Strand Boards), SV - particles from energy willow (*Salix viminalis*), and MIX - a 50:50 mix of particles from both. The raw materials were shredded in a laboratory ring-knife shredder and the obtained chips were sorted. The fractions obtained from the 2.0 mm sieve sorting machine were dried at 103°C to a moisture content of 2%. Under laboratory conditions, single-layer particleboards were produced with a nominal thickness of 16 mm, a nominal density of 670 kg/m³ and the resination ratio was 10%. Melamine-

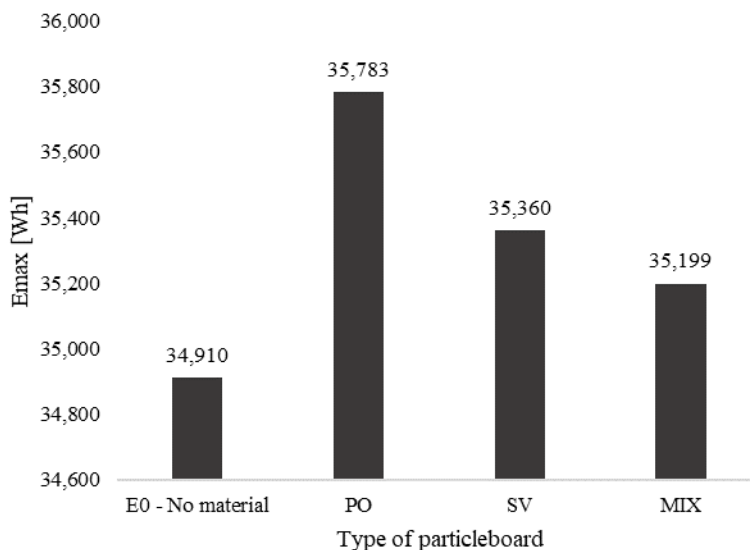
urea-formaldehyde (MUF) adhesive (Swiss Krono Sp. z o.o., Żary, Poland) was used, and the hardener was a 40% water solution of NH_4NO_3 . The resin used had a particulate content of 67.8%, dynamic viscosity of 305 mPa·s and the gel time of the adhesive mass at 100°C was about 93 s. The boards were pressed on a hydraulic single-level press (Simpelkamp, Krefeld, Germany) using the pressing parameters: unit pressure 2.5 MPa, temperature 180 °C, pressing factor 6 s per one mm of nominal board thickness. After manufacturing, respectively, the boards were conditioned in an air-conditioning chamber at a relative humidity of $65 \pm 5\%$ and a temperature of 20 ± 2 °C. Based on the mechanical strength results obtained, the manufactured boards were classified as P2 type (boards for interior fitments, including furniture) according to EN 312.

The energy consumption of the drilling process was tested using a PQ-box 150 energy quality analyzer. The analyzer was connected to the Felder Creator 950 CNC machine (Żory, Poland) for which programs were written. During each test cycle, 19 holes were drilled at 32 mm spacing, which had a diameter of 5 mm and a depth of 25 mm. The number of holes drilled was based on the size of the particleboard format. Leitz drills marked as HW-massive/D5/NL35/S10x27/GL70 were used during drilling. Tests were conducted using two feed rates of 0.2 and 2 m/min and a constant revolution of the cutting tool of 6000 rev/min. Energy consumption tests were conducted for each of the three variants of particleboard raw material used. The methodology for calculating energy consumption per hole is presented in (Pakuła et al., 2024). The energy consumption during the operation of the machine performing the assumed machining cycle (19 holes) without contact with the material was determined (this was to determine the energy consumption of the machine without taking into account the energy for the actual cutting) with two feed speeds, marked as E0. Subsequently, full machining of the 3 particleboards tested was carried out using 2 feed speeds, during which energy consumption was determined as Emax. The results obtained with the energy analyzer were used to calculate the energy consumed to make one hole in the particleboard at different speed variants - Ep. The volume was calculated using data from (Pakuła et al., 2024) and is 490,625 mm³. The specific cutting work (SCW) was calculated from the equation:

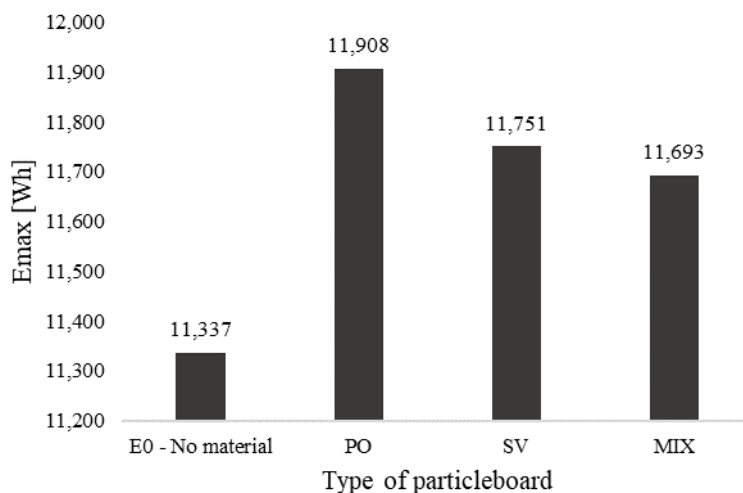
$$\text{SCW} = \frac{E_p}{V}$$

RESULTS

The results of energy consumption measurements making 19 holes are shown in Figures 1 and 2. Energy consumption for a feed rate of 2.0 m/min is on average three times lower than for a feed rate of 0.2 m/min. For a feed rate of 0.2 m/min, the lowest energy consumption was obtained for the MIX variant and amounted to 35,199 Wh, and increased by almost 0.5 and 1.7% for the SV and PO boards, respectively. For a feed rate of 2.0 m/min, consumption was also lowest for the MIX board and amounted to 11.693 Wh, increasing by about 0.5% for the SV board and 1.8% for the PO board. The value of energy consumption for drilling the 19 holes planned in the research was 11.337 Wh for a feed speed of 0.2 m/min and 34.910 Wh for a ten times higher speed rate of the cutting tools.

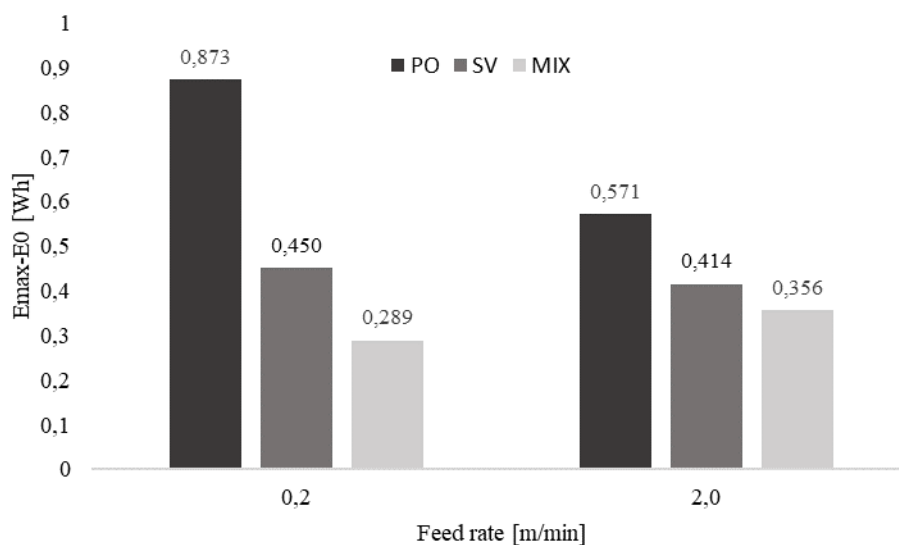


Ryc. 1. Energy consumption during the hole drilling cycle for 3 types of particleboards and a reference sample without material at a feed rate of 0.2 m/min.



Ryc. 2. Energy consumption during the hole drilling cycle for 3 types of particleboards and a reference sample without material at a feed rate of 2.0 m/min.

To obtain the energy consumption of drilling one hole in each board, the differences in energy consumption were first calculated for each board and the reference sample without material, the results are shown in Figure 3. Table 1 shows the energy consumption E_p calculated per drilled hole.



Ryc. 3. Difference in energy consumption between the researched samples and the reference sample without material.

Table 1. Energy consumption for drilling one hole in a particleboard at different feed rates and SCW results.

Parameter	Type of particleboard					
	PO		SV		MIX	
Feed rate [m/min]	0.2	2.0	0.2	2.0	0.2	2.0
Ep [Wh]	0.046	0.030	0.024	0.022	0.015	0.019
SCW [J/mm ³]	9.3621401E-05	6.12076E-05	4.82772E-05	4.44087E-05	3.09727E-05	3.81758E-05

The Ep values indicate that the particleboard material used affects energy consumption during drilling. For the PO board made from shredded laminated particleboard and OSB, the energy consumption for drilling one hole is 0.046 and 0.030 Wh. Using only 50% of the board waste for production, energy consumption can be reduced to 0.015 and 0.019 Wh, a decrease in energy consumption of as much as 48% at a feed rate of 0.2 m/min. For SV and MIX boards at higher feed speeds, the values are similar. However, a significant decrease of 37% in energy is seen at the lower feed rate after reducing the proportion of energy willow particles in favour of board shredding particles.

The specific cutting work indicates how much energy is required to turn a unit volume of material into a particle. Thus, low SCW values are advantageous, as lower resistance will also reduce cutting tool wear. Analysis of the data showed that SCW for PO and SV boards is higher for feed rates of 0.2 m/min. By far the highest SCW values are for the PO board and are 9.3621401E-05 and 6.12076E-05 J/mm³ for feed rates of 0.2 and 2.0 m/min. Adequately to the Ep results, small differences between the feed rates are for the SV board, and the smallest SCW values were shown for the MIX board, which were 3.09727E-05 and 3.81758E-05 J/mm³.

CONCLUSION

The type of raw material used in particleboard production affects energy consumption during hole drilling. Particleboards made from shredded wood-based panels and energy willow particles (MIX) have the lowest energy consumption and the best machinability. In this respect, it is the most energy-efficient material among those researched. Particleboards made from particles of shredded wood-based panels (PO), have the highest energy consumption and require the most energy for drilling. The SV boards rank in the middle on most parameters, making them a compromise between ease of processing and energy consumption. Combining several lignocellulosic materials to produce particleboards is advantageous in terms of technological properties. The type of material affects the cost of energy consumption during processing and tool wear, and this affects the technological profitability of using alternative raw materials for particleboard production. The results of the conducted work will provide the data necessary for the furniture industry to use particleboards from alternative raw materials in the production of products such as furniture.

REFERENCES

- Aladegboye, O.J., Oyedepo, O.J., Awolola, T.J., Oguntayo, O.D., Babatunde, O.Y., Ilesanmi, O.T., Ikubanni, P.P., 2024. Physicomechanical and Thermal Properties of Particle Board Produced Using Waste Ceramic Materials and Corncob. *Advances in Materials Science and Engineering* 2024, 8839814. <https://doi.org/10.1155/2024/8839814>
- Dukarska, D., Rogoziński, T., Antov, P., Kristak, L., Kmiecik, J., 2022. Characterisation of Wood Particles Used in the Particleboard Production as a Function of Their Moisture Content. *Materials* 15, 48. <https://doi.org/10.3390/ma15010048>
- Janiszewska-Latterini, D., Pizzi, A., 2023. Application of Liquefied Wood Products for Particleboard Manufacturing: a Meta-analysis Review. *Curr. For. Rep.* 9, 291–300. <https://doi.org/10.1007/s40725-023-00192-3>
- Langová, N., JOŠČÁK, P., 2019. Mechanical properties of confirmat screws corner joints made of native wood and wood-based composites. *Ann. WULS For. Wood Technol.* 76–84.
- Pakuła, W., Prałat, B., Potok, Z., Wiaderek, K., Rogoziński, T., 2024. Energy Consumption for Furniture Joints during Drilling in Birch Plywood. *Polymers* 16, 1045. <https://doi.org/10.3390/polym16081045>
- Pędzik, M., Tomczak, K., Janiszewska-Latterini, D., Tomczak, A., Rogoziński, T., 2022. Management of Forest Residues as a Raw Material for the Production of Particleboards. *Forests* 13, 1933. <https://doi.org/10.3390/f13111933>
- Rajemi, M.F., Mativenga, P.T., Aramcharoen, A., 2010. Sustainable machining: selection of optimum turning conditions based on minimum energy considerations. *Journal of Cleaner Production* 18, 1059–1065. <https://doi.org/10.1016/j.jclepro.2010.01.025>
- Reh, R., Kristak, L., Kral, P., Pipiska, T., Jopek, M., 2024. Perspectives on Using Alder, Larch, and Birch Wood Species to Maintain the Increasing Particleboard Production Flow. *Polymers* 16, 1532. <https://doi.org/10.3390/polym16111532>
- Tankut, N., 2009. Effect of various factors on the rigidity of furniture cases. *Afr. J. Biotechnol.* 8, 5265–5270.



SURFACE ROUGHNESS OF OIL SURFACE FINISHES ON BEECH WOOD IF THE RECOMMENDED APPLICATION PROCEDURE IS NOT FOLLOWED

Gabriela Slabejová – Mária Šmidriaková – Lukáš Adamčík
– Zuzana Vidholdová

Abstract

Surface Roughness of Oil Surface Finishes on Beech Wood if The Recommended Application Procedure is Not Followed. The article evaluates the differences in roughness of oil-wax surface finishes on beech wood with the zone of mature wood and false heartwood in the situation if all recommended application procedures for surface finishing were not followed. The final sanding was done with P120 grit sandpaper on one set of test bodies; and with P150 grit sandpaper on the other set. Beech wood were surface finished with two representative coating materials based on vegetable oils and waxes. The entire applied amount of the coating material was intentionally left on the surface; after 30 min, the unabsorbed coating material was not wiped off. The roughness R_a and R_z parameters were recorded on VHX-7000 digital microscope. The surface of beech wood sanded showed a lower roughness when using sandpaper P150 compared to P120 in the zone of mature wood and false heartwood both perpendicularly to the wood grain and along the grain. Oil-wax surface finishes reduced the surface roughness of beech wood if the principles of the technological procedure of applying coating materials were followed. If the principles are not followed, there is a high probability of defects in the coating film and this results in an increase in the surface roughness.

Key words: *beech wood, false heartwood, mature wood, oil surface finish, roughness*

INTRODUCTION

Beech wood is one of the most used types of wood for the production of furniture, floors and stairs. It has its own unmistakable texture. Beech is one of the tree species in which a false heartwood is formed. The occurrence of a false heartwood in beech wood is a common malformation encountered in practice (MICHALEC *et al.*, 2022, DZURENDA *et al.*, 2023).

The issue of how to eliminate the creation of false heartwood have been dealt by experts since the beginning of the last century. But we cannot prevent the occurrence of false heartwood yet. Perhaps it would be more interesting to consider the idea of using beech wood with a false heartwood (without rot) for the production of interior elements that are mentioned. The interior elements are usually surface finished. If we want to preserve the visible texture of the wood, transparent coatings are used. Currently, the trend is to use

ecological coating materials or natural-based ones (YAREMCHUK *et al.*, 2023; VIDHOLDOVÁ *et al.*, 2021; YAREMCHUK *et al.*, 2016). One type of coating material with a predominantly naturally occurring film-forming agent are oil-based coating materials (ARMINGER *et al.*, 2020). They harden on wood surface as thin films with sufficient resistance properties in the interior. Transparent oil surface finishes also have their negatives, such as low light fastness, lower hardness and lower abrasion resistance of the coating films. To improve the appearance of oil coating films, their mechanical and resistance properties, various additives are added to coating materials (CHENG *et al.*, 2020). Improvement of the mechanical properties of the coating film is achieved, for example, by adding waxes to the coating material. The quality of the surface finish is determined not only by the properties of the coating material, but also by the nature of substrate, especially its surface properties.

Surface properties of the substrate to be surface finished – roughness (PIERNIK *et al.*, 2023; ADAMČÍK *et al.*, 2023a; ZHU *et al.*, 2022; SMAJIC *et al.*, 2020;) wettability (JANKOWSKA *et al.*, 2021) and adhesion – are important characteristics. JOVANOVIĆ *et al.* (2020) dealt with the effect of different types of wood surface processing on surface roughness. Specifically, they investigated the roughness on beech wood and oak wood after surface processing by milling and grinding. KÚDELA *et al.* (2018) also dealt with a similar issue. They investigated the effect of wood surface processing by milling and grinding on surface morphology of beech wood and spruce wood. SLABEJOVÁ and MÓZA (2010) dealt with the influence of selected, water-dilutable coating materials on the final surface roughness of beech wood.

The aim of the work is to point out the roughness of oil-wax surface finishes on beech wood with a false heartwood in the situation if all recommended application procedures for surface finishing were not followed.

MATERIALS AND METHODS

Material

In the experimental tests, beech wood (*Fagus sylvatica* L.) originating from the Štiavnické vrchy mountains (Slovakia) was used. Test bodies with dimensions of 60 mm × 20 mm × 18 mm, without wood defects (bumps, cracks, etc.), were made of beech lumber.

Roughness was measured on test bodies with dimensions of 80 mm × 80 mm × 10 mm. They were made of beech wood with a false heartwood and conditioned at a temperature of 20 °C and a relative humidity of 60 % to a moisture content of 10 ± 1 %. Each test body contained a zone of mature wood and a zone of false heartwood. The bodies were grinded with an eccentric sander – Festool ETS 120, abrasive Rubin 2 with a diameter of 125 mm. The final sanding was done with P120 grit sandpaper on one set of test bodies; and with P150 grit sandpaper on the other set.

Coating materials

Two representative coating materials based on vegetable oils and waxes, suitable for interior use, were used to final treatment of the wood surface.

- Surface finish Wax-oil Original (acronym WOO) – hard waxy oil with a high content of solids, based on natural oils and waxes. It is applied with a brush or a roller in two thin layers. The dry matter content in the coating material is 50 % (URL1).
- Surface finish Wax-oil Naturalis (acronym WON) – hard waxy oil, composed of a mixture of hard waxy oil, siccative and solvent. Hard waxy oil can be applied using a brush or a roller in thin layers to already oiled surfaces. After 30 minutes, it is necessary to wipe

the remains of unabsorbed oil from the surface. The dry matter content in the coating material is 80 % (URL2).

Coating materials were applied using a brush according to the recommendations in the technical sheets. The exact spread of the coating materials was measured by the weighting method using laboratory scales KERN 573/DS with an accuracy of 0.01 g (see Table 1). The entire applied amount of the coating material was intentionally left on the surface; after 30 min, the unabsorbed coating material was not wiped off.

Table 1 Average spread of the coating materials immediately after application and subsequently after hardening

Surface finish	1 st coat [g]		2 nd coat [g]		Sum of coats [g]
	After application	After hardening	After application	After hardening	After hardening
WOO-P120	0.49	0.18	0.37	0.23	0.41
WOO-P150	0.38	0.17	0.30	0.21	0.38
WON-P120	0.29	0.19	0.56	0.48	0.67
WON-P150	0.21	0.19	0.49	0.43	0.61

Note: WOO, WON – surface finishes; P120, P150 – final sanding

The surface finishes were cured for 24 hours in laboratory conditions – the temperature $20\text{ }^{\circ}\text{C} \pm 2\text{ }^{\circ}\text{C}$ and relative humidity $60\text{ } \% \pm 5\text{ } \%$. After 24 hours, the second coat was applied and cured under the same conditions for 76 hours. After the coatings had hardened, the surface finishes were visually evaluated according to STN 91 0272: 1992. The following defects were monitored: orange peel, hardened impurities, craters and bubbles.

Defects were assessed visually with the naked eye from a distance of 250 – 750 mm at an angle of $0 - 90^{\circ}$ in daylight. For each defect, the incidence (Table 2) and size (Table 3) were evaluated.

Table 2 Evaluation scale for the occurrences of defects "M"

Grade	Density of defects; Affected area of the total surface of the sample (%)
1	$\leq 0.03\text{ } \%$
2	$\leq 1\text{ } \%$
3	$< 2\text{ } \%$
4	$< 5\text{ } \%$
5	$< 25\text{ } \%$

Table 3 Evaluation scale for size of defects "G"

Grade	Type of defect	Size of defect
1	Microscopic	Only visible at $7 - 10\times$ magnification
2	Tiny	Visible by eye
3	Clearly visible	The largest dimension $0.5 - 1.0\text{ mm}$
4	Visible very well	The largest dimension $1.0 - 3.0\text{ mm}$
5	Size of defect up to 1 cm	The largest dimension $3.0 - 10.0\text{ mm}$

Surface roughness before and after surface treatment

Surface roughness was measured using a VHX-7000 digital microscope (Keyence Corporation, Osaka, Japan). It is a non-contact optical method for surface observation using incident and reflected light. The main part of the microscope is a 100× to 1000× zoom lens connected to a VHX-7020 camera (Keyence Corporation, Osaka, Japan), placed on an observation stand. The lens and camera are connected to the observation stand by a motorized part, enabling movement along the Z axis. The device also includes an eccentric motorized stage and a main unit with a UHD LCD monitor.

The first roughness measurement was carried out on beech wood processed by final eccentric sanding with a Festool ETS 125 REQ-PLUS sander (Festool Group GmbH & Co. KG, Wendlingen, Germany) with sanding disc with grit size P120 or P150 type Rubin 2 (Festool Group GmbH & Co. KG, Wendlingen, Germany) before surface finishing. The surface of the samples was scanned using a digital microscope and converted into a 3D image. Scanning was performed on each sample in the mature wood zone and in the false heartwood zone (they were visually recognized). The size of the scanned surface was 20 mm × 20 mm at 100× magnification.

The roughness measurement was performed on the scanned 3D surface without surface finish. According to the ISO 21920-3 (2022) standard, values were set for the traverse length ($L_t = 17.5$ mm), which consisted of the pre-travel (run-up; $L_p = 2.5$ mm) and post-travel (over-travel; $L_p = 2.5$ mm) and the evaluated length ($L_e = 12.5$ mm). The evaluated length L_e consisted of five section lengths ($L_{sc} = \lambda_c$ (cutoff) = 2.5 mm).

The following roughness parameters were recorded and subsequently evaluated:

- R_a (arithmetic mean height),
- R_z (maximum height).

The descriptions of these roughness parameters are taken from the VHX-7000 digital microscope operating manual (Keyence Corporation, Osaka, Japan) and from currently valid technical standards.

The second roughness measurement was performed after the application and curing of the tested surface finishes.

Parameters R_a and R_z were evaluated using the software STATISTICA 12 (StatSoft, Tulsa, Oklahoma).

RESULTS AND DISCUSSION

After the coating films had hardened, the defects that could affect the roughness of the surface were visually evaluated (according to the tables 2 and 3 listed in the methodology – occurrence of defects "M" and size of defects "G"). Table 4 shows the evaluation of the defects on all surface finishes.

Table 4 Evaluation of defects on surface finishes

Surface finish	Defect							
	Orange peel		Hardened impurities		Craters		Bubbles	
	M	G	M	G	M	G	M	G
WOO	1	1	2	2	1	1	1	1
WON	5	5	2	2	1	1	1	1

On the surface finish WOO, very fine hardened impurities were visible to the naked eye – bristles from the brush used to apply the coating material (Fig. 1a). In addition to hardened impurities, the surface finish WON also contained orange peel (Fig. 1b), which significantly affected the overall surface roughness. We assume that the orange peel occurred as a result of not removing the unabsorbed coating material.

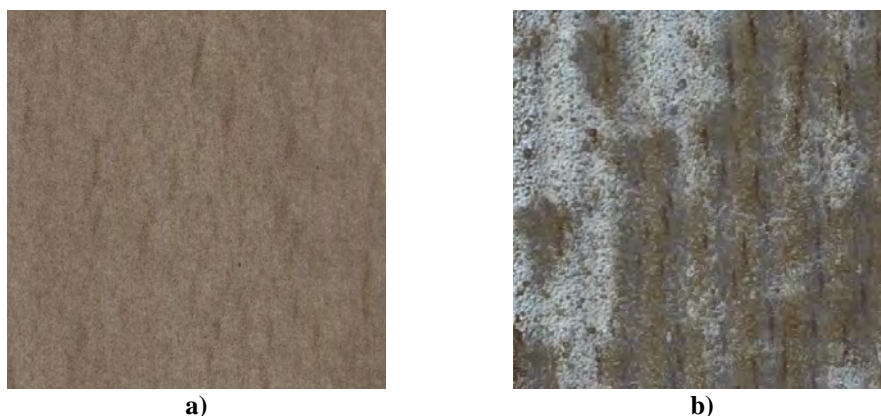


Fig. 1 Scanned area of the surface finish (20 mm × 20 mm): a) Wax-oil original, b) Wax-oil naturalis.

Surface roughness

Table 5 of the descriptive statistics lists arithmetic means, standard deviations and confidence intervals for roughness parameters R_a , R_z measured after eccentric grinding. The last sandpapers used were P120 or P150. Values were measured separately in the zone of false heartwood and in the zone of mature wood, in the directions perpendicular to the wood grain and along the grain.

Results (Tables 5 and 6) show a reduction in the surface roughness after the last sanding with sandpaper P150 compared to sanding with sandpaper P120. The values of the R_a parameter after the last sanding with P150 were lower in the zone of mature wood than in false heartwood, both in the direction perpendicular to the wood grain and along the grain. After sanding with P120, mature wood showed a higher roughness in both directions compared to false heartwood in both directions, but this difference was smaller when compared to sanding with P150.

Tables 7–10, which present the 95 % confidence intervals for the average values of R_a and R_z , show that the surface roughness of beech wood was lower in the direction along the wood grain than in the direction perpendicular to the grain, both in mature wood and in false heartwood. Beech wood surfaces showed lower roughness and improved surface quality after final sanding with P150 sandpaper compared to P120 sanding. Only on false heartwood in the direction perpendicular to the wood grain, there was a statistically insignificant difference in the roughness between the surfaces P120 and P150. The roughness reached statistically significantly higher values in the zone of mature wood compared to false heartwood; however, this difference was not statistically significant in the direction perpendicular to the wood grain after sanding P150.

Table 5 Roughness parameter R_a after grinding before surface finishing: arithmetic mean, standard deviation (SD) and 95 % confidence interval (n = 450)

Sandpaper	Zone	Direction of measurement relative to the wood grain	R_a Mean	R_a SD	R_a -95.00 %	R_a +95.00 %
P120	FH	perpendicular	3.57	0.76	3.50	3.64
P120	FH	along	3.14	0.49	3.10	3.19
P120	MW	perpendicular	3.70	0.79	3.63	3.77
P120	MW	along	3.36	0.57	3.30	3.41
P150	FH	perpendicular	3.50	0.80	3.42	3.57
P150	FH	along	3.03	0.50	2.99	3.08
P150	MW	perpendicular	3.52	0.78	3.45	3.59
P150	MW	along	3.15	0.60	3.09	3.21

Note: MW – mature wood, FH – false heartwood

Table 6 Roughness parameter R_z after grinding before surface finishing: arithmetic mean, standard deviation (SD) and 95 % confidence interval (n = 450)

Sandpaper	Zone	Direction of measurement relative to the wood grain	R_z Mean	R_z SD	R_z -95.00 %	R_z +95.00 %
P120	FH	perpendicular	16.96	3.00	16.68	17.24
P120	FH	along	14.60	2.18	14.40	14.80
P120	MW	perpendicular	17.88	3.36	17.57	18.19
P120	MW	along	15.66	2.69	15.41	15.91
P150	FH	perpendicular	16.12	3.10	15.83	16.40
P150	FH	along	13.58	2.15	13.38	13.78
P150	MW	perpendicular	16.42	3.26	16.12	16.73
P150	MW	along	14.28	2.82	14.02	14.54

Note: MW – mature wood, FH – false heartwood

Table 7 t-test for the surface finish Wax-oil original on false heartwood

Variables	Mean	SD	N	Difference	t	sv	p	-95.000 %	+95.000 %
R_a – before SF	3.32	0.72	-	-	-	-	-	-	-
R_a – after SF	2.82	0.63	360	0.50	10.53	359	0.000	0.41	0.60
R_z – before SF	15.40	3.17	-	-	-	-	-	-	-
R_z – after SF	13.52	2.51	360	1.87	9.95	359	0.000	1.50	2.24

Note: SF – surface finishing

Table 8 t-test for the surface finish Wax-oil original on mature wood

Variables	Mean	SD	N	Difference	t	sv	p	-95.000 %	+95.000 %
R_a – before SF	3.41	0.73	-	-	-	-	-	-	-
R_a – after SF	2.90	0.63	360	0.51	10.82	359	0.000	0.41	0.60
R_z – before SF	15.81	3.33	-	-	-	-	-	-	-
R_z – after SF	13.82	2.41	360	1.99	10.43	359	0.000	1.62	2.37

Note: SF – surface finishing

Table 9 t-test for the surface finish Wax-oil naturalis on false heartwood

Variables	Mean	SD	N	Difference	t	sv	p	-95.000 %	+95.000 %
R_a – before SF	3.28	0.66	-	-	-	-	-	-	-
R_a – after SF	5.13	1.22	360	-1.85	-26.82	359	0.000	-1.99	-1.72
R_z – before SF	15.13	2.93	-	-	-	-	-	-	-
R_z – after SF	29.40	8.10	360	-14.27	-32.80	359	0.000	-15.13	-13.41

Note: SF – surface finishing

Table 10 t-test for the surface finish Wax-oil naturalis on mature wood

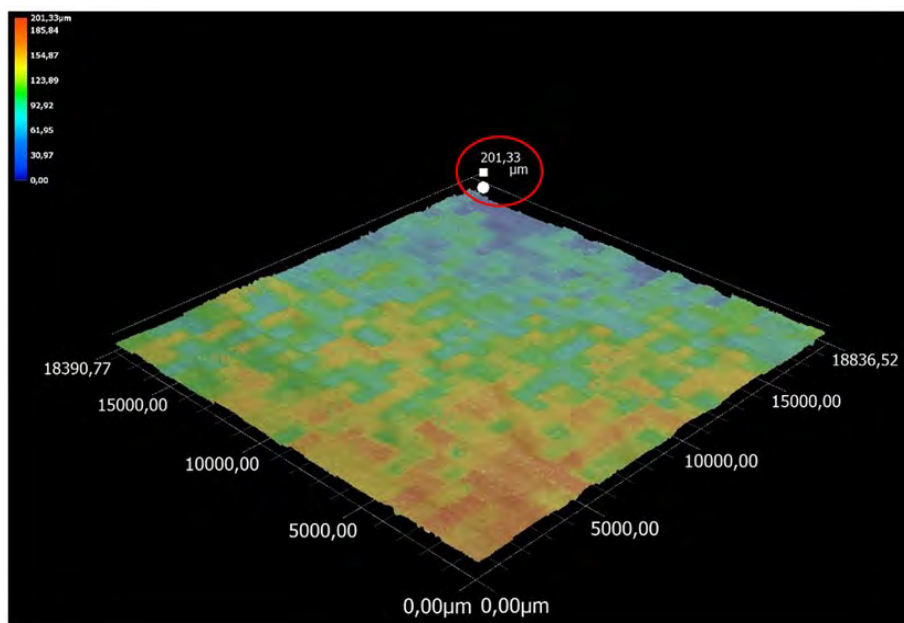
Variables	Mean	SD	N	Difference	t	sv	p	-95.000 %	+95.000 %
R_a – before SF	3.40	0.73	-	-	-	-	-	-	-
R_a – after SF	4.72	1.13	360	-1.32	-18.12	359	0.000	-1.46	-1.17
R_z – before SF	15.96	3.70	-	-	-	-	-	-	-
R_z – after SF	25.60	7.00	360	-9.64	-22.41	359	0.000	-10.49	-8.80

Note: SF – surface finishing

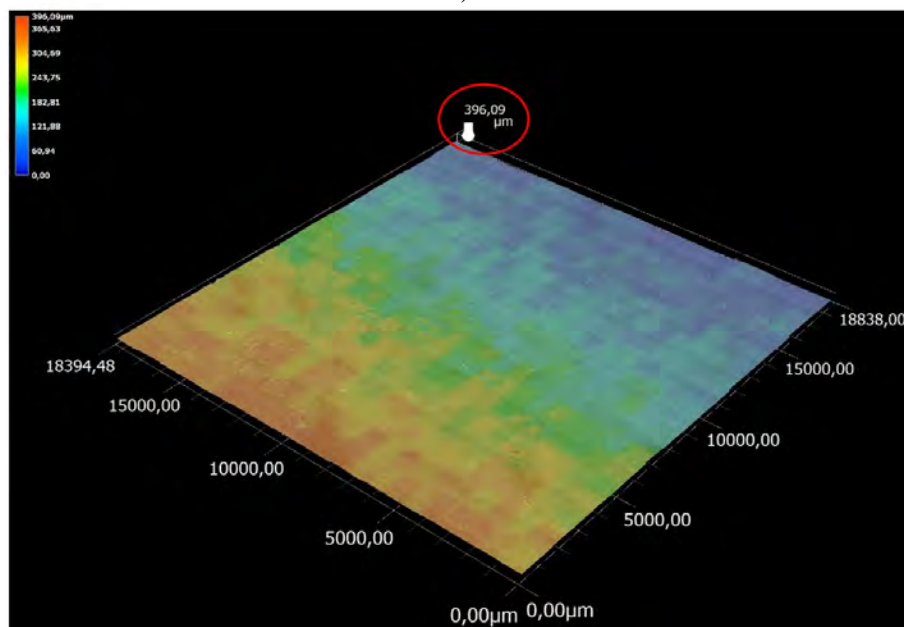
In the direction perpendicular to the wood grain, the surface roughness of beech wood was higher than the surface roughness in the longitudinal direction. This is in accordance with the literature (ADAMČÍK *et al.*, 2023b; KÚDELA *et al.*, 2020; GURAU and IRLE, 2019; KÚDELA *et al.*, 2018; KILIC *et al.*, 2006).

As mentioned in the methodology, the surfaces of beech wood were scanned using a digital microscope and converted into a 3D image. Figures 2 and 3 show the 3D images of the surfaces of beech wood without surface finish, after eccentric sanding P120 and P150, in the zone of mature wood and false heartwood, at a zoom of 200×. The circled values on the images indicate the heights of the highest protrusions in μm . We can also see that there was a slope on the individual beech bodies after operating the sander (manually). That is, one side of the bodies was sanded more than the other side, which would ultimately distort the values of R-parameters (Fig. 2 and 3). Also for this reason, a slope correction was performed on the samples before translating and evaluating the roughness profiles.

At visual evaluation of the surface finishes, a large occurrence of surface irregularities (orange peel) was detected on the wax-oil naturalis surface finish. For this very reason, the roughness of the surface of beech wood was higher after surface finishing than before it. When compared to unfinished bodies, the average value of the R_a parameter after surface finishing was 1.85 μm higher in the false heartwood zone (table 9) and 1.32 μm higher in the mature wood zone (table 10). The appearance of orange peel on surfaces with wax-oil naturalis caused that the surface roughness is higher when compared to the surfaces with no surface finish both after eccentric grinding P120 and P150.



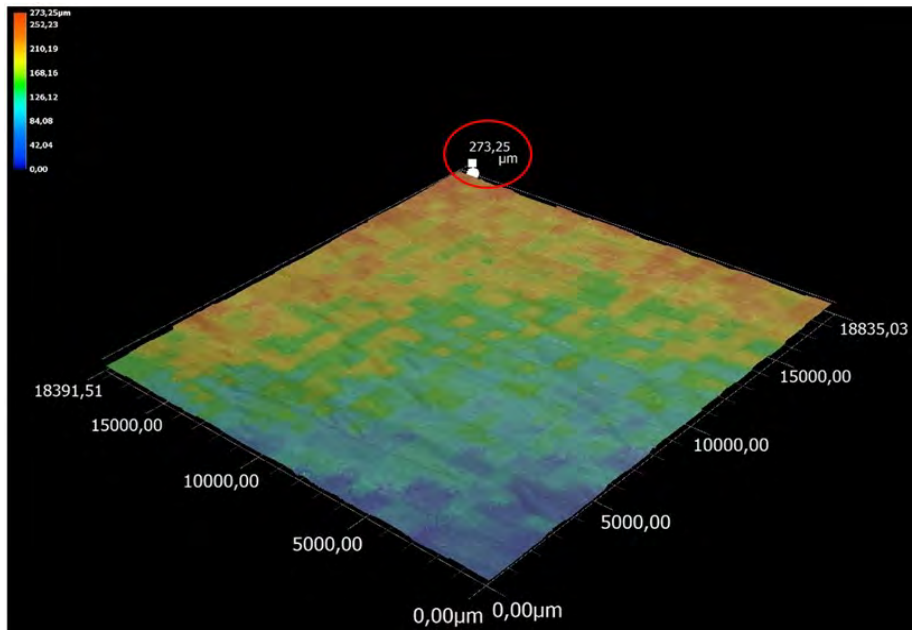
a)



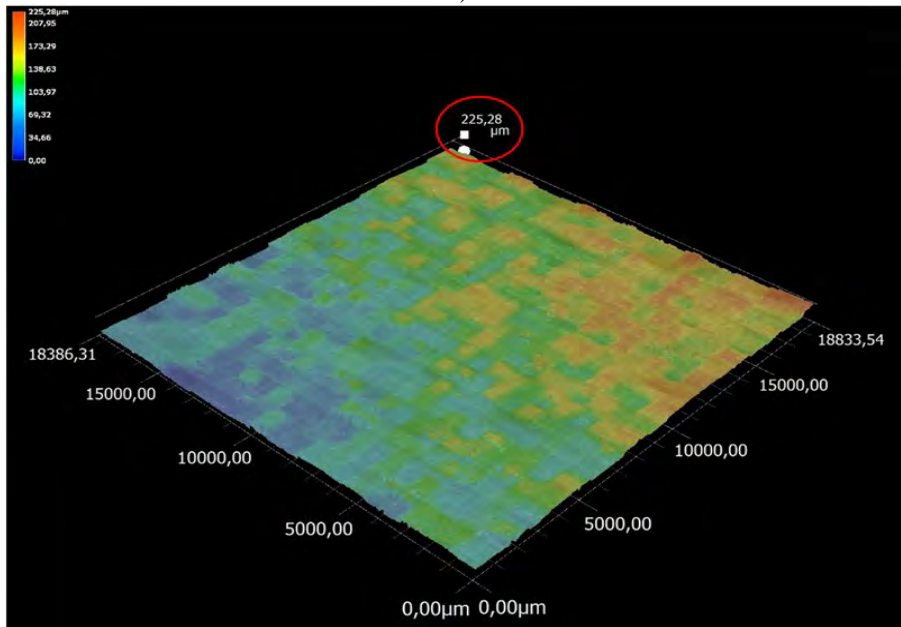
b)

Fig. 2 3D image of surface roughness of beech wood after sanding P120; a) false heartwood, b) mature wood.

Note: Without slope correction.



a)



b)

Fig. 3 3D image of surface roughness of beech wood after sanding P150; a) false heartwood, b) mature wood.

Note: Without slope correction.

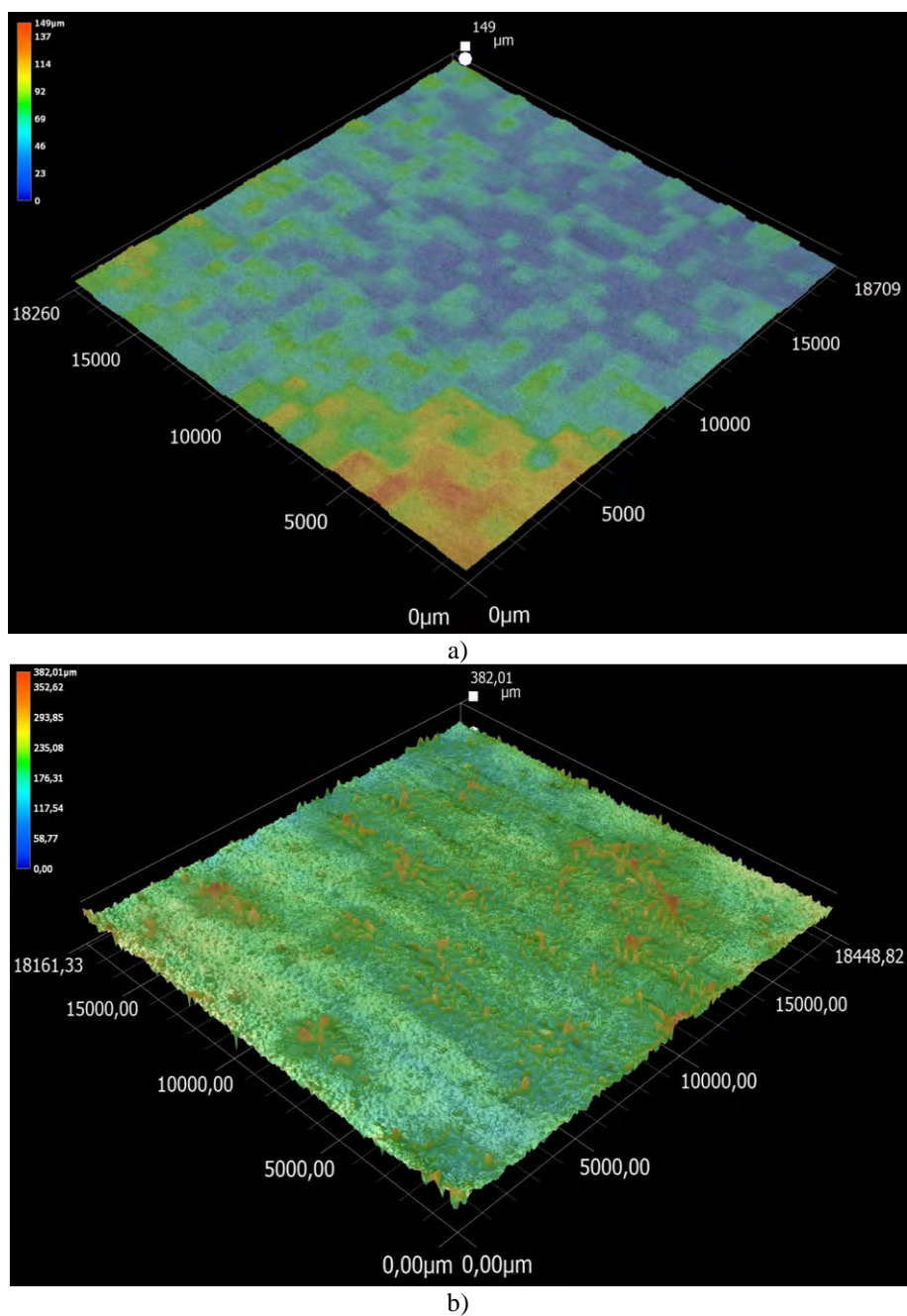


Fig. 4 3D image of surface roughness of mature wood after sanding P150, surface finished with: a) Wax-oil original, b) Wax-oil naturalis

Note: With slope correction.

The 3D image of the surface of mature wood with Wax-oil naturalis surface finish (Fig. 4b) shows how the occurrence of orange peel affected the roughness of the surface. While with the Wax-oil original surface finish (Fig. 4a), the height of the highest protrusion on the surface was around 150 μm , in the case of Wax-oil naturalis surface finish, the height reached the value of 382.01 μm . At the same time, the height of the highest protrusion on the surface after Wax-oil naturalis surface finishing was even higher than on unfinished bodies after sanding P120 in the zone of false heartwood and after sanding P150 in both zones (false heartwood and mature wood). The reduction of the surface roughness of beech wood after surface finishing was also confirmed by SLABEJOVÁ and MÓZA (2010) and RUŽINSKÁ (2006). In addition to the effect of surface finish and surface treatment, they also investigated the effect of the number of coats on surface roughness. It follows that, if the recommendations of the technological procedure for applying coating materials are followed, the surface finishes reduce the roughness of the surface.

CONCLUSIONS

The aim of the work was to determine the effect of sanding with P120 and P150 sandpapers on the surface roughness in the zones of mature wood and false heartwood. At the same time, the goal was to determine the effect of transparent oil-wax coating materials on the surface roughness of beech wood in the zone of mature wood and false heartwood when the principles of the application procedure were not followed. Based on the experiments and the evaluation of measured values, the following conclusions were reached:

- The surface of beech wood sanded with an eccentric sander showed a lower roughness when using sandpaper P150 compared to P120 in the zone of mature wood and false heartwood both perpendicularly to the wood grain and along the grain.
- In the direction perpendicular to the wood grain, the surface roughness of beech wood was higher than the roughness in the longitudinal direction.
- The surface roughness of beech wood reached was higher in the mature wood zone compared to the false heartwood zone.
- Oil-wax surface finishes reduced the surface roughness of beech wood if the principles of the technological procedure of applying coating materials were followed. If the principles are not followed, there is a high probability of defects in the coating film and this results in an increase in the surface roughness.

Acknowledgment

The authors express their gratitude to the Slovak Research and Development Agency, project no. APVV-21-0051.

REFERENCES

- ADAMČÍK, L., DZURENDA, L., BANSKI, A., KMINIAK, R. 2023a. Comparison of Surface Roughness of Beech Wood after Sanding with an Eccentric and Belt Sander. *Forests*, 15(1), 45.
- ADAMČÍK, L., KMINIAK, R., SCHMIDTOVÁ, J. 2023b. Measurement of the Roughness of the Sanded Surface of Beech Wood with the Profile Measurement Software of the Keyence VHX-7000 Microscope. *Acta Facultatis Xylogologiae Zvolen*, 65(1), 73-86.
- ARMINGER, B., JAXEL, J., BACHER, M., GINDL-ALTMUTTER, W., HANSMANN, C. 2020. On the drying behavior of natural oils used for solid wood finishing. *Progress in Organic Coatings*, 148, 105831.

- DZURENDA, L., DUDIAK, M., KUČEROVÁ, V. 2023. Differences in Some Physical and Chemical Properties of Beechwood with False Heartwood, Mature Wood and Sapwood. *Forests*, 14(6), 1123.
- GURAU, L., IRLE, M. 2019. Buchner, J. The surface roughness of heat treated and untreated beech (*Fagus sylvatica* l.) wood after sanding. *BioResources* 2019, 14, 4512–4531.
- CHENG, L., REN, S., LU, X. 2020. Application of eco-friendly waterborne polyurethane composite coating incorporated with nano cellulose crystalline and silver nano particles on wood antibacterial board. *Polymers*, 12(2), 407.
- JANKOWSKA, A., KOZAKIEWICZ, P., ZBIĘC, M. 2021. The Effects of Slicing Parameters on Surface Quality of European Beech Wood. *Drvna industrija*, 72(1), 57-63.
- JOVANOVIĆ, J., SMAJIĆ, S., BELJO LUČIĆ, R. 2020. Influence of different machining on the surface roughness of beech wood samples. In 13th International Scientific Conference WoodEMA 2020 and 31st International Scientific Conference ICWST 2020: Sustainability of Forest-Based Industries in the Global Economy (pp. 355-360)
- KILIC, M., HIZIROGLU, S., BURDURLU, E. 2006. Effect of machining on surface roughness of wood. *Building and environment*, 41(8), 1074-1078.
- KÚDELA, J., LAGAÑA, R., ANDOR, T., CSIHA, C. 2020. Variations in beech wood surface performance associated with prolonged heat treatment at 200 C. *Acta Facultatis Xylogologiae Zvolen res Publica Slovaca*, 62(1), 5-17.
- KÚDELA, J., MRENICA, L. JAVOREK, L. 2018. The influence of milling and sanding on wood surface morphology. *Acta Facultatis - Xylogologiae. Zvolen: Technická univerzita vo Zvolene*, 2018. Dostupné z: doi:10.17423/afx.2018.60.1.08
- MICHALEC, K., WASIK, R., GACH, M. 2022. The occurrence and size of false heartwood in beech timber. *Drewno. Prace Naukowe. Doniesienia. Komunikaty*, 65(209).
- PIERNIK, M., PINKOWSKI, G., KRAUSS, A. 2023. Effect of chip thickness, wood cross-sections, and cutting speed on surface roughness and cutting power during up-milling of beech wood. *BioResources*, 18(4), 6784.
- RUŽINSKÁ, E. 2006. Štúdium povrchových vlastností po aplikácii náterových látok na báze olejov a voskov: Zborník príspevkov z 37. medzin. konferencie "Coats and coatings technology". Univerzita Pardubice, 2006.
- SLABEJOVÁ, G., MÓZA, M. 2010. Vplyv vybraných faktorov na drsnosť povrchu dreva upraveného vodou riediteľnými náterovými látkami. *Acta Facultatis - Xylogologiae. Zvolen: Technická univerzita vo Zvolene*, 2010. ISSN 1336-3824.
- SMAJIC, S., JOVANOVIC, J., LUCIC, R. B. 202. Effect of Different Processing on the Roughness of Oak and Beech Wood. *DAAAM International Scientific Book*, 18, 217-226.
- STN 91 0272: 1992. Furniture. Testing furniture finishes. Evaluation of appearance properties. „Nábytok. Skúšanie povrchovej úpravy nábytku. Hodnotenie vzhľadových vlastností.“ Slovak Office of Standards, Metrology and Testing: Bratislava, Slovakia, 1992.
- URL1: <https://www.osmocolor.sk/p/447/osmo-tvrdy-voskovy-olej-original> [09.03.2024]
- URL2: https://www.renojva.sk/naturalis-oils-tvrdy-voskovy-olej?gloss_degree= [09.03.2024]
- VIDHOLDOVÁ Z, SLABEJOVÁ G, ŠMIDRIAKOVÁ M. 2021. Quality of Oil- and Wax-Based Surface Finishes on Thermally Modified Oak Wood. *Coatings*. 2021; 11(2):143. <https://doi.org/10.3390/coatings11020143>
- ZHU, Z., JIN, D., WU, Z., XU, W., YU, Y., GUO, X., WANG, X. 2022. Assessment of surface roughness in milling of beech using a response surface methodology and an adaptive network-based fuzzy inference system. *Machines*, 10(7), 567.
- YAREMCHUK, L., HOGABOAM, L., SLABEJOVÁ, G., SEDLIAČIK, J. 2023. Comparative Analysis of the Quality Properties of Oil-Based and Alkyd Coating Materials for Wood. *Acta Facultatis Xylogologiae Zvolen*, 65(1), 63-72.
- YAREMCHUK, L., OLYANYSHEN, T., HOGABOAM, L. 2016. Selection of coating materials for wood finishing based on a hierarchical analysis method of their technological, economic and ecological criteria. *International Journal of Energy Technology and Policy*, 12(3), 295-311.



IDENTIFICATION OF THE WORKPIECE MATERIAL BASED ON THE OF SIGNALS FROM THE CUTTING ZONE

Krzysztof Szwejka¹ – Joanna Zielińska-Szwejka²

Abstract

The fact is that hundreds of holes are drilled in the assembly process of furniture sets, so intelligent drilling is a key element in maximizing efficiency. Increasing the feed or cutting speed in materials with a higher machinability index is necessary. Smart drilling, i.e. real-time adjustment of cutting parameters, requires the evolution of cutting process variables. In addition, it is necessary to create and manage a database, process data and adjust processing parameters in real time. The article proposes methods for identifying the material in the drilling process in order to automatically adjust cutting parameters during machining based on force signals, cutting torque and acceleration signals. The results obtained during the tests showed that the selected signal measures in the time and frequency domain are constant for a given workpiece material and do not depend on the cutting parameters.

Key words: *drilling, cutting resistance, workpiece identification, STFT, permutation entropy*

INTRODUCTION

The hybrid structure of wood-based materials has become essential in building structures for economic and environmental reasons, as it allows maintaining good mechanical properties. Due to the different materials combined with each other, which have significantly different machinability, the cutting data must be changed during machining to enable this optimization. In the past, the procedure of optimizing cutting parameters was omitted in the production process. Currently, with the rapid development of Industry 4.0, real-time identification of parameters becomes necessary to improve the process in industrial reality [1, 2, 3]. Smart factories are a key feature of Industry 4.0. Industry 4.0 focuses on creating intelligent products, processes and procedures with an emphasis on sustainable development [4]. The essence of the process is comprehensive factory management, which allows for the reduction of erroneous factors. In such an environment, there is more efficient production and communication between people, machines and resources, in accordance with the principles of a social network. In Industry 4.0, it is assumed that standard jobs will be replaced by artificial intelligence (AI) or robots.

The enormous and continuous increase in the possibilities of using computers since the early 1990s and the simultaneous decline in their prices have resulted in more and more

¹ Department of Integrated Design and Tribology Systems, Faculty of Mechanics and Technology, Rzeszow University of Technology, ul. Kwiatkowskiego 4, 37-450 Stalowa Wola, Poland

² Department of Component Manufacturing and Production Organization, Faculty of Mechanics and Technology, Rzeszow University of Technology, ul. Kwiatkowskiego 4, 37-450 Stalowa Wola, Poland
e-mail: kszwejka@prz.edu.pl, j.zielinska@prz.edu.pl

manufacturers using IT techniques to control production in all phases of the production process.

There are many ways to process chipboard [6], so the machinability of these materials can be tested in many ways. Nevertheless, the machinability of any type of chipboard when drilled is one of the most important issues from a practical point of view. This general belief can be proven in many ways, but it seems that two basic arguments suffice. Firstly, resistance to axial screw removal is one of the most important technical parameters characterizing chipboards. This resistance should be determined experimentally in accordance with the detailed standard [7]. The experimental procedure requires drilling an appropriate hole in order to install the screw, which is why drilling is a very basic form of chipboard processing.

MATERIL AND METHODS

In the tests, four types of wood-based materials were used as the processed material: Medium-Density Fiberboard (MDF), chipboard, plywood and High Pressure Laminate (HPL). Figure 1 shows the materials processed during the tests. The first three materials belong to the group of materials most frequently used in the furniture industry. HPL, on the other hand, is a specially pressed plastic which, thanks to its high density and hardness, is very resistant to damage. The HPL board is characterized by a durable coating, resistant to fading and mechanical damage. This, in turn, makes it suitable for a wide range of applications in the finishing and furniture industries. Before starting the basic research, measurements of selected mechanical and physical properties of the processed materials were carried out. The density of the HPL board was measured in accordance with the ISO 1183-1:2019 standard for other materials in accordance with the EN 622-5 standard. Mechanical properties for HPL were determined in accordance with the EN ISO 178 standard. For other materials, in accordance with the EN 310 standard.



Figure 1. Cutting material.

The structure of the processed materials differs from each other. Figure 2 shows different arrangement of the structure and different density, which translates into, among other things, the hardness of the material. The HPL board is characterized by a uniform arrangement of layers, improving the properties of the material. In the case of plywood, you can notice layers of varying degrees of density. MDF board has a medium density structure. Due to the way it is made, chipboard has an irregular structure. The tests used a typical cutting tool intended for wood-based materials, a single-edge drill with a diameter of 10 mm with Polycrystalline Diamond (PCD) blades from Leitz® Diamaster PRO. The drill marking is: DP/D10/NL30/S10x27/GL70/RL. This drill is used in processing materials such as: wood, chipboards, resin boards, plastics, reinforced plastics.

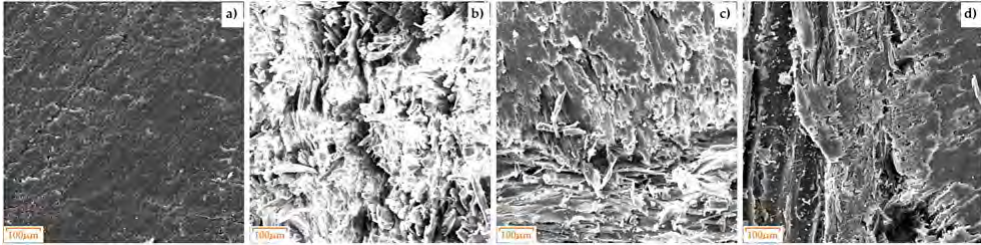


Figure 2. Cutting material SEM: (a) HPL; (b) MDF; (c) Chipboard; (d) Plywood.

As part of the research, holes were drilled on a CNC milling machine in prepared samples cut from processed materials with dimensions of $130 \times 30 \times 18$ mm (Fig. 1). Except for the HPL board, which was 10 mm thick. The acceleration signal value in three mutually perpendicular directions was measured using a KISTLER® 8763B piezoelectric acceleration sensor, which was mounted on the workpiece. The axial force (F_t) and cutting torque (M_s) signals were measured using a KISTLER® 9345B sensor. The acoustic emission signal was measured using a KISTLER® 8152C sensor. Signals from the sensors were recorded on the hard drive of a personal computer (PC) in digital form via a National Instruments® 6034E analog-to-digital card. The sampling frequency of signals during the experiments was 50 kHz, and the measurement resolution of the card was 16 bits. Table 1 lists the cutting parameters used during drilling experiments. Three repetitions were performed for each set of cutting parameters.

Table 1. Machining conditions.

Cutting speed (m/min)	Feed per tooth (mm)	Feed speed (mm/min)	Rotational speed of tool (rev/min)
78	0.15	375	2500
	0.20	450	
	0.25	525	
94	0.15	500	3000
	0.20	600	
	0.25	700	
109	0.15	625	3500
	0.20	750	
	0.25	875	

RESULTS AND DISCUSSION

The acceleration signal was measured in both the transverse (X), (Y) and axial (Z) directions. Acceleration signals on the analyzed directions contain information regarding:

(a) The vibrating length of the drill in the transverse and axial directions does not change during the drilling process, thus maintaining a rather constant frequency.

(b) Natural frequencies in the lateral and axial directions of the CNS during drilling are essentially insensitive to drill diameter, simplifying monitoring for a wide range of drill sizes.

(c) The vibration in the X, Y, and Z directions is influenced by torque and axial force, which are the main sources of excitation during drilling. Figure 3 shows typical signals in the time domain in the X and Y (lateral) and Z (vertical) directions, respectively, in one time interval, recorded for the selected sample.

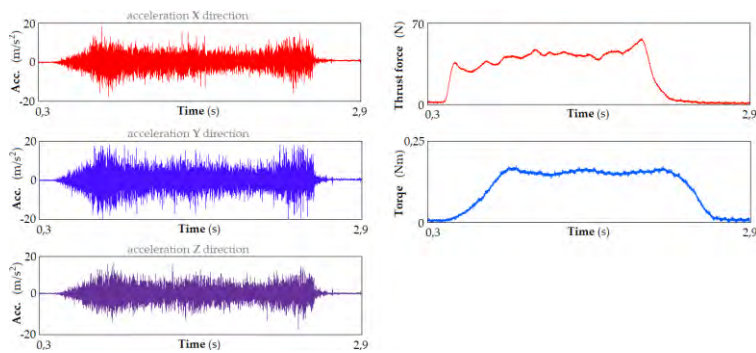


Figure 3. Vibration and thrust force signal.

Drilling was carried out with a spindle speed of $n = 3000$ rpm, a feed rate of $v_f = 750$ mm/min, and a drill diameter of 10 mm. As can be seen, the vibration signals can be characterized as consisting of short high-low frequency oscillatory transients occurring randomly over the duration until one hole is drilled. With the density of the material being cut, the amplitude of these signals begins to increase. Excitation of the CNS in the drilling process at a frequency independent of cutting conditions, such as feed and speed. By far the majority of vibration signals consist of frequency components related to the dynamics of the cutting system.

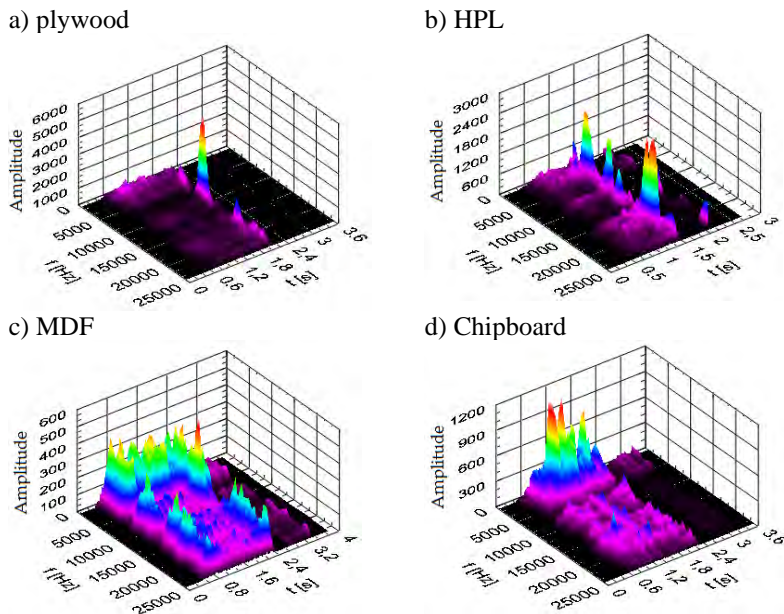


Figure 4. Spectrogram of the vibration signal in the X direction.

Figure 4 shows examples of the power spectra of vibration signals generated in the X direction during drilling in various types of workpiece materials. The cutting parameters are $n=3000$ rpm, $v_f=750$ mm/min. As shown in the figures, the maximum amplitude of the vibration signal in the frequency range varies in the range from 2-22 kHz depending on the type of material being processed. Figure 4 shows the effect of

the workpiece material on the vibration power spectra. It can be seen that when drilling into plywood, the power spectrum has characteristic increases in amplitude at frequencies around 10 kHz in the X direction. When drilling into HPL, the power spectrum has characteristic increases in amplitude at frequencies around 19 kHz in the X direction. When drilling into MDF material, the power spectrum has characteristic increases in amplitude at frequencies of about 10 kHz in the X direction. When drilling in a chipboard, the power spectrum has characteristic increases in amplitude at frequencies of about 2.5 kHz in the conclude that there is a significant impact of the processed material on the dominant frequency range in the signal. It can also be observed that there is a correlation between the hardness of the workpiece material and the dominant frequency range in the vibration signal. For example, for the HPL material, the value of the dominant frequency is approximately 19 kHz (material with the highest hardness) and for chipboard it is approximately 2.5 kHz (material with the lowest hardness).

PermEn for force signals (F_t) for the processed materials was calculated in a window of 1000 elements, moved by a step of 200. Changing the signal frequency affects the obtained permutation entropy values, it increases linearly with the increase in the signal frequency. *PermEn* is very sensitive to adding noise of different strengths. To eliminate the effects of unexpected noise in the signal, filters are used to process the signal's feature values before applying it to detect the change in workpiece material in the drilling process.

Figure 5 shows the thrust force signal and its permutation entropy H_p . The H_p permutation entropy values are low for materials with a homogeneous structure under normal cutting conditions because the force signal is similar to a regular periodic signal.

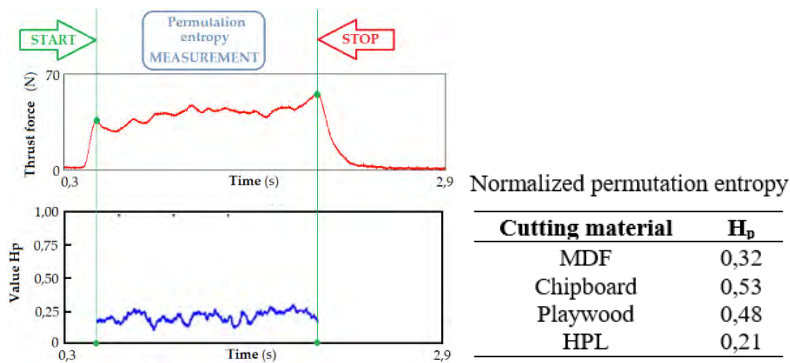


Figure 5. Thrust force signal and its permutation entropy H_p .

However, the force signals (F_t) have different waveforms due to various effects, including: different material density, hardness, friction coefficients in different positions. The H_p values changed within relatively small limits in the drilling processes of the tested workpiece materials. Table 2 shows the change in H_p values for the processed materials. The results show that the permutation entropy of force signals (F_t) can be applicable and indicate material change in the drilling process.

CONCLUSIONS

1. Identification of the material being processed during the drilling process is possible based on both force (F_c) and cutting torque (M_c) and acceleration (Acc.) signals.
2. Identification based on the signal of force and cutting torque is based on the value of the unit cutting resistance ($k_{c1.1}$) and on the basis of the change in the value of permutation entropy (H_p).
3. Identification based on STFT analysis of acceleration signals in specific directions (X, Y, Z) uses the assessment of the dominant frequency amplitude depending on the material being processed. There is no need to know the signal history needed to identify the processed material.
5. Also, the described material identification based on changes in the permutation entropy (H_p) value of the force signal (F_c) during the process works reliably for all analyzed processed materials. This measure turned out to be insensitive to the combinations of drilling parameters used in the studies. The proposed method enables reliable detection of tool contact with the workpiece material and identification of the material during the drilling process.

REFERENCES

1. Szwajka, K.; Zielińska-Szwajka, J.; Trzepieciński, T. Experimental Analysis of Smart Drilling for the Furniture Industry in the Era of Industry 4.0. *Materials* 2024, 17, 2033.
2. Szwajka, K.; Zielińska-Szwajka, J.; Trzepieciński, T. The Use of a Radial Basis Function Neural Network and Fuzzy Modelling in the Assessment of Surface Roughness in the MDF Milling Process. *Materials* 2023, 16, 5292.
3. Zhu, J.; Wang, X. Research on enabling technologies and development path of intelligent manufacturing of wooden furniture. *J. For. Eng.* 2021, 6, 177–183.
4. Wenkler, E., Arnold, F., Hänel, A., Nestler, A., & Brosius, A. (2019). Intelligent characteristic value determination for cutting processes based on machine learning. *Procedia CIRP*, 79, 9-14.
5. Vrchota, J.; Řehoř, P.; Maříková, M.; Pech, M. Critical Success Factors of the Project Management in Relation to Industry 4.0 for Sustainability of Projects. *Sustainability* 2020, 13, 281.
6. Szwajka K., and Trzepieciński T. On the Machinability of Medium Density Fiberboard by Drilling. *BioResources* 2018, 13(4), pp. 8263-8278.
7. Brozzi, R.; Forti, D.; Rauch, E.; Matt, D.T. The Advantages of Industry 4.0 Applications for Sustainability: Results from a Sample of Manufacturing Companies. *Sustainability* 2020, 12, 3647.



COMPARISON OF KERF WIDTHS AFTER CO₂ LASER CUTTING OF WOOD-BASED MATERIALS

Lukáš Štefancin – Rastislav Igaz – Ivan Kubovský – Richard Kminiak

Abstract

This study evaluates the consistency of kerf widths in CO₂ laser cutting of various species of woods and wood-based materials: Beech Plywood, Pine Plywood, High-Density Fiberboard (HDF), Beech, Oak, and Spruce. Samples were cut using a 135W CO₂ laser at power levels of 40%, 60%, 80%, and 100%, and speeds of 5, 10, 15, and 20 mm/s. Kerf widths were measured using a high-resolution digital microscope. Results indicate that HDF exhibits the smallest and most uniform kerf widths, suggesting its homogeneous properties lead to more uniform and precise kerf. In contrast, natural woods like Spruce and Oak show larger and more variable kerf widths due to their heterogeneous nature. Statistical analysis confirms that more uniform materials, such as Plywood and HDF, yield more consistent kerf widths compared to natural woods.

Key words: *Laser cutting, Kerf variation, Kerf width, CO₂ laser, Wood, Processing*

INTRODUCTION

CO₂ laser cutting is widely used in the woodworking and manufacturing industries due to its precision and efficiency [1,2]. The process involves using a high-powered CO₂ laser beam to cut through various materials, including different types of wood and composite materials. One of the critical factors in laser cutting is the kerf width, which is the width of the material removed by the laser. The uniformity of the kerf width is essential for achieving high-quality cuts and minimizing material waste.

Wood and wood-based composites, such as plywood and high-density fiberboard (HDF), are commonly used materials in laser cutting applications. Each material has unique properties that can affect the cutting process. For instance, solid wood has a natural grain and varying density, which can lead to non-uniform cuts. In contrast, engineered wood products like plywood and HDF have more consistent properties due to their manufacturing process [3,4].

Previous studies have shown that factors such as wood density, moisture content, and grain orientation can influence the kerf width and its uniformity [5]. However, there is limited research on comparing the kerf width uniformity across different types of wood-based materials. Understanding these differences can help optimize material selection and laser cutting parameters, improving the efficiency and quality of the cutting process [6–8].

Research has focused on optimizing cutting parameters to improve quality and minimize defects. Factors influencing cut quality include laser power, cutting speed, material properties, and cutting direction [9,10]. Higher cutting speeds generally result in narrower

kerf widths [11]. The relationship between processing parameters and wood properties affects geometric accuracy, material removal rate, and burn severity [10]. Visual inspection and measurement of kerf width are common methods for quality assessment [11]. Recent studies have investigated the laser cutting quality of various wood species used in industrial manufacturing, considering factors such as kerf width, heat-affected zone, and cutting direction [12]. Optimization of cutting parameters can lead to significant improvements in part quality, ranging from 3% to over 30% [9].

This study hypothesizes that wood-based materials with more uniform anatomical properties exhibit more consistent kerf widths when cut with a CO2 laser. Specifically, it is proposed that materials like HDF, which are engineered to have uniform density and structure, will show less variation in kerf width compared to natural woods and plywood with more heterogeneous anatomical properties.

The primary objective of this research is to investigate the relationship between the anatomical uniformity of different wood-based materials and the consistency of their kerf widths when subjected to CO2 laser cutting. The study aims to compare the kerf width variability among various types of wood, including hardwoods, softwoods, and composite materials like plywood and HDF.

MATERIALS AND METHODS

The samples used in this study consisted of various types of wood and wood-based materials. All samples were standardized to dimensions of 500 mm in length, 70 mm in width, and 6 mm in thickness. The specific materials included Beech (*Fagus sylvatica* L.), oak (*Quercus petraea*), and spruce (*Picea Abies* L.), Beech plywood, Pine plywood and High-Density Fiberboard (HDF). All samples were acclimated for interior use, maintaining a moisture content of 8-10%.



Figure 1. Laser cutting setup

The samples were cut using a 135W CO2 laser cutter. The laser cutting parameters were varied systematically to investigate their effect on kerf width. The parameters included four different cutting speeds and four different power levels. All parameters are detailed in Table 1.

Table 1: Parameters used in the laser experiment

Parameter	Value
Power output [W]	54 (40%), 81 (60%), 108 (80%), 135 (100%)
Cutting speed [$\text{mm}\cdot\text{s}^{-1}$]	5, 10, 15, 20
Wavelength [μm]	10.6
Length of the cut [mm]	40
Focal length [mm]	50.8
Beam radius [mm]	0.15
Nozzle standoff distance [mm]	10
Assistant gas	Compressed air
Assistant gas pressure [bar]	0.35

The resulting cuts were digitalized and measured using a Keyence VHX-7000 digital microscope. This high-resolution microscope allowed for precise measurement of the kerf widths, providing accurate data for subsequent analysis. The kerf widths were measured at multiple points along each cut to assess the consistency and variability.

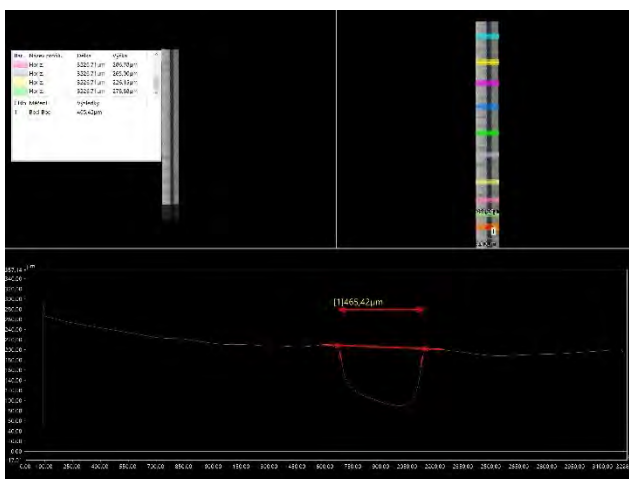


Figure 2: Kerf measuring inside the Keyence interface.

RESULTS

The dataset was subjected to statistical analysis using the STATISTICA 12 software. Prior to this, data was checked and any extreme outliers were removed to ensure normal distribution, while also confirming equal variances among groups. Subsequently, the data was categorized and descriptive statistics (Table 2.) were computed to validate the ANOVA assumptions. This was followed by a multi-factor analysis of variance with interaction. The p-values resulting from the analysis are presented in Table 3.

Table 2: Results of descriptive statistics for Kerf widths

Material	Position	N	Mean [μm]	Median [μm]	Std. Deviation	95% Confidence Interval for Mean					CV [%]
						Lower Bound	Upper Bound	Min [μm]	Max [μm]	Variance	
Beech Plywood	BTM	480	403.51	352.96	178.61	387.49	419.53	161.3	901.95	31903.01	44.27
Beech Plywood	TOP	480	392.96	380.88	66.00	387.04	398.88	266.03	621.44	4355.84	16.80
Pine Plywood	BTM	480	486.01	429.70	198.86	468.18	503.85	199.3	974.39	39543.61	40.92
Pine Plywood	TOP	480	406.37	417.38	56.01	401.34	411.39	251.04	557.88	3137.67	13.78
HDF	BTM	480	243.72	216.31	104.48	234.35	253.09	91.57	487.44	10916.49	42.87
HDF	TOP	480	387.21	383.36	45.56	383.12	391.29	276.85	498.47	2075.54	11.77
Beech	BTM	480	315.38	272.01	152.83	301.68	329.09	101.89	767.05	23358.09	48.46
Beech	TOP	480	482.22	469.21	80.45	475.00	489.44	344.21	731.24	6472.83	16.68
Oak	BTM	480	415.13	393.51	209.61	396.33	433.93	96.45	924.95	43936.21	50.49
Oak	TOP	480	466.51	461.88	53.64	461.70	471.32	309.52	682.42	2877.59	11.50
Spruce	BTM	480	591.10	509.22	236.09	569.92	612.27	225.71	1090.29	55737.47	39.94
Spruce	TOP	480	462.28	448.91	55.70	457.29	467.28	328.88	631.7	3102.43	12.05

Table 2. presents the descriptive statistics for kerf width measurements across various wood-based materials and positions (bottom and top) when cut with a CO2 laser. The results show that HDF consistently has the smallest and most uniform kerf widths, indicating high precision. In contrast, Spruce exhibits the largest and most variable kerf widths. Natural woods like Spruce and Oak demonstrate higher variability, as reflected by their larger standard deviations, variances, and wider confidence intervals. The coefficient of variation (CV) is lowest for HDF and Oak at the top position, indicating higher consistency, while Beech and Oak at the bottom position have the highest CVs, showing greater variability.

These findings support the hypothesis that materials with more uniform properties exhibit more consistent kerf widths. Engineered materials like HDF provide smaller and more consistent kerf widths compared to natural woods.

Table 3: Results from multi-factor analysis of variance (ANOVA)

	Kerf width F-value	Kerf width p-value
Material	4301.0	0.00
Position	749.4	0.00
Speed [mm·s ⁻¹]	16881.5	0.00
Power [%]	4254.8	0.00
Material*Position	3123.1	0.00
Material*Speed [mm·s ⁻¹]	178.7	0.00
Position*Speed [mm·s ⁻¹]	5476.4	0.00
Material*Power [%]	68.4	0.00
Position*Power [%]	831.5	0.00
Speed [mm·s ⁻¹]*Power [%]	104.7	0.00
Material*Position*Speed [mm·s ⁻¹]	236.4	0.00
Material*Position*Power [%]	80.0	0.00
Material*Speed [mm·s ⁻¹]*Power [%]	22.5	0.00
Position*Speed [mm·s ⁻¹]*Power [%]	101.7	0.00
Material*Position*Speed [mm·s ⁻¹]*Power [%]	22.3	0.00

The kerf width measurements for different wood-based materials cut with a CO2 laser at various power levels and cutting speeds are shown in Figure 3.

Across all materials, increasing cutting speed reduces kerf width at all power levels (40%, 60%, 80%, and 100%). Higher laser power results in wider kerf widths at lower speeds, but this effect lessens with increased speed. This finding is supported by studies from Eltawahni et al. (2013) and Rāviņš et al. (2024), who also observed that optimizing cutting parameters is crucial for improving cut quality and consistency [4,7].

Specifically, Beech Plywood and Pine Plywood show significant reductions in kerf width with higher cutting speeds, with Pine Plywood generally having slightly larger kerf widths. HDF consistently exhibits the smallest kerf widths, indicating its uniform density leads to more precise cuts. This aligns with previous findings by Eltawahni et al. (2011), who also reported high precision in CO2 laser cutting of MDF. The consistency in kerf widths for HDF is attributed to its uniform density and structure, which is a characteristic shared with MDF [3].

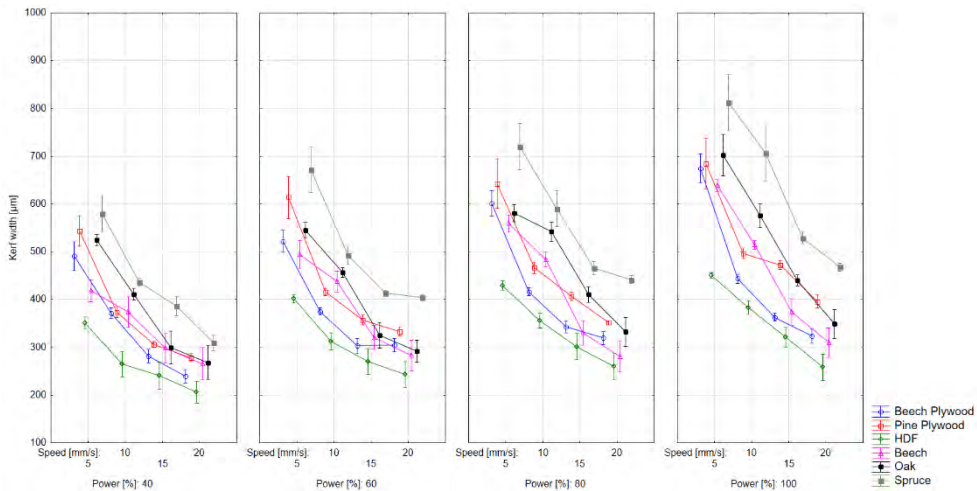


Figure 3. Kerf widths comparisons across different materials.

Beech shows a sharp decrease in kerf width with increasing speed, especially at higher power levels. Oak's kerf width decreases moderately with speed but remains larger than Beech and HDF. Spruce has the largest kerf widths at lower speeds, particularly at 40% and 60% power, and decreases with higher speeds but is still larger compared to other materials. This is consistent with the findings of Guo et al. (2021), who observed significant kerf width variation in pine wood due to its heterogeneous anatomical properties. The variability in natural woods can be attributed to differences in grain structure and density [5].

At lower power levels (40% and 60%), all materials exhibit a significant decrease in kerf width as speed increases. At higher power levels (80% and 100%), the decrease is less pronounced for Spruce and Oak due to their larger and more variable kerf widths. HDF achieves the smallest and most uniform kerf widths, likely due to its engineered homogeneity. Error bars indicate that HDF and Beech Plywood have smaller standard deviations, suggesting more consistent cuts, while Oak and Spruce have larger error bars, reflecting greater variability due to their heterogeneous properties.

These results highlight the influence of material properties, laser power, and cutting speed on kerf width in CO₂ laser cutting. Engineered materials like HDF and plywoods provide more consistent kerf widths compared to natural woods, which is advantageous for applications requiring precise and uniform cuts.

CONCLUSIONS

- **HDF Consistency:** High-density fiberboard (HDF) exhibited the smallest and most uniform kerf widths due to homogeneous property distribution.
- **Natural Wood Variability:** Natural woods like Spruce and Oak showed larger and more variable kerf widths, attributed to their heterogeneous properties.
- **Impact of Cutting Parameters:** Higher cutting speeds resulted in narrower kerf widths, while higher power levels led to wider kerf widths.

Future Research: Further investigation into microstructural and surface morphology changes during laser cutting and the impact of different laser parameters will be looked into.

ACKNOWLEDGMENTS

This work was supported by the Slovak Research and Development Agency under the contracts no. APVV-20-0159, VEGA Agency of the Ministry of Education, Research, Development and Youth of the Slovak Republic and the Slovak Academy of Sciences Grant no. 1/0577/22 and by the Internal project agency of the Technical University in Zvolen Proj. number IPA 3/2024.

REFERENCES

- [1] D. Schuocker, LASER CUTTING, *Materials and Manufacturing Processes* 4 (1989) 311–330. <https://doi.org/10.1080/10426918908956297>.
- [2] W.M. Steen, Laser material processing—an overview, *Journal of Optics A: Pure and Applied Optics* 5 (2003) S3. <https://doi.org/10.1088/1464-4258/5/4/351>.
- [3] H.A. Eltawahni, A.G. Olabi, K.Y. Benyounis, Investigating the CO₂ laser cutting parameters of MDF wood composite material, *Opt Laser Technol* 43 (2011) 648–659. <https://doi.org/https://doi.org/10.1016/j.optlastec.2010.09.006>.
- [4] H.A. Eltawahni, N.S. Rossini, M. Dassisti, K. Alrashed, T.A. Aldaham, K.Y. Benyounis, A.G. Olabi, Evaluation and optimization of laser cutting parameters for plywood materials, *Opt Lasers Eng* 51 (2013) 1029–1043. <https://doi.org/https://doi.org/10.1016/j.optlaseng.2013.02.019>.
- [5] X. Guo, M. Deng, Y. Hu, Y. Wang, T. Ye, Morphology, mechanism and kerf variation during CO₂ laser cutting pine wood, *J Manuf Process* 68 (2021) 13–22. <https://doi.org/https://doi.org/10.1016/j.jmapro.2021.05.036>.
- [6] A.S. Gusts, I. Adijāns, OPTIMIZATION OF PARAMETERS FOR LASER MARKING AND ENGRAVING ON PLYWOOD AND PINE WOOD MATERIALS, HUMAN. ENVIRONMENT. TECHNOLOGIES. Proceedings of the Students International Scientific and Practical Conference (2021) 145–150. <https://doi.org/10.17770/HET2021.25.6795>.
- [7] D. Rāviņš, I. Adijāns, E. Yankov, V. Bakakins, THE IMPACT OF CO₂ LASER POWER AND SCANNING SPEED ON VARIOUS WOOD AND THERMOWOOD SAMPLES, ENVIRONMENT. TECHNOLOGIES. RESOURCES. Proceedings of the International Scientific and Practical Conference 3 (2024) 434–439. <https://doi.org/10.17770/ETR2024VOL3.8170>.
- [8] V. Barnekov, C.W. McMillin, H.A. Huber, Factors influencing laser cutting of wood, *For Prod J* 36 (1986) 55–58. http://www.srs.fs.usda.gov/pubs/ja/ja_barnekov001.pdf.
- [9] I. Kubovský, L. Kristak, J. Suja, M. Gajtanska, R. Igaz, I. Ružiak, R. Réh, Optimization of Parameters for the Cutting of Wood-Based Materials by a CO₂ Laser, *Applied Sciences* 10 (2020) 8113. <https://doi.org/10.3390/app10228113>.
- [10] N. Yusoff, S. Ismail, A. Mamat, A. Ahmad-Yazid, Selected Malaysian Wood CO₂-Laser Cutting Parameters And Cut Quality, *Am J Appl Sci* 5 (2008). <https://doi.org/10.3844/ajassp.2008.990.996>.
- [11] A. Sobolewska, B. Cieczińska, Problems of Quality Assurance and Selection of Control Criteria in Laser Cutting Operations of Wood and Wood-Like Materials, *Multidisciplinary Aspects of Production Engineering* 4 (2021) 142–152. <https://doi.org/doi:10.2478/mape-2021-0013>.
- [12] C. Açıık, Research of computerized numerical control laser processing qualities of some wood species used in the furniture industry, *Maderas. Ciencia y Tecnología* 25 (2023). <https://doi.org/10.4067/S0718-221X2023000100433>.



MONITORING THE DIMENSIONAL STABILITY OF HORNBEAM LUMBER IN THE PROCESS OF AIR DRYING

Hugo M. Uličný – Peter Vilkovský – Ivan Klement

Abstract

*The dimensional stability of hornbeam lumber (*Carpinus betulus* L.) during air drying was tracked in the study, aiming to compare the shape changes in two types of logs, those with and with no spiral grain. The primary objective was to differentiate the impact of spiral grain on the warp cup and warp twist during air drying. Over three months, temperature and relative humidity were diligently measured. The statistical analysis revealed no statistically significant difference in warp cup between the samples with and with no spiral grain (p -value = 0.9599). However, a significant difference was observed in warp twist between the samples with spiral grain and those with no spiral grain. The p -value for this type of warp was (p -value = 0.00002). These findings have significantly contributed to a deeper understanding of the effect of spiral grain and the drying process on the dimensional stability of hornbeam lumber, which holds immense value for the woodworking industry.*

Keywords: *Hornbeam, Shape Changes, Air Drying, Lumber, Cup, Twist*

INTRODUCTION

Hornbeam (*Carpinus betulus* L.) is a tree that has yet to find its place in the woodworking industry. Its relatively large shape instability makes it problematic for final wood products. Despite its high density and strength, like beech (*Fagus sylvatica* L.), its low durability hinders outdoor use (FANNI FODOR A COL., 2017). The Green Report 2023 from the Ministry of Agriculture and Rural Development of the Slovak Republic indicates a growing share of hornbeam in our forests yearly, even at the expense of other valuable trees, such as those from the genus (*Quercus*). The current percentage representation is at the level of 6% with a growing tendency. The percentage representing similar trees in beech forest is at the level of 35.1%. These two trees are found in the same stands, which can save harvesting funds in the future. The research by the authors (KIAEI A ABADIAN, 2018) on the physical and mechanical properties of the common hornbeam (*Carpinus betulus* L.), with an emphasis on its location in the stand, revealed significant differences in the mechanical properties of hornbeam lumber growing in denser stands. In terms of physical properties, it was found that the tree location does not affect its physical properties. According to other studies, the trees on the forest border have a more pronounced spiral grain than those inside the forest stand (WELLNER A LOWERY, 1967).

Shape changes caused by changes in humidity during drying or operation are a significant problem for lumber intended for timber structures. Changes in moisture content are

accompanied by significant drying shrinkage or swelling of the material. The stability of structural lumber is often associated mainly with the so-called cylindrical geometry caused by growth rings, the orthotropic nature of the wood material, and the tendency of the wood fibers to grow spirally around the trunk, which is often considered the most damaging deformation of lumber (ORMARSSON A KOL., 1998). (FORSBERG A WARENSJÖ, 2010) found that the angle of rotation of the fibers on the surface of the trunk and the slope of the angle of the fibers of the curve is strongly correlated with the angle of rotation. In the study of (EKEVAD, 2005), he described the basic mechanical understanding of the causes of shape changes associated with the spiral grain. In his study, Shape changes in dried lumber can depend on several factors. One of them is the original position of the lumber in the log before the cut. This issue was addressed by several authors (ORMARSSON A KOL., 1999), (ORMARSSON A KOL., 2000), (ORMARSSON A JOHANSSON, 2006) and (STRAZE A KOL., 2011) who focused on the original position of the lumber in the log with subsequent comparison of shape stability. The warps created during the log processing and the remaining growth stresses affect the shape changes after drying (ORMARSSON A JOHANSSON, 2006).

MATERIAL METHODS

The sampling for the research was conducted in the district of Žiar nad Hronom, in the cadastral territory of the village of Hronská Dúbrava, at an altitude of 457 a.s.l. The research was conducted on two logs, one with spiral grain and one with no. The ages of logs ranged from ± 52 to ± 60 years. The density was measured according to the standards STN EN 384+A2 (49 1533) on Structural wood and (EN 384: 2016 + A2: 2022) on Determination of characteristic values of mechanical properties and density. The dimensional characteristics of the logs are detailed in Tab. 1.

Tab. 1 Dimensional characteristics of selected logs

	Log with no spiral grain.	Log in with the spiral grain.
Small end diameter	0.380 m	0.350 m
Center diameter	0.410 m	0.370 m
Large end diameter	0.490 m	0.430 m
Log length	2.965 m	3.040 m
Deviation per 1 m of length before air drying \bar{x}	0°	5.8°
Deviation per 1 m of length after air drying \bar{x}	3°	10.6°
Sample density ρ_0	1158.14 kg/m ³	1151.56 kg/m ³

A live sawing pattern (Fig.1), the most used sawing pattern for hardwoods, made the log. The sawing was processed on a Mebor 1200 log horizontal band saw. Unplastered boards were produced and subsequently plastered into samples with dimensions (t) = 0.025 m, width (w) = 0.095 m, and length (l) = 2 m. The length of 2 m was chosen based on the standard STN EN 1309-3 (49 1013). Finally, samples for the research were made from the lumber.

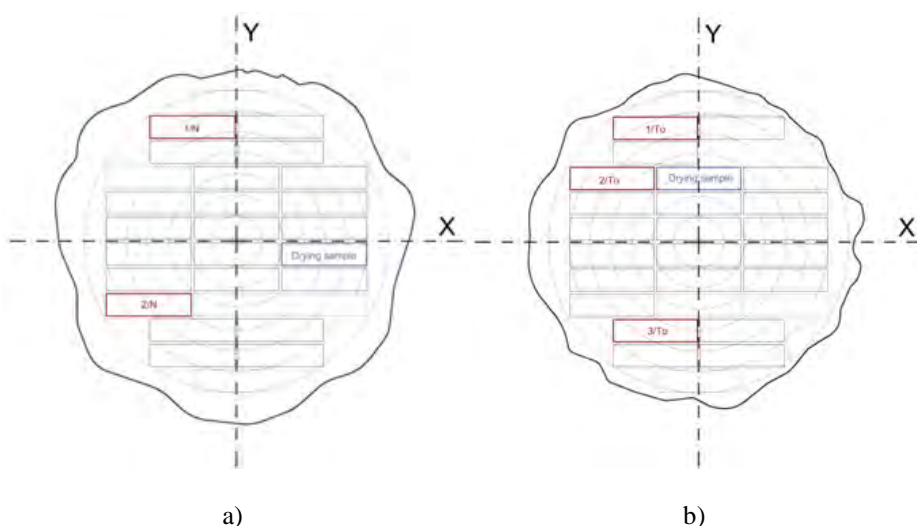


Figure 1. Position of the samples in the log a) with no spiral grain and b) with spiral grain

Air Drying Conditions

The samples were stored in cages during air drying. Air drying occurred from November 10, 2022, to February 14, 2023. Air drying conditions were recorded using the Data device Logger Comet S3631. The device recorded temperature in °C and relative humidity in % at hourly intervals. One piece was selected from the remaining ten pieces of lumber, from which drying samples were sawn for monitoring and calculating moisture content during the drying process. Moisture samples with spiral grain and with no spiral grain had the fronts on both sides covered with a silicone layer, which served against rapid moisture loss. Moisture samples were weighed once a week.

Measured Change of Shape by STN EN 1309-3.

Shape changes were measured once a week throughout the entire course of the research. The size of the shape changes depends on the density and the orientation of the wood fibers. In our logs, ρ_0 in the log with no spiral grain density was 1158.14 kg/m^3 , and in the log with spiral grain density, it was 1151.56 kg/m^3 . On the pieces of lumber from the top layer of the drying cages, which were intended for research, shape changes were measured according to the standard STN EN 1309-3 (49 1013) (Logs and lumber. Methods of measuring dimensions. Part 3: Signs and biological damage).

During the research, absolute warp cup and warp twist were measured. The measurement methods are shown in Fig 2. Measurements were made using a measuring device on a flat surface in the laboratories of the Technical University in Zvolen.

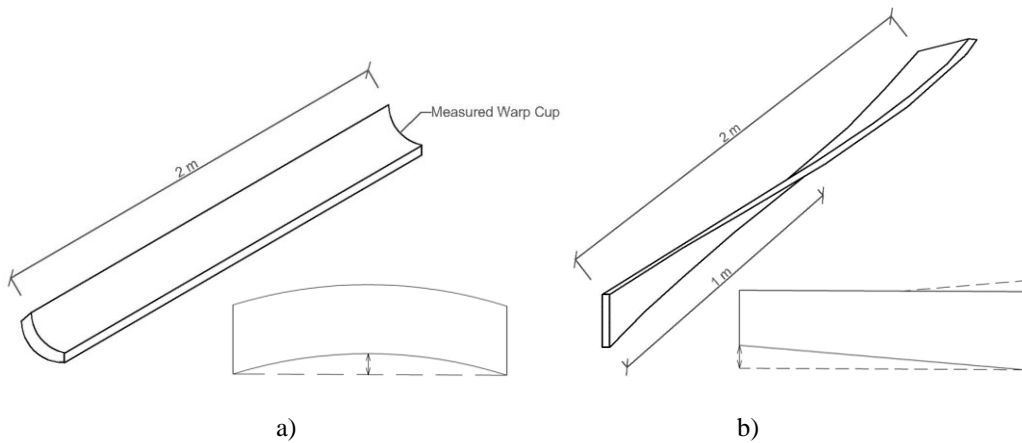


Figure 2. Measured shape change– a) warp cup and b) warp twist

RESULTS

Air drying conditions (Fig.3) were recorded, and temperatures ranged from 9°C in November to 15°C in February. Humidity ranged from 90% in November 2022 to 60% in February.

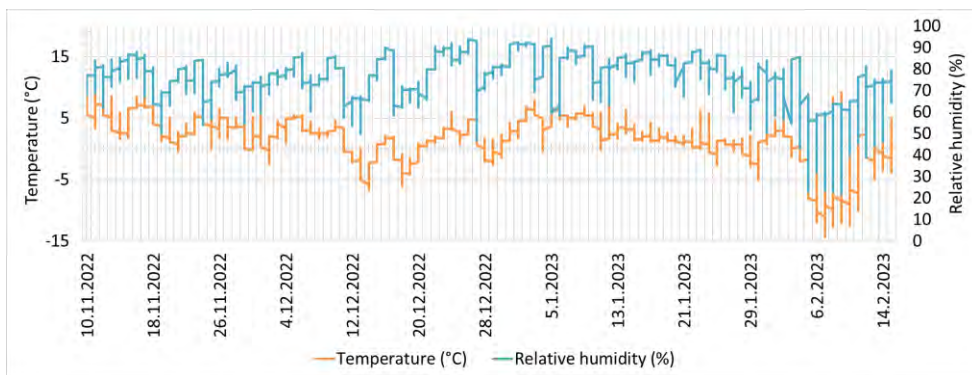


Figure 3. The conditions of air drying during three months of research

Warp cup

The warp cup of the samples due to air drying with and with no spiral grain is approximated in Figure 4. In the case of warp, approximately the same increase in warp for both types of samples can be observed. The rise in warp occurred at the material moisture content $M_c = 59.38\%$. In samples without spiral grain (1/N, 2/N), an interesting situation was observed over two months, as the warp cup increased from the beginning and then decreased from 1.96 mm to 1.12 mm. This phenomenon occurred at almost final moisture content $M_c = 33.57\%$. After a week of decreasing warp, all samples leveled off with other values. The warp values of the spiral grain samples ranged from 0.7 mm to 1.09 mm. The drying curve, determined from the drying samples, is shown by the red dotted curve (Fig.

4). The moisture content of the drying sample was at the M_c level at the end of air drying = 33.82%.

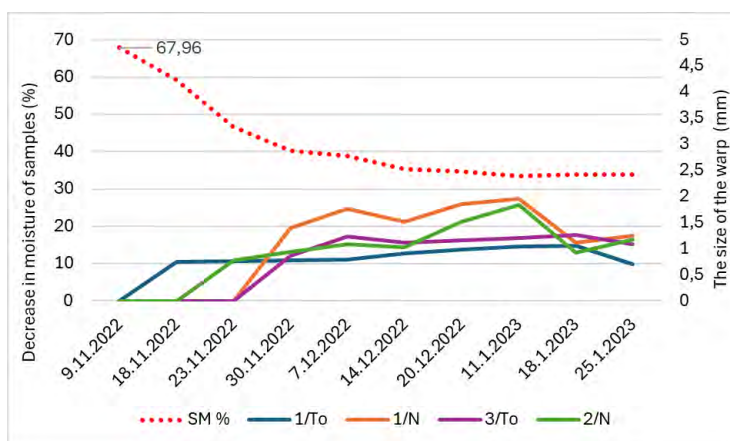


Figure 4. The warp cup during the three-month research

There is no statistically significant difference in warp cup between the samples with and without spiral grain. The p -value = 0.9599 means that the warp cup did not depend on the spiral grain in the research (Fig. 5).

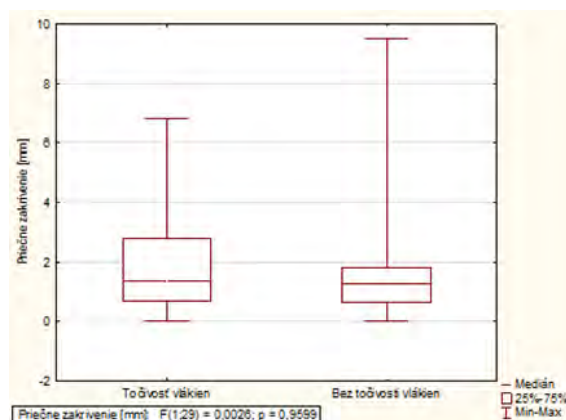


Figure 5. Statistical evaluation – warp cup

Warp twist

(Fig.6) show warp twist during three months of air drying on samples with spiral grain and without spiral grain. An increase in warp occurred at the same angle in the second week of measurements. An increase in warp occurred at $M_c = 52.11\%$. The warp values ranged from 16.83 to 23.96 mm for spiral grain samples. Conversely, the values ranged from 4.36 to 7.87 mm for samples with no spiral grain. An increase in warp was linear until the end of the research.

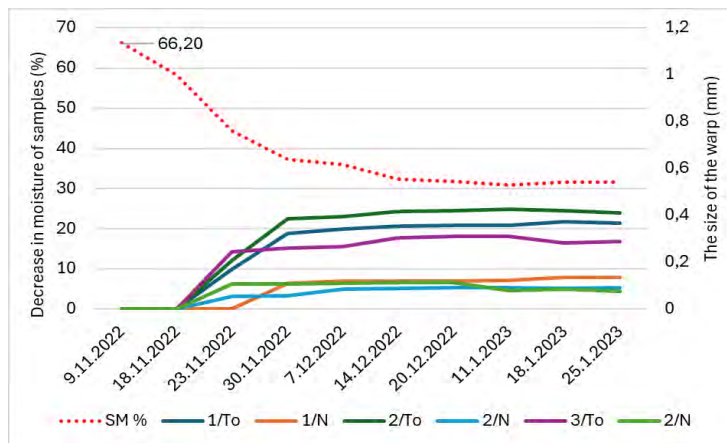


Figure 6. The size of the warp twist during the three-month research

A significant difference in warp twist exists between samples with spiral grain and with no spiral grain. The p-value for this type of warp is 0.00002, indicating that the spiral grain affects the warp (Fig. 7).

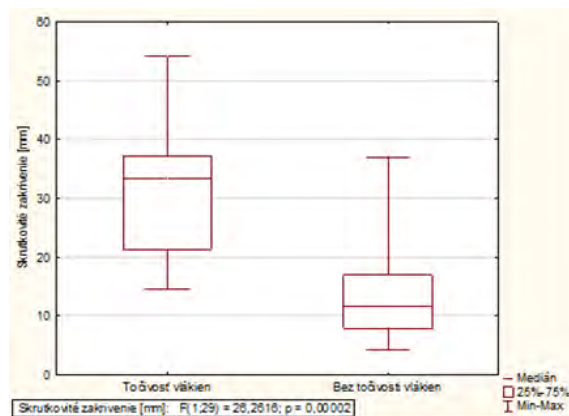


Figure 7. Statistical evaluation – Warp twist

DISCUSSION

In the research on monitoring the dimensional stability of hornbeam lumber in the air drying process, it was found that spiral grain affected warp twist but not warp cup. Similar findings were also reported by (ORMARSSON, 2000), who simulated board drying using three-dimensional theory to numerically simulate shape changes caused by humidity fluctuations. (ORMARSSON, 2000) conducted research on spruce (*Picea abies* (L.) H. Karst.), emphasizing the dependence of shape changes on the original position of samples for both species. This observation is also noted by other authors (STRAZE A KOL., 2011), (SANDBERG, 1997), and (ORMARSSON A KOL., 2000). According to (HARALD SÄLL, 2002), warp cup primarily arises due to humidity changes, a conclusion with which we concur

following the completion of our research. Over subsequent weeks, as temperatures dropped below freezing, warp cup increased. Warp cup was not observable before air drying, especially on samples without spiral grain, a finding similarly noted in research by (ORMARSSON A JOHANSSON, 2006). (ZHAN JIAN-FENG A KOL., 2007) assert that sample width can significantly influence the final warp cup size.

Warp twist is predominantly influenced by samples with spiral grain. Following one week of air drying, warp increased dramatically and continued to grow significantly over the next two weeks. Our research data indicate that warp was not influenced by the initial sample position but was affected by the presence of spiral grain.

CONCLUSION

- The warp cup of the samples during air drying was not significantly affected by the presence of spiral grain.
- No statistically significant difference was found in warp cup between the samples with spiral grain and with no spiral grain. The p-value was 0.9599, indicating that spiral grain did not affect the warp cup in our research.
- There is a significant difference in the warp twist between the samples with spiral grain and with no spiral grain. The p-value achieved was well below 0.05 (0.00002), indicating that spiral grain affects warp.
- According to the measured values for warp twist, the warp depends on the spiral grain.
- The shape stability can also be influenced by the drying conditions in which the material was located.

ACKNOWLEDGMENTS

This work was supported by the Slovak Research and Development Agency under contract no. APVV-21-0049. This work was supported by the Scientific Grant Agency of the Ministry of Education, Science, Research and Sport of the Slovak Republic and the Slovak Academy of Sciences — project VEGA no. 1/0063/22.

This work was supported by project IPA 13/2024.

REFERENCES

Ekevad, M. Twist of wood studs: dependence on spiral grain gradient. *J Wood Sci* 51, 455–461 (2005). <https://doi.org/10.1007/s10086-004-0679-2>

Fodor, Fanni, et al. "Testing common hornbeam (*Carpinus betulus* L.) acetylated with the Accoya method under industrial conditions." *Iforest - Biogeosciences and Forestry* 10 (2017): 948-954.

Forsberg D. and Warensjö M. Grain Angle Variation: A Major Determinant of Twist in Sawn *Picea abies* (L.) Karst, *Scandinavian Journal of Forest Research*, 16:3, 269-277 (2001). <https://doi.org/10.1080/713785122>

Kiaei, M., and Abadian, Z. Physical and Mechanical Properties of Hornbeam Wood from Dominant and Suppressed Trees. *Grinder Industry*, 69, 63-69, (2018) <https://doi.org/10.5552/drind.2018.1705>

Lowery David P. and Wellner Charles A. *Spiral grain: a cause of pole twisting*. Ogden, Utah: Intermountain Forest and Range Experiment Station, Forest Service, US Dept. of Agriculture, vol: no.38, (1967) ISBN-13 : 978-1390408867

Ministry of the Environment of the Slovak Republic. *Green Report 2023*. Ministry of the Environment of the Slovak Republic, 2023.

Ormarsson, S., and Johansson, M. Finite element simulation of growth stress formation and related board distortions resulting from sawing and forced drying. *New Zealand Journal of Forestry Science* vol. 36 no. (2/3): p. 408–423 (2006).

Ormarsson, S., Dahlblom , O. & Petersson, H. A numerical study of the shape stability of sawn timber subjected to moisture variation Part 1: Theory. *Wood Sci. Technol .* 32, 325–334 (1998). <https://doi.org/10.1007/BF00702789>

Ormarsson, S., Dahlblom , O. & Petersson, H. A numerical study of the shape stability of sawn timber subjected to moisture variation. Part 2: Simulation of drying board. *Wood Science and Technology* 33, 407–423 (1999). <https://doi.org/10.1007/s002260050126>

Ormarsson, S., Dahlblom , O. & Petersson, H. A numerical study of the shape stability of sawn timber subjected to moisture variation. *Wood Science and Technology* 34, 207–219 (2000). <https://doi.org/10.1007/s002260000042>

Säll, H. (2002). *Spiral Grain in Norway Spruce* (PhD dissertation, Växjö University Press).

Sandberg, D. Radially sawn timber. *Holz als Roh-und Werkstoff* 55, 175–182 (1997). <https://doi.org/10.1007/BF02990541>

Straze, A, et al. The influence of material properties on the amount of twist of spruce wood during kiln drying. *Eur. J. Wood Prod.* 69, 239–246 (2011). <https://doi.org/10.1007/s00107-010-0422-1>

Vilkovský, P.; Uličný, H.M.; Klement, I.; Vilkovská, T. The Differences in Shape Stability for Hornbeam (*Carpinus betulus* L.) Lumber with and without Spiral Grain. *Appl. Sci.* (2024), 14, 5250. <https://doi.org/10.3390/app14125250>

Zhan, JF, & Avramidis, S. Impact of conventional drying and thermal post-treatment on the residual stresses and shape deformations of larch lumber. *Drying Technology*, 35(1), 15–24. (2016) <https://doi.org/10.1080/07373937.2016.1156123>

STN EN 1309-3 (49 1013): 2018. Logs and lumber, Methods measurements dimensions, Part 3: Signs and biological damage.

STN EN 384+A2 (49 1533): Structural wood.

EN 384: 2016 + A2: 2022: Determination of characteristic values of mechanical properties and density.



MODEL OF ENERGY CONSUMPTION IN DRILLING PROCESSES OF WOOD-BASED MATERIALS BASED ON CUTTING FORCE

Joanna Zielińska-Szwajka¹ – Krzysztof Szwajka²

Abstract

Wood-based boards are becoming more and more widely used in many areas of industrial production. Their growing popularity is determined by numerous advantages over natural wood. Smart drilling, i.e. real-time adjustment of cutting parameters, requires the evolution of cutting process variables. In addition, it is necessary to create and manage a database, process data and adjust processing parameters in real time. Machinability is one of the most important technological properties in the machining process, enabling the determination of the material's susceptibility to machining. One of the machinability indicators is the unit cutting resistance ($k_{c1.1}$). An innovative method for determining the value of unit cutting resistance ($k_{c1.1}$) was proposed. The obtained results were used to determine the machinability index. The results obtained during the tests showed that the specific cutting resistance is constant for a given workpiece and does not depend on the cutting parameters.

Key words: *drilling, cutting resistance, cutting force, torque*

INTRODUCTION

There are many ways to process chipboard [1, 2], so the machinability of these materials can be tested in many ways. Nevertheless, the machinability of any type of chipboard when drilled is one of the most important issues from a practical point of view. This general belief can be proven in many ways, but it seems that two basic arguments suffice. Firstly, resistance to axial screw removal is one of the most important technical parameters characterizing chipboards. This resistance should be determined experimentally in accordance with the detailed standard [3]. The experimental procedure requires drilling an appropriate hole in order to install the screw, which is why drilling is a very basic form of chipboard processing. There are many ways to process chipboard [4], so the machinability of these materials can be tested in many ways. Nevertheless, the machinability of any type of chipboard when drilled is one of the most important issues from a practical point of view. This general belief can be proven in many ways, but it seems that two basic arguments suffice. Firstly, resistance to axial screw removal is one of the most important technical parameters characterizing chipboards. This resistance should be determined experimentally in accordance with the detailed standard [5]. The experimental procedure requires drilling an appropriate hole in order to install the screw, which is why drilling is a

¹ Department of Component Manufacturing and Production Organization, Faculty of Mechanics and Technology, Rzeszow University of Technology, ul. Kwiatkowskiego 4, 37-450 Stalowa Wola, Poland

² Department of Integrated Design and Tribology Systems, Faculty of Mechanics and Technology, Rzeszow University of Technology, ul. Kwiatkowskiego 4, 37-450 Stalowa Wola, Poland
e-mail: j.zielinska@prz.edu.pl, kszwajka@prz.edu.pl

very basic form of chipboard processing. Secondly, drilling is now used not only to make holes for construction purposes. Drilling tests are widely considered the most convenient (fastest and most economical) method for the relative assessment of the machinability of any wood or wood-based materials [4, 5, 6]. Any scientific study of machinability must be strictly experimental. In general, it has long been known that any attempts to theoretically determine (predict) machinability based on the mechanical properties of the material are pointless [6]. This may contradict the belief that, for example, knowledge of the tool geometry, cutting parameters and standard material properties allows for the theoretical determination of cutting forces. Previous research shows that real cutting processes, such as drilling, are too complex from a physical point of view to find a direct relationship between cutting forces and the tensile or shear strength of the processed material [4, 5]. We are simply forced to conduct experimental research. Unfortunately, there is no generally accepted standard that can be directly applied to testing the machinability of particleboard. The problem of machining quality may significantly limit the scope of application of the construction material, and excessive drilling resistance may result in the need to limit the feed speed and reduce machining efficiency.

MATERIAL AND METHODS

In the tests, four types of wood-based materials were used as the processed material: Medium-Density Fiberboard (MDF), chipboard, plywood and High Pressure Laminate (HPL). The tests used a typical cutting tool intended for wood-based materials, a single-edge drill with a diameter of 10 mm with Polycrystalline Diamond (PCD) blades from Leitz® Diamaster PRO. The drill marking is: DP/D10/NL30/S10x27/GL70/RL. This drill is used in processing materials such as: wood, chipboards, resin boards, plastics, reinforced plastics.

As part of the research, holes were drilled on a CNC milling machine in prepared samples cut from processed materials with dimensions of 130 × 30 × 18 mm. Except for the HPL board, which was 10 mm thick. The axial force (F_t) and cutting torque (M_s) signals were measured using a KISTLER® 9345B sensor. Signals from the sensors were recorded on the hard drive of a personal computer (PC) in digital form via a National Instruments® 6034E analog-to-digital card. The sampling frequency of signals during the experiments was 50 kHz, and the measurement resolution of the card was 16 bits. Table 1 lists the cutting parameters used during drilling experiments. Three repetitions were performed for each set of cutting parameters.

Table 1. Machining conditions.

Thickness of the cutting layer (mm)	Feed per tooth (mm)	Feed speed (mm/min)
0,05	0,07	177
0,10	0,14	354
0,15	0,21	530
0,20	0,28	707
0,25	0,35	884
0,30	0,42	1061
0,35	0,49	1237

The research involved drilling with a drill with a diameter of 10 mm, after previously drilling a hole in the material with a drill with a diameter of 3 mm. In this case, only the axial force (F_t) and cutting torque (M_s) signals were recorded. The above-described

research methodology was repeated for all four types of processed materials. This allowed for the experimental determination of cutting resistance. Figure 2 shows the distribution of cutting forces and torque during drilling.

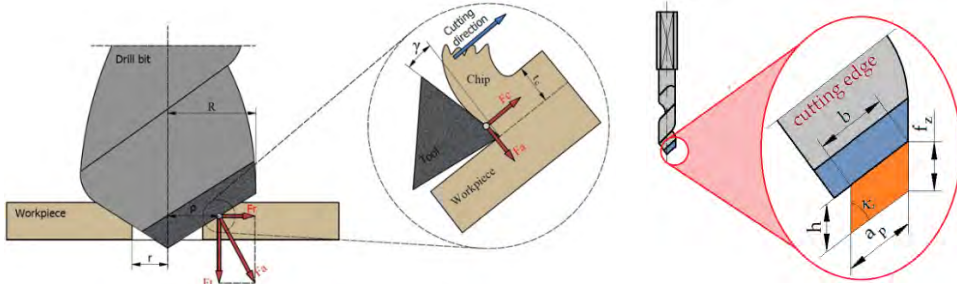


Figure 1. Distribution of forces.

After a preliminary analysis, it was determined that in the case of tests during drilling in wood-based materials, an effective solution would be to carry out the drilling process using different thicknesses of the cut layer. It was assumed that to determine the cutting resistance for each of the tested materials, it would be optimal to determine seven values of the thickness of the cut layer, starting from 0.05 mm and successively in steps of 0.05 mm up to 0.35 mm. For each cutting depth, the feed per tooth and the feed speed increased similarly. Before starting the research, the basic geometry of the drill cutting edge was determined. The entering angle of the drill's cutting edge is: $\kappa_r=45^\circ$, which means that $\sin\kappa_r=0.707$. Determining the cutting depth, we obtain: $a_p=3.5$ mm. Then, the cutting width (b) was determined, which was a constant parameter for all drilling tests: $b=a_p/\sin\kappa_r=4.95$ mm.

RESULTS AND DISCUSSION

Analyzing the course of the axial force (F_t) and cutting torque (M_s) recorded during the tests (Fig. 2), it can be noticed that there are characteristic fragments in the signals, i.e. the entries and exits of the tool from the material, in which the value of the axial force signal and cutting torque characteristically increases or decreases accordingly. Force fluctuations can be distinguished in the signal, related to the passage of the cutting tool through layers of workpiece material of different density. It was noticed that during drilling, characteristic fragments of the axial force (F_t) signal could be extracted. The first fragment is the area where the drill enters the workpiece material, the axial force increases, and the drill point presses the workpiece material (just before cutting starts). Then the drill starts cutting the outer layer of the material with the highest density. In the case of HPL boards, this does not occur because the density of the material is similar throughout the entire cross-section of the board. When the drill leaves the area of the material with increased density, the force decreases because the drill cuts in the lower density middle layer. Then there is a signal fragment in which the drill penetrates to a depth equal to the height of the drill's cutting blades. This is cutting with a constant cross-section of the cut layer in the middle layer of the plate. This results in stabilization of the axial force value. At the beginning of the next signal fragment, the value of the axial force begins to increase due to the fact that the drill begins to enter the outer layer of the material with a higher density. The value of the axial force drops to zero at the end of the last signal fragment, when the drill is already leaving

the workpiece. In the case of cutting torque (M_s), there is a fragment of the signal in which there is no cutting action and only the cutting edge is pressed into the workpiece.

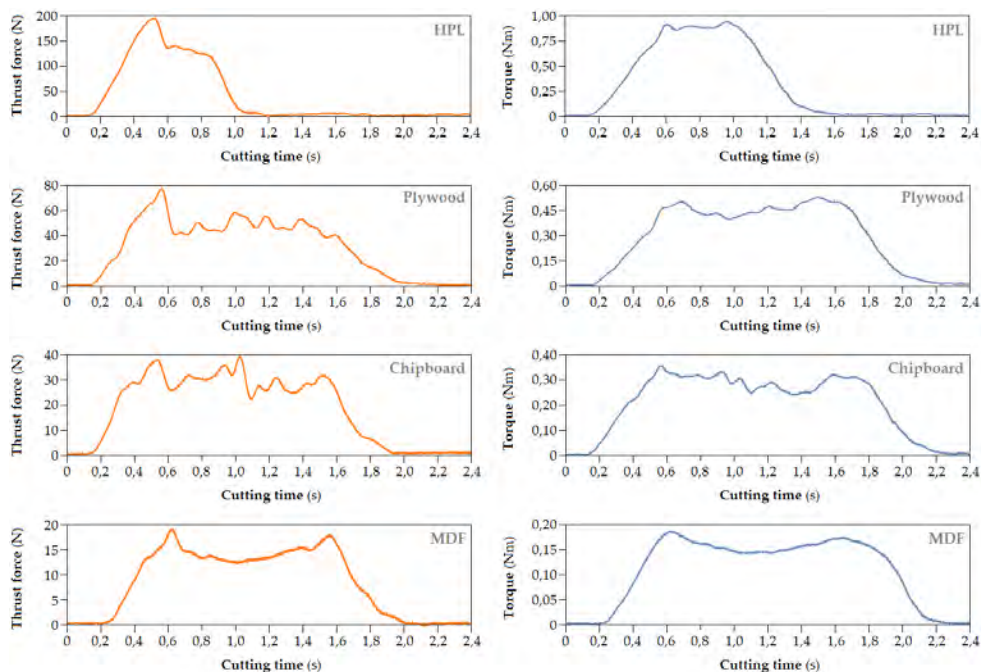


Figure 2. Torque and thrust force signal.

In this part of the signal, the cutting torque value is close to zero. The drill then sinks into the workpiece material, which increases the cutting torque value. The period of this increase lasts until the drill reaches the maximum cross-section of the cut layer. The next fragment of the signal is cutting with a constant cross-section of the cut layer in the middle layer of the plate. This results in stabilization of the cutting torque value. In the next signal fragment, as in the case of the axial force, the cutting torque value begins to increase. This is due to the fact that the drill begins to penetrate the outer layer of the material with increased density. As the drill begins to exit the workpiece, the cutting torque value begins to decrease. The cutting torque value drops to zero at the end of the signal when the drill has exited the workpiece. As mentioned earlier, the specific cutting resistance is defined as the quotient of the cutting force to the cross-sectional area of the cut layer and it is experimentally derived from this relationship. To determine the cutting resistance parameters (k_c) for the tested materials, it was necessary to determine the instantaneous value of the cutting torque (M_s) occurring in the drilling process. The cross-sectional area of the cut layer was variable, depending on the feed speed values used. The cutting width (b) remained constant, while the thickness of the cut layer changed depending on the drilling parameters, therefore, before determining the specific resistance, it was necessary to calculate the surface area of the cut layer for all drilling tests using the equation:

$$A_d = hb \quad (1)$$

Knowing the values of the cutting force (F_c) and the cross-sectional area of the cut layer (A_d), the values of specific cutting resistance were determined at given drilling parameters for all tested materials. For this purpose, the distribution of cutting resistance values

depending on the considered point on the cutting edge was described (Fig. 3). As can be seen from Fig. 3, the cutting resistance $k_{c(\rho)}$ acting on the infinitesimal element dA_d of the cross-section of the drill cutting edge gives the elementary moment dM_s relative to the drill axis:

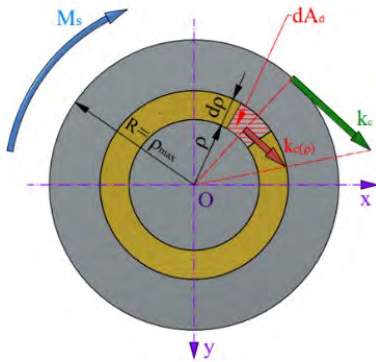
$$dM_s = k_{c(\rho)} \cdot \rho \cdot dA_d \quad (2)$$

where:

$k_c(\rho)$ - cutting resistance on the radius ρ ,

ρ – radius,

dA_d – elementary area of the cutting layer.



$$M_s = \int_{A_d} dM_s = \int_{A_d} k_{c(\rho)} \cdot \rho \cdot dA_d \quad (3)$$

Figure 3. Distribution of cutting resistance along the cutting edge of the drill..

The equilibrium conditions show that the sum of these elementary moments collected over the entire length of the drill's cutting edge must be equal to the moment M_s acting on the drill:

After transforming expression, we obtain the relationship determining the cutting resistance:

$$k_c = \frac{3 \cdot M_s \cdot R}{h \cdot (R^3 - r^3)} \quad (\text{N/mm}^2) \quad (4)$$

The procedure for determining the cutting resistance from equation (4) was repeated for all tested materials. In such a case, it was possible to obtain the value of the unit cutting resistance ($k_{c1.1}$) and the exponent (mc) for each tested material. The charts and the results obtained are presented below.

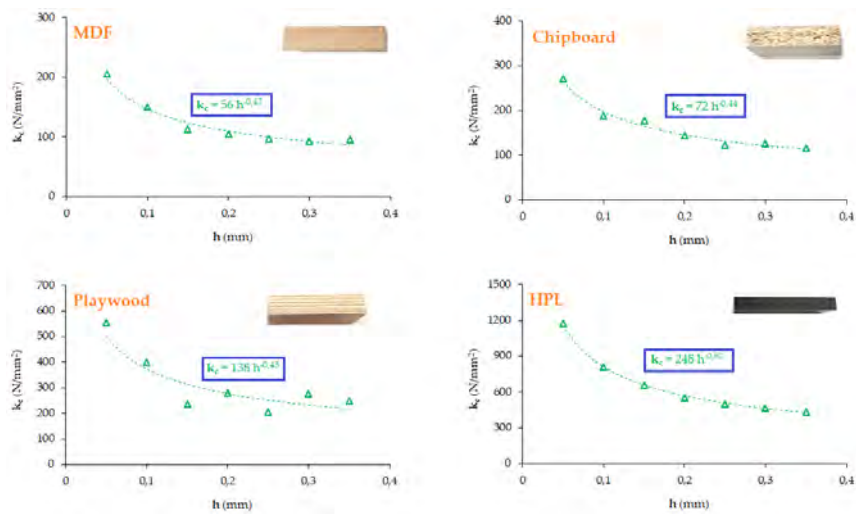


Figure 4. Cutting resistance in the drilling process.

CONCLUSIONS

1. Determination of cutting energy based on the signal of force and cutting torque is based on the value of unit cutting resistance ($k_{c1.1}$).
2. As expected, the specific cutting resistance ($k_{c1.1}$) varied in value depending on the type of material being processed, which allows for a clear distinction between materials. The results show that the proposed methodology can be used as an intelligent technique in the drilling process to identify machined materials.

REFERENCES

1. Szwajka, K.; Zielińska-Szwajka, J.; Trzepieciński, T. Experimental Analysis of Smart Drilling for the Furniture Industry in the Era of Industry 4.0. *Materials* 2024, 17, 2033.
2. Zhu, J.; Wang, X. Research on enabling technologies and development path of intelligent manufacturing of wooden furniture. *J. For. Eng.* 2021, 6, 177–183.
3. Wenkler, E., Arnold, F., Hänel, A., Nestler, A., & Brosius, A. (2019). Intelligent characteristic value determination for cutting processes based on machine learning. *Procedia CIRP*, 79, 9-14.
4. Vrchota, J.; Řehoř, P.; Maříková, M.; Pech, M. Critical Success Factors of the Project Management in Relation to Industry 4.0 for Sustainability of Projects. *Sustainability* 2020, 13, 281.
5. Szwajka K., and Trzepieciński T. On the Machinability of Medium Density Fiberboard by Drilling. *BioResources* 2018, 13(4), pp. 8263-8278.
6. Brozzi, R.; Forti, D.; Rauch, E.; Matt, D.T. The Advantages of Industry 4.0 Applications for Sustainability: Results from a Sample of Manufacturing Companies. *Sustainability* 2020, 12, 3647.



DECAY RESISTANCE VALUATION FOR FALSE HEARTWOOD AND MATURE BEECH WOOD

Zuzana Vidholdová – Gabriela Slabejová

Abstract

Timber made of beech (*Fagus sylvatica*, L.) is frequently used indoors, mostly in the production of flooring and furniture, but its higher susceptibility to decay by fungal attack is of great concern. This study examines the influence of mature beech wood and native false heartwood on its resistance to selected wood rot fungi - the brown rot fungi *Coniophora puteana* and *Serpula lacrymans* as well as the white rot fungus *Trametes versicolor*. It has been found that (a) mature beech wood and native false heartwood are highly susceptible to decomposition by brown and white rot fungi, (b) mature beech wood and native false heartwood are equally resistant to brown and white rot fungi, (c) Fungi species have an influence on the resistance of beech wood – very significantly in the “wood part*fungus” interaction. Both the formation of a large amount of free water and an increase in their moisture content occur in tandem with the decomposition process.

Key words: beech, false heartwood, fungi, mature wood

INTRODUCTION

Indoor wood rot fungi cause many problems worldwide; Fungi that attack roofs, walls, ceilings, floors, doors, windows, etc. represent a group of different basidiomycetes and their degradation modes can be divided into white rot or brown rot. Typical brown rot fungi are *Serpula lacrymans*, *Coniophora puteana* and *Gloeophyllum trabeum*. *S. lacrymans* is a fungus that causes more damage to buildings than its close relatives and other wood-decaying fungi found in forests (Watkinson and Eastwood 2012). Several characteristics of the fungus probably contribute to this. Its ability to infect and colonize wood in buildings has long been linked to its ability to survive and thrive in a spatially discontinuous supply of moisture and nutrients. This adaptation was likely refined during its evolution by ancestors that grew in temperate and boreal regions. *C. puteana* is a fungus that is very common in buildings (Rypáček 1957, Reinprecht 2008, Watkinson - Eastwood 2012, Gabriel - Švec 2017).

It is often used as an important test fungus in rot tests that determine a fungus's tolerance to several organic wood preservatives. *Rhodonina (Postia) placenta* is one of the most common types of brown rot on wood products. It is also tolerant of copper-based preservatives and is often used as a test fungus in evaluating new wood preservatives. *S. lacrymans* and *C. puteana* are the most common fungi found in damaged buildings in Europe (Gabriel – Švec 2017). Woods do not necessarily occupy the same relative position in the order of rot resistance when in contact with the ground as when in contact above

ground. Results with the test fungi *R. placenta* and *Trametes versicolor* provide information about the class of rot resistance that can be expected when in contact with soil. Although *G. trabeum* is less able to attack resistant woods than the others, it is believed to be a better indicator of the resistance class expected above ground.

Beech (*Fagus sylvatica* L.) is abundant and grows in managed forests throughout Europe. Due to its significant occurrence in the forest, it is one of the most commonly used commercial hardwoods. In Slovakian forests, deciduous trees predominate at 64.5%, including mainly beech (35.1%) and oak (10.4%) (Green Report 2023). Long-term forest planning assumes a lower proportion of spruce and a higher proportion of beech. It is a challenge for wood processors who need to forecast and align their production towards higher value-added end products. The disadvantage of beech wood is its relatively low proportion of trunk wood, which is only around 50% compared to 90% for spruce (Pöhler et al. 2006). Another disadvantage of beech wood is that it is not durable (EN 350:2016) and is therefore not suitable for outdoor use and uses such as garden furniture, decking or flooring. But beyond that, beech is an excellent hardwood for a variety of applications, from construction and furniture making to flooring and sports equipment. Due to its strength and smooth surface, beech wood is also widely used in the manufacture of furniture, flooring, plywood, veneers, musical instruments, sports equipment, construction, furniture, turned items and small wooden items. Beech wood is easy to work with. It is easy to machine, cut, glue, turn, plan, drill, mill and machine. It can be stained and polished (Slabejová 2013). Because beech wood is easy to bend and turn, it is often used to make turned objects such as toys, kitchen utensils, tools, and decorative items. Beech is also used in model making. Beech is an extremely hard and strong wood, making it an excellent choice for flooring, especially in busy commercial areas. Beech floors do not wear out as quickly. However, it is prone to decay and cannot be used outdoors. Beech is also commonly used to make household furniture, chairs, beds, tables and more. Beech furniture is very stable and heavy and lasts a very long time with little maintenance. Beech is also used for making parts of musical instruments such as guitar bodies, drums, etc. When making drums, beech is often used as a substitute for maple. Beech veneer is used for structural and decorative purposes. Beech wood is less prone to warping or splitting. However, false heartwood is an important factor affecting wood use, quality and its aesthetic appearance, as it could limit the processing options of beech wood and reduce its market price (Trenčiansky et al. 2017, Klement and Vilkovská 2019, Rohanová 2022).

False heart wood is classified as a wood structural defect and is known for its great variability of morphological forms. The formation of a false heart in a living tree as well as a colour change during storage or drying leads to a significant loss of financial value of the beech (Pöhler et al. 2006). Log quality standards are already based on the presence of certain types of false hearts in the logs and automatically classify these logs into lower quality classes.

The aim of this study is to determine the resistance of false heartwood and old beech wood to selected wood rot fungi. For this purpose, a laboratory mycological test was carried out.

MATERIALS AND METHODS

European beech (*Fagus sylvatica* L.) from the Štiavnické vrchy region in Slovakia was used to prepare the test samples. Three sections of different trees with healthy, round pseudo-heartwood were selected for the research. Lumber was made by sharp cutting. By

spreading the middle wood with a thickness of 50 mm and handling it crosswise, blanks with dimensions of $32 \times 50 \times 800$ mm were produced (Figure 1). A total of 270 beech microsamples measuring $25 \text{ mm} \times 25 \text{ mm} \times 5 \text{ mm}$ (longitudinal \times tangential \times radial) were used in the experiment (180 from heartwood and 90 from mature wood). In addition, 60 samples of pine wood (*Pinus sylvestris* L.) were used as samples for the virulence test for brown rot fungi and 30 mature samples of beech wood were used as samples for the virulence test for white rot fungi. All samples were oven-dry in the Memmert UNB 100 oven (Mettmert GmbH + CoKG, Schwabach, Germany) at 103 ± 1 °C, then cooled in desiccators to 20 ± 2 °C and finally weighed with an accuracy of 0.001 g (m_0).

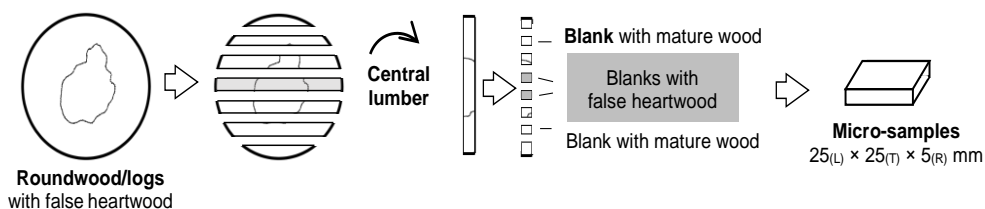


Figure 1. Scheme of preparation of samples.

Micro-samples of the mature and false heart beech wood and 2 virulence woods were attacked with the brown rot fungi *Coniophora puteana*, BAM Ebw. 15 and *Serpula lacrymans* BAM 87, and the white rot fungus *Trametes versicolor*, CTB 863A, respectively. Mycological tests were performed in glass Petri dishes with diameter of 100 mm. The microsamples were placed on plastic mats under which a fungal mycelium had already grown on a 3–4 mm thick solidification layer of 4.5% malt agar (HiMedia Ltd., India). Two microsamples of the false beech wood species, one microsample of the mature beech wood and one microsample of the virulence wood were placed in each petri dish (Figure 2). The reference woods were selected based on the types of fungi used (pine sapwood for brown rot fungi and beech wood for white rot fungi).

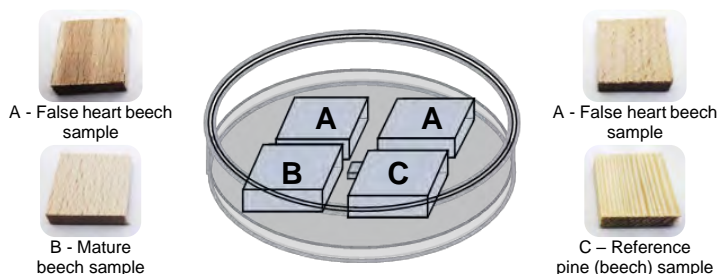


Figure 2. Mycological test in Petri dishes – scheme of test samples for introduction.

The incubation period for fungi lasted 8 weeks at a temperature of 24 ± 2 °C and a relative humidity of $90 \pm 5\%$. After fungal attacks, the microsamples were carefully lifted from plastic mats, cleaned of fungal mycelia and weighed with an accuracy of 0.001 g ($m_{\text{Fungal Attack}}$). Likewise, microsamples after drying at 103 °C until a constant weight was achieved weighed with an accuracy of 0.001 g ($m_{0-\text{Fungal Attack}}$).

The decay resistance of false heartwood and mature beech wood was evaluated based on their mass loss (Δm), which was determined in percent [%] for each microsample in the absolutely dry state before (m_0) and after fungal attack ($m_{0-Fungal\ Attack}$) by Equation 1:

$$\Delta m = \frac{m_0 - m_{0-Fungal\ Attack}}{m_0} \cdot 100 \quad (1)$$

The moisture content – *MC* of false heartwood and mature beech wood samples after fungal attack was determined using the gravimetric method. The moisture content in percent (%) was calculated using Equation 2,

$$MC = \frac{m_{Fungal\ Attack} - m_{0-Fungal\ Attack}}{m_{0-Fungal\ Attack}} \cdot 100 \quad (2)$$

RESULTS

The mass loss - Δm [%] of the tested beech microsamples with false heartwood or mature wood against the brown rot fungi *C. puteana* and *S. lacrymans* as well as the white rot fungus *T. versicolor* is given in Table 1.

Following the standard EN 350:2016, it is suggested that the median (central trend) can be determined better than the average. The influence of certain deviating data with extreme value deviations was eliminated by using the median value. The validity of the test was confirmed by the satisfactory virulence of each brown rot fungal strain, which in the reference samples of sapwood of pine wood caused a mass loss of 20.02% for *C. puteana* and 26.09% for *S. lacrymans* - i.e. more than that for this reference type of wood requires 20% according to EN 113-2:2020. For the white rot fungus *T. versicolor* it was 27.06%, although according to EN 113-2:2020 it is very close to the threshold value (more than 20%).

Table 1 Basic statistical characteristics of mass loss – Δm [%] of beech wood part by selected fungi after 8 weeks.

Fungi		Mass loss – Δm [%]					
		<i>C. puteana</i>		<i>S. lacrymans</i>		<i>T. versicolor</i>	
Wood Part		False Heart	Mature	False Heart	Mature	False Heart	Mature
Median	\tilde{x}	14.50	28.73	24.99	15.14	20.42	27.95
Average	\bar{x}	17.11	25.78	25.68	17.22	21.31	27.23
Minimum	x_{min}	5.78	6.46	13.33	12.00	7.45	21.19
Maximum	x_{max}	36.46	42.64	43.94	32.57	38.18	33.11
Standard Deviation	<i>SD</i>	9.68	10.64	7.51	4.87	7.99	3.40

Based on the results (Tables 1 and 2), we can say that the influence of the type of decaying fungi and the “wood part*fungus” interaction on the mass loss is statistically significant. However, the influence of part of the beech wood – false heartwood or mature wood – is statistically insignificant. The dependence of the mass loss on the selected rotting fungus species and the wood content is shown graphically in Figure 3.

False heartwood and mature wood from beech woods were also resistant to rotting fungi. These results are also influenced by the increased variation in the mass loss values of

individual samples, which is reflected in the determined minimum and maximum values or standard deviations.

Table 2 Analysis of variance for mass loss – Δm [%] of beech wood part by selected fungi after 8 weeks.

	Sum of Squares	Degrees of Freedom	Deviation	F test	Significance Level – p
Absolute member	99 586	1	99 585	1 628	0.000
Wood Part	206.6	1	206.6	3.378	0.067
Fungus	384.0	2	192.0	3.139	0.045
Wood Part *Fungus	2 718	2	1359	22.22	0.000
Error	13 760	225	61.16		

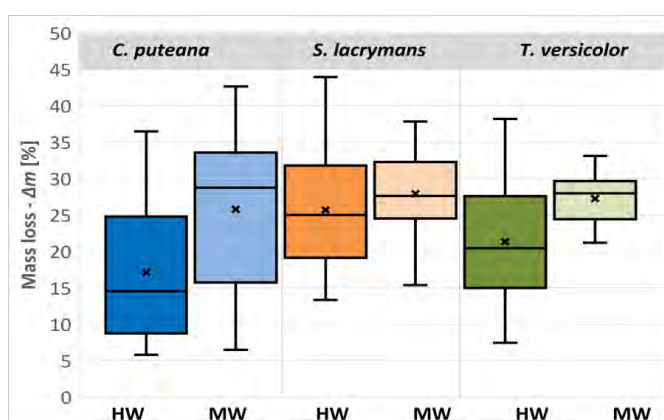


Figure 3. Mass loss – Δm [%] for beech wood withdrawn to fungi species (*C. puteana*, *S. lacrymans*, and *T. versicolor*) and wood part (HW – heartwood and MT – mature wood).

After the decay resistance test, a moisture content that was significantly above the fiber saturation point was achieved in all cases (Table 3). As expected, these fungi showed the ability to produce significant amounts of free water by decomposing relevant basic components of the wood structure (polysaccharides or lignin) in mature and false core beech wood.

Table 3 Basic statistical characteristics of moisture content – MC [%] of beech wood by selected decaying fungi after 8 weeks.

Fungi		Moisture content – MC [%]					
		<i>C. puteana</i>		<i>S. lacrymans</i>		<i>T. versicolor</i>	
Wood Part		False Heart	Mature	False Heart	Mature	False Heart	Mature
Average	\bar{x}	51.26	53.40	54.64	57.27	55.31	58.30
Median	\tilde{x}	52.22	54.76	55.16	57.44	55.93	58.68
Minimum	x_{min}	41.92	29.51	21.50	49.81	45.02	54.07
Maximum	x_{max}	57.98	44.10	43.83	62.34	61.55	61.54
Standard Deviation	SD	4.58	5.43	4.64	2.59	4.02	2.32

RESULTS

The results of this laboratory study on decay resistance of beech wood are as follows:

- Native false heartwood and mature wood are equally resistant to brown and white rot fungi;
- Fungi species have an influence on the resistance of beech wood – very significantly in the “wood part*fungus” interaction;
- The decomposition process is accompanied by the formation of a significant amount of free water and an increase in their moisture content.

Acknowledgment

This work was supported by the Slovak Research and Development Agency under the contract no. APVV-21-0051.

REFERENCES

- EN 350:2016. Durability of wood and wood-based products – Testing and classification of the durability to biological agents of wood and wood-based materials.
- EN 113-2:2020. Durability of wood and wood-based products – Test method against wood destroying basidiomycetes - Part 2: Assessment of inherent or enhanced durability.
- Gabriel, J., Švec, K. 2017. Occurrence of indoor wood decay Basidiomycetes in Europe. *Fungal Biology Reviews*, 31: 212-217.
- Geen Report 2023. Report on the Forestry Sector of the Slovak Republic 2022 – Green report. Ministry of Agriculture and Rural Development of the Slovak Republic: Bratislava, Slovak Republic, 2023; 66 p. <https://www.mpsr.sk/zelena-sprava-2023/123---19005/>
- Klement, I, Vilkovská, T., 2019. Color characteristics of red false heartwood and mature wood of beech (*Fagus sylvatica* L.) determining by different chromacity coordinates. *Sustainability*, 11(3): 690.
- Pöhler, E., Klingner, R., Künniger, T., 2006. Beech (*Fagus sylvatica* L.) – Technological properties, adhesion behaviour and colour stability with and without coatings of the red heartwood. *Annals of forest science*, 63(2): 129-137.
- Reinprecht, L. 2008. Wood Protection, Zvolen: Technical university in Zvolen, 453 p.
- Rohanová, A. 2022. The influence false heartwood on the quality of beech structural timber. *Chip and Chipless Woodworking Processes*. 13(1): 87-94.
- Rypáček, V. 1957. Biology of wood decay fungi. Prague: Publishing House of the Czechoslovak Academy of Sciences, 209 p.
- Slabejová, G. 2013. Photostability of transparent surface coatings of beech wood. *Acta Facultatis Xylogiae Zvolen*. 55(2): 5-12.
- Trenčiansky, M., Lieskovský, M., Merganič, J., Šulek, R., 2017. Analysis and evaluation of the impact of stand age on the occurrence and metamorphosis of red heartwood. *iForest-Biogeosciences and Forestry*, 10(3): 605-610.
- Watkinson, S., Eastwood, D. 2012. *Serpula lacrymans*, wood and build-ings. *Advances in Applied Microbiology*, 78: 121-149.